Understanding the early mechanisms of graft union formation in Arabidopsis

Clément Chambaud

université de BORDEAUX

THÈSE PRÉSENTÉE

POUR OBTENIR LE GRADE DE

DOCTEUR DE

L'UNIVERSITÉ DE BORDEAUX

ÉCOLE DOCTORALE DES SCIENCES DE LA VIE ET DE LA SANTE

SPÉCIALITÉ BIOLOGIE VEGETALE

Par Clément CHAMBAUD

COMPREHENSION DES MECANISMES PRECOCES DANS L'ETABLISSEMENT DE LA RELATION PORTE GREFFE-GREFFON

Sous la direction de : Lysiane BROCARD
(co-directeur : Sarah COOKSON)

Soutenue publiquement le 19 Décembre 2019

Membres du jury :

M. MOREAU Patrick	Directeur de recherche CNRS	Président
Mme BENITEZ-ALFONSO Yoselin	Maitre de conférences Université de Leeds	Rapporteur
Mme VERNHETTES Samantha	Directeur de recherche INRA	Rapporteur
Mme POURTAU Nathalie	Maitre de conférences Université de Poitiers	Examinateur
Mme BAYER Emmanuelle	Directeur de recherche CNRS	Examinateur
Mme OLLAT Nathalie	Ingénieur de recherche INRA	Invité

COMPREHENSION DES MECANISMES PRECOCES DANS L'ETABLISSEMENT DE LA RELATION PORTE GREFFE-GREFFON

Le greffage est une pratique qui consiste à couper et joindre les appareils racinaires et aériens de deux plantes pour former un organisme chimérique unique, combinant au sein d'un même individu, les caractéristiques biologiques les plus avantageuses de ces deux plantes, telles que la résistance aux agents pathogènes du sol et la production fruitière. Pour survivre, les plantes greffées, où toutes les communications cellulaires entre les parties aériennes et racinaires ont été interrompues par la coupe, doivent interagir ensemble pour établir de nouvelles voies d'échange. De nos jours, des efforts considérables ont été déployés pour comprendre les mécanismes de développement sous-jacents à la formation d'une union au niveau de la greffe en termes de signalisation hormonale, d'expression génique et d'histologie ; mais les données ultrastructurales sont encore insuffisantes.
En raison de la difficulté de cibler de manière fiable l'interface de greffe en microscopie électronique, très peu de données ultrastructurales de l'interface de greffe sont disponibles. Cependant, ces données sont essentielles pour comprendre l'établissement de communications greffons / porte-greffes.

Dans ce contexte, l'objectif de ma thèse était de caractériser les développements ultrastructuraux survenant au cours de la formation de cette union afin de caractériser les mécanismes cellulaires impliqués. Tout d'abord, une approche par microscopie correlative (CLEM) a été développée sur des hypocotyles greffés d'Arabidopsis thaliana et des greffes in vitro de vigne. Bien que la qualité obtenue sur le modèle de la vigne doive encore être améliorée, la préservation de la fluorescence et de l'ultrastructure obtenue pour A. thaliana a permis de révéler au moins quatre voies de communication entre le greffon et le porte-greffe : exosomes, plasmodesmes, phloème et xylème. La caractérisation ultrastructurale des plasmodesmes formés de novo à l'interface de greffe, par tomographie électronique, a montré que plus de 30% des tentatives pour former une connexion symplastique échouaient et aboutissaient à la formation d'hémi-plasmodesmes ne traversant pas la paroi cellulaire, aussi bien du côté du greffon que du porte-greffe. De plus, les observations d'événements de biogenèse de plasmodesmes secondaires semblent indiquer que ces plasmodesmes seraient formés dans des cellules présentant un amincissement synchrone de la paroi cellulaire. Enfin, pour la première fois, des échanges cytoplasmiques ont été observés à l'interface de greffe. Ainsi, le processus de greffage combiné à notre approche de CLEM pourrait être un moyen d'induire et d'étudier des événements de transplastomiques. Ces fusions cytoplasmiques pourraient jouer un rôle dans la cicatrisation des blessures ou la reconnexion vasculaire. Finalement, des lignées

transgéniques d'Arabidopsis ont été mises au point pour suivre, à l'avenir, la perméabilité des plasmodesmes à l'interface de greffe. L'intégration d'études ultrastructurales et d'études dynamiques lors du greffage de différents mutants permettra d'élucider la fonctionnalité de la connexion de cellule à cellule pendant la formation de la greffe.

Mots clés : Greffe, Arabidopsis, Microscopie Correlative, Plasmodesme, Comminucation cellulaire

---

UNDERSTANDING THE EARLY MECHANISMS OF GRAFT UNION FORMATION

Grafting consists of the cutting and joining of two plants together to form one unique chimeric organism; it is done to combine biological traits of the two plants such as resistance to soil borne pathogens and high fruit quality in one plant. To survive, grafted plants, where all physical cell communications between aerial and root parts are interrupted by cutting, have to interact together to establish new exchange pathways. Nowadays, considerable efforts have been done to understand the developmental mechanisms underlying graft union formation in terms of hormone signaling, gene expression and histology however ultrastructural data are still lacking.

Because of the difficulty of reliably targeting the graft interface under the electron microscope very few ultrastructural data of the graft interface are available; however, such precise data is essential to understand the establishment of scion/rootstock communications.

In this context, the aim of my thesis was to characterize the ultrastructural developments occurring during graft union formation to provide insights into the cellular mechanisms involved. First, a correlative light and electron microscopy (CLEM) approach was implemented on grafted hypocotyls of Arabidopsis thaliana and in vitro grafts of grapevine. Although quality obtained on the grapevine model still needs to be improved, the fluorescence and ultrastructure preservation obtained for A. thaliana allowed me to reveal four potential pathways of communication between the scion and rootstock: exosomes, plasmodesmata, phloem and xylem. The ultrastructural characterization of de novo plasmodesmata formed at the graft interface, by electron tomography, showed that more than 30 % of the attempts to form symplastic connection failed and resulted in the formation, both at scion or rootstock side of the cell wall, of hemi-plasmodesmata that do no span the cell wall. Moreover, the observations of events of secondary plasmodesmata biogenesis seem to indicate that plasmodesmata can be formed successfully between cells where there is a synchronous thinning of

the cell wall. Finally, for the first time cytoplasmic exchanges were shown to happen at the graft interface and confirm that grafting combined with our CLEM approach could be a way to induce and study transplastomic events. They could play a role in wound healing or vascular reconnection. Additionally, biological tools have been developed to follow, in the future, the permeability of plasmodesmata at the graft interface of A. thaliana. The integration of ultrastructural and dynamic studies on different mutants will allow us to decipher the functional establishment of the cell-to-cell connectivity during the graft union formation.

Keywords: Graft, Arabidopsis, Correlative microscopy, Cell communication, Plasmodesmata

---

Ecophysiologie et génomique fonctionnelle de la vigne
INRA UMR 1287

ISVV Bordeaux-Aquitaine
210 Chemin de Leysotte, 33140 Villenave-d'Ornon, France

Résumé détaillé en français

Le greffage est une pratique qui consiste à assembler deux plantes vivantes en une seule, pour former un organisme chimérique unique. La partie aérienne, qui est sélectionnée en fonction de ses avantages de production, est appelée greffon. Elle est greffée sur un système racinaire appelé porte-greffe, qui est sélectionné en fonction de son adaptation aux conditions du sol. Bien que les origines exactes du greffage soient incertaines, il est probablement originaire de Chine quelques siècles avant J.-C. De nos jours, c'est une pratique largement utilisée pour les cultures pérennes telles que les *Citrus spp*, *Prunus spp*, les pommiers et les vignes, ainsi que certaines cultures annuelles comme les melons et les tomates. Historiquement, la principale utilisation du greffage a été la propagation végétative d'espèces pour assurer la stabilité du phénotype. De plus, le greffage permet d'éviter de passer par une multiplication sexuelle qui implique une longue période de juvénilité où la plante est incapable de fleurir et donc de produire. Il existe aujourd'hui de nombreuses applications à la greffe, notamment la réduction de la taille de la partie aérienne, qui améliore l'allocation du carbone aux fruits et augmente le rendement par unité de surface, mais aussi la résistance aux stress biotiques et abiotiques. Aujourd'hui, l'amélioration de la résistance aux stress biotiques et abiotiques conférée par le greffage peut même contribuer à réduire l'utilisation des traitements phytosanitaires, un sujet d'intérêt dans une société confrontée au changement climatique et à la diminution de la biodiversité.

Malgré un intérêt scientifique de longue date pour la greffe, les processus biologiques à l'origine de la formation d'une greffe fonctionnelle ne sont pas encore totalement élucidés, en particulier les problèmes liés à la compatibilité entre greffons et porte-greffes, car tous les génotypes ne peuvent pas être greffés ensemble avec succès. Comprendre les mécanismes de développement de cette union et la manière dont les plantes interagissent à l'interface de greffe est une priorité. Les études récentes de Melnyk *et al.* décrivent les mécanismes de formation de l'union porte-greffe/greffon et les gènes différentiellement exprimés entre les deux partenaires durant la greffe d'hypocotyles d'*Arabidopsis thaliana*. Ces études ouvrent la voie à la compréhension des processus qui se produisent pendant la formation de cette union, notamment les voies de signalisation hormonale, de cicatrisation des blessures et de reconnexion vasculaire impliquées. Cependant, la connaissance des développements ultrastructuraux à l'interface de greffe est encore insuffisante. Cela est dû en grande partie à la difficulté d'identifier l'origine des cellules, soit du greffon, soit du porte-greffe, dans le cal cellulaire à l'interface en microscopie électronique.

Pendant la greffe, toutes les communications cellulaires sont interrompues par la coupe au point de greffe et les deux organismes greffés doivent interagir ensemble assez rapidement et efficacement pour survivre. En raison de la complexité à cibler de manière fiable l'interface de greffe en microscopie électronique, les données ultrastructurales font toujours défaut. Kollmann & Glockmann (1985), en travaillant sur un modèle d'hétérogreffe de *Vicia faba* et d'*Helianthus annuus*, qui présentent des marqueurs ultrastructuraux cytologiques spécifiques à chacun (noyaux, plastes), ont réussi à démontrer la présence de plasmodesmes, des canaux intercellulaires spécifiques des plantes, à l'interface de greffe. Toutefois, cette approche ne permettait pas d'identifier sans ambiguïté chaque cellule étudiée en raison de l'hétérogénéité ultrastructurale intrinsèque entre des cellules différenciées. Plus de 30 ans après, aucune étude fiable n'a été publiée concernant les événements ultrastructuraux se produisant spécifiquement à l'interface. La connaissance des détails ultrastructuraux fins nécessaires pour comprendre la biogenèse des plasmodesmes et l'établissement de la communication à l'interface de greffe fait toujours défaut et ne peut être évaluée qu'avec de nouvelles méthodes.

L'utilisation de protéines étiquetées par des protéines fluorescentes offre la possibilité de marquer les cellules des échantillons vivants. En outre, des protéines fluorescentes de différentes couleurs (rouge, RFP ou jaune, YFP) peuvent être utilisées pour marquer spécifiquement chacun des partenaires de la greffe. Malheureusement, avec la microscopie à fluorescence, l'environnement cellulaire n'est pas accessible et la résolution atteinte est limitée par la diffraction. Pour accéder à l'échelle de l'ultrastructure cellulaire, la microscopie électronique à transmission est essentielle cependant, la fluorescence ne peut être observée. Ainsi, l'accès à l'ultrastructure de l'environnement d'une protéine fluorescente n'est pas directement possible.

Grâce à l'émergence de nouveaux outils en microscopie, l'ultrastructure de l'interface de greffe pourrait être étudiée et offrir de nouvelles perspectives pour la compréhension des mécanismes de communications qui s'y établissent chez des plantes modèles comme *Arabidopsis thaliana*. En effet, des méthodes de microscopie corrélative permettent de combiner les informations obtenues par la microscopie optique, par exemple l'étude de la dynamique d'un processus dans un tissu vivant, avec l'analyse de l'ultrastructure des composants sub-cellulaires impliqués dans ce processus grâce à la microscopie électronique. C'est cette approche de microscopie corrélative que nous avons décidé de développer pour accéder à l'ultrastructure de l'interface de greffe afin d'y décrypter l'établissement de communications cellulaires. La microscopie corrélative est devenue une technique de choix au cours des dernières années, car elle a un large éventail d'applications chez de nombreux organismes modèles mais elle reste pourtant peu développée chez les plantes. Le premier objectif de cette thèse

a donc été de mettre en place une méthode de microscopie corrélative adaptée à l'étude ultrastructurale de l'interface de greffe.

Les travaux de l'équipe de Kukulski (Kukulski *et al.*, 2011), réalisés sur des cellules en culture, chez la levure et sur des échantillons de mammifères, ont permis d'obtenir une bonne préservation ultrastructurale ainsi qu'une bonne préservation du signal de fluorescence. C'est pour cela nous avons choisi d'adapter leur protocole de microscopie corrélative "In Resin Fluorescence" à des échantillons végétaux. En outre, cette approche est compatible avec la tomographie électronique permettant d'atteindre une résolution à l'échelle du nanomètre dans les trois dimensions, indispensable pour accéder à l'ultrastructure des plasmodesmes. Nos principales modifications ont consisté à trouver les bonnes conditions de préparation de nos échantillons en ajustant la température et la durée de chaque étape de la "Freeze Substitution" et de l'imprégnation. Comme la fluorescence diminuait pendant la préparation des échantillons, l'étape la plus difficile était la visualisation du signal de fluorescence. L'épaisseur des coupes, la fragilité de la grille de microscopie électronique, le montage de l'échantillon, la sensibilité du système d'acquisition du signal fluorescent ont été adaptés pour permettre une approche de microscopie corrélative réussie. Pour visualiser l'interface de greffe d'*Arabidopsis thaliana*, nous avons utilisé la séquence HDEL, motif de rétention au réticulum endoplasmique, fusionnée aux protéines fluorescentes ; YFP et RFP pour chaque partenaire de greffe respectivement. Après avoir vérifié que ce signal de rétention HDEL ne peut se déplacer de cellule en cellule, ces constructions ont été utilisées pour marquer l'interface de greffe. Sur la vigne, en raison des difficultés à établir de nouvelles lignées transgéniques, une seule lignée de cultivars *in vitro* de Pinot Noir exprimant 35S::HDEL_GFP était disponible et a été greffée sur des cultivars de Pinot Noir de type sauvage. Le système de vigne, avec un seul des deux partenaires marqué est moins pratique que celui d'*Arabidopsis thaliana.* En effet, si une cellule n'est pas fluorescente, elle pourrait appartenir au partenaire n'exprimant pas la GFP. En revanche, on ne peut pas exclure que le signal puisse être trop faible pour être détecté. Des premiers résultats encourageants, permettant de conserver la fluorescence, ont été obtenu chez la vigne. Concernant l'ultrastructure, celle-ci a été insuffisamment préservée pour permettre d'observer l'ultrastructure fine, notamment des plasmodesmes mais permettait néanmoins l'observation des types cellulaires et des formes de plasmodesmes. En revanche, notre approche microscopie corrélative nous a permis de cibler sans ambiguïté l'interface de greffe d'hypocotyles d'*Arabidopsis thaliana* avec une conservation de l'ultrastructure fine pour la première fois. Combinée à la tomographie électronique, elle nous a permis d'atteindre un niveau de détail sans précédent et de suivre l'établissement des communications à l'interface de greffe. La mise au point d'un tel protocole de microscopie corrélative couplée à la tomographie électronique constitue une avancée technologique significative pour l'imagerie chez plantes pour accéder à des évènements

rares ou difficile à cibler de plus, cette approche pourrait être étendue à d'autres organes de plantes, telles que la pointe racinaire.

Le deuxième objectif de cette thèse a été l'utilisation de cette approche sur des hypocotyles greffés *d'Arabidopsis thaliana* afin de mieux comprendre les processus ultrastructuraux se produisant lors de la formation cette union. En effet, lors de la greffe, toutes les communications sont interrompues et l'établissement de communications *de novo* est essentiel pour la survie et le développement des deux partenaires. Les mécanismes ultrastructuraux mis en place pour former ces nouvelles communications (plasmodesmes, xylème, phloème) restent non connus. Pour établir une chronologie des évènements se déroulant à l'interface de greffe, deux temps ont été étudiés : 3 et 6 jours après la greffe. Au temps le plus précoce, les greffes sont dans un état transitoire où les nouvelles connexions entre les partenaires sont en cours d'établissement avec des plasmodesmes et des vaisseaux qui se connectent mais alors que d'autres régions restent séparées par des couches de paroi cellulaires avec des résidus denses aux électrons. De plus, 3 jours après la greffe, les cellules ne sont toujours pas complètement différenciées, alors que le processus de différenciation semble achevé 6 jours après la greffe, montrant des tubes criblés déjà matures et des vaisseaux du xylème connectés à l'interface.

Les plasmodesmes dits "primaires" se forment entre deux cellules filles par le piégeage de brins de réticulum endoplasmique dans la paroi végétale en expansion. Dans le cadre de la greffe, l'établissement d'une connexion de cellule à cellule entre les partenaires greffés implique nécessairement la biogenèse de plasmodesmes "*de novo*", dans des parois préexistantes. Les mécanismes de biogenèse à l'origine de ces derniers ne sont pas connus à ce jour. L'étude de leurs caractéristiques ultrastructurales et leur environnement cellulaire peuvent nous donner des clefs pour comprendre ce mécanisme de biogenèse particulier. Nous avons donc particulièrement recherché des évènements pouvant correspondre à la biogenèse de plasmodesmes. Grâce à la tomographie, qui donne accès à une vue tridimensionnelle, des plasmodesmes de différentes formes ont été observées dès 3 jours après la greffe et répartis en quatre classes : les simples, les branchés, les "twins" et les "hémis". Les simples, branchés et "twins" traversent complètement la paroi cellulaire. La dernière classe, les hémi-plasmodesmes, les plus fréquemment observés à l'interface de greffe, ne traversent pas complètement la paroi cellulaire. Ces plasmodesmes se trouvent indépendamment du coté greffon ou porte-greffe indiquant que la biogenèse de plasmodesmes est initiée aussi bien par des cellules de greffon ou de porte-greffe. De plus, lorsque la lamelle moyenne est visible, la progression des hémi-plasmodesmes dans la paroi cellulaire semble bloquée par celle-ci. Une modification préalable de la composition de la paroi à l'établissement d'un plasmodesme semble donc nécessaire. Presque tous les hémi-plasmodesmes observés forment des structures en boucle avec au moins deux ouvertures

cytosoliques dans la même cellule. Certains hémi-plasmodesmes ayant une structure en « pelote de laine » ont été observés à deux reprises dans des parois cellulaires épaisses. Ces derniers ont une grande cavité centrale dans laquelle le desmotubule est comprimé et accumulé. Finalement, les hémi-plasmodesmes ont été généralement observé dans des parois plus épaisses que celles des autres classes. Alors que d'après les données obtenues par Melnyk (2015), le greffon a tendance à impulser les processus développementaux au sein de la greffe, tandis que le porte-greffe est plus passif, les deux partenaires sont capables d'initier la biogenèse des plasmodesmes.

L'observation de ces différentes formes de plasmodesmes en trois dimensions nous indiquent que différents mécanismes de biogénèse peuvent coexister simultanément à l'interface de greffe, probablement en fonction du contexte cellulaire au moment de la formation de ces plasmodesmes. La première hypothèse est qu'elle pourrait être initiée par un accolement de la membrane de réticulum endoplasmique à la membrane plasmique, simultanément à un amincissement local et une modification de la composition de la paroi cellulaire. Ensuite, des brins de réticulum endoplasmisque pourraient être piégées dans la paroi lorsque du matériel pariétal est amené à cet endroit par la cellule, conduisant ainsi à la formation d'un hémi-plasmodesme. Finalement, un événement similaire pourrait se produire de manière synchrone du côté opposé de la paroi cellulaire, chez l'autre partenaire, suivie d'une fusion des deux hémi-plasmodesmes et formation d'un plasmodesme branché. Cela impliquerait l'existence de voie de signalisation permettant de coordonner spatialement et temporellement ces événements symétriques. L'autre hypothèse est qu'une seule des deux cellules, nécessitant une augmentation de ses communications cellule à cellule, envoie des ramifications vers l'autre, par un mécanisme actif tel qu'en témoigne la présence de plasmodesmes en « pelote de laine » avec une accumulation de réticulum endoplasmique dans la paroi ou de plasmodesmes simple. Ainsi, si la cellule en face se trouve dans un état "accepteur", il y aura formation de plasmodesmes simples. Si les conditions ne sont pas réunies, car une seule cellule initie le processus de biogenèse et les cellules réceptrices ne donnent pas leur accord, la progression de plasmodesmes est bloquée au milieu de la paroi cellulaire. Il en résultera la formation d'hémi-plasmodesmes de ce côté. Il est possible que ces différents types de biogenèse co-existent au sein d'un même greffe. Le choix entre l'un ou l'autre des mécanismes pourrait dépendre par exemple des types cellulaires impliquées (parenchyme, précurseurs de vaisseaux,…). Pour répondre à cette question, il est cependant nécessaire de disposer de davantage de données. Il est intéressant de noter que de nombreux hémi-plasmodesmes ont été observés à l'interface du greffe et cela même dans un contexte d'homogreffe d'*Arabidopsis thaliana.* Ces "demi" plasmodesmes ne sont donc pas la conséquence d'une incompatibilité entre les deux partenaires.

Trois jours après greffe, une grande partie de l'interface de greffe contient des débris de cellules et de parois cellulaires. Au sein de ces parois, nous avons observé plusieurs types de vésicules extracellulaires, de tailles et d'aspects differents. Elles pourraient être originaire des résidus formés à partir de cellules sectionnées, mais elles pourraient également être le résultat d'un processus cellulaire actif. Les vesicules extracelullaires sont connues pour jouer un rôle dans les réactions de stress, l'immunité et la médiation des interactions plantes-pathogènes (Rutter & Innes, 2017, 2018 ; Rybak & Robatzek, 2019). Elles peuvent transporter des petits ARN, des enzymes, des ribosomes d'une cellule à une autre ou dans la paroi cellulaire. En outre, les vésicules extracellulaires ont été associées au plasmodesmes, en agissant pour réduire leur perméabilité et arrêter la propagation de la réponse hypersensible en réponse à l'attaque d'un agent pathogène. Dans le contexte de la greffe, notre hypothèse est que ces vesicules extracellulaires pourraient assurer les premières étapes de la communication cellulaire entre le greffon et le porte-greffe en passant à travers les couches de paroi cellulaire qui séparent les deux partenaires et en transportant des molécules de signalisation d'un partenaire à l'autre. Cela pourrait, entre autre, permettre la synchronisation spatio-temporelle des deux partenaires. Elles pourraient également apporter le matériel nécessaire à la digestion de la couche nécrotique pour remodeler la paroi cellulaire et créer une paroi cellulaire unique commune à l'interface du greffe, première étape clef pour la mise en place d'une communication entre les partenaires.

Enfin, lors de l'observation des interfaces de greffe d'*Arabidopsis thaliana*, 3 jours après greffe, des cellules bicolores, présentant les signaux fluorescent YFP et RFP ont été observées. Ces cellules correspondent à des évènements de fusions cytoplasmiques induites par des amincissements de parois cellulaires, conduisant à la formation d'ouvertures pariétales jusqu'à 2 µm. Ces évènements ont été observés rarement. Nous avons pu vérifier la spécificité du signal fluorescent dans la cellule bicolore grâce à un immuno-marquage à l'or avec des anticorps dirigés contre la YFP. Un marquage spécifique du réticulum endoplasmique a été observé. Notre hypothèse est qu'au cours de la biogenèse des plasmodesmes, si l'amincissement de la paroi cellulaire est excessif, une fusion partielle de la membrane plasmique entre les deux cellules pourrait se produire à cet endroit et conduire à la formation de cellules bicolores. Des transferts d'organelles et de cytoplasmes entre des cellules partiellement fusionnées pourrait alors se produire. Ces événements de mélange cellulaire pourraient également expliquer la possibilité d'obtenir des plantes hybrides à partir de cellules de cals de tabac greffées, caractérisé dans les études de Bock et Stegemann (2009, 2017). Ces échanges pourraient être très importants pour la communication entre les partenaires greffés. Ils permettraient d'accélérer les

échanges de molécules de signalisation entre les deux partenaires en fusionnant deux cellules et en formant une zone hybride, où l'interface de greffe n'est pas bien définie.

En résumé, la microscopie corrélative a été une approche innovante et robuste pour étudier l'ultrastructure de l'interface de greffe et la formation de connexions symplastiques chez *Arabidopsis thaliana*. Elle nous a permis de cibler de manière fiable, pour la première fois, l'interface de greffe et d'y révéler la présence de plasmodesmes. Par ailleurs, la tomographie nous a permis d'identifier différentes formes de plasmodesmes (simple, branché, twins et hémi), nous permettant ainsi d'émettre des hypothèses sur leur biogenèse dans ce contexte particulier. Nous avons pu notamment voir que les deux partenaires sont capables d'initier la biogenèse de plasmodesmes à l'interface de greffe. Ensuite, les plasmodesmes traversant l'interface sont soit le resultat d'une synchronisation des deux partenaires par fusion d'hémi-plasmodesmes soit issus d'un mécanisme unidirectionnel (un seul partenaire envoi son "plasmodesme" vers l'autre). Comprendre précisément comment ces connexions de cellule à cellule sont établies et sont fonctionnelles dans le temps (en particulier dans les cultures pérennes), reste un enjeu majeur pour déchiffrer les mécanismes de compatibilité/incompatibilité lors de l'établissement de l'union porte-greffe/greffon.

ACKNOWLEDGMENTS

First of all, I am very grateful to all the people who have made possible this thesis work notably Remi Lemoine, his team, and Charles Melnyk for the Arabidopsis grafting training and Cyril Hévin for the *in vitro* grapevine grafting training. I wish to express my deepest gratitude to all persons I met and that brought me a lot during these 3 years; Marie Brault that helped me a lot in the molecular biology, Claire Brehelin and Emmanuelle Bayer for the plant materials and all the other members of UMR 5200, laboratory of membrane biogenesis, that welcomed me for my experiments.

I am also very grateful to my office companions throughout this thesis: Leslie Bancel-Vallée, Brigitte Batailler and Catherine Cheniclet of the Plant Imaging Platform of Bordeaux, which whom we shared a lot of nice discussions and very good cakes at every opportunity.

Finally, I would like to thank two supervisors Sarah Cookson from the lab of Ecophysiology and Grape Functional Genomics and especially Lysiane Brocard, from the Plant Imaging Platform, who accompanied me throughout this project and since my master internship. She has always been available to guide me, to give me precious advices and pushed me to the best of myself, even during the most difficult moments. I am more than grateful that she gave me all her trust.

Last but not the least, I would like to thank my family and my friends for supporting me spiritually throughout writing this thesis and my life in general. I would like to express my deepest gratitude to Lycia, the magnificent person who shares my life since more than 10 years, my unconditional support in the moments when there was no one else to answer my queries.

To my beloved grandfather

Grafting is defined as the art of joining two living plants together into one, to form a unique chimeric organism. The aerial part, which is selected based on its production advantages is called scion. It is grafted on a root system called rootstock, which is selected based on its adaptation to soil conditions. Although the exact origins of grafting are uncertain, it probably originates from China a few centuries BC (Mudge, 2009), it is now a practice widely used in the culture of perennial crops such as *Citrus spp, Prunus spp*, apples and grapevines, as well as some annuals crops such as melons and tomatoes. The principal historical use of grafting has been for the vegetative propagation of species that ensure the phenotype stability. Moreover, grafting avoid to pass through a sexual propagation that involves a long period of juvenility where plant is unable to flower and thus produce. There is now a broad range of uses for grafting, notably the reduction of scion size which improves carbon allocation to fruits and increases yield per unit area, but also for the resistance to biotic and abiotic stresses. Nowadays, improvement of resistance to biotic and abiotic stresses conferred by grafting may contribute to reduce the use of phytosanitary treatments, an increasing topic of interest in a society facing climate change, decrease in biodiversity and where ecological issues hold a fundamental place (May *et al.,* 1994; Mudge, 2009).

Despite a long history of scientific interest in grafting (Bailey, 1923), the biological processes underlying graft union formation are yet to be fully elucidated, in particular, the problems associated with graft compatibility as not all genotypes can be grafted together successfully. Concerning graft compatibility, a generally admitted condition is the high grafting success rate of grafting (early compatibility) is characterized by the vascular continuity of phloem and xylem, but long-term survival of the grafted plant (late compatibility) is no less important.

Considerable effort is done to understand the developmental mechanisms underlying graft union formation and how plants interact at the graft interface (Albacete *et al.,* 2015; Gautier *et al.,* 2019; Harrison *et al.,* 2016). The recent studies of Melnyk *et al*. describe the mechanisms of graft union formation (Melnyk *et al.,* 2015) and the genes differentially expressed in *Arabidopsis thaliana* hypocotyl grafts (Melnyk *et al.,* 2018). These studies pave the way to understand the fine processes occurring during the graft union formation especially in terms of hormone signaling pathways, wound healing and vascular reconnection. However, knowledge of the ultrastructural developments at the graft interface is still lacking. This is largely due to the difficulty to identify the origin of cells, from scion and rootstock, in the cell mixture at the graft interface under the electron microscope. Only one team, by using the hetero-grafting model *Vicia faba* and *Helianthus annuus,* succeeded to reveal reliably the presence of plasmodesmata (PD), crucial inter-cellular channels specific of plants, at the graft interface (Kollmann & Glockmann, 1985, 1991; Kollmann *et al.,* 1985). Plasmodesmata

might be observed on a homograft of tomato (Jeffree & Yeoman, 1982) but in this case, targeting the graft interface was not very reliable. Thus, more than 30 years after, no reliable report was published on the ultrastructural events occurring specifically at the graft interface. Knowledge of the fine ultrastructural details required to understand PD biogenesis and the establishment of communication across the graft interface are still lacking, and can only be assessed with modern, state of the art techniques.

In this context, the aims of my thesis were to develop an approach to access specifically the ultrastructure at the graft interface in order to decipher the communication establishments at the scion/rootstock interface. Two models were used: Grapevine and *A. thaliana*. Thanks to a correlative light and electron microscopy (CLEM) approach, the targeting of the ultrastructure of the graft interface became accessible on both *A. thaliana* and grapevine. As the quality of ultrastructure was better preserved on *A. thaliana*, the studies were firstly done on this model. A special focus was made on the ultrastructure of the PD formed at the graft interface.

My thesis comprises five chapters:

1. Introduction
2. Context and objectives
3. Results
4. Discussion and perspectives
5. References

To complement the introduction to this thesis, I integrate the *Expert View* in *Journal of Experimental Botany* in which I actively participated as co-first author. The review will cover the scion and rootstock interactions in a first part, introducing how the choice of a specific scion can induce modifications of the phenotype of the rootstock and *vice versa*. The second part of this review focuses on the graft union formation and graft incompatibility, which has become a hot topic since grafting is widely used, but very little is known about this processes. This part highlights the recent breakthroughs in understanding this union and emphasizes on the gaps in our knowledge especially our understanding of how partners make new connections through vascular tissues and PD.
In this review, I actively participated in the writing of the second part and I wrote the box 1 and designed the figure of box 2.

The results obtained during my thesis allowed me to write two articles. A first one, which constitutes the first part of my results, concerns the development of a CLEM approach for *A. thaliana* hypocotyl grafts that allowed us to unequivocally target the graft interface and study its ultrastructure. This methodological article can be more generally applied to *A. thaliana* roots tips and hypocotyls. This article will be submitted to *Bioprotocols* after the publication of the second article, which will constitute the main part of my result chapter that we will submit to *Plant Journal.* The second article will bring a new level of details to understanding the ultrastructural organization of the graft interface and especially how both partners make new connections. It will particularly highlight the ultrastructure of PD and bring new data on their *de novo* biogenesis across a pre-existing cell wall.

LIST OF ABBREVIATIONS

1103P: 1103 Paulsen

BSA: Bovine Serum Albumin

CC: Companion Cell

CLEM: Correlative Light Electron Microscopy

DAG: Day After Grafting

EM: Electron Microscopy

ER: Endoplasmic Reticulum

ET: Electron Tomography

EVs: Extracellular Vesicles

FPs: Fluorescent Proteins

FS: Freeze Substitution

GFP: Green Fluorescent Protein

GMA: Glycol Methacryate

HPF: High Pressure Freezing

LM: Light Microscopy

MCS: Membrane Contact Site

MCTP: Multiple C2 and Transmembrane domain-containing Protein

mRFP: Monomeric Red Fluorescent Protein

MS: Murashige and Skoog

PD: Plasmodesmata

PD-PM: Plasmodesmata located Plasma Membrane

PFA: Paraformaldehyde

PM: Plasma Membrane

PN: Pinot Noir

RGM: Riparia Gloire de Montpellier

RT: Rootstock

RTNLB: Reticulon-like B

SBF: Serial Block Face

SC: Scion

SE: Sieve Element

SEL: Size Exclusion Limit

SEM: Scanning Electron Microscope

SIM: Structured Illumination Microscopy

STED: Stimulated Emission Depletion

STEM: Scanning Transmission Electron Microscope

SWEET: Sugars Will Eventually Be Exported Transporters

TagRFP: Tag Red Fluorescent Protein

TE: Tracheary Element

TEM: Transmission Electron Microscopy

YFP: Yellow Fluorescent Protein

TABLE DES MATIÈRES

INTRODUCTION

1. General introduction

1.1. Plant grating: a long history and new applications

Plant grafting is a technique that consists of connecting (at least) two cut plants together: a scion that acts as the new shoot system and the rootstock that acts as the new root system. The grafted plant functions as a unique plant with vascular continuity established between them (Pina & Errea, 2005). The first historical evidence to report grafting attributes its emergence in East Asia already thousands of years ago (Mudge *et al.,* 2009). The occurrence of natural grafting of stems or roots that spontaneously fuse, may have inspired people to use grafting in order to combine plants. To some extent, grafting has been more efficient than cutting for the domestication of certain plants such as apples, pears and plums. Indeed, originally grafting brought the advantage to combine a scion and an already developed root system. By avoiding the immature stage of the plants, the fruit production is accelerated. The use of grafting has extended to many plant species of woody (*e.g. Citrus spp.* and grapevines) and vegetables (especially among Solanaceae (*i.e.* tomatoes, eggplants and peppers) and cucurbits (Kousik *et al.,*2018)). Grafting has been used historically to combine certain agronomical or ornamental traits that are difficult to obtain with simple cuttings or breeding. One important example is the use of dwarfing rootstocks in apples to control growth of the scion, which increases the productivity of the orchards. Nowadays, many plants are grafted to introduce crop resistances to abiotic stresses such as salinity, water deficit, deleterious soil conditions (*i.e.* concerning pH, nutrient availability), in particular because of the increasing concern in regard to climate change (Gregory *et al.,* 2013). In viticulture, nearly all grapevines are grafted, especially in Europe since the invasion of Phylloxera in the late XIXth century. Phylloxera is a soil-dwelling aphid that feeds from the roots and causes death of the plant. *Vitis vinifera*, the European grapevine species, is susceptible to Phylloxera, but it used for its organoleptic properties in wine making. Because Phylloxera originates from America, American *Vitis spp*. are naturally resistant but unsuitable for winemaking. So, grafting *V. vinifera* onto American *Vitis spp.* was introduced (Mudge *et al.,* 2009). Nowadays, grafting could be a key in the limitation of phytosanitary treatments and fertilizers as well as to obtain plants that are better adapted to their environmental conditions such as nature of the soil and climate conditions (May *et al.,* 1994) (Fig. 1).

In recent years, grafting was used in the scientific community as a research tool to understand signaling and transport by studying the movement of mobile elements such as metabolites, proteins and RNAs (Notaguchi *et al.,* 2008; Thieme *et al.,* 2015; Turnbull, 2010; Turnbull *et al.,* 2002).

Figure 1. Examples of horticultural, agricultural and natural grafting. (A) A grafted apple tree. **(B)** An orange tree scion grafted to a rootstock, most likely to improve cold tolerance or for dwarfing. **(C)** An American grape rootstock grafted to a European grape scion to confer resistance to the pathogen Phylloxera. **(D)** An example of natural grafting in Persian Ironwood (*Parrotia persica*) where branches and limbs in contact can fuse. **(E)** A ruby ball or moon cactus, formed by grafting a chlorophyll-deficient cactus species (red) onto a different species that is capable of photosynthesis. The graft takes, but often after time, the lower cactus will outgrow the upper cactus and the plants will separate. An example of an initially compatible graft that with time can fail. **(F)** Grafting of a standard beech rootstock (*Fagus sylvatica*) to a weeping beech scion (*Fagus sylvatica* 'Miltonensis'). A–F: Photos by C.W. Melnyk (Extracted from Melnyk *et al.,* 2015)

1.2. Graft compatibility in agriculture

The implementation of new scion/rootstock combinations constitutes a challenge for breeders. However, grafting process forces the coexistence of two organisms with different genotypes that could interact more or less well (Cordeau, 1998). Early detection of compatible grafts would be highly beneficial to nurseries, and thus, it is of a great interest to understand this process to predict compatible grafts. For Goldschmidt (2014), there is no precise definition of 'graft compatibility'. It generally means establishment of successful graft union, with high success rate (early compatibility) and, no less importantly, the long-term survival and proper functioning of the composite plant (late compatibility). For example, a vascular continuity of phloem and xylem must be established between both partners. This event involves a first establishment of cell-to-cell communication between scion and rootstock, which probably must be renewed each spring for perennial plants that resume growth each year. Indeed, even after a successful union at first, a too high percentage of plants begin to die prematurely, several years after grafting. Unfortunately, despite the widespread use of grafting, mechanisms at the origin of graft compatibility/incompatibility remain to be elucidated. In perennial plants, several processes such as oxidative stress (Nocito *et al.,* 2010; Zarrouk, 2010) or the accumulation of phenolic compounds have been proposed to be involved in graft compatibility (Pina & Errea, 2005, 2008). Differential transcriptomic studies on grafted and non-grafted ligneous grapevine revealed that homo-grafting (grafting the same genotype with itself) is associated with a transcriptional deregulation of genes associated with phloem and xylem development, cell-wall biogenesis and secondary metabolism (particularly wounding responses)(Cookson *et al.,* 2013). A recent transcriptomic study (Assunção *et al.,* 2019) also observed that early steps of a compatible graft are related to the induction of signaling pathways with notably hormone one, leading to a good communication between partners. In hetero-grafting, additional transcripts associated with stress and defense responses are accumulated at the graft interface (Assunção *et al.,* 2019; Cookson *et al.,* 2014; Irisarri *et al.,* 2015). However, transcriptomic studies although very informative have to face the challenge of separating transcripts which are specific to the wood development and transcripts which are specific to the graft process. This is because, in perennial crops such as grapevine, grafting is done on dormant wood, so that the formation of the graft union coincides with the reactivation of the cambium in the spring. Furthermore, to date, all transcriptomic studies on the graft interface have been done on heterogeneous cell populations (including wood cells and callus cells of both scion and rootstock) and have lacked sufficient sampling depth or all the necessary controls to adequately interpret the data (Chen *et al.,* 2017; Cookson *et al.,* 2014). Above all, these transcriptomic studies pinpoint the great importance of communication establishment from the very beginning of graft union formation to ensure a long term survival of the graft. Indeed, to survive,

grafted plants, where all physical cell communications between the scion and the rootstock are interrupted by cutting, need at first to establish new exchange pathways.

1.3. Intercellular plant communication: communication via plasmodesmata (PD)

For the development of multicellular organisms such as higher plants, intercellular communications are crucial and, in plants, many molecules are transported from cell-to-cell through PD. These nanometric channels, with a diameter from 20 to 40 nm, span the cell wall to connect the symplast of two neighboring cells. They were firstly observed by Eduard Tangl in 1880 between cotyledon cells of *Strychnos nuxvomica* and were already hypothesized to unite the cells as a higher entity, introducing for the first time, the concept of symplastic domains. Plasmodesmata allow the cell-to-cell communication between almost all plant cells by establishing both cytosolic and membrane continuities between cells of the entire plant body. These channels are required for the entire plant life cycle because of their role in key biological processes such as photoassimilate distribution (Turgeon, 1996) and developmental events (as reviewed by Otero *et al.,* 2016) through the transports of transcription factors, RNA and metabolites (Lucas & Lee, 2004; Furuta *et al.,* 2012 Benitez-alfonso *et al.,* 2009; Stonebloom *et al.,* 2009; Xu *et al.,* 2011). They can also be hijacked by viruses (Kumar *et al.,* 2014). The work of Yin *et al.* (2012) showed a high expression levels of PLASMODESMATA-LOCATED PROTEIN 1 (PDLP1), a protein located at PD. PDLP1 participates in PD trafficking (Thomas *et al.*, 2008), suggesting that PD could contribute to cell-to-cell communication in graft union formation. The first model of PD described a membraned-line pore, traversed by a central cylindrical element (López-Sáez *et al.,* 1966; Robards, 1971) (Fig. 2). Later, studies on the formation of cell plates during cytokinesis showed that these channels are formed between two daughter cells. Endoplasmic reticulum (ER) strands are being trapped in the newly developing cell wall and form the central part of the PD called the desmotubule (Ding *et al.,* 1992; Hepler, 1982; Tilney *et al.,* 1991). The desmotubule is a highly compressed ER presumably associated with RETICULON-LIKE B proteins (RTNLB 3 and 6), a protein family that is associated with ER tubuling. Reticulon could be responsible of the tight compression of ER into the desmotubule (K. Knox *et al.,* 2015). The outer limit of PD is a specialized plasma membrane (PM) domain called PD-PM (Grison *et al.,* 2015), which is enriched in sterols while starved of glycerolipids. This specific composition permits the regulation of PD permeability by notably recruiting glycosyphosphatidylinositol (GPI) anchored proteins at the entrance of PD. Different morphotypes of PD were recently described and could be associated with differential permeability. The PD of type II, mostly found in mature tissues, align with the conventional model proposed by Ding (Ding *et al.,* 1992). It shows a space between the desmotubule and the PD-PM that forms the cytoplasmic sleeve and in which cytosolic molecules can traffic from cell-to-cell. The PD of type I,

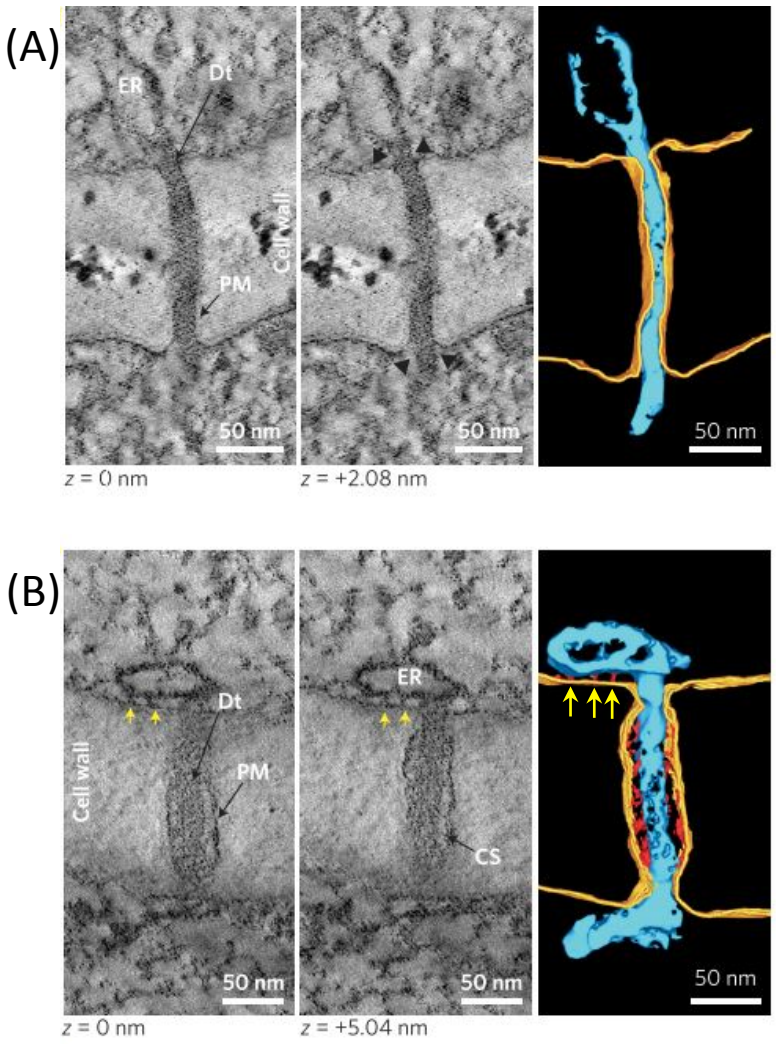

Figure 2. Different morphotypes of PD at *the Arabidopsis thaliana* root tip

(A) Two electron tomogram Z-plans and the 3D segmentation of plasmodesmata of type I showing a dense desmotubule (blue) and no cytoplasmic sleeve, **(B)** two electron tomogram Z-plans and the 3D segmentation of plasmodesmata of type II showing a cytoplasmic sleeve between desmotubule (blue) and the plasma membrane (yellow) of plasmodesmata. The space is populated by dense spoke-like elements (red). Yellow arrows indicate membrane contact site (MCS) between the endoplasmic reticulum and the plasma membrane.

Dt, desmotubule; ER, endoplasmic reticulum; PM, plasma membrane; CS, cytoplamic sleeve

(adapted from Nicolas et *al.*, 2017)

which are described to occur in post-cytokinesis cell walls, show a very tight contact between the ER and the PD-PM with no visible remaining space (Fig. 2A). Surprisingly the lack of visible cytoplasmic sleeve is associated with a cell-to-cell movement of cytosolic green fluorescent protein (GFP). Interestingly, one study address the potential role of the desmotubule, which is still unclear, but could play a role in a trafficking pathway from cell-to-cell for lipids and membranous proteins (Cantrill *et al.,* 1999). In PD of type II, the cytoplasmic sleeve is punctuated by straight electron dense structures called spoke-like elements (Fig. 2B). Their natures and functions remain largely unknown (Ding *et al.,* 1992; Nicolas *et al.,* 2017; Tilney *et al.,* 1991). It is hypothesized that they could be seen as a particular type of Membrane Contact Site (MCS) maintaining the two membranes relatively close, to control maybe the width of the cytoplasmic sleeve. In addition, these MCS elements could be a way for molecules transfer from one membrane to the other one (Brault *et al.,* 2018; Tilsner *et al.,* 2016; Overall & Blackman, 1996; Radford & White, 2011).

Plasmodesmata have long been considered as simple holes connecting neighboring cells through the cell wall, but studies demonstrated the importance of the regulation of PD permeability, which needs to be adjusted permanently throughout the development of the plant, *e.g.* for the emergence of new organs (Benitez-Alfonso *et al.,* 2013). The Size Exclusion Limit (SEL), reflecting the aperture of PD can vary from an “open” to a “closed” state. The study of Pina *et al.,* (2009) investigate on the potential role of PD permeability in the different graft compatibility state on tree grafted cells. Their hypothesis is that a late compatibility could be predetermined at the initial step by the contact between the grafted partners. In this study, the compatible/incompatible grafting effect of on the global PD permeability is measured between cells not positioned at the graft interface. They show that a global decreased of cell-to-cell permeability is induced in an incompatible grafting context. This result suggests that the problem of incompatibility in grafted *Prunus* trees, and thus potentially of other species, may be related to low intercellular transport capacity. Functional PD may be a key parameter for grafting success. The most known factor to regulate cell-to-cell trafficking is the modification of SEL through the homeostasis of callose, that could be deposited at neck regions of PD, which results in pushing the PM against the desmotubule and therefore occluding PD. On the contrary, callose can be degraded to open the PD (Guseman *et al.,* 2010; Levy *et al.,* 2007; Storme *et al.,* 2014; Wu *et al.,* 2018). This callose homeostasis is governed by two families of proteins: (1) the β-1,3-glucanases such as the PD located β-1,3-GLUCANASE 1 (PDBG1) and PDBG2 that are responsible for callose degradation (Benitez-Alfonso *et al.,* 2013), (2) callose synthase such as GLUCAN SYNTHASE-LIKE 8 (GSL8) and CalS3, that are responsible for synthesis of callose (Cui *et al.,* 2016; Dettmer *et al.,* 2011; Guseman *et al.,* 2010).

Plasmodesmata are subject to structural modifications and degeneration events , depending on developmental or environmental cues that could lead to intercellular connectivity modifications

(Sager & Lee, 2014). For example, as guard cells become mature and differentiated, the PD that connect them to neighboring pavement cells are lost because they require a complete symplastic isolation to function. Interestingly, a completely opposite phenomenon also occurs, where PD become large channels without desmotubule between the cells in anthers or at the junction of sieve elements (SE) to form pores. Another common feature, which could play a role in regulation of communication, is PD density, *i.e.*, their number per area unit. Indeed, PD could be form *de novo* outside the cytokinesis process. For example, in the shoot apex, the number of PD can be transiently extended during floral development by the formation of secondary PD between non-daughter cells (Ormenese *et al.,* 2000).

As wrote previously, PD are present between almost every plant cells governing key events during the plant life. How a graft union could be efficient in cell-to-cell communication without PD between the scion and the rootstock? Only the works of Kollmann and Glockmann (Kollmann & Glockmann, 1985, 1991; Kollmann *et al.,* 1985) can reliably localize the graft interface ultrastructure and show unequivocally the presence of PD interconnecting the rootstock and scion cells. Kollmann and Glockmann studied the ultrastructure of the graft interface thanks to the use of a heteroplastic graft of *Vicia faba* on *Helianthus annuus* (Fig. 3A). This graft combination is not a highly compatible because grafted plants cannot be maintained in life during long time. These two plants have species-specific cell markers that can be identified under the electron microscope. *V. faba* cells are characterized by a large nucleus with lots of heterochromatin, while the nucleus of *H. annuus* is smaller and shows less heterochromatin. Moreover, these two distant plants have structural differences in their plastids such as the presence of dilated thylakoids with no starch in *H. annuus* while plastids of *V. faba* usually contain starch and do not have dilated thylakoids (Fig. 3B). The mechanisms leading to the formation of these PD at the graft interface is still unknown. In fact, in contrast to primary PD, which are formed during cytokinesis, the PD formed across the graft interface must have been formed *de novo* in pre-existing walls. As they are formed after the cell wall, they are called secondary PD. The observations revealed that secondary PD were mostly arranged in small groups where the cell wall was thinner than in other regions, as cell wall regions with PD in pitfields (Faulkner *et al.,* 2008). They were able to observe mainly branched PD that can succeed or fail to connect the two adjacent cells at the graft interface. PD that did not span the cell wall were called hemi-PD. The authors proposed that continuous secondary PD could form only if both the scion and rootstock part of the cell wall was thinned. They proposed a mechanism in which regions where ER cisternae and PM have strong interactions could invaginate in the cell wall and form so-called PD precursors. Finally, to establish a continuous PD, these PD precursors need to be established synchronously from both sides of adjacent cell walls and fuse. On the contrary, if PD

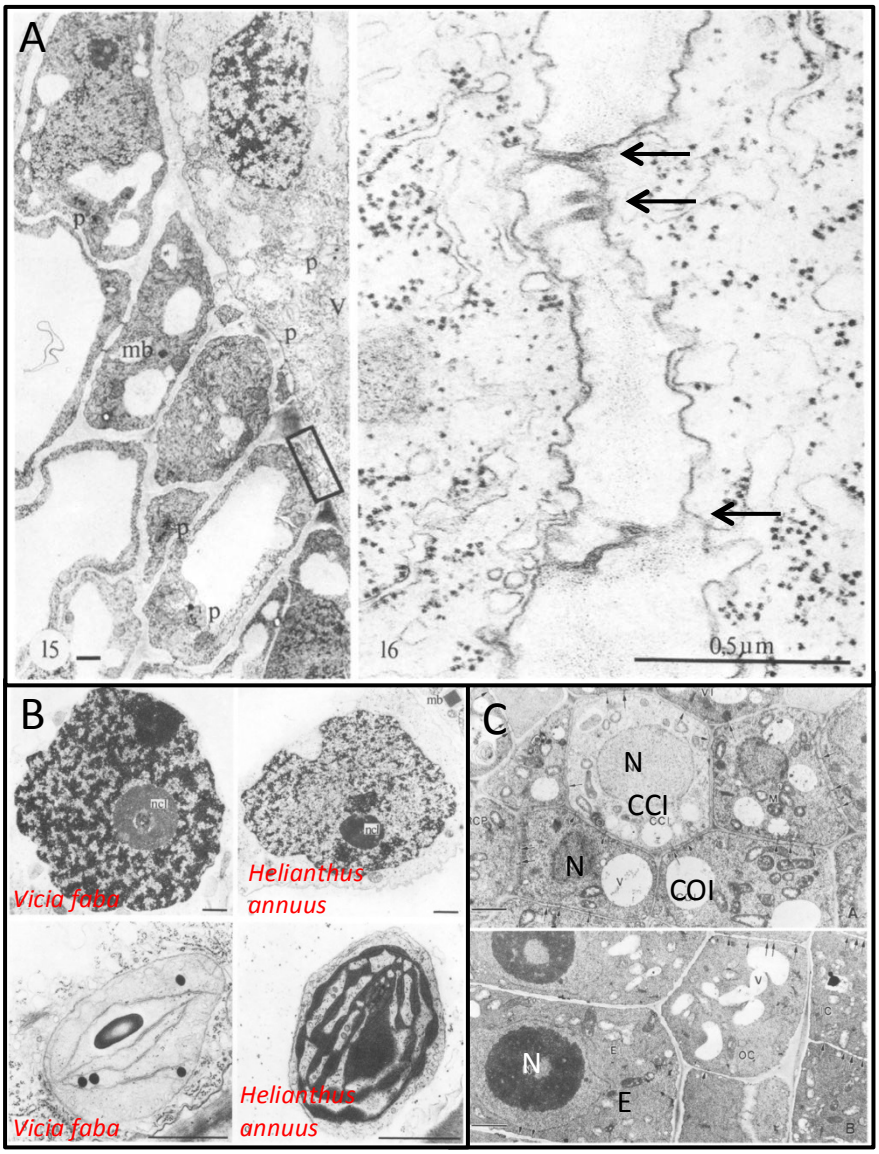

Figure 3. Plasmodesmata found at the graft interface of *Vicia faba/Helianthus annuus* and ultrastructural organite diversitity

(A) In their study, Kollmann and Glockmann (1985) were able to find plasmodesmata (black arrows) at the graft interface of *Vicia faba* and *Helianthus annuus* **(B)** To target the graft interface, they used the difference in ultrastructure of the two partners, allowing them to identify cells at the graft interface. *Vicia faba* cells have a nucleus with dense heterochromatin and chloroplasts with starch and flattened thylakoids, while *H. annuus* have a less dense nucleus and plastids with dilated thylakoids and electron dense content. **(C)** In *Arabidopsis thaliana* roots, ultrastructure of the cells is very heterogeneous and depends on the cell type and developmental stage. The central cortex initials (CCI) do not have a dense cytoplasm and nucleus (N) content, while surrounding columella initials have a dense cytoplasm content, denser nucleus, and epidermal cells (E) have a large nucleus with a dense nucleolus.

(adapted from Kollmann and Glockmann (1985) and Zhu et al., 1998)

precursors are only formed at one side of the cell wall, or in too thick walls, it results in the formation of hemi-PD that do not entirely span the cell wall. This failure could take part in the incompatibility state between both plants. It is proposed that modifications of the cell wall have to be targeted to sites of future PD formation, synchronously at the two sides of the cell wall, in order for the PD to progress and fuse in a thinner wall. These specific regions of cell walls may have a modified composition in order to have a loosed matrix, thus facilitating the progress and fusion of PD precursors.

Up until now, the mechanism of formation of secondary PD, especially in the context of the graft interface remains to be elucidated, but as proposed by Kollmann and Glockmann, modifications of the cell wall composition are likely to play a crucial role.

1.4. Cell wall characteristics around PD

Plasmodesmata are structures formed in the cell wall. Some genes are known to play a role on secondary PD formation, as an example, mutants of INCREASED SIZE EXCLUSION LIMIT 1 and 2 (ISE1 and ISE2) display more secondary PD. INCREASED SIZE EXCLUSION LIMIT 1 is a mitochondrial DEAD-box RNA helicase, while ISE2 is a DEVHRNA helicase therefore, their link to PD biogenesis is not clear. However, they have been identified to be involved in the signaling pathways to regulate the reduction-oxidation reaction (redox) status. Reactive oxygen species (ROS) generated in the apoplast have been proposed to act as cell wall softening molecules, which might physically influence PD ultrastructure and their formation (Ehlers & van Bel, 2010). An augmentation in the concentration of ROS is known to induce PD structural modifications by altering the activity of callose synthase at PD-associated cell walls. Lastly, hydrogen peroxide and class III peroxidases have been found to accumulate at PD regions in the stem cambial zone of tomato accompanying changes in PD structure. Calcofluor staining and immunoanalysis of freeze-fractured tobacco trichome cells revealed that there is an enrichment in pectin polysaccharides and there is a reduction in cellulose content in cell walls around PD (Faulkner *et al.,* 2008). Pectin network is made of polysaccharides, principally homogalacturonan (HG) and rhamnogalacturonan-I (RG-I). The arabinan and galactan compose side chains of RG-I and arabinan-rich domains are associated with cell wall flexibility whereas galactan-rich domains are associated with more rigid cell walls. These different properties suggest PD-specific RG-I polymers may be inserted around PD to maintain a flexible state of the cell wall, compatible with PD changes in permeability or PD biogenesis. Interestingly, low-esterified HG and (1-5)-α-L-arabinan domains are preferentially localized at PD whereas (1-4)-β-galactan is specifically absent. Pectin methyl esterase (PME), the enzyme involved in pectin HG de-esterification in the cell wall and is associated with PD in *Linum usitatissimum* hypocotyls, modifies elastic properties of the cell wall.

Thereby, it is supposed that they could play a role in stabilizing or regulating PD structure and also in the formation of secondary PD which need a remodeling of the cell-wall (Knox *et al.*, 2014).

Along with pectins, cellulose is a major component of the cell wall. Several enzymes, including glycosyl transferases and reversibly glycosylated polypeptides, implicated in the biosynthesis of cell wall polysaccharides have been found in the PD proteome (Vaten *et al.,* 2011). As example, KOBITO1 is a glycosyl transferase-like protein that may play a role in the synthesis of cellulose (Pagant *et al.,* 2002). In some KOBITO1 mutant (kob1-3), stomata differentiation is affected. This alteration could be linked to modifications of cell wall composition permitting an increase of cell-to-cell diffusion of cytosolic GFP and SPEECHLESS transcription factor after biolistic experiments. Then, due to the aberrant SPEECHLESS diffusion, cells underwent differentiation and stomata appeared aggregated together (Kong *et al.,* 2012). However, how enzymes like glycosyl transeferase could act to modify PD permeability by changing cell wall composition is still unknown.

1.5. Plant vascular tissues

While PD are crucial for cell-to-cell communications in plant, long distance signaling is ensured by vascular tissues: phloem and xylem. They are responsible for the transport of water, nutrients, hormones and other molecules such as proteins or mRNA (Thieme *et al.,* 2015) throughout the plant and also provide physical support. Vascular specification in *A. thaliana* occurs during the early globular stage of embryogenesis during which four meristematic cells, procambium, divide and give rise to cells having a cellular identity that will be at the origin of all xylem and phloem cells in the root and the hypocotyl (Rybel et *al.* 2015). At the end of embryogenesis, although they are not fully differentiated, all vascular cells, phloem, xylem and procambial cells, are present.

The phloem is responsible for the shoot to root transport of photoassimilates and signaling molecules. Sieve elements (SEs) are the conductive cells of phloem. Sieve elements usually have thicker cell walls than parenchyma cells. The differentiation process of SE is characterized by the draining of most of the cytoplasm and the progressive loss of several organelles, including rough ER, vacuoles and at the final stage nuclei. The only remaining organelles in mature SE are plastids, mitochondria and smooth ER that occupy a parietal position within the cell. Moreover, these organelles are subjected to a change in morphology by becoming smaller with a more spherical shape. Accumulation of the phloem proteins (P-proteins) in the lumen of SE and sieve plates pores is one of the earliest markers of differentiation of SE followed by hydration of the cytoplasm after the breakdown of the tonoplast. Finally, degeneration of the nucleus occurs during the late stages of differentiation. This enucleation is mediated by two NAC-type transcription factors (NAC45 and NAC86) that are the downstream target of ALTERED PHLOEM DEVELOPMENT (APL) transcription factor. They notably permit the beginning of enucleation possess and the perinuclear recruitment of

mitochondria. Furthermore, NAC45 and NAC86 target a family of nucleases, NAC45/86-DEPENDENT EXONUCLEASE- DOMAIN PROTEIN (NEN1 to NEN4), which is required to finish the enucleation process (Batailler *et al.,* 2012; Froelich *et al.,* 2011; Furuta *et al.,* 2014). Despite the loss of most of its components, SE are still alive and form functional units with their respective companion cell (CC). Companion cells present a denser cytoplasm, large nucleus, high number of dense mitochondria and starch-free plastids (Esau, 1973). Ontogenically, SE and CC are coming from the division of the same cambial cell that engages the differentiation process through the APL pathways. Sieve elements and companion cells remain connected together through PD that are formed during the cambial cell division (Cheadle *et al.,* 1962; Esau & Thorsch, 1985). Companion cells are highly specialized for metabolically support the SE. They are also involved in the phloem loading and unloading of nutrients (Paultre *et al.,* 2016). Lastly, phloem parenchyma cells have the role of support cells. They can be distinguished by a larger vacuole and fewer ribosomes than the young sieve elements. Parenchyma cells have also been described to take part in the phloem loading, in concert with CC as they are connected to them through PD. Parenchyma cells also actively secrete photosynthetic products in the apoplast through sucrose efflux carriers such as the SUGARS WILL EVENTUALLY BE EXPORTED TRANSPORTERS (SWEET) family (Sleighter *et al.,* 2012). To ensure the continuum, SE are aligned together and have perforated end walls, the sieve plate, where there are specialized pores deriving from PD in which the desmotubule was lost.

On the other hand, xylem is notably composed of tracheary elements (TE) and parenchyma cells. In contrast to the phloem, TE translocate fluids in the apoplast. Tracheary elements are lignified dead cells responsible for the transport of water and minerals from root to shoot. Tracheary element differentiation is characterized by the deposition of secondary cell wall, composed of lignin at the lateral sides of the cells. The deposition of secondary cell wall occurs in parallel with an induction of a programmed cell death at the late stages of differentiation. During the programmed cell death, the vacuole collapses, the nucleus is digested and all the cell content is removed (Groover *et al.,* 1997). Vacuole collapse may play a role in the digestion of the nucleus and cell components, by releasing its contents into the cytosol, such as DNAses, RNAses and proteases (Funk *et al.,* 2002; Ito & Fukuda, 2002; Lehmann *et al.,* 2001). The principal regulators of xylem cell fate are the NAC transcription factors VASCULAR-RELATED NAC-DOMAIN 6 (VND6) and VND7. They positively regulate genes that are involved in programmed cell death and secondary cell wall deposition (Kubo *et al.,* 2005; Ohashi-Ito *et al.,* 2010). One the other hand, differentiation of xylem is repressed by two peptides from the Clavata3-like/ESR (CLE) family; CLE41 and CLE44 (Ito *et al.,* 2006). At the end of the differentiation, the cell walls between TE are perforated leading to the formation of continuous tubes. Xylem parenchyma cells do not have a well-defined secondary cell walls. They are known to help in the

lignification of secondary cell walls of the neighboring TE by exporting monolignols to the cell wall after TE death (Smith *et al.,* 2013).

1.6. Developmental framework of the graft union formation

Wounding partially interrupt cell exchanges. However, for grafting, all cell communications are interrupted completely by cutting at the grafting point. Thus, the formation of new vascular tissues and exchange pathways must be urgently established. In various species (e.g. grapevine (Cookson *et al.,* 2014), prickly pear cactus (Estrada-Luna *et al.,* 2002), *A. thaliana* flowering stem grafting (Flaishman *et al.,* 2008) and tomatoes (Fernández-García *et al.,* 2004)), grafting was described to begin by the formation of a necrotic layer between the two grafted partners. However, formation of this necrotic layer has not been systematically observed in all graft systems, for example in passion fruit (Ribeiro *et al.,*2015) or surprisingly in another *A. thaliana* hypocotyl grafting study (Yin *et al.,* 2012). This necrotic layer is likely to be formed of collapsed cell debris produced by the wounding and forms a barrier, preventing the establishment of a direct contact between the two partners. The proliferation of cells produces a callus that restores the contact by filling the gaps of lost tissues (Estrada-Luna *et al.,* 2002). Once cells are in contact, they can begin to form common cell walls and eventually form PD across these newly formed cell walls. Finally, callus cells differentiate and form vascular tissues: phloem and xylem, to reestablish the vascular continuum (Jeffree & Yeoman, 1982; Lindsay *et al.,* 1974; Moore & Walker, 1981) (Fig. 4). Recent progress has been made in understanding of graft union formation by using the *A. thaliana* hypocotyl grafting model. In this model, developmental framework (Melnyk *et al.,* 2015) and transcriptomic events (Melnyk *et al.,* 2018) have been well-documented. Melnyk *et al.* described in 2015 that the establishment of a vascular continuum begins by phloem reconnection at 3 day after grafting (DAG) and then, is followed by xylem reconnection from 5 to 7 DAG. New vascular tissue formation is initiated above, and then below, the graft interface indicating that the scion could be the leader of this cellular differentiation processes. At the graft interface, new differentiated vascular cells expand and divide to bypass the wounded regions and permit the vascular reconnection between both partners (Melnyk *et al.,* 2015). One of the early plant responses is the detection of wounding and the activation wounding responses. In his study, Melnyk focused notably on the role of the phytohormone auxin. Auxin is known to be involved during the vascular tissue differentiation (Sieburth, 1999). The role of many phytohormones remains unknown (*i.e.* abscisic acid and salicylic acid) or seems to have little effect (*e.g.* ethylene, jasmonic acid, strigolactones, brassinosteroids and cytokinins) on hypocotyl graft formation. Auxin appears to be a major regulator of vascular cell differentiation and patterning at the graft interface. When grafting *A. thaliana* hypocotyls, the disruption of vascular tissues induces an asymmetry between the scion and the rootstock. For

example, substances generally transported basipetally such as photosynthetic products and auxin, accumulate above the grafting point. Auxin accumulation above the cut site activates the ARABIDOPSIS NAC DOMAIN CONTAINING PROTEIN 71 (ANAC071) expression, whereas auxin depletion below the cut site activates RAP2.6L (Satoh *et al.,* 2011). ANAC071 and RAP2.6L are two transcription factors, they promote pith cell division and their expression is important for successful tissue reunion of incised stems (Satoh *et al.,* 2011). The accumulation of auxin above the graft junction allows a depolarization following by new polarization of its transporter, PIN-FORMED 1 (PIN1), in cells above the graft junction. This new polarization leads to the channeling that facilitates the cell alignment of future vascular cells (Mazur *et al.,* 2016). Interestingly, Melnyk et *al*. (2015) demonstrated that *A. thaliana* mutants deficient for auxin biosynthesis/transport can reconnect their phloem with a similar dynamics as wild-type plants. However, some mutants affected in auxin perception or auxin response have a delayed phloem reconnection during hypocotyl grafting. This suggests that auxin signaling in the graft is mostly sensing relative level of auxin rather that the exact concentration. They propose that ABERRANT LATERAL ROOT FORMATION 4 (ALF4) functions as a sensor in the rootstock for auxin coming from the scion, and promotes vascular formation from the rootstock to the scion.

Along with auxin, cytokinins could also play a role in graft union formation, notably for the vascular reconnection. Grafting promotes the cytokinin responses above and below the graft junction in pericycle cells and vascular cambium. However, grafting mutants of cytokinins biosynthesis or cytokinin responses did not affect significantly phloem connection at the graft interface. Moreover, for vascular differentiation, their effects often occur through the interaction with the auxin signaling pathway (reviewed in Kieber & Schaller, 2014; Osugi & Sakakibara, 2015; Schaller *et al.,* 2015).

Lastly, in grafted *A. thaliana* hypocotyls, gibberellins seem important to control the cell expansion in the cortex to seal the wound. Indeed, when gibberellin biosynthesis or signaling is inhibited, it suppressed the expansion of cortex cells, but did not inhibit cell proliferation in the vascular tissue (Matsuoka *et al.,* 2016). The importance of gibberellins in the expansion of cortex cells has also been demonstrated for tissue reunion during wounding in cucumber and tomatoes hypocotyls (Asahina *et al.,* 2002).

However, even though these studies are very important to understand the graft development, by helping to understand key processes, in terms of hormones, cell division and patterning, these studies on hypocotyls may not be applicable to other models such as ligneous plants. As an example, while ethylene did not show a crucial role for the development of *A. thaliana* hypocotyl grafts, this is different in wounding of mature inflorescence stems, where ethylene response is required for healing and pith division after cutting (Satoh *et al.,* 2011).

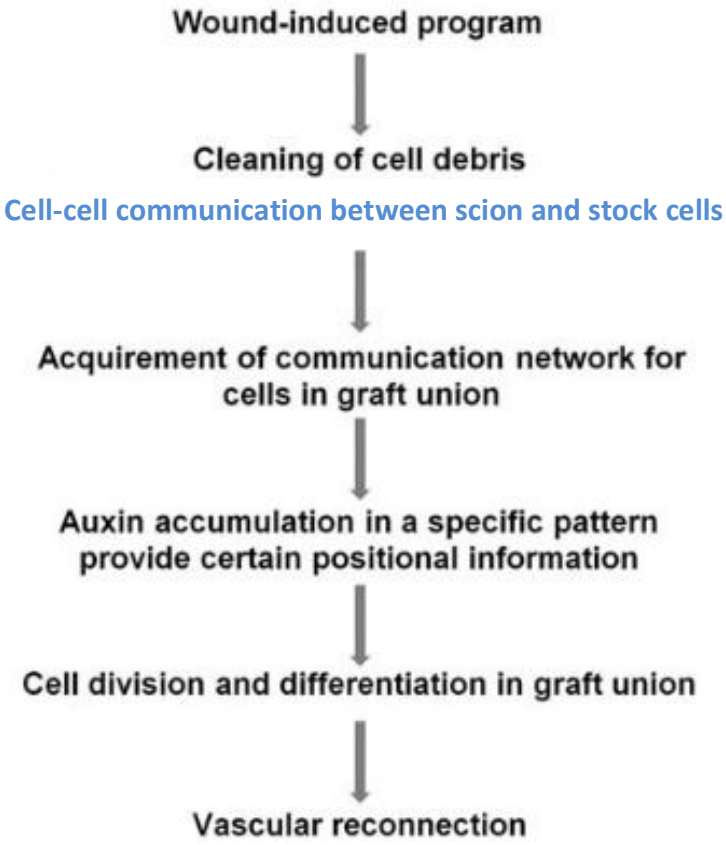

Figure 4. Model for graft-union developmental stages
(extracted from Yin et al., 2012)

1.7. Organelle and genetic exchanges at the graft interface

In 1976, Pandey proposed that when tissues are cut for grafting, some cells might have parts of their wall removed and this could result in fusion of rootstock and scion cells at the graft union.

Recently, horizontal gene transfer has been documented at the graft interface (Fuentes *et al.,* 2014; Lu *et al.,* 2017; Sidorov *et al.,* 2018; Stegemann & Bock, 2009). These exchanges of genetic material could occur between callus cells harvested at the graft interface. The induction of these genetic transferts was realized by grafting lines of tobacco plants that either express a resistance transgene encoded by nuclear DNA or another resistant transgene encoded by plastid DNA. The selection of the transfert events was realized afterwards thanks a selective medium. *In vitro* regeneration process from these grafted selected cells could permit to obtain plants which exhibited a combination of characters of both rootstock and scion. Moreover, they showed that these genetic exchanges of plastid DNA can occur in both directions, but are limited only to the grafting site. Later, Fuentes *et al.,* (2014) demonstrated with similar experiments that entire nuclear genomes could be transferred across the graft junction to generate allopolyploid plants.

Nowadays, this transfer of genetic material is used as a biotechnological tool. The work of Lu et *al*., (2017) showed that this approach could be a new method to perform transplastomic into non transformable species. Most recently, a new approach based on mixing and wounding of callus cells was used to transfer nuclear or plastid DNA between plant cells (Sidorov *et al.,* 2018).

However, these exchanges have only been demonstrated with *in vitro* callus system. The frequency of these events *in planta* and their possible biological relevance during grafting stay to be addressed.

2. **Introductory review: "Merging Genotypes: graft union formation and scion/rootstock interaction". *Expert View, Journal of Experimental Botany***

Journal of Experimental Botany, Vol. 70, No. 3 pp. 747–755, 2019
doi:10.1093/jxb/ery422 Advance Access publication 27 November 2018

EXPERT VIEW

Merging genotypes: graft union formation and scion–rootstock interactions

Antoine T. Gautier[1,†], Clément Chambaud[1,†], Lysiane Brocard[2], Nathalie Ollat[1], Gregory A. Gambetta[1], Serge Delrot[1] and Sarah J. Cookson[1,*]

[1] EGFV, Bordeaux Sciences Agro, INRA, Université de Bordeaux, ISVV, 210 Chemin de Leysotte, Villenave d'Ornon, France
[2] Université de Bordeaux, CNRS, INSERM, UMS 3420, INRA, Bordeaux Imaging Center, Plant Imaging Plateform, Villenave d'Ornon, France

* Correspondence: sarah.cookson@inra.fr
† These authors contributed equally to this work.

Received 10 August 2018; Editorial decision 19 November 2018; Accepted 20 November 2018

Editor: Christine Raines, University of Essex, UK

Abstract

Grafting has been utilised for at least the past 7000 years. Historically, grafting has been developed by growers without particular interest beyond the agronomical and ornamental effects, and thus knowledge about grafting has remained largely empirical. Much of the commercial production of fruit, and increasingly vegetables, relies upon grafting with rootstocks to provide resistance to soil-borne pathogens and abiotic stresses as well as to influence scion growth and performance. Although there is considerable agronomic knowledge about the use and selection of rootstocks for many species, we know little of the molecular mechanisms underlying rootstock adaptation to different soil environments and rootstock-conferred modifications of scion phenotypes. Furthermore, the processes involved in the formation of the graft union and graft compatibility are poorly understood despite over a hundred years of scientific study. In this paper, we provide an overview of what is known about grafting and the mechanisms underlying rootstock–scion interactions. We highlight recent studies that have advanced our understanding of graft union formation and outline subjects that require further development.

Keywords: Graft compatibility, grafting, phloem, plasmodesmata, rootstock, scion, xylem.

Introduction

Grafting is one of the most ancient horticultural techniques, originating prior to 7000 BC in China (Mudge *et al.*, 2009), and even today most commercial perennial fruit production is still dependent upon grafting with rootstocks. More recently, vegetable grafting has been increasing, especially in cucurbits and solanaceous crops (Bie *et al.*, 2017). The use of grafted plants provides flexibility, allowing growers to combine different scion and rootstock traits independently. During grafting, tissues cut from different genotypes are brought into contact so that the plants join together to form one composite organism. During this process two individuals are forced to interact, and their survival depends on the efficiency of this interaction. Integrating the tissues of two individuals implies that adult, differentiated tissues engage in a process during which they de-differentiate and form new conducting structures (as reviewed by Pina *et al.*, 2017). The underlying mechanisms must be significantly different for the xylem vessels (dead cells) and the sieve elements of the phloem (living cells). The mechanisms responsible for the integration remain poorly understood (as reviewed by Melnyk, 2017*a*, 2017*b*; Pina *et al.*, 2017) and the

ability to be grafted is not ubiquitous across taxa; dicotyledonous plants graft together easily, whereas grafting is not possible in monocots as they lack a vascular cambium.

Natural variation in the adaptation of different species or accessions to specific biotic and/or abiotic soil conditions has been exploited to generate many rootstocks (as reviewed by Warschefsky *et al.*, 2016; Colla *et al.* 2017). One of the most famous examples comes from the world of wine. Nearly all wine grapes are different varieties of the same European *Vitis* species, *V. vinifera*. At the end of the 19th century a soil-dwelling insect pest, *Phylloxera*, was accidentally introduced to Europe from North America, devastating European vineyards. Researchers at the time quickly realised that the roots of American *Vitis* species provided a natural tolerance and began grafting *V. vinifera* onto American *Vitis* species and hybrid derivates (Ollat *et al.*, 2016). Today, despite the continuing importance of *Phylloxera*-resistant rootstocks to viticulture, we know little of the molecular basis of this trait.

Phenotype modifications via scion–rootstock interactions

How do rootstocks modify scion phenotypes?

Rootstocks confer differences in salinity tolerance, drought tolerance, water-use efficiency, scion vigour, scion architecture, mineral element composition and use efficiency, phenology, and fruit quality and yield in a wide range of species (Warschefsky *et al.*, 2016; Colla *et al.*, 2017; Kumar *et al.*, 2017). Traditionally, rootstock-conferred differences in scion phenotypes have been determined empirically with little or no attention paid to the underlying mechanisms. However, it is clear that there is a genetic control of rootstock-conferred modifications of scion phenotypes, since the parentage of a given rootstock is frequently observed to indicate its behaviour in the field (Cordeau, 1998; Pico *et al.*, 2017) and quantitative trait loci (QTLs) for a variety of rootstock-conferred traits have been identified (Rusholme Pilcher *et al.*, 2008; Estañ *et al.*, 2009; Asins *et al.*, 2010, 2015, 2017; Marguerit *et al.*, 2012; Bert *et al.*, 2013; Fazio *et al.*, 2014; Raga *et al.*, 2014; Foster *et al.*, 2015; Knäbel *et al.*, 2015; Tandonnet *et al.*, 2018).

One important example of the use of rootstocks to confer traits to the scion is the use of dwarfing rootstocks of the Malling series in commercial apple orchards (Hatton, 1917). Dwarfing has been extensively studied with these rootstocks and three QTLs have been identified in populations containing the M9 dwarfing rootstock (Rusholme Pilcher *et al.*, 2008; Fazio *et al.*, 2014; Foster *et al.*, 2015; Harrison *et al.*, 2016*b*;). Recently, the apple WRKY transcription factor family has been targeted as candidate genes of dwarfing control in the M26 rootstock and MdWRKY9 has been identified as a potential candidate based on its differential expression between different dwarfing and non-dwarfing rootstocks (Zheng *et al.*, 2018). The over-expression of *MdWRKY9* represses *MdDWF4*, which controls the rate-limiting step in brassinosteroid synthesis, thereby reducing brassinosteroid production and triggering dwarfing (Zheng *et al.*, 2018). However, the ability of these transgenic rootstocks to confer dwarfing to a wild-type scion (given that brassinosteroids are not considered as long-distance signalling molecules; Symons *et al.*, 2008) and whether MdWRKY9 is the underlying cause of one of the QTLs of M9-conferred dwarfing in apple are still unknown.

Rootstocks could influence scion phenotypes via a variety of mechanisms, as follows.

(1) Rootstocks could differ in their functioning, i.e. their ability to capture soil resources (via differences in root system architecture, functioning, and interactions with the rhizosphere) and transport them to the scion. For example, both grapevine and citrus rootstocks have different root architectures (Sorgona *et al.*, 2007; Dumont *et al.*, 2016) and different capacities to take up phosphate and remobilise phosphorus reserves (Zambrosi *et al.*, 2012; Gautier *et al.*, 2018). Similarly, greater root length is associated with greater stomatal conductance and transpiration in grafted grapevine under low and moderate water deficit (Peccoux *et al.*, 2018). Furthermore, grapevine rootstocks differ in their pH exudation response to iron deficiency (Ollat *et al.*, 2003) and alter the microbiome of the soil (Marasco *et al.*, 2018).

(2) The graft interface itself could alter scion development directly; however, although frequently suggested in the literature, this seems unlikely in compatible grafts once the connections across the interface have been well established. In general, once established, the graft union offers little resistance to water movement (Clearwater *et al.*, 2004; Nardini *et al.*, 2006; Adams *et al.*, 2018) and there has been no clear evidence of the interface sequestering molecules despite there being numerous suggestions of this in the literature (Webster, 2004; Gregory *et al.*, 2013).

(3) Rootstocks could differ in their regulation of shoot–root signalling in terms of both the concentration and fluxes of signalling molecules. A number of reviews have been devoted to the potential roles of long-distance signalling molecules in regulating scion–rootstock interactions (Goldschmidt, 2014; Albacete *et al.*, 2015; Venema *et al.*, 2017). Grafting rootstocks that have been genetically modified to alter long-distance signal molecules (such as hormones) can affect scion phenotypes. For example, the overexpression of isopentenyltransferase (IPT), a key enzyme of cytokinins biosynthesis, in tomato rootstocks increases the cytokinin content of the scion and its resistance to salinity stress (Ghanem *et al.*, 2011). Similarly, a recent study has shown that methylation of the promoter of IPT5B is greater in roots of the dwarfing apple rootstock M9 compared to a high-vigour rootstock, and that this is correlated with reductions in IPT5B expression in the root and cytokinin content in the shoot (Feng *et al.*, 2017). There are also numerous examples of specific signals being associated with rootstock-conferred traits. For example, grapevine rootstocks can confer differences in shoot behaviour (e.g. shoot branching) that are consistent with differences in the biosynthesis of mobile signalling molecules (e.g. strigolactones) (Cochetel *et al.*, 2018). In tomato grafts, growth and plant responses to the abiotic environment have been associated with modifications of the concentration of certain hormones, for example under low potassium supply, shoot biomass is negatively correlated with the concentration of the ethylene precursor aminocyclopropane-1-carboxylic acid (Martínez-Andújar *et al.*, 2016). Similarly, in some cases, apple rootstocks have been shown to alter the concentration of gibberellins in the scion (Tworkoski and Fazio, 2016), and the over-expression of an artificially generated apple *Mhgai1*,

a GA-insensitive allele, in tomato rootstocks confers dwarfing to the wild-type tomato scion (Wang *et al.*, 2012); this suggests that gibberellin signalling could be a potential mechanism of dwarfing by apple rootstocks. As genetic resources are limited for most commercial crops, unequivocal experimental proof of the molecular mechanisms underlying genotypic variation in rootstock-conferred traits is difficult to obtain.

(4) In perennials crops, rootstocks and scions could differ in their perception of seasonal environmental signals related to dormancy; seasonal changes in climate have to be coordinated between two different species potentially adapted to different temperature regimes. There have been reports of rootstocks altering bud-break, leaf senescence, and the cessation of growth at the end of the growing season (Wang *et al.*, 1994; Dong *et al.*, 2008; Prassinos *et al.*, 2009; Loureiro *et al.*, 2016;), but the mechanisms remain unknown. In kiwifruit, rootstocks differ in the development of root pressure in the spring and this is associated with the vigour conferred to the scion, with high-vigour rootstocks more rapidly increasing root pressure (Clearwater *et al.*, 2007). Similarly, if grafted plants consist of two individuals with different biological clocks and rhythms, it is possible that rootstocks can influence the circadian rhythms of the scion, and vice versa.

How do scions modify rootstock phenotypes?

Rootstocks are known to alter a wide range of scion phenotypes, but little attention has been paid to scion effects on rootstock phenotypes despite the fact that such effects have long been recognised (Amos *et al.*, 1930). The characterisation of scion effects on rootstock development has been largely limited to effects on root biomass or total root length (Amos *et al.*, 1930; Tandonnet *et al.*, 2010; Harrison *et al.*, 2016*a*). There are numerous examples of shoot-borne signals regulating root development in model species (Ko and Helariutta, 2017), for example metabolites, hormones, peptides, HY5 (which regulates whole-plant carbon and nitrogen status; Chen *et al.*, 2016), microRNA 156 (which regulates tuber formation in potato; Bhogale *et al.*, 2014), and microRNA 399 (which regulates phosphate uptake and translocation under phosphorus starvation conditions; Lin *et al.*, 2014). Studying how scions alter rootstock phenotypes is of particular importance for root crops, and future work in this area is a priority.

Future research directions

Our knowledge of the signals associated with rootstock modifications of scion phenotypes is growing rapidly and many QTLs regulating conferred traits have been identified. However, experiments designed to understand the genetic architecture of rootstock-conferred traits have generally been restricted to the study of only one scion variety and have rarely included self-grafted controls. One exception is the study by Bert *et al.* (2013) on grapevine, in which tolerance to lime-induced iron deficiency in grafted rootstocks (with a unique scion) and un-grafted cuttings was compared. The authors found that the genetic architecture of rootstock versus whole-plant responses to iron deficiency were different; thus, future research directions should address the roles of both the shoot and the root in regulating traits of interest and plant responses to the environment.

The idea that the graft interface could sequester or physically alter the movement of signals between the scion and the rootstock originates from experiments on apple grafts without homo-grafted controls (Jones, 1974, 1976; Else *et al.*, 2018), but further experiments are required to confirm this hypothesis.

Numerous small RNAs are found in the phloem sap (Buhtz *et al.*, 2008) and are graft-transmissible (as reviewed by Tamiru *et al.*, 2018), suggesting that they could modify scion–rootstock signalling. As interspecific grafting can modify DNA methylation patterns in the grafted partner (Wu *et al.*, 2013), it is possible that epigenetic modifications underlie many rootstock-conferred traits in crop species and this topic will be of interest in the future.

Graft incompatibility and graft union formation

What are the causes of graft incompatibility?

The commercial use of grafting depends upon the degree of graft compatibility, i.e. the ability of the assembled scion–rootstock to form and sustain a successful graft union. It is generally considered that graft incompatibility increases with the taxonomic distance, but predicting compatibility is not always easy. Most intraspecific grafts and interspecific grafts (from within the same genus) are compatible; however interspecific graft incompatibility has been widely reported in fruit trees such as *Prunus* species (Pina *et al.*, 2017). Intrafamilial grafts are rarely compatible, except within the Solanaceae and Cucurbitaceae in which compatibility between different genera is exploited in commercial grafting. Similarly, in Rosaceae certain cultivars of pear (*Pyrus communis*) are compatible with rootstocks of quince (*Cydonia oblonga*). Interfamilial grafts are almost always incompatible; however, some may survive in the short-term (weeks) such as Arabidopsis–tomato grafts (Flaishman *et al.*, 2008). This short-term survival of interfamilial grafts can be used to graft-inoculate pathogens for scientific study (Vigne *et al.*, 2005; Aryan *et al.*, 2016). Graft incompatibility can express itself over various time-frames, from poor success soon after grafting to the dieback of grafted plants several years after planting in the field. This delayed dieback may simply be the appearance of incompatibility symptoms that have been progressing, unobserved, since shortly after the grafting was performed. Despite its importance in horticulture, little is known about the mechanisms that cause graft compatibility/incompatibility except for the special case of certain pear–quince grafts (Gur *et al.*, 1968). Certain quince rootstocks contain prunasin, a cyanogenic glycoside, which can move into the pear scion where hydrolysis by β-glicosidases releases toxic cyanide that causes tissue necrosis and graft incompatibility.

There have been a small number of studies of the transcripts or proteins accumulated at the graft interface during graft union formation that have been aimed at trying to understand the molecular basis of graft incompatibility and differences between hetero- and homo-grafting (Prassinos *et al.*, 2009; Cookson *et al.*, 2014; Wang *et al.*, 2016; Chen *et al.*, 2017; Ren *et al.*, 2018).

Generally, these studies have lacked appropriate controls (such as homo-grafts and cut, but un-grafted scions and rootstocks) and/or sufficient sampling to accurately identify the transcripts or proteins involved. This analysis is particularly complicated in perennial crops; grafting typically occurs when the wood is dormant during the winter months as such the graft union develops at the same time as the spring reactivation of the cambium (Cookson *et al.*, 2013). The activation of the cambium may be different between the different genotypes studied, thus requiring that changes in transcription expression are studied over time so that the profiles associated with differences in the reactivation of the cambium can be separated from those associated with the incompatibility responses. Furthermore, no attempts have been made so far to assign the transcripts harvested from the mixture of cells at the graft interface to either of the grafting partners, although this is theoretically possible if there is sufficient variation between the scion and rootstock genotype and long reads are used. A similar technique has been used to determine the parental origin of transcripts identified in RNA sequencing data from allopolyploid species (Peralta *et al.*, 2013).

How does the graft union form?

The process of graft union formation begins with formation of a necrotic layer, followed by adhesion of the two grafted partners, callus cell formation, and the establishment of a functional vascular system; this has been extensively studied in hypocotyl grafts of Arabidopsis (Box 1). The role of different hormones

Box 1. Key developments in understanding graft union formation

- **Auxin response genes are essential for phloem connection in Arabidopsis hypocotyl grafting, but less so for xylem connection**
  Melnyk *et al.* (2015) showed that in Arabidopsis hypocotyl grafts, auxin accumulated above the graft interface just after cutting and is key to forming vascular connections between the scion and rootstock. By grafting scions labelled with green fluorescent protein onto rootstocks defective in auxin signalling, they demonstrated that movement of the fluorescent protein from the scion to the rootstock was delayed up to 2-fold. However, transport assays from rootstock to scion showed that the xylem connection was not significantly impaired.
- **Genes are asymmetrically expressed between the scion and the rootstock around the graft interface of Arabidopsis hypocotyl grafts**
  Melnyk *et al.* (2018) characterised the genome-wide changes in gene expression induced during hypocotyl grafting in Arabidopsis (at 0–240 h after grafting). The authors observed that the gene expression response was very different between the scion and rootstock, and that many of the differences were driven by accumulation of carbon in the scion and limitation of carbon in the rootstock (until the phloem reconnected). Interestingly, many genes associated with vascular formation were up-regulated in grafted tissues in comparison to the cut and separated tissues before the formation of functional vascular connections, indicating that a recognition mechanism was activated.
- **Grafted partners can exchange nuclear and plastid genetic material in tobacco grafts**
  By grafting two transgenic tobacco lines, one carrying a kanamycin-resistance gene and the yellow fluorescent protein gene in its nuclear genome, and the other one carrying a spectinomycin-resistance gene and the green fluorescent protein gene in its chloroplast genome, Stegemann and Bock (2009) were able to select double-resistant cells from callus cells at the graft interface on selective media. Double-resistant lines could not be obtained from tissues far from the graft interface, suggesting that these genome transfer events were restricted to the graft interface itself. In a second paper (Fuentes *et al.* 2014), the same group showed in a similar fashion that not only chloroplast genomes were exchanged between the scion and rootstock at the graft interface, but nuclear genomes were also exchanged and that allopolyploid cells could be selected for in the callus tissues.
- **Mitochondria are able to move from cell to cell through the graft junction in tobacco grafts**
  To demonstrate the transfer of mitochondria at the graft interface, Gurdon *et al.* (2016) grafted two tobacco species, *Nicotiana tabacum*, which has male-sterile flowers due to cytoplasmic male sterility carried by mitochondria, and *N. sylvestris*, which has fertile flowers. As in the Stegemann and Bock (2009) and Fuentes *et al.* (2014) studies, thanks to resistant genes carried in the nucleus and the chloroplast, they selected and regenerated hybrid lines from the callus cells at the graft interface. The regenerated plants were chimeric, showing three types of flowers: sterile, fertile, and an intermediate phenotype, suggesting that a mitochondrial transfer also occurs at the graft interface.

in graft union formation and wound healing has been recently reviewed by Nanda and Melnyk (2018). Although auxins have been used to improve grafting success in viticulture since 1934 (according to Fallot, 1970), their precise role in phloem reconnection during graft union formation has only recently been identified (Melnyk *et al.*, 2015). In perennial crops, grafting is traditionally performed on over-wintering woody tissues in the spring, whereas commercial vegetable grafting is generally done on hypocotyls or stems of actively growing plants soon after germination (Box 2), suggesting that the signalling processes involved may be different.

The development of the graft interface has been of scientific interest for nearly a hundred years, with the first classical microscopy studies being published in the 1920s (Bailey, 1923). More recently, 3D imaging techniques have improved our understanding of the graft union in perennial crops, but with limited resolution (Bahar *et al.*, 2010; Milien *et al.*, 2012). Significant progress has been made in understanding the early stages of vascular reconnection in hypocotyl grafts of Arabidopsis. Melnyk *et al.* (2015) showed that the scion and rootstock adhere 1–2 d after grafting, and the use of fluorescent dyes and proteins demonstrated that the phloem reconnects 3–4 d after grafting (which coincides the resumption of root growth). The xylem reconnects 6–7 d after grafting (Box 1). This study was restricted to the first week after grafting, so we still have no knowledge of the organisation of the limited secondary growth of grafted hypocotyls and how the newly formed xylem and phloem develop. In a subsequent paper, Melnyk *et al.* (2018) described in detail the genes differentially expressed during the time-course of graft union formation and highlighted the up-regulation of many genes associated with vascular regeneration (Box 1).

There are many difficulties associated with studying cellular development at the graft interface of woody perennial species: the tissues are large, very hard, and the identification of the exact location of the graft interface is impossible if the scion and rootstock have morphologically indistinct callus cells. Furthermore, using assays similar to those described by Melnyk *et al.* (2015) to quantify the function of xylem and phloem across the interface of woody grafts of perennial crops is technically challenging because plants are grafted before bud break, so there are no leaves to drive transpiration and movement of labelled molecules.

In addition to the connection of vascular tissues across the graft interface, cell-to-cell contacts via plasmodesmata are presumably also important to the function of grafted plants. Plasmodesmata are small membrane channels of about 30 nm in diameter that pass through the plant cell wall, and provide membrane and cytosolic continuity between most cells of the plant. They are composed of a central element originating from the endoplasmic reticulum, the desmotubule. The unequivocal presence of plasmodesmata at the scion–rootstock interface has only been demonstrated in one study, in which the scion and rootstock could be identified using electron microscopy thanks to histological differences between the two genotypes (Kollmann and Glockmann, 1985). Many questions remain concerning the formation of plasmodesmata at the graft interface: (1) are they essential for grafting success and/or long-term plant survival? (2) How do they form across the pre-existing cell walls of the scion and rootstock? (3) Where does the endoplasmic reticulum of the desmotubule originate, from the scion, from the rootstock, or from both grafted partners? Different models of plasmodesmata formation across the graft union are outlined in Box 3. In the first, (A), the

Box 2. Comparison of grafting in herbaceous versus woody plants

Herbaceous grafting	Woody grafting
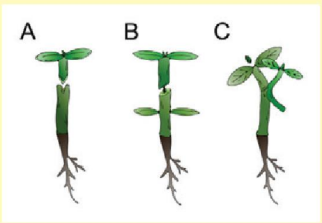	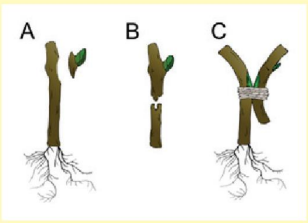
Diagrams of (A) hypocotyl grafting, (B) stem grafting, and (C) approach grafting of herbaceous tissues	Diagrams of (A) chip budding, (B) omega table-top grafting, and (C) approach grafting of woody tissues
Tissues active and rapidly growing when grafted	Tissues dormant when grafted
Leaves and/or cotyledons photosynthesising and transpiring when grafted	Buds dormant when grafted
Carbon accumulates in the scion, whereas the rootstock is starved of carbon until the phloem reconnects	Large supplies of starch in dormant wood of scion and rootstock
Root growth depends upon phloem connections with scion	Bud-break and adventitious root formation largely independent of graft union development
Limited secondary growth	Considerable secondary growth

Box 3. Models of *de novo* plasmodesmata biogenesis and organelle transfer events at the graft interface

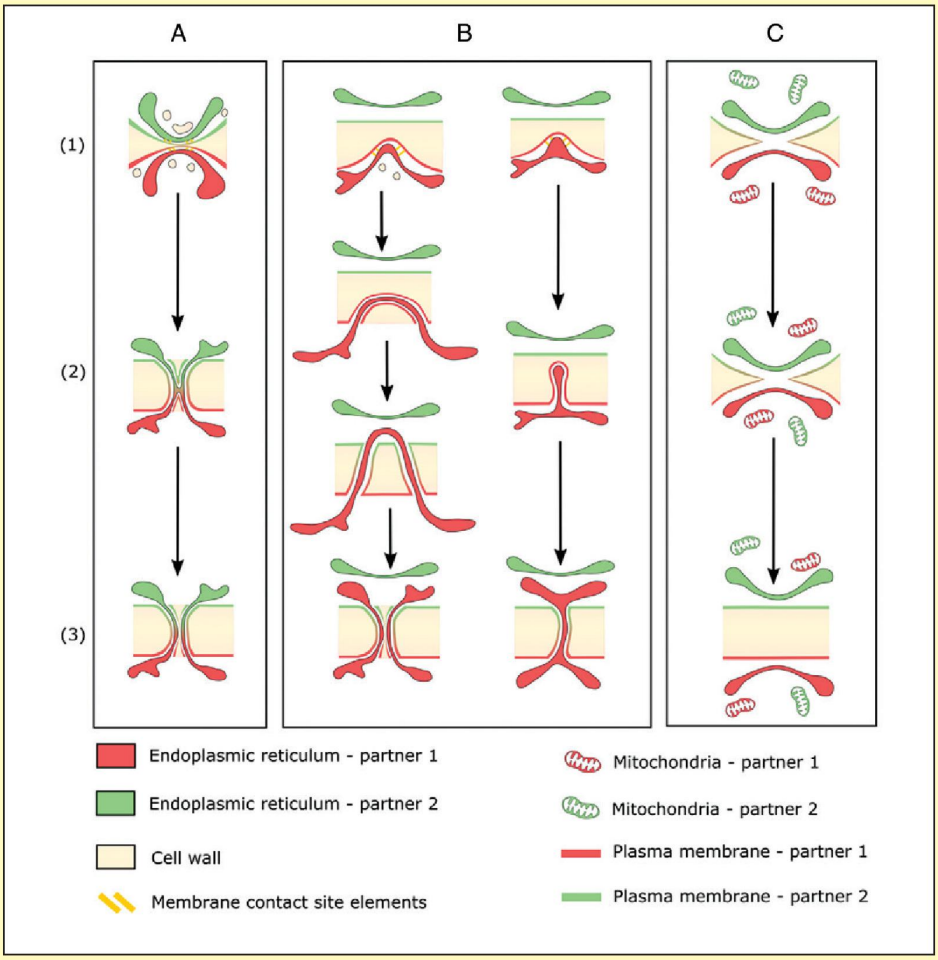

(A) Model of spatio-temporal coordination between both partners for plasmodesmata biogenesis. (1) Tethering of endoplasmic reticulum to the plasma membrane at both sides of the graft interface and thinning of the cell wall; (2) endoplasmic reticulum and plasma membrane fusions leading to the formation of branched plasmodesmata and thickening of the cell wall through callose deposition; (3) maturation from branched into twin plasmodesmata. (B) Biogenesis of plasmodesmata initiated by only one partner. (1) Tethering of endoplasmic reticulum to the plasma membrane at one side of the graft interface with thinning of the cell wall; (2) invagination of endoplasmic reticulum into the cell wall; (3) new twin or simple plasmodesmata are formed. (C) Organelle transfer events at the graft interface. (1) Cell wall opening at the graft interface; (2) organelles transfer; (3) pore closing.

scion and rootstock coordinate to form a new plasmodesmata by thinning the cell wall and tethering endoplasmic reticulum to it. This is followed by the fusion of the endoplasmic reticulum from both grafting partners, cell wall thickening, and the formation of a mature plasmodesmata. This would result in the formation of a desmotubule that originates from both grafted partners. In the second model, (B), the formation of plasmodesmata is initiated by only one of the grafted partners (the rootstock in the example shown). The endoplasmic reticulum of the rootstock invaginates into the cell wall and new plasmodesmata are formed with desmotubules originating from only one grafted partner.

The unprecedented work of Stegemann and Bock (2009) and Fuentes *et al.* (2014) has shown that entire chloroplast and nuclear genomes can be horizontally transferred across the graft union (Box 1). These authors suggest two potential mechanisms for this process: (1) fusion of neighbouring cells at the graft site, or (2) migration of nuclei from cell-to-cell through plasmodesmata in a cytomixis-like process. To date, we do not know the mechanisms of organelle exchange at the

graft interface (a model for this process is shown in Box 3C), or when, or in which cell type(s) it occurs. However, given that these exchanges appear to be fairly frequent, cell fusion or migration of nuclei may actually be an essential component of the graft union formation process.

Future research directions

We still have little understanding of how the physical connections across the graft interface are formed, how the vascular tissue is integrated, how plasmodesmata are formed, and how organelles are exchanged; future research should address these fundamental questions using fluorescent markers and correlative light-electron microscopy techniques.

In addition, to expand the range of rootstocks compatible with existing scion varieties, we need to advance the identification of the molecular elements underlying graft union formation and graft incompatibility. A clear understanding of the transcript or protein accumulation profiles at the graft interface associated with incompatibility is still lacking. Although it is logistically challenging to graft hundreds of different scion–rootstock combinations with a sufficient number of replicates to accurately quantify graft compatibility, QTL studies of graft compatibility should be done in the future.

Conclusions

Despite thousands of years of agronomic use, science is just beginning to reveal the mechanisms underlying graft union formation and scion–rootstock interactions. Understanding how rootstocks can modify scion phenotypes will be valuable in aiding plant adaptation to climate change via the creation of new rootstocks. The increasing commercial use of grafted vegetables has renewed scientific interest in grafting because it holds the promise of providing sustainable solutions to numerous agronomic challenges.

References

Adams S, Lordan J, Fazio G, Bugbee B, Francescatto P, Robinson TL, Black B. 2018. Effect of scion and graft type on transpiration, hydraulic resistance and xylem hormone profile of apples grafted on Geneva (R) 41 and M.9-NIC (TM) 29 rootstocks. Scientia Horticulturae **227,** 213–222.

Albacete A, Martínez-Andújar C, Martínez-Pérez A, Thompson AJ, Dodd IC, Pérez-Alfocea F. 2015. Unravelling rootstock×scion interactions to improve food security. Journal of Experimental Botany **66,** 2211–2226.

Amos J, Hatton RG, Hoblyn TN, Knight RC. 1930. The effect of scion on root: II. Stem-worked apples. Journal of Pomology and Horticultural Science **8,** 248–258.

Aryan A, Musetti R, Riedle-Bauer M, Brader G. 2016. Phytoplasma transmission by heterologous grafting influences viability of the scion and results in early symptom development in periwinkle rootstock. Journal of Phytopathology **164,** 631–640.

Asins MJ, Albacete A, Martinez-Andujar C, Pérez-Alfocea F, Dodd IC, Carbonell EA, Dieleman JA. 2017. Genetic analysis of rootstock-mediated nitrogen (N) uptake and root-to-shoot signalling at contrasting N availabilities in tomato. Plant Science **263,** 94–106.

Asins MJ, Bolarín MC, Pérez-Alfocea F, Estañ MT, Martínez-Andújar C, Albacete A, Villalta I, Bernet GP, Dodd IC, Carbonell EA. 2010. Genetic analysis of physiological components of salt tolerance conferred by *Solanum* rootstocks. What is the rootstock doing for the scion? Theoretical and Applied Genetics **121,** 105–115.

Asins MJ, Raga V, Roca D, Belver A, Carbonell EA. 2015. Genetic dissection of tomato rootstock effects on scion traits under moderate salinity. Theoretical and Applied Genetics **128,** 667–679.

Bahar E, Korkutal I, Carbonneau A, Akcay G. 2010. Using magnetic resonance imaging technique (MRI) to investigate graft connection and its relation to reddening discoloration in grape leaves. Journal of Food Agriculture & Environment **8,** 293–297.

Bailey JS. 1923. A microscopic study of apple graft unions. MS Thesis. Ames: Iowa State University of Science and Technology.

Bert PF, Bordenave L, Donnart M, Hévin C, Ollat N, Decroocq S. 2013. Mapping genetic loci for tolerance to lime-induced iron deficiency chlorosis in grapevine rootstocks (*Vitis* sp.). Theoretical and Applied Genetics **126,** 451–473.

Bhogale S, Mahajan AS, Natarajan B, Rajabhoj M, Thulasiram HV, Banerjee AK. 2014. MicroRNA156: a potential graft-transmissible microRNA that modulates plant architecture and tuberization in *Solanum tuberosum* ssp. *andigena*. Plant Physiology **164,** 1011–1027.

Bie ZL, Nawaz MA, Huang Y, Lee JM, Colla G. 2017. Introduction to vegetable grafting. In: Colla G, Perez Alfocea F, Schwarz D, eds. Vegetable grafting: principles and practices. Wallingford, UK: CABI, 1–21.

Buhtz A, Springer F, Chappell L, Baulcombe DC, Kehr J. 2008. Identification and characterization of small RNAs from the phloem of *Brassica napus*. The Plant Journal **53,** 739–749.

Chen X, Yao Q, Gao X, Jiang C, Harberd NP, Fu X. 2016. Shoot-to-root mobile transcription factor HY5 coordinates plant carbon and nitrogen acquisition. Current Biology **26,** 640–646.

Chen Z, Zhao JT, Hu FC, Qin YH, Wang XH, Hu GB. 2017. Transcriptome changes between compatible and incompatible graft combination of *Litchi chinensis* by digital gene expression profile. Scientific Reports **7,** 3954.

Clearwater MJ, Blattmann P, Luo Z, Lowe RG. 2007. Control of scion vigour by kiwifruit rootstocks is correlated with spring root pressure phenology. Journal of Experimental Botany **58,** 1741–1751.

Clearwater MJ, Lowe RG, Hofstee BJ, Barclay C, Mandemaker AJ, Blattmann P. 2004. Hydraulic conductance and rootstock effects in grafted vines of kiwifruit. Journal of Experimental Botany **55,** 1371–1382.

Cochetel N, Météier E, Merlin I, *et al*. 2018. Potential contribution of strigolactones in regulating scion growth and branching in grafted grapevine in response to nitrogen availability. Journal of Experimental Botany **69,** 4099–4112.

Colla G, Perez Alfocea F, Schwarz D. eds. 2017. Vegetable grafting: principles and practices. Wallingford, UK: CABI.

Cookson SJ, Clemente Moreno MJ, Hevin C, Nyamba Mendome LZ, Delrot S, Magnin N, Trossat-Magnin C, Ollat N. 2014. Heterografting with nonself rootstocks induces genes involved in stress responses at the graft interface when compared with autografted controls. Journal of Experimental Botany **65,** 2473–2481.

Cookson SJ, Clemente Moreno MJ, Hevin C, Nyamba Mendome LZ, Delrot S, Trossat-Magnin C, Ollat N. 2013. Graft union formation in grapevine induces transcriptional changes related to cell wall modification, wounding, hormone signalling, and secondary metabolism. Journal of Experimental Botany **64,** 2997–3008.

Cordeau J. 1998. Création d'un vignoble. Greffage de la vigne et porte-greffes. Elimination des maladies à virus. Bordeaux: Editions Féret.

Dong H, Niu Y, Li W, Zhang D. 2008. Effects of cotton rootstock on endogenous cytokinins and abscisic acid in xylem sap and leaves in relation to leaf senescence. Journal of Experimental Botany **59,** 1295–1304.

Dumont C, Cochetel N, Lauvergeat V, Cookson SJ, Ollat N, Vivin P. 2016. Screening root morphology in grafted grapevine using 2D digital images from rhizotrons. In: Gaiotti F, Battista F, Tomasi D, eds. Proceedings of the I international symposium on grapevine roots. Acta Horticulturae **1136,** 213–219.

Else MA, Taylor JM, Young S, Atkinson CJ. 2018. The effect of the graft union on hormonal and ionic signalling between rootstocks and scions of grafted apple (*Malus pumila* L. Mill.). Environmental and Experimental Botany **156,** 325–336.

Estañ MT, Villalta I, Bolarín MC, Carbonell EA, Asins MJ. 2009. Identification of fruit yield loci controlling the salt tolerance conferred by solanum rootstocks. Theoretical and Applied Genetics **118,** 305–312.

Fallot J. 1970. Callogèse, soudure, culture des tissus. Bulletin de l'Office International de la Vigne et du Vin **469,** 908–918.

Fazio G, Wan YZ, Kviklys D, Romero L, Adams R, Strickland D, Robinson T. 2014. *Dw2*, a new dwarfing locus in apple rootstocks and its relationship to induction of early bearing in apple scions. Journal of the American Society for Horticultural Science **139,** 87–98.

Feng Y, Zhang X, Wu T, Xu X, Han Z, Wang Y. 2017. Methylation effect on *IPT5b* gene expression determines cytokinin biosynthesis in apple rootstock. Biochemical and Biophysical Research Communications **482,** 604–609.

Flaishman MA, Loginovsky K, Golobowich S, Lev-Yadun S. 2008. *Arabidopsis thaliana* as a model system for graft union development in homografts and heterografts. Journal of Plant Growth Regulation **27,** 231–239.

Foster TM, Celton JM, Chagné D, Tustin DS, Gardiner SE. 2015. Two quantitative trait loci, *Dw1* and *Dw2*, are primarily responsible for rootstock-induced dwarfing in apple. Horticulture Research **2,** 15001.

Fuentes I, Stegemann S, Golczyk H, Karcher D, Bock R. 2014. Horizontal genome transfer as an asexual path to the formation of new species. Nature **511,** 232–235.

Gautier A, Cookson SJ, Hevin C, Vivin P, Lauvergeat V, Mollier A. 2018. Phosphorus acquisition efficiency and phosphorus remobilisation mediate genotype-specific differences in shoot P content in grapevine. Tree Physiology **38,** 1742–1751.

Ghanem ME, Albacete A, Smigocki AC, *et al*. 2011. Root-synthesized cytokinins improve shoot growth and fruit yield in salinized tomato (*Solanum lycopersicum* L.) plants. Journal of Experimental Botany **62,** 125–140.

Goldschmidt EE. 2014. Plant grafting: new mechanisms, evolutionary implications. Frontiers in Plant Science **5,** 727.

Gregory PJ, Atkinson CJ, Bengough AG, Else MA, Fernández-Fernández F, Harrison RJ, Schmidt S. 2013. Contributions of roots and rootstocks to sustainable, intensified crop production. Journal of Experimental Botany **64,** 1209–1222.

Gur A, Samish RM, Lifshitz E. 1968. Role of cyanogenic glycoside of quince in incompatibility between pear cultivars and quince rootstocks. Horticultural Research **8,** 113–134.

Gurdon C, Svab Z, Feng Y, Kumar D, Maliga P. 2016. Cell-to-cell movement of mitochondria in plants. Proceedings of the National Academy of Sciences, USA **113,** 3395–3400.

Harrison N, Barber-Perez N, Pennington B, Cascant-Lopez E, Gregory PJ. 2016a. Root system architecture in reciprocal grafts of apple rootstock-scion combinations. In: Tustin DS, VanHooijdonk BM, eds. XXIX International Horticultural Congress on Horticulture: sustaining lives, livelihoods and landscapes: international symposia on the physiology of perennial fruit crops and production systems and mechanisation, precision horticulture and robotics. Acta Horticulturae **1130,** 409–414.

Harrison N, Harrison RJ, Barber-Perez N, Cascant-Lopez E, Cobo-Medina M, Lipska M, Conde-Ruíz R, Brain P, Gregory PJ, Fernández-Fernández F. 2016b. A new three-locus model for rootstock-induced dwarfing in apple revealed by genetic mapping of root bark percentage. Journal of Experimental Botany **67,** 1871–1881.

Hatton RG. 1917. 'Paradise' apple stocks. Journal of the Royal Horticultural Society of London **42,** 361–399.

Jones OP. 1974. Xylem sap composition in apple trees – effect of graft union. Annals of Botany **38,** 463–467.

Jones OP. 1976. Effect of dwarfing interstocks on xylem sap composition in apple trees – effect on nitrogen, potassium, phosphorus, calcium and magnesium content. Annals of Botany **40,** 1231–1235.

Knäbel M, Friend AP, Palmer JW, *et al*. 2015. Genetic control of pear rootstock-induced dwarfing and precocity is linked to a chromosomal region syntenic to the apple *Dw1* loci. Bmc Plant Biology **15,** 230.

Ko D, Helariutta Y. 2017. Shoot–root communication in flowering plants. Current Biology **27,** R973–R978.

Kollmann R, Glockmann C. 1985. Studies on graft unions. 1. Plasmodesmata between cells of plants belonging to different unrelated taxa. Protoplasma **124,** 224–235.

Kumar P, Rouphael Y, Cardarelli M, Colla G. 2017. Vegetable grafting as a tool to improve drought resistance and water use efficiency. Frontiers in Plant Science **8,** 1130.

Lin WY, Huang TK, Leong SJ, Chiou TJ. 2014. Long-distance call from phosphate: systemic regulation of phosphate starvation responses. Journal of Experimental Botany **65,** 1817–1827.

Loureiro MD, Moreno-Sanz P, Garcia A, Fernandez O, Fernandez N, Suarez B. 2016. Influence of rootstock on the performance of the Albarin Negro minority grapevine cultivar. Scientia Horticulturae **201,** 145–152.

Marasco R, Rolli E, Fusi M, Michoud G, Daffonchio D. 2018. Grapevine rootstocks shape underground bacterial microbiome and networking but not potential functionality. Microbiome **6,** 3.

Marguerit E, Brendel O, Lebon E, Van Leeuwen C, Ollat N. 2012. Rootstock control of scion transpiration and its acclimation to water deficit are controlled by different genes. New Phytologist **194,** 416–429.

Martínez-Andújar C, Albacete A, Martínez-Pérez A, Pérez-Pérez JM, Asins MJ, Pérez-Alfocea F. 2016. Root-to-shoot hormonal communication in contrasting rootstocks suggests an important role for the ethylene precursor aminocyclopropane-1-carboxylic acid in mediating plant growth under low-potassium nutrition in tomato. Frontiers in Plant Science **7,** 1782.

Melnyk CW. 2017a. Connecting the plant vasculature to friend or foe. New Phytologist **213,** 1611–1617.

Melnyk CW. 2017b. Plant grafting: insights into tissue regeneration. Regeneration **4,** 3–14.

Melnyk CW, Gabel A, Hardcastle TJ, Robinson S, Miyashima S, Grosse I, Meyerowitz EM. 2018. Transcriptome dynamics at Arabidopsis graft junctions reveal an intertissue recognition mechanism that activates vascular regeneration. Proceedings of the National Academy of Sciences, USA **115,** E2447–E2456.

Melnyk CW, Schuster C, Leyser O, Meyerowitz EM. 2015. A developmental framework for graft formation and vascular reconnection in *Arabidopsis thaliana*. Current Biology **25,** 1306–1318.

Milien M, Renault-Spilmont AS, Cookson SJ, Sarrazin A, Verdeil JL. 2012. Visualization of the 3D structure of the graft union of grapevine using X-ray tomography. Scientia Horticulturae **144,** 130–140.

Mudge K, Janick J, Scofield S, Goldschmidt EE. 2009. A history of grafting. In: Janick J, ed. Horticultural reviews, **Vol. 35**. Hoboken, NJ: John Wiley & Sons, Inc., 437–493.

Nanda AK, Melnyk CW. 2018. The role of plant hormones during grafting. Journal of Plant Research **131,** 49–58.

Nardini A, Gascó A, Raimondo F, Gortan E, Lo Gullo MA, Caruso T, Salleo S. 2006. Is rootstock-induced dwarfing in olive an effect of reduced plant hydraulic efficiency? Tree Physiology **26,** 1137–1144.

Ollat N, Bordenave L, Tandonnet JP, Boursiquot JM, Marguerit E. 2016. Grapevine rootstocks: origins and perspectives. In: Gaiotti F, Battista F, Tomasi D, eds. Proceedings of the I International Symposium on grapevine roots. Acta Horticulturae **1136,** 11–22.

Ollat N, Laborde W, Neveux M, Diakou-Verdin P, Renaud C, Moing A. 2003. Organic acid metabolism in roots of various grapevine (*Vitis*) rootstocks submitted to iron deficiency and bicarbonate nutrition. Journal of Plant Nutrition **26,** 2165–2176.

Peccoux A, Loveys B, Zhu J, Gambetta GA, Delrot S, Vivin P, Schultz HR, Ollat N, Dai Z. 2018. Dissecting the rootstock control of scion transpiration using model-assisted analyses in grapevine. Tree Physiology **38,** 1026–1040.

Peralta M, Combes MC, Cenci A, Lashermes P, Dereeper A. 2013. SNiPloid: a utility to exploit high-throughput SNP data derived from RNA-Seq in allopolyploid species. International Journal of Plant Genomics **2013,** 890123.

Pico MB, Thompson AJ, Gisbert C, Yetisir H, Bebeli PJ. 2017. Genetic resources for rootstock breeding. In: Colla G, Perez Alfocea F, Schwarz D, eds. Vegetable grafting: principles and practices. Wallingford, UK: CABI, 22–69.

Pina A, Cookson SJ, Calatayud A, Trinchera A, Errea P. 2017. Physiological and molecular mechanisms underlying graft compatibility. In: Colla G, Perez Alfocea F, Schwarz D, eds. Vegetable grafting principles and practices. Wallingford, UK: CABI.

Prassinos C, Ko JH, Lang G, Iezzoni AF, Han KH. 2009. Rootstock-induced dwarfing in cherries is caused by differential cessation of terminal meristem growth and is triggered by rootstock-specific gene regulation. Tree Physiology **29,** 927–936.

Raga V, Bernet GP, Carbonell EA, Asins MJ. 2014. Inheritance of rootstock effects and their association with salt tolerance candidate genes in a progeny derived from 'Volkamer' lemon. Journal of the American Society for Horticultural Science **139,** 518–528.

Ren Y, Xu Q, Wang L, Guo S, Shu S, Lu N, Sun J. 2018. Involvement of metabolic, physiological and hormonal responses in the graft-compatible process of cucumber/pumpkin combinations was revealed through the integrative analysis of mRNA and miRNA expression. Plant Physiology and Biochemistry **129,** 368–380.

Rusholme Pilcher RL, Celton JM, Gardiner SE, Tustin DS. 2008. Genetic markers linked to the dwarfing trait of apple rootstock 'Malling 9'. Journal of the American Society for Horticultural Science **133,** 100–106.

Sorgona A, Abenavoli MR, Gringeri PG, Lupini A, Cacco G. 2007. Root architecture plasticity of citrus rootstocks in response to nitrate availability. Journal of Plant Nutrition **30,** 1921–1932.

Stegemann S, Bock R. 2009. Exchange of genetic material between cells in plant tissue grafts. Science **324,** 649–651.

Symons GM, Ross JJ, Jager CE, Reid JB. 2008. Brassinosteroid transport. Journal of Experimental Botany **59,** 17–24.

Tamiru M, Hardcastle TJ, Lewsey MG. 2018. Regulation of genome-wide DNA methylation by mobile small RNAs. New Phytologist **217,** 540–546.

Tandonnet JP, Cookson SJ, Vivin P, Ollat N. 2010. Scion genotype controls biomass allocation and root development in grafted grapevine. Australian Journal of Grape and Wine Research **16,** 290–300.

Tandonnet JP, Marguerit E, Cookson SJ, Ollat N. 2018. Genetic architecture of aerial and root traits in field-grown grafted grapevines is largely independent. Theoretical and Applied Genetics **131,** 903–915.

Tworkoski T, Fazio G. 2016. Hormone and growth interactions of scions and size-controlling rootstocks of young apple trees. Plant Growth Regulation **78,** 105–119.

Venema JH, Giuffrida F, Paponov I, Albacete A, Perez-Alfocea F, Dodd IC. 2017. Rootstock-scion signalling: key factors mediating scion performance. In: Colla G, Perez Alfocea F, Schwarz D, eds. Vegetable grafting: principles and practices. Wallingford, UK: CABI, 94–131.

Vigne E, Demangeat G, Komar V, Fuchs M. 2005. Characterization of a naturally occurring recombinant isolate of *Grapevine fanleaf* virus. Archives of Virology **150,** 2241–2255.

Wang L, Li G, Wu X, Xu P. 2016. Comparative proteomic analyses provide novel insights into the effects of grafting wound and hetero-grafting *per se* on bottle gourd. Scientia Horticulturae **200,** 1–6.

Wang SS, Liu ZZ, Sun C, Shi QH, Yao YX, You CX, Hao YJ. 2012. Functional characterization of the apple *MhGAI1* gene through ectopic expression and grafting experiments in tomatoes. Journal of Plant Physiology **169,** 303–310.

Wang ZY, Patterson KJ, Gould KS, Lowe RG. 1994. Rootstock effects on budburst and flowering in kiwifruit. Scientia Horticulturae **57,** 187–199.

Warschefsky EJ, Klein LL, Frank MH, Chitwood DH, Londo JP, von Wettberg EJB, Miller AJ. 2016. Rootstocks: diversity, domestication, and impacts on shoot phenotypes. Trends in Plant Science **21,** 418–437.

Webster AD. 2004. Vigour mechanisms in dwarfing rootstocks for temperate fruit trees. In: Sanchez MA, Webster AD, eds. Proceedings of the 1st International Symposium on Rootstocks for Deciduous Fruit Tree Species, Vols 1 and 2. Leuven, Belgium: International Society for Horticultural Science, 29–41.

Wu R, Wang X, Lin Y, Ma Y, Liu G, Yu X, Zhong S, Liu B. 2013. Inter-species grafting caused extensive and heritable alterations of DNA methylation in Solanaceae plants. PLoS ONE **8,** e61995.

Zambrosi FCB, Mattos D, Boaretto RM, Quaggio JA, Muraoka T, Syvertsen JP. 2012. Contribution of phosphorus (^{32}P) absorption and remobilization for citrus growth. Plant and Soil **355,** 353–362.

Zheng X, Zhao Y, Shan D, *et al*. 2018. *MdWRKY9* overexpression confers intensive dwarfing in the M26 rootstock of apple by directly inhibiting brassinosteroid synthetase *MdDWF4* expression. New Phytologist **217,** 1086–1098.

CONTEXT AND OBJECTIVES

The research team of Nathalie Ollat where I did my Ph.D. project focuses on the scion/rootstock interactions in grapevine and the effects of this union on the development of the whole plant. The team aim to understand the mechanisms governing scion/rootstock interactions in different environmental conditions. My Ph.D. was focused on understanding the process of graft union formation at an ultrastructural level. Indeed, grafting is crucial to the culture of numerous perennial plants, especially grapevine. During grafting, all physical cell communications are interrupted by cutting at the grafting point and the two grafted organisms have to interact together enough quickly and effectively to survive. Because of the complexity to reliably target the graft interface under the electron microscope very few work has be done and fine ultrastructural data is still lacking. One of the only approaches that permitted us to reach reliably the ultrastructure of graft interface was published in 1985 by Kollmann & Glockmann. They used two phylogenetically distant plants (*Vicia faba* and *Heliantus annuus*) that show cytological differences, recognizable under electron microscopy (EM). However, this approach did not allow the identification without ambiguity of every cell studied because of the intrinsic ultrastructural cell heterogeneity between differentiated cells (Fig. 3C). Moreover, this method restricted to the study models ultrastructural differences and cannot be applied to model plants such as *A. thaliana*. Thanks to the emergence of new tools in microscopy, the ultrastructure of the graft interface could be assessed and could provide new insights into the establishment of new communications at the scion/rootstock interface. To this end, we decided to develop correlative light and electron microscopy approach (CLEM) which permits us to access the ultrastructure of the graft interface. Indeed, by grafting plants expressing different fluorescent proteins we will be able to take advantage of light microscopy (LM) to reliably target the graft interface and further characterize its ultrastructure under Transmission Electron Microscope (TEM).

In this context, my challenge was to develop CLEM on the graft interface of grapevines and *A. thaliana* in order to gather data on the ultrastructural organization of the graft interface to shed light on the developmental processes underpinning the establishment of communication between the grafted partners. As a large part of my Ph.D. work consisted of developing CLEM methods, I was mainly supervised by Lysiane Brocard, a research engineer on the plant imaging platform of the Bordeaux Imaging Centre.

3. Correlative Light Electron microscopy (CLEM)

Correlative Light Electron Microscopy has become a choice technique over the last few years as it has a broad range of applications (as reviewed in Müller-Reichert & Verkade, 2012). It combines the valuable information obtained through light microscopy (LM), for example studying the dynamic of a process in a living tissue, with a study of fine ultrastructural details of the sub-cellular structures involved in the process of interest with EM. The outline of a first approach that could be defined as an attempt of CLEM, where both LM and EM were performed on the exact same sample, was done by Abandowitz & Geissinger (1975). At this time, they only performed scanning EM followed by interference microscopy. It is only later in 1978, with the work of Webster *et al.*, on the visualization of cytoskeleton protein of *Potorous tridactylis* epithelial kidney (PtK2) cells, where they begin to use first light microscopy (LM) with immunofluorescence followed by EM.

Since then, the direct use of fluorescently labeled proteins (such as GFP fusion proteins) offers the possibility to observe directly the localization of proteins in living samples. In addition the combination of different variants of fluorescent proteins (FPs) such as red fluorescent protein (mRFP) and yellow fluorescent protein (YFP) together (Shaner *et al.,* 2005) can be used to follow relative localization of two different proteins within the same sample (Brocard *et al.,* 2017). Unfortunately, with LM, cell environment is not accessible and the resolution reached is not always sufficient. To overcome these limits, TEM observations can be performed to access the ultrastructural level. But no fluorescence can be observed by TEM. Thus, the localization of a FP within its ultrastructural environment is not directly possible. Immuno-labelling with a secondary gold-conjugated antibody, directed against primary antibody itself directed against the FP, has to be performed. Usually, secondary antibodies are conjugated with gold beads with a diameter from five to 15 nm. To succeed, immuno-labelling has to be performed on samples where the antigenicity is well preserved. Unfortunately, the preservation of antigenicity avoids the using of efficient chemical fixative compounds that ensure the well-ultrastructural preservation (Ripper *et al.,* 2008). Nevertheless, when the labelling succeeds, it is often light because antigen accessibility is restricted to the surface of the resin section (Glauert & Lewis, 2014). Moreover, on large samples and/or for rare proteins, nanometric gold-labelling observations can be like looking for a needle in a haystack. A solution to facilitate the ultrastructure observation of fluorescent events would be to get the possibility to observe the fluorescence and the ultrastructure of exactly the same sample. Thus, the fluorescence signal could be observed and mapped by observing an ultrathin resin section before its TEM observation. Unfortunately, fluorescence is lost during the steps of conventional TEM sample preparation. This is because conventional EM preparation methods involve the use of chemical compounds, such as glutaraldehyde and osmium tetroxide, which react with the FPs (Watanabe *et al.,* 2011). Furthermore, glutaraldehyde is known to induce auto-fluorescence (Biberfeld *et al.,* 1974),

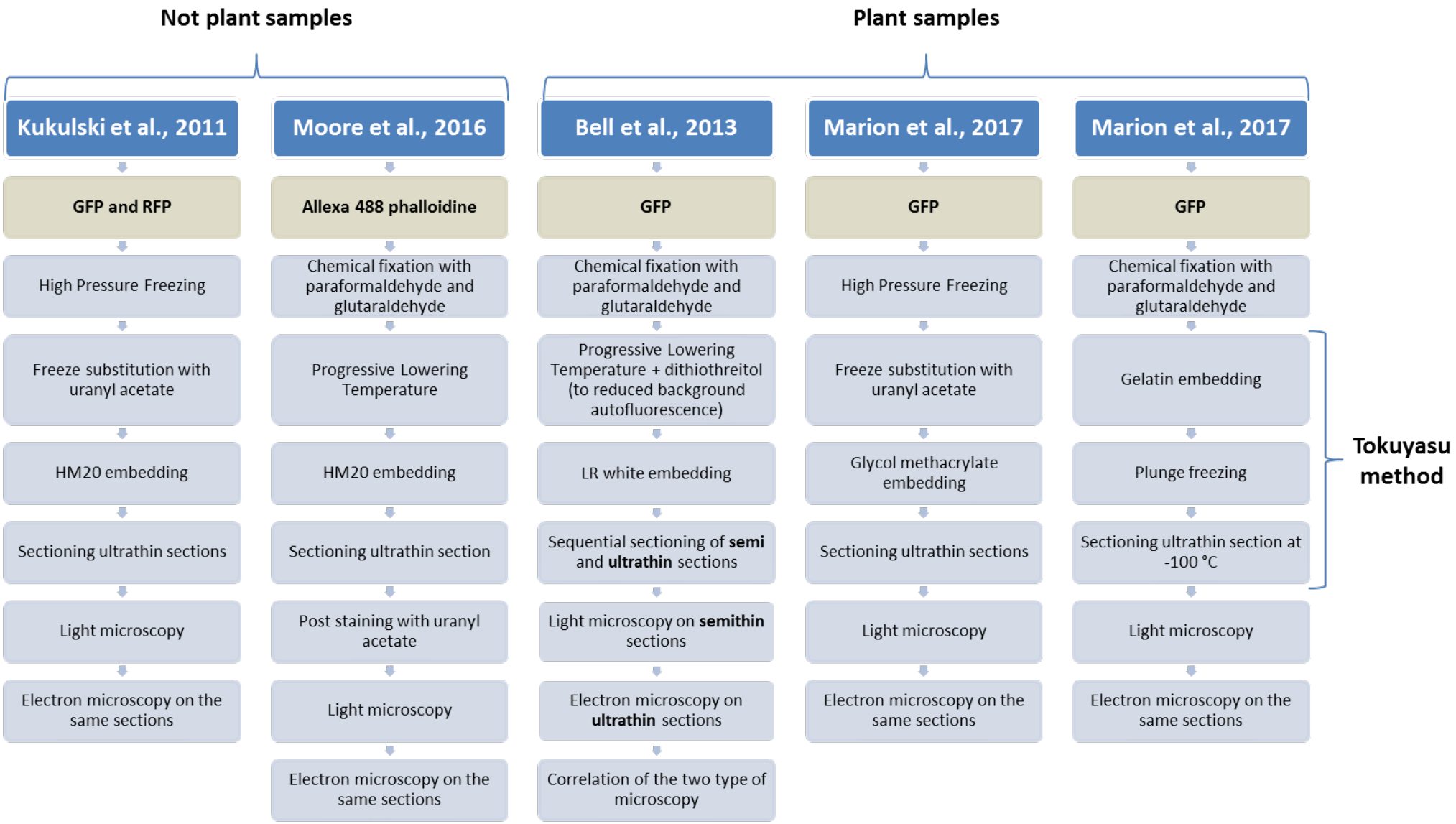

Figure 5. Workflows of Correlative Light Electron Microscopy (CLEM)

which impairs the detection of specific signals from FPs by impairing drastically the signal-to-noise ratio. Thus, the main challenge for one CLEM method called In Resin Fluorescence (IRF) was to sufficiently maintain fluorescence properties of FPs during the sample preparation while preserving a good ultrastructure for TEM (Fig. 5) (Carron *et al.,* 2012; Kukulski *et al.,* 2012; Kukulski *et al.,* 2011; Watanabe *et al.,* 2011). The work of Nixon *et al.,* 2009 on zebrafish and Kukulski *et al.,* 2011 on the localization of Human Immunodeficiency Viruses (HIV) particles on mammalian cells and microtubule structures in yeast proposed the use of cryofixation methods over conventional chemicals methods as a starting point for CLEM. Cryo-methods permit to limit the use of fixative compounds to the use of uranyl acetate alone. Indeed, they observed a very good preservation of the GFP signal along with ultrastructural preservation using cryofixation methods. The freeze-substitution, *i.e.* working with very low temperature until full dehydration, needs a resin which can polymerize at a low temperature for embedding. The use of a combination of High Pressure Freezing (HFP) and Lowicryl resins that polymerize at negative temperatures under UV, such as HM-20 or LR White, lead to obtain a preserved ultrastructure and also a sufficient signal of the GFP. Importantly, the protocol described by Kukulski *et al.,* (2011) demonstrates that both RFP and GFP can be preserved at the same time, opening the door of colocalization and grafted tissues studies. Working directly 'in-resin', with ultrathin sections deposited on TEM grids, allows a precise correlation on the same region of interest between LM and TEM because LM and TEM imaging are performed directly on the TEM grids. To achieve this, grids are mounted in water before LM observations with water or oil immersion objectives with high numerical aperture to get the best resolution and sensitivity. Transmission electron microscope grids can be then transferred to the TEM to access to the ultrastructure. The fluorescence pattern of cell shapes is then correlated to the shape of cells observed by TEM. Moreover, to reach this precise correlation (under 100 nm) it is possible to use fluorescent electron-dense fiducials deposited on grids. They are beads electron-dense under the TEM that have been coated with fluorescent probes, making them visible both under LM and TEM. The set of coordinates provided by the positions of the beads in LM and in TEM allows the precise correlation between both microscopies. Afterwards, thanks to the triangulation method, the FP spots can be positioning relatively to the fiducials on the TEM images with a precision around 100 nm in a 2D plan.

Despite this success, CLEM approaches are still challenging. Thus, Bell *et al.,* (2013) were the first one to use an IRF approach in plant samples (Fig. 6G, H and I). They used chemical fixation and particular dehydration steps where dithiothreitol was added to ethanol. Dithiothreitol allows improving the signal-to-noise by decreasing the autofluorescence induced by glutaraldehyde. Nevertheless, the signal-to-noise ratio obtained for the GFP was not good enough for its observation on ultrathin sections. They need to firstly observe on semi-thin sections (1 to 2 µm) by LM before to correlate

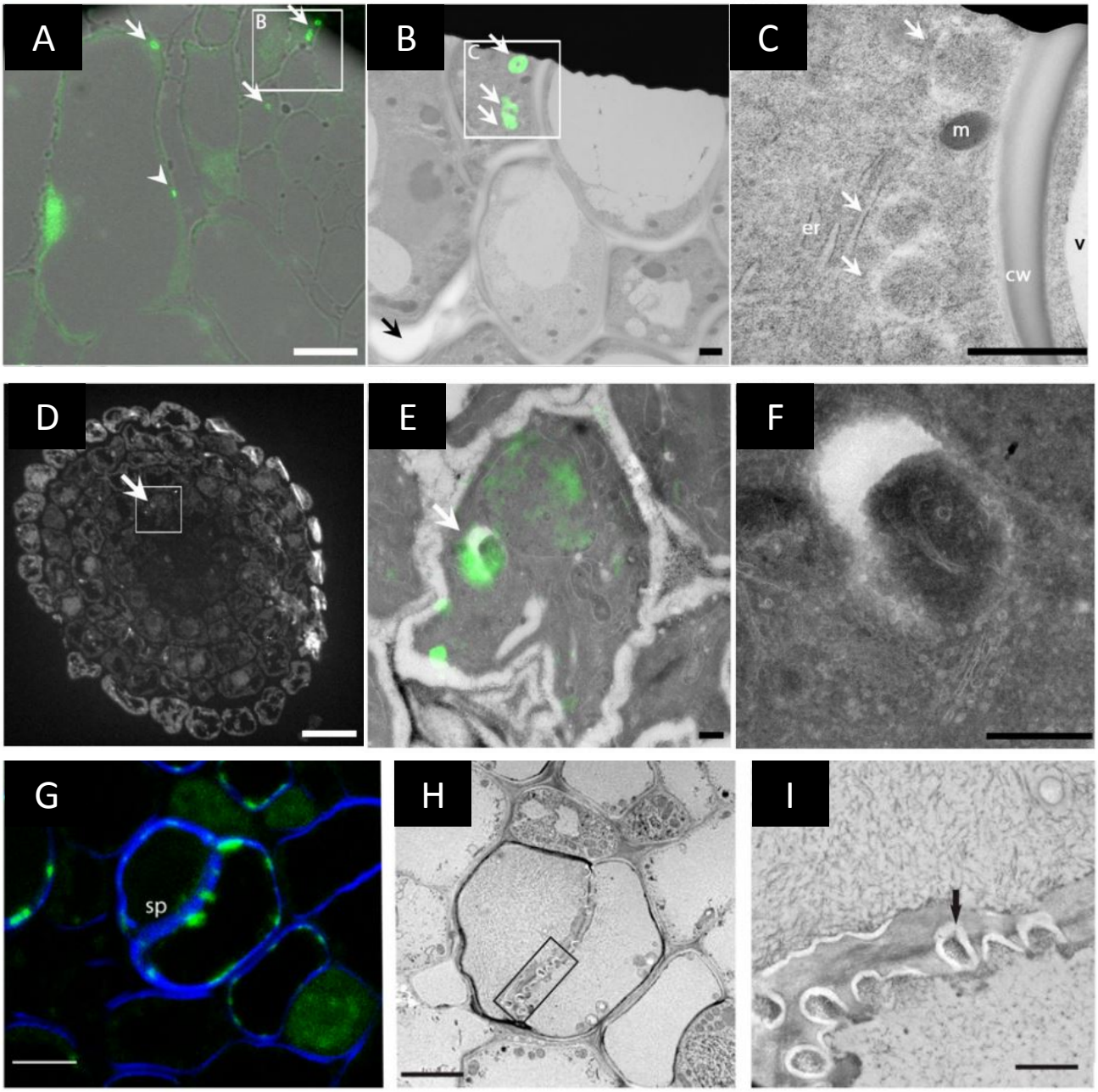

Figure 6. In Resin Fluorescence Correlative Light Electron Microscopy (CLEM) on plant samples (A-C) High pressure freezing followed by Glycol Methacrylate (GMA) embedding preserve the fluorescence of green fluorescent protein (GFP), however GMA infiltration is poor and leads to cells that detach from each other , **(D-F)** the Tokuyasu methods permits the preservation of GFP, but the chemical fixation induces shrinking of tissues and wrinkled membranes **(G-I)** In Bell *et al.* (2013) cold chemical fixation did not preserve sufficiently the fluorescence of GFP, thus making mandatory to work with alternating sections of different thicknesses for fluorescence microscopy and electron microscopy.
(A and B, adapted from Marion *et al.,* 2017; C adapted from Bell *et al.,* 2013)

with the ultrastructure observed on the following ultrathin section by TEM. Moreover, the ultrastructure preservation is limited. In 2017, the second and most recent plant CLEM paper was published, using a cryosectioning Tokuyasu method (Fig. 6 D, E, F) or cryofixation (Fig. A, B and C) and embedding in the acrylic resin Glycol Methacrylate (GMA). This resin allowed them to preserve GFP fluorescence a little during the processing of samples (Marion *et al.,* 2017). Despite precautions, both methods led to insufficient ultrastructure preservation for fine ultrastructural studies. Glycol methacrylate infiltration was bad, causing cells detachment other and making it inappropriate to study fine structures located in the cell wall such as PD. On the other hand, results obtain with Tokuyasu method showed a shrinking of tissues and wrinkled membranes and is not appropriate for ultrastructural studies

4. Establishing the CLEM approach on plant samples

To perform CLEM on our grafted hypocotyls of *A. thaliana* and *in vitro* grapevine micro grafts, we decided to adapt the in resin fluorescence protocol that Kukulski *et al.,* (2011) used on yeast and mammal samples to plant samples. The results obtained in these studies permitted us to reach a high ultrastructural quality with preservation of fluorescence signal. Moreover, this approach is compatible with electron tomography allowing reaching a resolution at the nm scale in the three dimensions. Our main modifications consisted of finding the right conditions of freeze substitution and embedding both in terms of temperature and duration of each step. As fluorescence decreased during samples preparation, the bottleneck step was the visualization of the fluorescence signal. The thickness of the section, the fragility of the TEM grid, the montage of the sample in water between the glass slide and the coverslip, the photonic system, the collection of the signal are in fact the real crucial points of this CLEM approach. All these steps constitute a significant technological advance for imaging the plant samples because this approach could be extended to other parts of plants such as the root tip.

To visualize the graft interface of *A. thaliana*, we used the ER retrieval sequence HDEL fused to FPs; YFP and mRFP for each grafting partner respectively. The HDEL retrieval signal has been shown to not move cell-to-cell (Knox *et al.,* 2015) and thus is appropriate to label the graft interface. On grapevine, due to the difficulties in establishing new transgenic lines only one line of *in vitro* Pinot Noir cultivars expressing 35S::HDEL_GFP was available and was grafted on wild type cultivars of Pinot Noir. This makes the grapevine system less convenient than *A. thaliana* one, but still permitted us to visualize the graft interface.

Although quality obtained on the grapevine model still needs to be improved, our CLEM approach permits the unambiguous targeting of the graft interface of *A. thaliana* hypocotyl grafts and its ultrastructure for the first time. Combined with ET, it allows us to reach an unprecedented level of

detail and follow the establishment of communications at the graft interface. As this protocol could be extended to other plant tissues, we describe to integrate our results in a methodological article that we plan to publish in *Bioprotocols*. These results constitute the first part of my manuscript and highlight all the crucial criteria to fulfill to access the ultrastructure of the graft interface. The second part of the results are based on what we discovered using this protocol, we are planning to submit this work to *Plant Journal.* Additionally, the third part of my results section will further focus on the preliminary results obtained to assess the trafficking of molecules between the scion and rootstock.

5. Imaging the three dimensions of the graft interface

To integrate the results obtained through CLEM to a more global scale, the 3D of the graft interface should be resolved. Until now, it was only assessed through low resolution techniques such a magnetic resonance imaging (MRI) (Baharet *et al.*, 2010) or X-ray tomography (Milien *et al.,* 2012). These techniques have allowed the analysis of the vascular connection in the graft. X-ray tomography permitted the identification of the main tissues in a graft union of grapevines (the pith, xylem vessels, phloem and necrotic tissues) with a significantly higher resolution than MRI. Moreover, X-ray is non-destructive (although high doses of X-rays can be toxic); it could be used to evaluate graft success in woody plants. Also, it may be of great interest to study living plants and the development of the graft interface on the same plant overtime. It presents a great interest, mostly for woody species, to understand grafting success or failure and/or incompatibility. However, these techniques do not provide enough resolution to understand all the fine developmental events occurring at the graft interface. They do not permit us to reach a perfect reliability at the cellular level. Moreover, even if they are suitable, especially for woody species, they seem not appropriate for the plant model *A. thaliana* where lots have been done to understand developmental framework and where a variety of molecular tools, such as FPs are available. Additionally, they cannot be linked to ultrastructural data. Thus, a last axis of my thesis was to begin to develop other techniques of 3D imaging of the graft interface, using CLEM and clearing approaches.

RESULTS

1. Setting up the Correlative Light and Electron microscopy on grafted plant samples

1.1. Article 1: “A Correlative Light Electron Microscopy Approach to Target Ultrastructural Events at the Graft Interface of Arabidopsis thaliana”, *Bioprotocols*

A Correlative Light Electron Microscopy Approach to Target Ultrastructural Events at the Graft Interface of Arabidopsis thaliana

Clément Chambaud[1], Sarah J. Cookson[1], Lysiane Brocard[2*]

[1] EGFV, Bordeaux Sciences Agro, INRA, Université de Bordeaux, ISVV, 210 Chemin de Leysotte, Villenave d'Ornon, France

[2] Université de Bordeaux, CNRS, INSERM, UMS 3420, INRA, Bordeaux Imaging Center, Plant Imaging Plateform, Villenave d'Ornon, France

[*]For correspondence: lysiane.brocard@inra.fr

Abstract

Combining two different plants together through grafting is one of our oldest horticultural techniques (Mudge *et al*., 2009), and in order to survive, both partners must form a vascular *continuum* via the *de novo* formation of connections between the scion and rootstock. Despite the importance of grafting, the key ultrastructural processes permitting successful graft union formation remain largely unknown because of the technical difficulty of precisely locating the site of contact between the scion and rootstock in the disorganized, wounded tissues of the graft interface zone. To date, only the studies of Kollmann and Glockmann (1985) and Kollmann et al. (1985) were able to reliably localize the grafting interface at the cellular level, thanks to grafting plants with species-specific cytological markers, which were visible under Electron Microscopy (EM). As such, studies requiring the precise identification of the graft interface are restricted to studying plants with species-specific cytological markers. However, today grafted plants can be made from scions and rootstocks labeled with specific fluorescent proteins and visualized with Light Microscopy (LM). Here, we describe a protocol permitting the study of ultrastructural events occurring precisely at the graft interface thanks to a Correlative Light Electron Microscopy (CLEM) approach. We applied this method to the model plant *Arabidopsis thaliana.* For the first time, the graft interface can be unambiguously localized and studied at the ultrastructural level. Moreover, the well-preserved ultrastructure and antigenicity is compatible with immunolocalization and electron tomography.

Keywords:

Plant grafting, correlative microscopy, *Arabidopsis thaliana*, plant vasculature, plant communication, plasmodesmata, electron microscopy, electron tomography, callus, xylem, phloem, wounding, healing, hypocotyl

Background

Combining plants together through grafting have been used for millenia in agriculture (Mudge *et al*., 2009). Today, most commercial perennial fruit production and some vegetables are grafted to improve agronomically interesting traits such as resistance to abiotic or biotic stress. Despite its widespread use, the ways in which the two partners of a grafted plant interact and communicate remain poorly understood; both in terms of the processes occurring during graft union formation and long-distance signaling mechanisms (Gautier et al., 2019).

During graft union formation, adult and differentiated tissues from both partners have to undergo a process of dedifferentiation to form callus cells and new conducting structures (phloem and xylem) (Pina et *al.,* 2017). In addition, cell-to-cell contact needs to be established between the scion and rootstock via plasmodesmata. Knowledge of the cellular mechanisms underpinning graft union formation is currently very limited (Kollmann & Glockmann, 1985; Kollmann et al., 1985; Melnyk *et al.*, 2015; Pina *et al.*, 2017) because precisely locating the site of contact between the two grafted partners under electron microscopy (EM) is a challenge. A first attempt was successfully made by Kollmann and Glockmann (1985) using *Helianthus annuus* grafted onto *Vicia faba*. These two plants have cytological differences in the callus cells produced at the graft interface that are visible under EM. Kollmann and Glockmann (1985) revealed the existence of plasmodesmata at the graft interface for the first time. Unfortunately, this technique is very limited as plants need to have obvious cytological differences, which is inappropriate in most cases of grafting of agronomic interest where the two plants are generally closely related to each other.

To overcome this constraint, correlative light and electron microscopy (CLEM) could be used; the precise location of the graft interface can be determined by light microscopy (LM) in scions and rootstocks transformed with different fluorescent proteins, and its ultrastructure studied by EM. Correlative light and electron microscopy approaches have been developed for several model organisms, but usually not for plant tissues. So far only one protocol has been described to study *Arabidopsis thaliana* root tips (Marion *et al.*, 2017). This protocol is based on either High Pressure Freezing (HPF) or Tokuyasu techniques followed by acrylic resin GMA (Glycol Methacrylate) embedding. This resin has the advantage of being hydrophilic and maintaining around 5 % of water in the sample, thus it could maintain the structure and properties of fluorescent proteins. However, handling this resin is not particularly user-friendly, it is very long and tedious, and the resin is fragile under EM so that it is impossible to do electron tomograms.

Here, we describe in detail a first protocol to get access with a very high reliability to the ultrastructure of the graft interface of the model plant A. thaliana based on the in-resin fluorescence CLEM methods published by Kukulski et al. (2012) that we adapted for plant samples. We grafted a scion and a rootstock expressing different fluorescent proteins (yellow fluorescent protein (YFP) and

red fluorescent protein (RFP) respectively) fused to the cell specific, endoplasmic reticulum retention HDEL sequence. We were able to preserve both YFP and RFP signal during sample processing. With CLEM, it was then possible to localize precisely the graft interface in both LM and EM. Moreover, our protocol is compatible with immunolocalization and electron tomography.

Materials and Reagents

A. Plant Culture

1. Eppendorf 1.5 mL tubes (Sarstedt, catalog number: 72.708)
2. Bleach (Orapi Europe, 'Pastilles chlorées effervescentes', catalog number: OR0011) (See recipe 1)
3. 12 N or 37 % Hydrochloric acid (Carlo Erba, catalog number: 524526)
4. Eppendorf 1.5 mL tube rack (Ratiolab cardboard grid, inserts for cryobox, catalog number 5020147)
5. Square plastic culture plates for *A. thaliana* seedlings vertical culture (VWR, catalog number: 391-0444)
6. Murashige and Skoog (MS) medium + vitamins (Duchefa Biochemie, catalog number: M0222.0050) for seedlings
7. Plant agar for seedlings culture and grafting (Duchefa Biochemie, catalog number: P1001.1000)
8. Culture medium for seedling (see Recipe 2)
9. Water medium for grafting (see Recipe 2)
10. Anapore tape (Euromedis, catalog number:135320) to seal culture plates

B. Plant grafting

1. Round petri dishes 90x14.2mm for grafting (generally used for bacterial culture) (VWR, catalog number 391-0439)
2. Neutral Nylon Membrane Hybond-N (GE Healthcare, catalog number: RPN 203 N)
3. Paraffin films (Bemis, Parafilm 'M') cut into strips of approximately 1 cm wide to seal the petri dishes

C. High pressure freezing

1. Cryotubes (VWR, catalog number: 479-1207)
2. Screw top 2 mL tubes (SARDTEDT, catalog number: 72.693)
3. Tooth picks
4. Bovine Serum Albumine (BSA) fraction V (Sigma-Aldrich, catalog number: 05482)
5. Methyl Cyclohexane (MCH) (Merck Schuchardt OHG 85662 Hohenbrunn, Germany)
6. BSA solution for cryoprotection during HPF (see Recipe 3)

7. Distilled water to cut sample

8. Membrane carriers (100 µm deep with a diameter of 1.5 mm) (Leica Microsystems, catalog numbers: 16707898)

D. Freeze substitution

1. Screw top 2 mL tubes (SARDTEDT, catalog number: 72.693)

2. Disposable regular pipettes 1, 2 and 3 mL (VWR, catalog number: 612-2850, 612-2851 and 612-1681) and Freeze Substitution specific 1 mL pipettes with thin tips (Ratiolab, catalog number: 2600155)

3. Wheaton glass sample vials with snap-cap for cryomix preparation (DWK Life Sciences, WHEATON, catalog number: 225536.)

4. Personal cartridge half mask 6100 (Honeywell International, catalog number: 1029471)

5. Aluminum foil

6. Uranyl acetate powder (Merck, catalog number: 8473)

7. Pure methanol (Fisher Scientific, catalog number: M/4062/17)

8. Ultra-pure 100 % ethanol and acetone (VWR, catalog numbers: 83813.440 and 20066.558, respectively)

9. Colored nail polish (color does not matter)

10. Reagent containers 12.5 mL with screw caps (Leica microsystems, catalog number: 16707158)

11. Cryosubstitution Uranyl-acetate stock solution (20 %) (see Recipe 4)

12. Cryosubstitution mix (see Recipe 5)

13. HM20 resin (Electron Microscopy Sciences, catalog number 14345)

14. HM20% solutions (see recipe 6)

15. Reagent bath (Leica microsystems, catalog number: 16707154)

16. Plastic mold 'Flow-through rings' (Leica microsystems: 16707157)

E. Ultramicrotomy

1. Crystalizing dish (Fisher Scientific, catalog number: 11766582) Manufacturer: DWK Life Sciences, DURAN, catalog number: 213133408.

2. Fast absorbent paper filters (Whatman, Filter papers 41) (GE Healthcare, catalog number: 1441-070)

3. Glass rods (Fisher Scientific, catalog number: 12441627) Manufacturer: MBL, catalog number: SRF380.

4. Grids with 200 L/inch square mesh Fine Bar (Electron Microscopy Sciences, catalog number: G200HS-Cu) to coat with parlodion or commercial grids with formvar (Electron Microscopy Sciences, catalog number: FCFT200-CU)

5. Razor blades for coarse block preparation (Electron Microscopy Sciences, catalog number: 71990)
6. Pasteur pipet (VWR, catalog number: 612-1720)
7. 0.2 µm Syringe filter (VWR, catalog number: 514-0061)
8. 10 mL Syringe (Terumo, catalog number: SS+10ES1)
9. Solid parlodion (Electron Microscopy Sciences, catalog number: 19220) Isoamyl-acetate (Sigma-Aldrich, catalog number: W205532)
10. Toluidine blue powder (Sigma-Aldrich, catalog number: T3260)
11. Sodium Borate powder
12. Ultrapure (MilliQ) water
13. 2 % Parlodion solution for grid filming (see Recipe 7)
14. Toluidine blue solution (see Recipe 8) for screening block sections on table top microscope during resin block milling

Equipment

A. Plant culture
   1. Desiccator used as hermetic chamber
   2. Fume hood
   3. Glass crystalizing dish
   4. Fridge for vernalization
   5. -80 °C Freezer for sterilization

B. Plant grafting
   1. Dissecting microscope with a minimal working distance of 5 cm (Leica Microsystems, model: Leica MZFLIII)
   2. Glass beaker for sterilization of tools with ethanol
   3. Spray for ethanol
   4. Dissecting Microknives 15° 5 mm (Fine Science Tools, catalog number: 72-1551)
   5. Precision tweezers (EMS style 5X, catalog number: 78320-5X (soft) and 78520-5X (hard))

C. High Pressure Freezing
   1. Liquid nitrogen, liquid nitrogen container and adapted personal protection gear
   2. Air compressor (JUN-AIR)
   3. Leica EM-PACT1 machine (Leica Microsystems)
   4. Leica loading system
   5. Pod holders (Leica, catalog number: 16706832)
   6. Pods (Leica, catalog number: 16706838)

7. Regular biomolecular pipettes from 2 µL to 1,000 µL range
8. Binocular with transmission illumination for root dissection (Nikon, model: SMZ-10A)
9. Heating surface for quick drying of Pods and pod holders during the session
10. Insulated tweezers for manipulation in liquid nitrogen (VOMM Germany, 22 SA ESD)
11. Metal containers for frozen sample transfer and associated screw driver for lifting procedures (provided with EMPACT1)
12. Torque screwdriver (TOHNICHI, Torque driver RTD60CN) set to 30 N.cm

D. Freeze-substitution
1. Leica Automatic Freeze Substitution AFS2 (Leica Microsystems, model: Leica AFS2)
2. Leica Freeze Substitution Processor FSP (Leica Microsystems, model: Leica FSP)
3. Metal socket for mold containers
4. Micro needles for separating the membrane carriers from frozen samples (Micro needle 0.025 mm, Electron Microscopy Science, catalog number 62091-01 and Micro needle 5 µm, Ted Pella, catalog number: 13625)
5. Ventilated fume hood

E. Ultramicrotomy
1. Block holders
2. Diamond trimming knife for first milling steps to reach the sample (Drukker 8 mm Histoknife Dry, discontinued)
3. Diamond knives Trim20 dry (Diatome, catalog number: DTB20), Ultra wet 45° (Diatome, catalog number: DU4530) and Histo wet (Diatome, catalog number: DH4560)
4. ELMO Glow discharger (optional) (CORDOUAN Technologies)
5. Grid carriers for grid storage
6. Leica Ultracut UC7 (Leica Microsystems, model: Leica Ultracut UC7)
7. Table top microscope (Olympus, model: CX-41)
8. Precision weight scale for parlodion weighting (Sartorius, model: TE124S)

F. Confocal Microscopy
1. Sensitive Confocal microscope equipped with spectral detector (Zeiss Microscopy, model Zeiss LSM 880) and 63x NA 1.4 oil immersion objective.

G. Electron Microscopy
1. FEI Tecnai G2 Spirit 120 kV equipped with Eagle 4Kx4K High sensibility CCD Camera
2. FEI Standard Single Tilt Holder (FEI, catalog number: 5322 695 15868)
3. Advanced Tomography Holder (Fischione instruments, model 2020)

Software

1. Zeiss Zen Dark software (https://www.zeiss.com/microscopy/int/products/microscope-software/zen.html) used for confocal acquisition.
2. Tecnai imaging and analysis (TIA) software (https://www.fei.com/software/) TEM User Interface was used in conjunction with Tecnai Imaging and Analysis (TIA) software to control and acquire micrographis with the EM (https://www.fei.com/software/)
3. Xplore3D (FEI) was used for automated tilt series acquisitions (https://www.fei.com/software/)
4. ImageJ (https://imagej.nih.gov/ij/download.html) with the Bio-Format plugin (https://www.openmicroscopy.org/bio-formats/) to open and process the Zeiss .czi files and to open the .mrc tilt series files and tomograms.
5. IMOD suite (http://bio3d.colorado.edu/imod/). All processing of tomograms was done using the IMOD suite (Kremer *et al.*, 1996) from the alignment of the tilt series to tomogram reconstruction.
6. For visualization purpose only, Adobe Photoshop is used for TEM mosaic assembling using photomerge function and coarse correlated view of confocal and TEM using layers and blending mode superposition.

Procedure

A. Plant Grafting

The *A. thaliana* hypocotyl grafting procedure is adapted and simplified from the 'two Segment Shoot-Root Graft' part of the protocol of Melnyk (Melnyk, 2017a). Finding the good level of humidity is the trickiest part of Melnyk's protocol, thus we replaced the water-soaked whatmaan paper by a water-based agar medium that maintains a constant humidity from several days after grafting. To target the graft interface with CLEM, we decided to use the endoplasmic reticulum retention signal HDEL, expected to not move from one partner to the other, labeled with a different fluorescent protein for each partner (i.e. YFP and RFP) (Dean & Pelham, 1990; Knox *et al.*, 2015). The plant should have a strong fluorescent signal as it will be partially degraded during the protocol. For other projects, different lines could also be used depending on the mechanisms, tissues (e.g. vessels) and organelles (e.g. mitochondria, plastids and nucleus) studied

1. Plant culture
    a. Sterilize *A. thaliana* seeds with chlorine gas (adapted from Iii et *al.*, 2017).

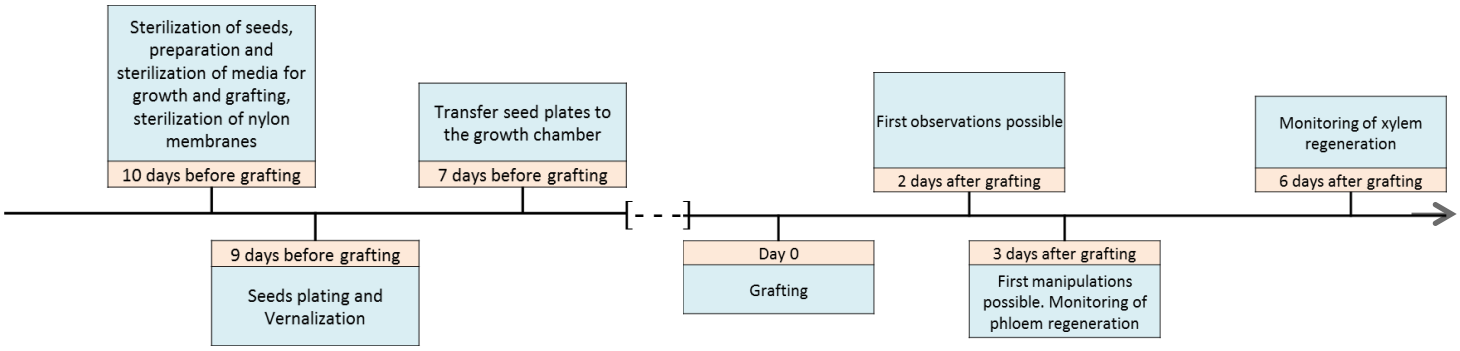

Figure 2. Workflow of grafting experiments

i. Aliquot a small amount of seeds (around 100 to 150) into a 1.5 mL centrifuge tube labeled with a permanent pen (covered in adhesive tape to avoid washing off of the ink), close the caps and place them for 20 min in a -80 °C freezer (Figure 1A).

ii. The sterilization will take place in a hermetic chamber, typically a glass desiccator, under a fume hood. In the desiccator, place a small glass crystalizing dish containing 50 mL of bleach solution (see recipe 1) (Figure 1C and D).

iii. Place the uncapped centrifuge tubes in a tube rack in the chamber, add 1.5 mL of 12 N chloridric acid into the crystalizing dish and quickly close the chamber. The yellow haze of chlorine gas should be visible at this point (Figure 1B, D and E).

iv. Incubate the seeds for at least 4 h, or overnight (e.g. 6 pm-9 am). Note that if the seed germination is affected, shorter time (from 1 to 3 h) should be preferred. Open the chamber and close the centrifuge tube.

v. Leave the chamber open under the fume hood until the reaction between chloridric acid and bleach ends. The reaction produces chlorine gas, sodium chloride and water as products. You can then dispose the solution.

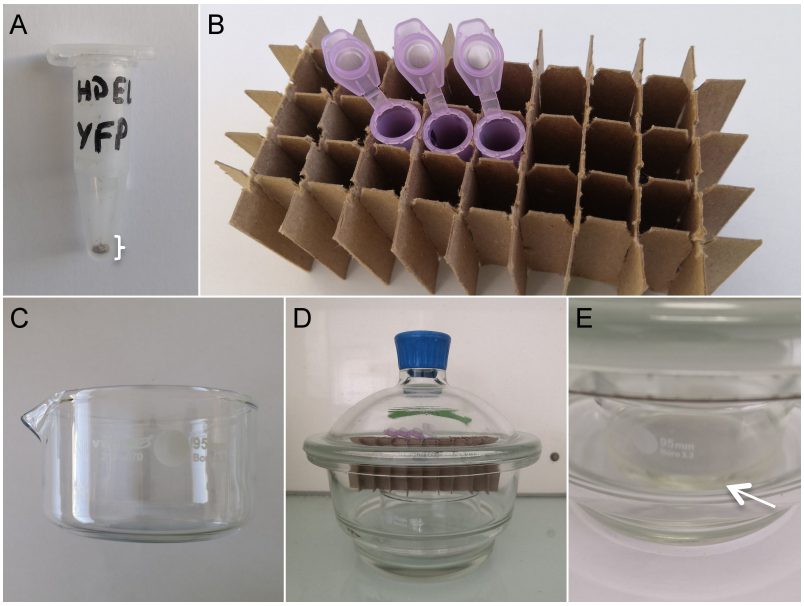

Figure 1. Seed sterilization procedure
(A) Appropriate amount of seeds in a 1.5 mL Eppendorf tube to have a proper sterilization. **(B)** For gas sterilization, place them open in a tube rack. **(C)** Glass crystalizing dish to use to put bleach inside the hermetic chamber. **(D)** Hermetic chamber with glass dish, tube rack and open Eppendorf tube containing seeds. **(E)** When mixing bleach with chloridric acid, the solution becomes yellow (white arrow), a faint yellow haze of chloride gas can be also visible

b. Under a laminar flow hood, plate the sterilized seeds on half concentrated MS medium with vitamins. Label the plates with the stock name, date and all pieces of information you may need (your name, culture medium, etc.). Gently sprinkle the seeds over the plates. Thanks to chloride gas sterilization, homogeneous distribution of the dry seeds is easily achieved.

c. Leave the plates at 4 °C in the dark for 2 to maximum 5 d for vernalization and stratification.

d. Transfer the plates to a growth chamber regulated at 20-23 °C with photosynthetic photon flux density (PPFD) of 100 µmol.m^{-2}.s^{-1} of light. Put the plates vertically so that the hypocotyls grow as straight as possible. Note that short day growing conditions (such as 8 h light per day) give rise to more elongated and thinner hypocotyls, which facilitate grafting procedure and microscopy experiments. Once the two first leaves can be slightly distinguished under the binocular microscope, grafting can be done. In general, seedlings grown under short or long day growing conditions (8 h and 16 h of light) have to be 7 or 5 days-old respectively. At all times, you need to monitor plant growth to graft at the more appropriate time.

2. Grafting

The absence of sucrose in the culture and grafting media makes it possible to graft in non-sterile conditions if you do not plan to keep the grafts *in vitro* for more than 6 d. Nevertheless, it is recommended to work on a 70 % ethanol pre-cleaned bench with sterilized tools to limit contamination.

The dissecting microscope used must allow you to work both with a low and a higher magnification (between 6x and 20x is a convenient compromise) and have a sufficient working distance, not less than 5 cm to have enough space for the manipulations required. We recommend using an anular illumination system which provides a homogeneous light during the grafting process. When performing grafting, as it is tedious and needs to be very precise and quick, you should be as calm as possible, try to avoid coffee or other stimulants before attempting grafting experiments. After practicing, the grafting technique presented here allows you to reach a success rate around 80 to 90 % with a speed of 70 grafts per h.

a. Before grafting, prepare and autoclave grafting medium with 1.6 % phytoagar and distilled water, buffer the medium to pH 5.8 with 1 N KOH. Under a laminar flow hood, before the medium cools fill ther petri dishes with approximately 20 mL of Agar. For each plate, cut nitrocellulose membrane in pieces of 2x5 cm, wrap them in aluminum foil before autoclaving. The membrane is used as a cutting surface. It is convenient to cut on it without damaging the expensive microknife. You will be able to do 10-12 grafts in each box.

b. Just before grafting, gather plants, petri dishes, microknives, forceps, nylon membranes, permanent pen and strips of parafilm (Figure 3). Clean the dissecting microscope, microknives and forceps by spraying 70% ethanol and allow them to dry completely before using them. Carefully label your petri dishes with the lines you will use as the scion and rootstock. Put a piece of Nylon membrane in each box.

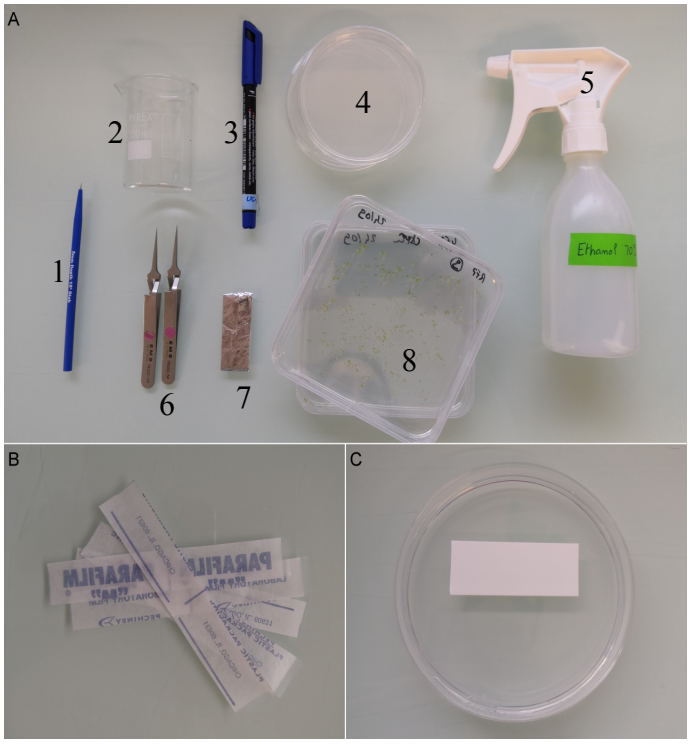

Figure 3. Grafting tools
(A) 1. dissecting microknife for grafting, 2. glass beaker for sterilization of tools, 3. Permanent marker to label petri dishes, 4. round petri dishes for grafting, 5. Spray with ethanol for tools and bench cleaning, 6. Fine tweezers, 7. Sterile nylon membrane wrapped in aluminum foil, 8. Plants to graft. **(B)** Parafilm strips to seal petri dishes after grafting. **(C)** Positionning of nylon membrane prior to grafting

c. Optional, but highly recommended, if the expression of your tag is not homogeneous in your plants, select plants that have the strongest fluorescence signal.

d. Then, carefully select the best plants for grafting: homogeneous size, hypocotyls as straight as possible and cotyledons not bent over hypocotyls (Figure 4A). Put them in a row on the membrane (Figure 4B and C). To move them you can use the forceps, taking the plant by a cotyledon or simply sticking to it without pinching it. In all cases you have to avoid ANY damage to the hypocotyl, shoot and root. If you want to use the two genotypes as scion or rootstock, you will put six plants of the first genotype in a row with six plants of the second genotype (Figure 4B). Scion will be prepared from the two genotypes as described in the following e. part. If you are interested in using a genotype only as scion and the other only as rootstock, you have dispose

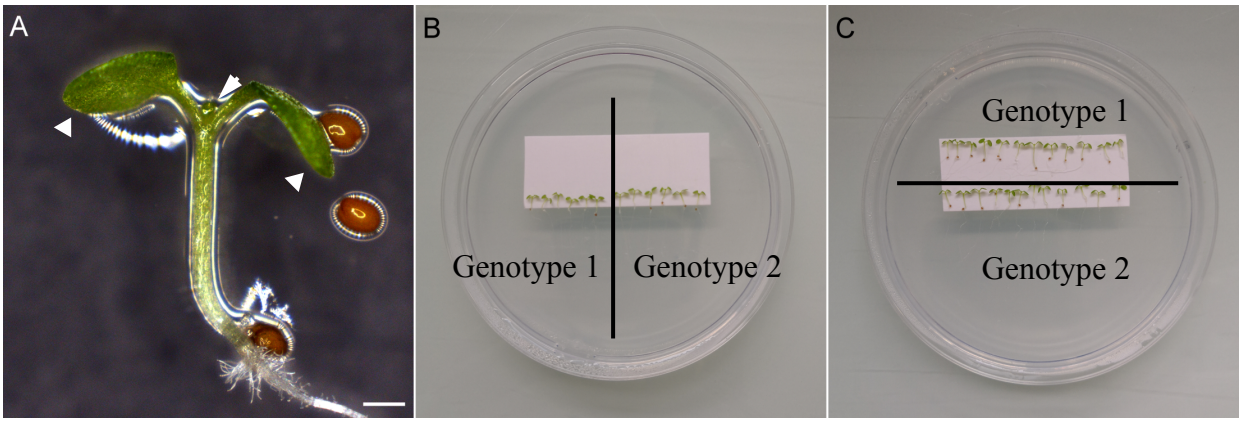

Figure 4. Ideal plant to graft and positionning of plants in petri dish prior to grafting
(A) An ideal *Arabidopsis thaliana* seedling for grafting has a straight hypocotyl, very small first leaves and cotyledon not bent over the hypocotyl. **(B)** When interested in keeping both direction of grafting (genotype 1/genotype 2 and genotype2/genotype1), a 6/6 graft scheme can be used. Scions and rootstocks will be prepared, cut and exchanged between the two genotypes. **(C)** When interested in only one direction of grafting (genotype 1/genotype 2 as above), a 12/12 graft scheme can be used. The top row (genotype 1) contains scions, their roots will be cut and discarded. The bottom row (genotype 2) contains rootstocks, their apical part will be cut and discarded. Scions prepared from genotype 1 will be moved and grafted to rootstocks from genotype 2
Scale bar: 500 µm

the plant in two rows of 12 plants (Figure 4C). Scion will be prepared from the top row while rootstock will be prepared from the bottom row as described is the following e. part.

e. Preparation of scions and rootstocks: under a cleaned dissecting microscope, cut off and discard one cotyledon (choose the smallest, most damaged or cotylon bent over the hypocotyl) to allow the seedling to lie flat on the membrane. Cut transversally through the hypocotyl just under the cotyledons without crushing the plant to obtain a cut shoot to use as a scion and a cut hypocotyl plus root to use as a rootstock. Avoid cutting too low in the hypocotyl to prevent adventitious root development on the scion and graft abortion (Figure 5A – E).

f. Take the scion from a plant by the petiole of the cut cotyledon and place it close to the rootstock from another plant. As the cut rootstock is very fragile and easy to damage, we recommend you do not move this part if possible, or do so very carefully with the tip of closed forceps. Assemble the graft by gently pushing the cut scion against the cut rootstock with the closed forceps (Figure 5F, G and H).

The moisture level is crucial during graft union formation, compared to Melnyk's protocol in

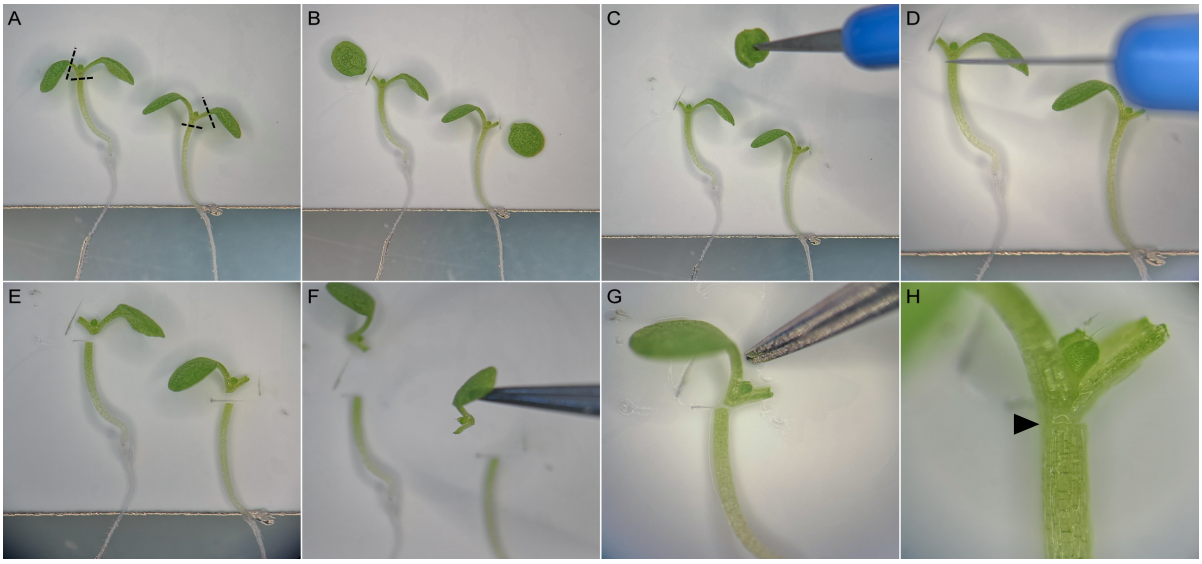

Figure 5. The step-by-step procedure of grafting
The two plants are disposed side by side on a nylon membrane and one cotyledon of each plant is cut along the black dashed lines **(A and B)** and then discarded **(C)**. Hypotocyls are cut just bellow the petiole of cotyledons **(D and E)**. Scions are exchanged between plants by sticking then to the tip of the tweezers **(F)**. Scion is carrefully brought close to the rootstock with the tip of the tweezers **(G)**. When properly grafted, the graft junction (black arrowhead) is barely visible **(H)**.

which water must be adjusted permanently by adding or removing sterile water on the Whatman papers, here, grafting onto grafting medium (water with 1.6 % agar) keeps the moisture level constant and allows us to keep the grafts *in vitro* long time after grafting.

g. Repeat d. and e. steps until all the plants on the plate are grafted. To save time, you can do this in a row: (1) cut and discard one cotyledons on each seedling, (2) then cut all the shoots, (3) move them next to the prepared rootstocks, (4) align and push the scions onto the rootstocks.

h. When grafting is done, be very cautious with the plate to avoid the scion falling off the rootstock. Close the lid and seal the plate with a Parafilm strip. You can label the plate with the time you ended grafting so that you know the age of the graft. If you have several plates, clean the dissecting microscope, forceps and knife with 70 % ethanol every 1 or 2 plates and let dry. Carefully put the plate vertically back to the growth chamber at 20-23 °C in PPFD of 100 $\mu mol.m^{-2}.s^{-1}$ light in either short- or long-day conditions.

i. If you grafted properly, you can begin to manipulate your graft (i.e. observing it under a microscope, fix tissues, transferring it to a new medium, etc.) from 48 h after grafting. After 3 d, the grafts become slightly more robust as phloem should be connected. After 6 to 7 d, xylem is connected and the grafted plant becomes quite robust.

j. When beginning grafting experiments you may need to assess your grafting success rate at first. You can rely on several criteria to evaluate grafting success (Melnyk, 2017b) such as the resumption of root growth, usually with emergence of lateral roots, and the absence of adventitious root formation in the scion. You can also monitor the phloem connection by grafting scions expressing pSUC2::GFP (i.e. green fluorescent protein (GFP) under the phloem-specific SUC2 promoter) and observing the movement of GFP to the rootstock, or by applying arboxyfluorescein diacetate (CFDA) to the scion or rootstock to evaluate phloem and xylem connectivity as described in the Melnyk's protocol (Melnyk, 2017b).

B. CLEM

1. High Pressure Freezing (HPF)

a. High Pressure Freezing was done using Leica EM-PACT1. A detailed protocol to use this machine is available in Nicolas' protocol (Nicolas *et al,.* 2018). With the EM-PACT1, we used the 100 µm deep carriers that involve to fix thin enough samples to fit in them. We recommend you to process all your samples of one condition as a batch, before to fix the next one. It will help you to avoid mixing up the different grafts.

b. If your samples are thicker than 100 µm, you will have to use a deeper carrier. With the 200 µm-deep carriers for EM-PACT1 we lost a lot of our samples and therefore to use 200 µm-deep carriers, we used the Leica HPM100.

2. Freeze Substitution (FS)

Our FS and embedding protocol is based on the protocol published by Kukulski et al., 2012 ; it was initially designed for yeast and mammalian cells but we have adapted it for our plant tissues (Table 1).

In comparison to a standard FS protocol, osmium tetroxyde and glutaraldehyde are avoided to preserve fluorescence of the YFP and mRFP without the autofluorescence background (Biberfeld *et al.*, 1974; Watanabe *et al.*, 2011). 0.1 % uranyl acetate during the first 44 h of FS can give enough contrast with the electron lucent HM20 resin. The properties of polymerization at -50 °C of HM20 allow us to limit the use of fixative agents. In comparison to Kukulski *et al. (2012),* for our plant samples, shorter FS and embedding time is convenient and can help to maintain fluorescence properties of fluorescent proteins. We recommend starting the FS either on Mondays or Tuesdays so all steps requiring handling could be finished either Thursdays or Fridays (table 2).

Table 1. Plant correlative light electron microscopy – freeze substitution program compared to plant freeze substitution and yeast correlative light and electron microscopy- freeze substitution

A. Standard plant freeze substitution (Nicolas *et al,*. 2018)			B. Yeast CLEM freeze substitution (Kukuski *et al,*. 2011)			C. Plant CLEM freeze substitution		
Media	Temperature	Duration	Media	Temperature	Duration	Media	Temperature	Duration
FS mix: Uranyl acetate 0,1 %, Glutaraldehyde 0,5 % OsO4 2 % in Acetone 100 %	-90 °C	48 h	FS mix: Uranyl acetate 0,1 % in Acetone 100 %	-90 °C	48 h	FS mix: Uranyl acetate 0,1 % in Acetone 100 %	-90 °C	30 h
FS mix: Uranyl acetate 0,1 %, Glutaraldehyde 0,5 % OsO4 2 % in Acetone 100 %	-90 °C to -50 °C	13h20	FS mix: Uranyl acetate 0,1 % in Acetone 100 %	-90 °C to -45 °C	9 h	FS mix: Uranyl acetate 0,1 % in Acetone 100 %	-90 °C to -50 °C	13h20
3 washes in Acetone 100 %	-50 °C	10 min/each	3 washes in Acetone 100 %	-45 °C	10 min/each	3 washes in Acetone 100 %	-50 °C	10 min/each
3 washes in EtOH 100 %	-50 °C	10 min/each	HM20 10 % in Acetone	-40 °C	4 h	3 washes in EtOH 100 %	-50 °C	10 min/each
HM20 20 % in EtOH	-50 °C	2 h	HM20 25 % in Acetone	-35 °C	4 h	HM20 20 % in EtOH	-50 °C	2 h
HM20 50 % in EtOH	-50°C	2 h	HM20 50 % in Acetone	-30 °C	4 h	HM20 50 % in EtOH	-50 °C	2 h
HM20 75 % in EtOH	-50 °C	15 h/Overnight	HM20 75 % in Acetone	-25 °C	4 h	HM20 75 % in EtOH	-50 °C	15 h/Overnight
HM20 100 %	-50 °C	2 h	HM20 100 %	-25 °C	10 h	HM20 100 %	-50 °C	2 h
HM20 100 %	-50 °C	2 h	HM20 100 %	-25 °C	10 h	HM20 100 %	-50 °C	2 h
HM20 100 %	-50 °C	8 h	HM20 100 %	-25 °C	10 h	HM20 100 %	-50 °C	6 h
		93h20min			**103h30**			**73h20min**

Table 2. Timetable of the cryo-fixation and freeze substitution for plant correlative light and electron microscopy

<table>
<tr><th></th><th>Monday</th><th>Tuesday</th><th>Wednesday</th><th>Thursday</th><th>Friday</th><th>Saturday</th><th>Sunday</th></tr>
<tr><td>Early morning</td><td rowspan="3">High Pressure Freezing of samples</td><td rowspan="4">Ongoing Freeze Substitution (-90 °C)</td><td rowspan="2">Ongoing Freeze Subsitution (transition from 90 °C to -50 °C)</td><td>1st HM20 100% for 2 h (-50 °C)</td><td rowspan="3">Ongoing UV polymerization for 24 h at -50 °C</td><td rowspan="2">Ongoing UV polymerization for 12h at 20 °C</td><td rowspan="4">Preservation of samples in the AFS chamber at -20 °C until next Monday</td></tr>
<tr><td>Late morning</td><td>2nd HM20 100% for 2 h (-50 °C)</td></tr>
<tr><td>Noon</td><td>3x Rising with Acetone, 3x with Ethanol (-50 °C)</td><td rowspan="2">3rd HM20 for 6 h (-50 °C) and setting up AFS and FSP for UV polymerization</td><td rowspan="2">End of polymerization and preservation of samples in the AFS chamber at -20 °C until next Monday</td></tr>
<tr><td>Early afternon</td><td>Separatation of samples from carrier and start of embedding (-50 °C)</td></tr>
<tr><td>Late afternoon</td><td>Freeze substitution : sample in cryomix for 30 h (-90 °C)</td><td>Continue embedding until 75 % HM20 overnight (-50 °C)</td><td>UV polymerization for 24 h at -50 °C</td><td>UV polymerization for 12h at 20 °C</td></tr>
</table>

a. Under a flow hood, prepare the cryomix (see recipe 5) in a glass sample vials with snap-cap. Close it before transferring it to the Automatic Freeze Substitution (AFS) chamber set to -90 °C and wait until it cooled down for 20 min.

b. During the cooling, prepare Leica plastic reagent baths for each type of samples you have from the HPF. You can label them on the outside using colored nail polish.

c. When mix is cooled, distribute it in the baths.

d. Transfer your frozen sample to the chamber and put them in the cryomix.

e. After 30 h FS in the cryomix, samples are washed 3 times in pre-cooled pure acetone and then 3 times in pre-cooled pure ethanol in the AFS chamber for at least 10-20 min.

f. Samples can be then removed from the metal carriers using thin needles and transferred to the plastic mold 'flow-through' for impregnation and polymerization. A step-by-step guide and illustration of this procedure is described in Nicolas et al., 2018.

g. For our protocol, we reduced also polymerization time under UV to limit photobleaching. A polymerization time of 24 h at -50 °C followed by 12 h at 20 °C get resin blocks hard enough for ultra-microtomy. If you started as recommended on Mondays or Tuesdays, polymerization will begin on Thursday or Friday and will continue over the week end. The samples are then stored at -20 °C in the Leica AFS chamber for the end of the week (Table 3). If your samples are not well impregnated, HM20 resin concentration can be increased progressively (i.e. 10 % by 10 %) and the total length of this step could be increased by a few h.

A. Standard plant freeze substitution (Nicolas *et al,*. 2018)		B. Yeast CLEM (Kukulski *et al.,* 2011)		C. Plant CLEM freeze substitution	
Temperature	Duration	Temperature	Duration	Temperature	Duration
-50 °C	24 h	-25 °C	48 h	-50 °C	24 h
20 °C	24 h	20 °C	48 h	20 °C	12 h
				-20 °C	Stay

Table 3. Standard plant freeze substitution (A) vs. Correlative Light Electron Microscopy (CLEM)-FS polymerization programs for yeast (B) and plant (C)

h. After polymerization, the samples should be stored at -20 °C in a freezer, protected from light and processed within a few weeks or months. We noticed that for our 1 to 2 year old graft samples, the YFP signal tends to be weak or even completely bleached, while the RFP signal seems to be better preserved. In our opinion the preservation time greatly depends on the fluorescent protein used, but also on the signal intensity before sample processing and probably the type of tissues and the labeled organelles.

3. Ultramicrotomy.

As samples are embedded in HM20, sections need to be harvested on film-coated grids. A detailed protocol of grid filming and resin block preparation is described in Nicolas et al., 2018. We recommend working with 200 square mesh copper grids with thin bars that give a good compromise between the field of view and the robustness. Also, working with square meshes is more suitable than hexagonal ones for correlation under the microscope. During the sample trimming step, thick sections of 500 nm are periodically harvested and stained with toluidine blue until the region of interest is reached. For an optimal balance between resolution under EM and signal quantity under confocal microscope, sections of 150 nm thick work best with our 120 kV EM. The thicker the sections are, the more you will have fluorescence under the confocal microscope, but at the same time the section will become less electron lucent and you will degrade the signal-noise ratio and the resolution under EM. If your fluorescence signal is very intense, you can reduce the thickness of sections and if you have access to an EM with a greater high voltage (such as 200 kV), you will be able to work with thicker sections (up to 200 nm). To study small structures, such as plasmodesmata, you should consider doing electron tomography that will reveal a high three dimensional level of detail and restore the contrast leading to a very high resolution.

Under the microtomes, at all time, you should work with as little light as possible, and protect the block for direct light when not cutting. When sections are done and harvested on parlodion filmed copper grids, they need to be processed as quickly as possible. If possible, prepare grids the same day of confocal observations to avoid loss of fluorescence due to photooxidation. Nevertheless, in case you prepared your sections in advance, we recommend that you store them at -20 °C in the dark to slow the photooxidation reactions. Allow the sections on the grid to dry completely to ensure a perfect adhesion between the section and the parlodion film before making microscopy observations, otherwise the sections can move off the grid during the transfer from LM to EM, making the following correlation step more complicated.

4. Confocal microscopy.

For LM, as signal in the sections will be low, you need to use a very sensitive detector such as GaSP detector (instead of the conventional PMT) or a spectral detector. Moreover, you will have to work with high numerical aperture objectives, which are usually oil-immersion and high magnification, thus, you will have to mount your samples between a slide and coverslip. You should have a motorized stage and consider doing Z stack to acquire all the information possible in your section. Also, to facilitate correlation and be sure to observe the same region of interest, doing a tiles scan (to have an overview with good resolution) and acquiring the transmission image will help.

a. Glow discharge.

This step is not mandatory but could help a lot to prevent air bubbles when mounting your grids between slide and coverslip. As both HM20 resin and parlodion film are hydrophobic, grid mounting for LM is hard and subjected to the formation of many air bubbles that disturb imaging due to changes in the refraction index. Glow discharge your grids one-by-one, just before the confocal observation as the effect will last only about 30 min.

i. Turn on the glow discharge system.

ii. Clean the glow discharge chamber by doing a cycle without microscopy grids (only the glass slide that will be used as a support for EM grids). Place glass slide inside the vacuum bell and close the chamber. Close the air valve and let the pressure goes down to $2*10^{-1}$ mbar. Press the High Voltage button and adjust the voltage until the current reaches 15-20 mA. Maintain the high voltage during 30 s. gradually remove the vacuum by opening very carefully the air valve to avoid a too high depressurization.

iii. Repeat the step ii., this time with your grid inside the chamber and maintain the high voltage for 1 min.

b. Montage of grids for confocal microscopy to prevent air bubbles (Figure 6A-F)

For this step, we recommend using inverted forceps (that close automatically).

i. Take your grid out of the grid box with forceps and place the forceps on the table.

ii. With a syringe and a 0.2 µm filter, put a drop of water on a cleaned microscope slide.

iii. Approach a coverslip vertically until it touches the water drop.

iv. Carrefully take the forceps and dip the grid into the drop of water between the slide and the coverslip. Release the grid from the forceps and with the tip, hold the grid on the slide and lay down the coverslip on the forceps.

v. Release the grid from the tip of the forceps and use it as a guide to slowly place the coverslip.

vi. Remove the excess of water with blotting paper or paper towels. You can now place the slide under the LM.

c. Removal of the EM grid (Figure 6G-L)

Long observation under confocal microscope can lead to evaporation of the water between slide and coverslip with a risk of the EM grid to sticking to the glass. This can greatly increase the chance of breaking the parlodion film and the sample when trying to remove the grid. To remove the coverslip

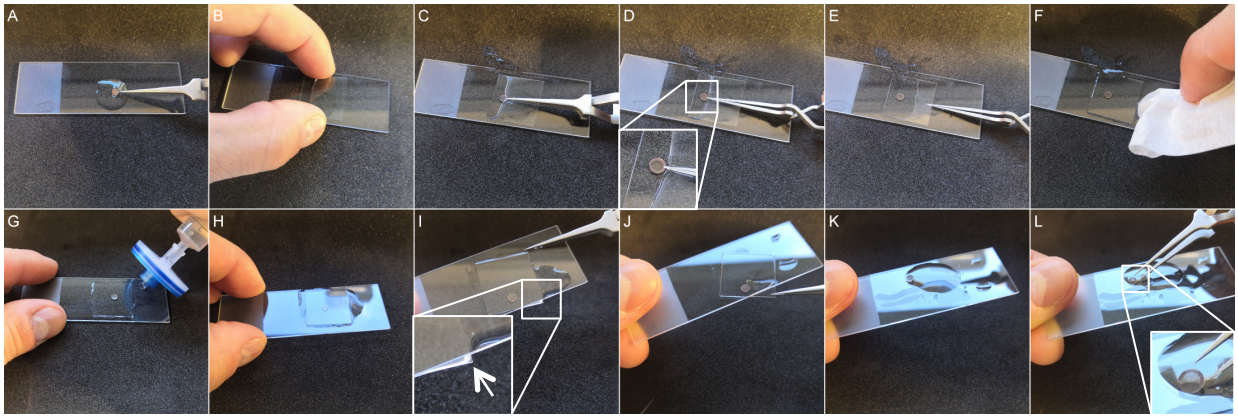

Figure 6. Mounting and unmounting of the Transmission Electron Microscopy (TEM) grids for Light Microscopy (LM) observation

(A – F) Mounting of the TEM grids. **(A)** Prior to observation, the slide is cleaned with ethanol to get rid of dust that can pollute the TEM grids. After that put a drop of filtered water with a syringe, you can wet the TEM grids on both sides so it will be easier to dip it into water later. Position the ultrathin section on the side of observation to visualize fluorescence signal even where they are bars from the TEM grid. **(B)** Approach the coverslip until it touches water. **(C)** Place carefully the grid between glass slide and coverslip with very thin forceps. Avoid air bubbles formation at the surface of the grid by plunging the grid into water. **(D)** Release the grid from the forceps and hold the grid in the water with the tip of the forceps so the grid does not move when lying down the coverslip. **(E)** Release the grid from the tip and use the tip as a guide to slowly place the cover slip. **(F)** Finally dry the excess of water with blotting paper prior to imaging.

(G-L) Unmounting the TEM grids **(G and H)** Add filtered water with a syringe at the side of the coverslip and wait few minutes **(I)** The excedent water permits to detach easily the coverslip from the glass slide. Tilt slowly the glass slide until a corner of the coverslip is outside the slide. **(J)** Remove very carefully the coverslip. At this step, there should be no resistance to avoid breaking the parlodion film. **(K-L)** Add more filtered water until the TEM grids unstick from the slide before taking it with the forceps.

without breaking the film, put water with the syringe (and filter) at the side of the coverslip and take the grid out with the forceps. If a grid is stuck against the glass, put a drop of water on top of it and gently take it off with the tip of forceps. The grid should now float on a water drop on the slide. Dry the grids with blotting paper and put it back in the grid box for subsequent EM observations. Be sure to remember on which side of the grid your sample is so you can observe the same side under EM (otherwise, you will have a mirror image of your sample so the correlation and localization of your region of interest will be much harder). The fluorescence pattern observed under the confocal microscope permits to identify cells under the EM based on their shapes.

Data analysis

This grafting protocol combined with HPF and our FS protocol adapted for CLEM allowed us to preserve fluorescence of the samples together with good ultrastructural resolution. At the graft interface of *A. thaliana*, the origin of the cells now can be determined without any ambiguity thanks to the expression of different fluorescent proteins for each partner (Figure 7A, B and C). Under the EM, different types of cell are identifiable, such as parenchyma cells and sieve elements (Figure 7D). In comparison to standard FS with osmium tetroxyde, lipidic components such as membranes are less contrasted, but still clearly visible (Figure 7F). Moreover, if necessary, to improve the resolution, electron tomography could be applied (Figure 7G, H and I). It restored the contrast quality leading to a very high resolution. Cytoplasm and plasmodesmata observed by conventional EM (Figure 7F) were indistinct, while they appeared much sharper, more highly contrasted and with a higher resolution with electron tomography; details such as membranes of plasmodesmata, clear ribosomes either free or associated with endoplasmic reticulum and small vesicules were clearly visible. Electron tomography permit us to reach a high three dimensional-level of detail for the structures of interest such as plasmodesmata and to study their shapes in three dimensions while this was not possible with conventional EM images (Figure 7J, K and L).

Addionnaly, our protocol is suitable both for super resolution with AiryScan detector, allowing to attribute very precisely the signal observed to the structure of interest such as ER strands and plasmodesmata at the graft interface (Figure 8) and it preserve antigenicity, thus make possible immunolabelling of desired structure for further identification under EM (Figure 9).

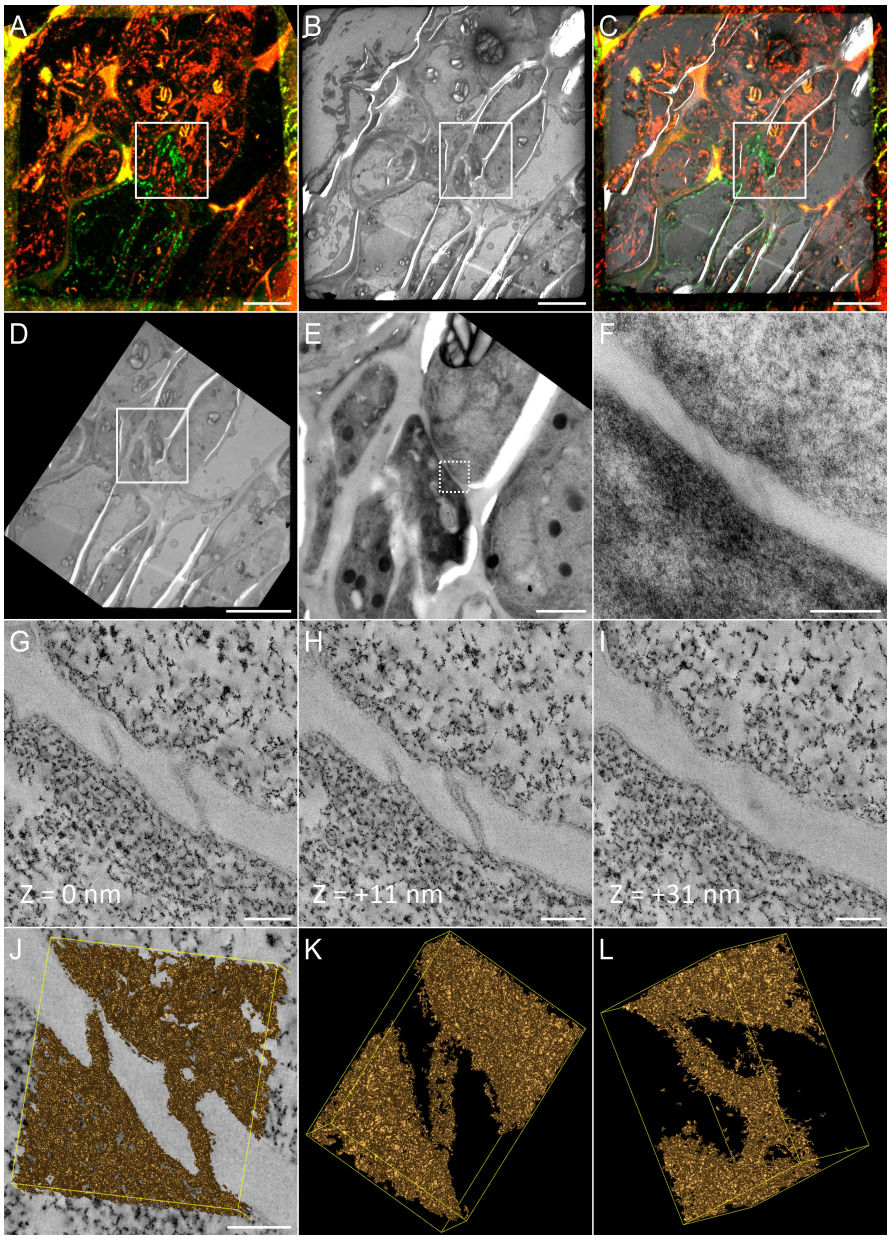

Figure 7. Studying the graft interface of *Arabidopsis thaliana*, from the confocal microscopy to the resolution of three dimensional shapes of nanometric structure: the plasmodesmata (PD)

(A) Z projection of confocal (Airyscan) micrograph of 150 nm ultrathin section of graft interface of 35S::HDEL_mRFP grafted onto 35S::HDEL_YFP. Origin of the cells, *i.e.* scion or rootstock, is easily determined thanks to the fluorescent proteins. **(B)** Overview of the same section in (A) is observed under transmission electron microscope **(C)** Correlated image of confocal and TEM is used for vizualisation and targeting of the graft interface. **(D)** Higher magnification of (B) **(E)** Higher magnification of the region highlighted with a white square in (A, B, C and D). **(F)** Higher magnification of the region highlighted with a white dotted square showing PD visible at the interface between the 2 grafted partners. **(G)** Tomogram of the PD observed in (F) z= 0 nm, **(H)** Tomogram of the PD observed in (F) z= + 11 nm, **(I)** Tomogram of the PD observed in (F) z= + 31 nm, **(J)** Isosurface segmentation permits to access to the three dimensionnal shapes of PD (K, L)

Scale bars: (A-D) 10 µm, (E) 2 µm, (F) 200 nm, (G-J) 100 nm

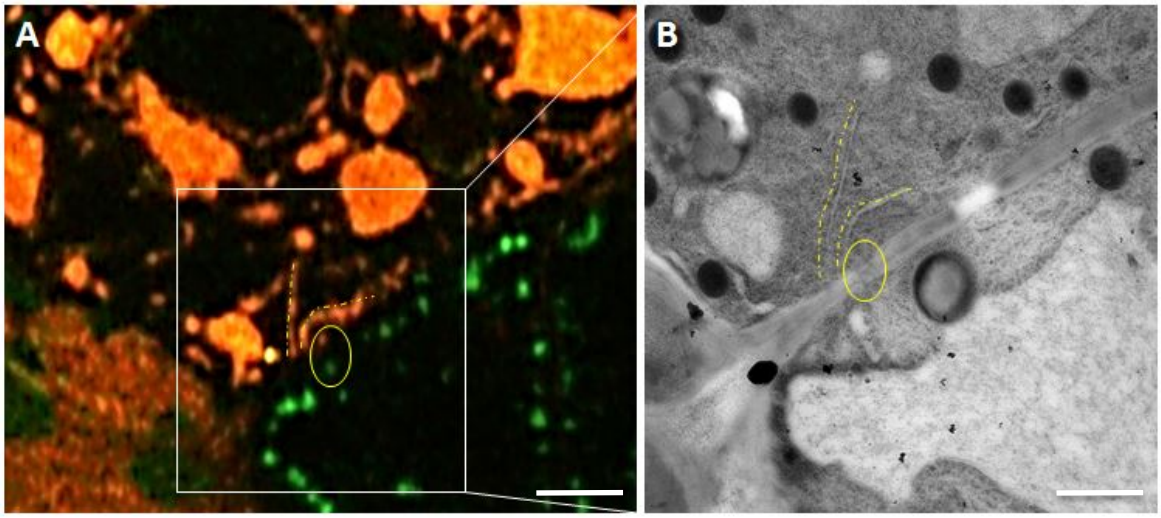

Figure 8. Improved resolution correlative light electron microscopy

(A) Confocal imaging with Airyscan detector of a graft interface of HDEL_FPs lines. **(B)** Transmission electron micrograph of the white square in A. Yellow dashed lines correspond to ER pattern and the yellow circle to plasmodesmata

Scale bars: 2 µm

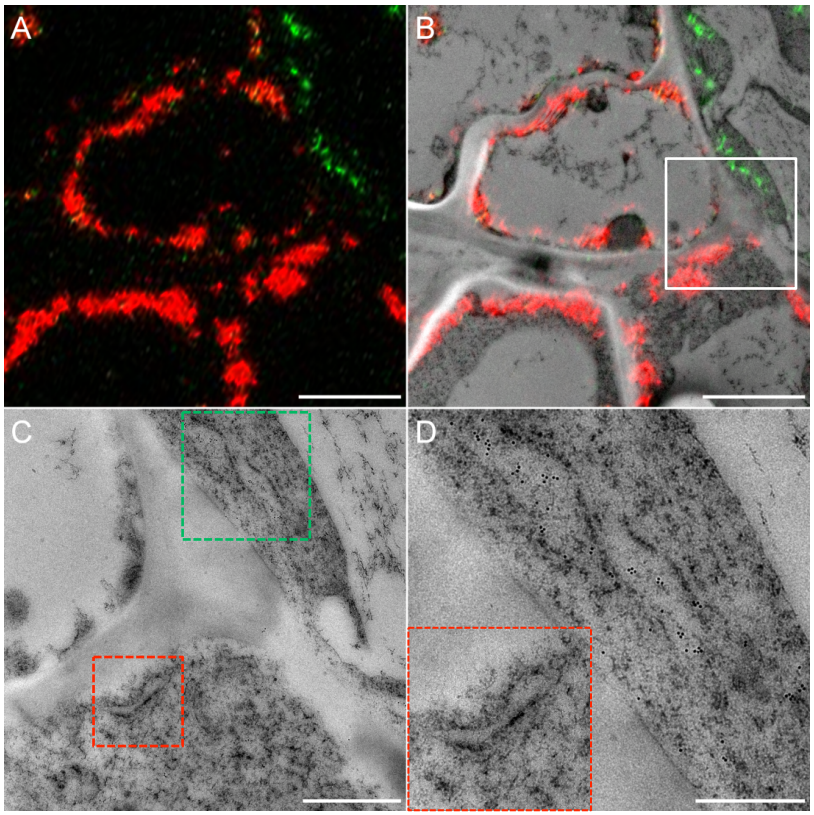

Figure 9. Immunolocalization of the Yellow Fluorescent Protein (YFP)

(A) Confocal observations of a graft interface of HDEL_YFP grafted onto HDEL_mRFP and **(B)** the corresponding correlated view. **(C)** Magnification of region highlighted by the white square in (B) showing endoplasmic reticulum (ER) of HDEL_mRFP (red dotted squared) and ER of HDEL_YFP (green dotted squared). **(D)** Magnification of these regions reveal the presence of ER immunolabeled with gold particules for HDEL_YFP cell, while there are no gold particules in the ER of HDEL_mRFP cell.

Scale bars: (A and B) 3 µm, (C) 1 µm, (D) 500 nm

Notes

When doing the seed sterilization, you need to work with bleach and acid separately to prevent an accidental mix of the two reagents in case of spills. Always use the appropriate protective equipment as gloves and a lab coat.

Recipes

1. Bleach solution for seeds sterilization

Disolve one tablet in 50 mM of distilled water

2. Culture mediums for seedlings and grafting

a. Half Murashige and Skoog medium for seedling (1 L)

Murashige and Skoog medium + vitamins (Duchefa Biochemi): 2.2 g

Plant agar (Duchefa Biochemi): 8 g

Adjust pH with 1 N KOH solution to 5.8

Autoclave flasks 120 °C for 20 min

b. Water medium for grafting

Put the autoclaved medium directly in the petri dishes while it is still hot as 1.6 % agar is long to melt again. Prepare only the amount of medium you need according to the number of graft you plan to do.

Volume (mL)	100	200	300	400	500	1000
Approximate number of petri dishes	5	10	15	20	25	30
Agar (g)	1.6	3.2	4.8	6.4	8	9.6

Adjust pH with 1 N KOH solution to 5.8

3. 20 % BSA solution for cryoprotection during HPF

Weigh 0.4 g of BSA and put it into a 2 mL screw top Eppendorf tube

Complete with water (or your medium culture) up to the 2 mL label

Alter quick centrifugations and vortex until BSA is dissolved entirely

Complete if necessary with water up to the 2 mL label to get a final concentration of 20 %

4. Cryosubstitution Uranyl-acetate stock solution (20 %, 500 µL)

Weigh 0.1 g of uranyl acetate powder (gloves and dust mask required) and put in 2 mL screwtop tube

Add pure methanol (under ventilated hood) up to 500 µL

Wrap the tube in tinfoil and store in the dark, at -20 °C in dedicated cryosubstitution box

5. Cryosubstitution mix for 3 mL

Compound (inititial concentration)	Volume (mL)	Final concentration
Uranyl acetate (20 %)	0.015	0.1 %
Pure Acetone	2.985	-

6. HM20 solutions

Make the solution in the FS Leica plastic solvent containers and cool the solution for 10-15 min in AFS chamber before use.

HM20 concentration	HM20 volume (mL)	Pure ethanol (mL)
20 %	2	8
50 %	5	5
75 %	7.5	2.5

7. 2 % Parlodion solution for grid filming

Only prepare a small quantity of parlodion, in a small glass flask as it is very sensitive to humidity and will not preserve properly over long time.

Weigh a small piece of solid parlodion -approximately 0.01 g-

Add isoamyl-acetate (store in a vented solvent cupboard and keep away from humidity) up to 1 mL

Wrap the flask in tinfoil and seal the lid with Parafilm

Before the first use, agitate to homogeneize the solution. Always seal the lid and protect from light.

8. Toluidine blue solution

Make mother solution with 1 g of Toluidine blue powder (Sigma-Aldrich) and 1 g of sodium borate (Sigma-Aldrich) in 20 mL of distilled water.

Dilute 25 times to prepare working solution.

Acknowledgments

This work was supported by the French Nationnal Institute for Agronomical Research (INRA), the Region Nouvelle Aquitaine and the Institute of Vine and Wine Science (ISVV) (travel grant to Melnyk's lab to learn grafting procedure). Thanks to Charles Melnyk and Remi Lemoine that invited me to learn the grafting procedure of *A. thaliana*. All sample preparation and imaging was done on the Pôle

Imagerie du Végétale, from Bordeaux Imaging Centre (http://www.bic.u-bordeaux.fr/). The authors declare having no conflicts of interests.

References

Biberfeld, P., Biberfeld, G., Molnar, Z., & Fagraeus, A. (1974). Fixation of cell-bound antibody in the membrane immunofluorescence test. Journal of Immunological Methods, 4(2), 135–148. https://doi.org/10.1016/0022-1759(74)90056-8

Dean, N., & Pelham, H. (1990). Recycling of proteins from the Golgi compartment to the ER in yeast. The Journal of Cell Biology, 111(2), 369–377. https://doi.org/10.1083/jcb.111.2.369

Gautier, A. T., Chambaud, C., Brocard, L., Ollat, N., Gambetta, G. A., Delrot, S., & Cookson, S. J. (2019). Merging genotypes: Graft union formation and scion-rootstock interactions. Journal of Experimental Botany, 70(3), 805–815. https://doi.org/10.1093/jxb/ery422

Iii, B. E. L., Rivero, L., Calhoun, C. S., Grotewold, E., & Brkljacic, J. (2017). Standardized Method for High-throughput Sterilization of Arabidopsis Seeds, (October), 1–7. https://doi.org/10.3791/56587

Knox, K., Wang, P., Kriechbaumer, V., Tilsner, J., Frigerio, L., Sparkes, I., … Oparka, K. (2015). Putting the Squeeze on Plasmodesmata: A Role for Reticulons in Primary Plasmodesmata Formation. Plant Physiology, 168(4), 1563–1572. https://doi.org/10.1104/pp.15.00668

Kollmann, R., & Glockmann, C. (1985). Studies on graft unions. I. Plasmodesmata between cells of plants belonging to different unrelated taxa. Protoplasma, 124(3), 224–235. https://doi.org/10.1007/BF01290774

Kremer, J. R., Mastronarde, D. N., & McIntosh, J. R. (1996). Computer visualization of three-dimensional image data using IMOD. Journal of Structural Biology, 116(1), 71–76. https://doi.org/10.1006/jsbi.1996.0013

Kukulski, W., Schorb, M., Welsch, S., Picco, A., Kaksonen, M., & Briggs, J. A. G. (2012). Precise, Correlated Fluorescence Microscopy and Electron Tomography of Lowicryl Sections Using Fluorescent Fiducial Markers. Methods in Cell Biology (Vol. 111). Elsevier. https://doi.org/10.1016/B978-0-12-416026-2.00013-3

Marion, J., Le Bars, R., Satiat-Jeunemaitre, B., & Boulogne, C. (2017). Optimizing CLEM protocols for plants cells: GMA embedding and cryosections as alternatives for preservation of GFP fluorescence in Arabidopsis roots. Journal of Structural Biology, 198(3), 196–202. https://doi.org/10.1016/j.jsb.2017.03.008

Melnyk, C. W. (2017a). Grafting with Arabidopsis (Vol. 137).

Melnyk, C. W. (2017b). Monitoring Vascular Regeneration and Xylem Connectivity in Arabidopsis thaliana, 1544, 91–102. https://doi.org/10.1007/978-1-4939-6722-3

Melnyk, C. W., Schuster, C., Leyser, O., & Meyerowitz, E. M. (2015). A developmental framework for graft formation and vascular reconnection in arabidopsis thaliana. Current Biology, 25(10), 1306–1318. https://doi.org/10.1016/j.cub.2015.03.032

Mudge, K. (2009). A History of Grafting, 35, 437–494.

Nicolas, W. J., Bayer, E., & Brocard, L. (2018). Electron Tomography to Study the Three-dimensional Structure of Plasmodesmata in Plant Tissues–from High Pressure Freezing Preparation to

Ultrathin Section Collection, 8, 1–25. https://doi.org/10.21769/BioProtoc.2681

Pina, A., Cookson, S. J., Calatayud, A., Trinchera, A., & Errea, P. (2017). Physiological and molecular mechanisms underlying graft compatibility ({Chapter} 5). Vegetable {Grafting}. {Principles} and {Practices}, 132–154. Retrieved from http://www.cabi.org/bookshop/book/9781780648972

Watanabe, S., Punge, A., Hollopeter, G., Willig, K. I., Hobson, R. J., Davis, M. W., … Jorgensen, E. M. (2011). Protein localization in electron micrographs using fluorescence nanoscopy. Nature Methods, 8(1), 80–84. https://doi.org/10.1038/nmeth.1537

1.2. Application of the Correlative Light Electron Microscopy approach to the study of grapevine grafts

1.2.1. Context

Arabidopsis is a very convenient model to study graft establishment because it is quite fast to graft many plants and the graft develops rapidly in only several days. Moreover, the graft development and changes in gene expression have been documented (Melnyk *et al.,* 2018, 2015). More importantly mutant and transgenic fluorescent lines are also available, permitting the study of very specific aspects of graft development. However, *A. thaliana* is a model plant that is relatively far from plants that are traditionally grafted, in particular perennial woody plants, such as grapevine. Thus, transferring the CLEM approach to grapevine is an important challenge of my research team. The management of the *in vitro* grafting of grapevine as well as the availability of one 35S::HDEL_GFP line of Pinot Noir (PN) could permitted us to target the graft interface. Moreover, cultures of callus cells of grapevine and notably the 35S::HDEL_GFP line of Pinot Noir (PN), are also available in our laboratory. For the micro-grafting model, the scion was always PN that express 35S::HDEL_GFP (PN-GFP) and the rootstock was always *V. riparia* cv. Riparia Gloire de Montpellier (RGM). PN is a *V.vinifera* cultivar which is traditionally used for wine production and RGM is a wild type cultivar of *V. riparia*. For callus grafting, the combination PN-GFP and 1103 Paulsen (1103P), that is a hybrid between *V. berlandieri* and *V. rupestris*, was used. Riparia Gloire de Montpellier and 1103P are traditionally used as rootstocks for their resistance to Phylloxera. The PN grafted onto RGM and 1103P are considered as a compatible combinations.

In this context, first experiments were done on two grapevine systems; micro-grafting of *in vitro* plants and callus grafting. Micro-grafting consist of cutting and assembling two stem segments of *in vitro* grapevine through a split graft. On top segment that constitutes the scion, one axillary bud is preserved while one the rootstock no axillary but are preserved. The low end of the rootstock is in a culture medium inducing root formation and the graft interface must be above to not induce adventitious root formation in the scion and lead to graft failure. Callus grafting growth consists of depositing callus cells on top of each other and growth on agar medium in petri dish as described in (Pina *et al.,* 2009). The advantage of model species such as grapevine is that several scion/rootstock combinations are already reported as more or less compatible. Thus, secondary PD number and ultrastructure could be studied in different contexts of compatibility (Fig. 7).

1.2.2. Results

The *in vitro* micro-grafts of PN-GFP grafted onto RGM permitted the localization of the graft interface in grapevine (27 DAG) (Fig. 7C and 8A). HDEL_GFP signal is clearly visible. Callus cells from both genotypes are formed at the contact point between scion and rootstock. To study the ultrastructure

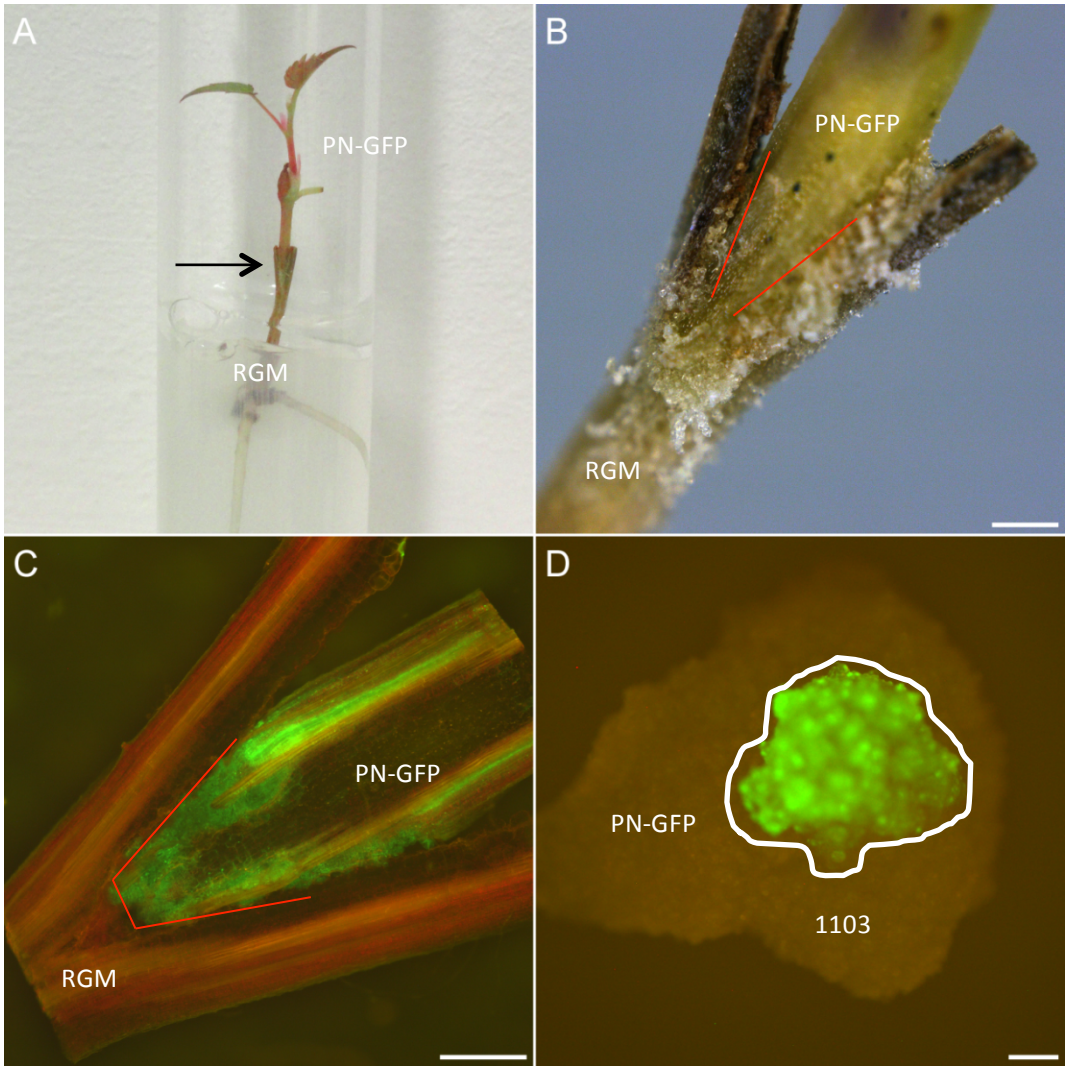

Figure 7. Grafts of grapevine samples

(A) *In vitro* grapevine Pinot Noir-GFP grafted onto Riparia Gloire de Montpellier (RGM), black open arrow shows graft interface **(B)** Magnification of the graft interface of Pinot Noir-GFP grafted onto RGM, **(C)** Vibratome 150 µm thick section of the graft interface of Pinot Noir-GFP grafted onto RGM observed with a macroscope **(D)** Callus cells of Pinot Noir GFP "grafted" onto 1103 Paulsen

Red lines indicate the V-type graft, PN-GFP: Pinot Noir-GFP, RGM: Riparia Gloire de Montpellier, 1103P: 1103 Paulsen.

Scale bars: (B, C and D) 500 µm

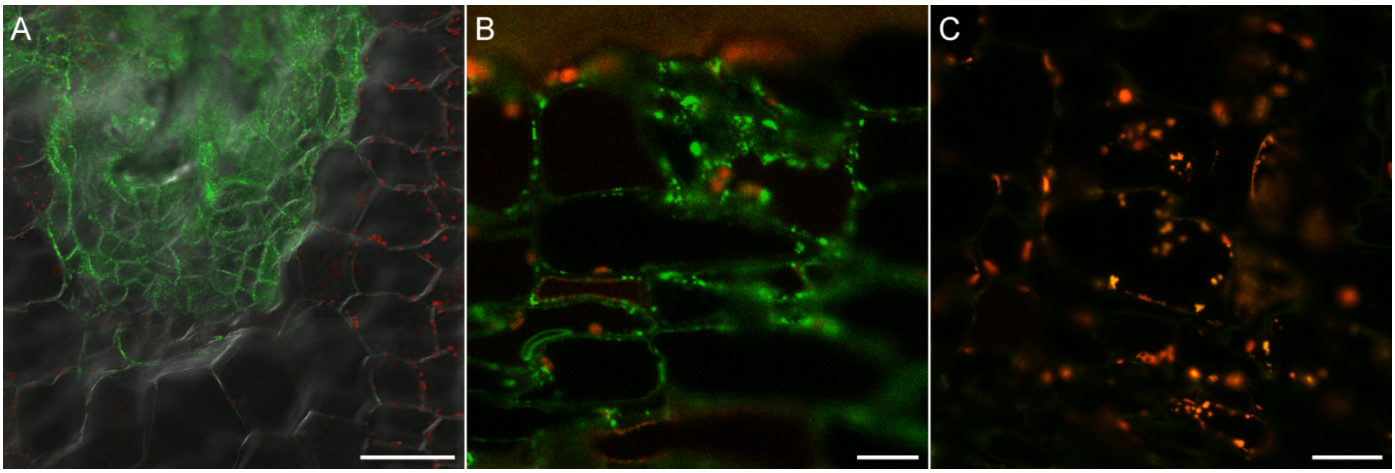

Figure 8. Confocal imaging of grafts of grapevine samples

(A) Vibratome 150 µm thick sections of *in vitro* grapevine Pinot Noir-GFP grafted on Riparia Gloire Montpellier allows to visualize the graft interface between GFP and non-GFP cells **(B)** The fluorescence of Pinot Noir – GFP is maintained using Progressive Lowering Temperature (PLT) methods, **(C)** No GFP fluorescence is observed in the RGM rootstock. On (A), (B) and (C), chlorophyll auto fluorescence appears in red.

Scale bars: (A) 100 µm, (B and C) 20 µm

of the graft interface of *in vitro* micro-grafts of grapevine, chemical fixation was firstly done because the diameter of the micro-graft is of several mm. This size is incompatible with HPF. The graft interfaces were sectioned above and below the graft point before sectioning in half longitudinally. The samples were rapidly chemical fixed with either only 4 % of paraformaldehyde (PFA) or supplemented with 0.1 % of glutaraldehyde in phosphate buffer 0.1 M pH 7.2. A light fixation was selected in order to conserve the fluorescent preservation. Nevertheless, small concentration of glutaraldehyde was used in order to improve the ultrastructural preservation despite the risk of producing autofluorescence signals. Fixation was followed by a progressive dehydration with increasing ethanol concentration from 30 % to 100 % at room temperature before a staining step with uranyl acetate 0.1 % in ethanol 100 %. The samples were then impregnated with increasing concentration of HM20 diluted in ethanol (HM20 25 % 2 h, HM20 50 % overnight, HM20 75 % 2 h, HM20 100% 2 h, HM20 100 % overnight and a last HM20 100 % 4 h). Polymerization was performed under UV light for 48 h at 20 °C. However, the graft interfaces, that are approximately 2 mm x 2 mm, even sectioned in half were still too big. Thus resin infiltration was incomplete and did not permit us to perform ultrathin sections for CLEM. Graft interfaces need to be sectioned longitudinally in several thinner sections before being fixed and impregnated.

Thus, sections of 150 µm thick were performed on live grafts using vibratome (Fig. 7A and 8C). Sections were rapidly chemically fixed on 4 % PFA. This time, fixation was followed by a Progressive Lowering Temperature dehydration (PLT) (as reported in (Moore *et al.,* 2016)) to limit the extraction of lipids (Table 1) during dehydration before staining with Uranyl Acetate. The PLT starts at 0 °C with 30 % ethanol until 100 % ethanol at – 50 °C. Subsequent HM20 impregnation was done at – 50 °C with increasing concentration of HM20. Polymerization was done under UV during 36 h at -50 °C and 12 h at 20 °C. In parallel, sections of 70 µm were also prepared for HPF and Freeze substitution as described previously for the *A. thaliana* CLEM part (see results 1.1.).

The PLT allowed us to maintain the fluorescence of GFP in the PN-GFP scion on semi thin sections of 500 nm. Moreover, no autofluorescence background was observed in the rootstock (Fig. 8). Unfortunately, the ultrastructure was not fully preserved with several empty cells. But vascular tissues and PD could be easily observed (Fig. 9). Correlative approach was very difficult due to difficulty to localize the cells on the ultrathin sections. In fact, on ultrathin sections, the contrast obtained with the transmitted light does not always permit the observation of the cell contours. Moreover, the very light fluorescent signal of GFP, which tends to photobleach on ultrathin section, does not allow us to find the cells. Grafting with a rootstock expressing a fusion protein with mRFP could be helpful, although this was unavailable to the project. With HPF (Fig. 10), we did not succeed in obtaining samples well infiltrated. Still, few sections have been done, allowing us to confirm the preservation of GFP fluorescence, however the ultrastructure was not well preserved, with no visible

	Initial temperature (° C)	End temperature (° C)	Lenght of the steps	
Ethanol 30 %	0	0	30 min	
Ethanol 50 %	0	- 15	30 min	
Ethanol 70 %	- 15	- 15	30 min	
Ethanol 95 %	- 15	- 30	25 min	+ U. A.
Ethanol 100 % (1)	- 30	- 30	25 min	+ U. A.
Ethanol 100 % (2)	- 30	- 50	25 min	
Ethanol 100 % (3)	- 50	- 50	30 min	
HM20 25 %	- 50	- 50	1 h	
HM20 50 %	- 50	- 50	Overnight	
HM20 75 %	- 50	- 50	4 h	
HM20 100 % (1)	- 50	- 50	2 h	
HM20 100 % (2)	- 50	- 50	Overnight	
HM20 100 % (3)	- 50	- 50	4 h	
Polymerization under UV	- 50	- 50	36 h	
	- 50	20	2 min	
	20	20	12 h	

Table 1: Progressive Lowering Temperature steps for grapevine *in vitro* micro-grafts

U.A.: 1% Uranyl acetate

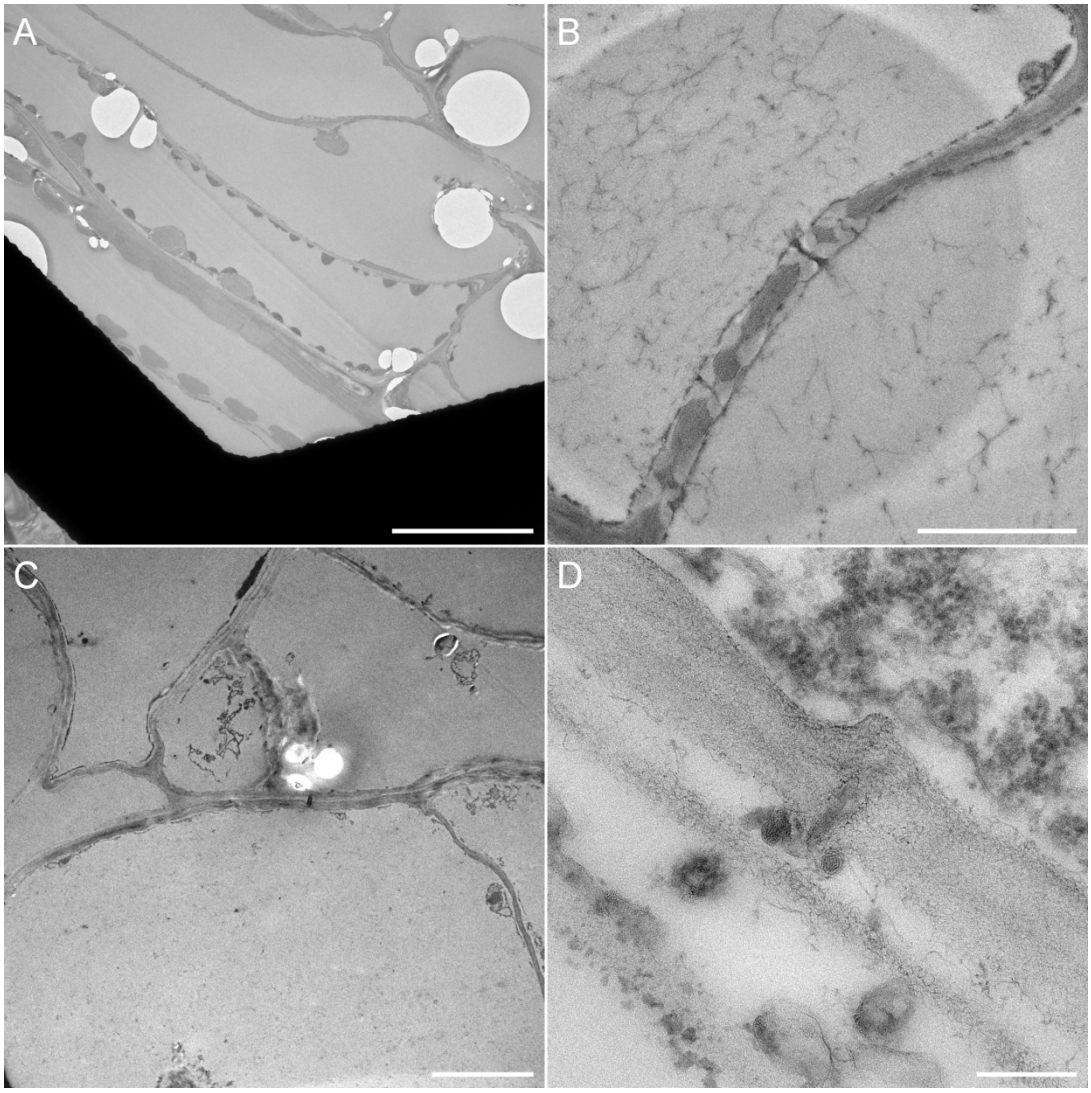

Figure 9. Ultrastructure of *in vitro* grapevine using Progressive Lowering Temperature (PLT)

(A) With PLT, tracheary elements and sieve elements are well preserved. The sample is not perfectly infiltrated **(B)** Sieve plates are visible between sieve elements, **(C)** Outside vascular tissues, cells appeared empty and not well-preserved **(D)** Plasmodesmata have been observed outside the graft interface

Scale bars: (A) 10 µm, (B) 2 µm, (C) 5 µm, (D) 200 nm

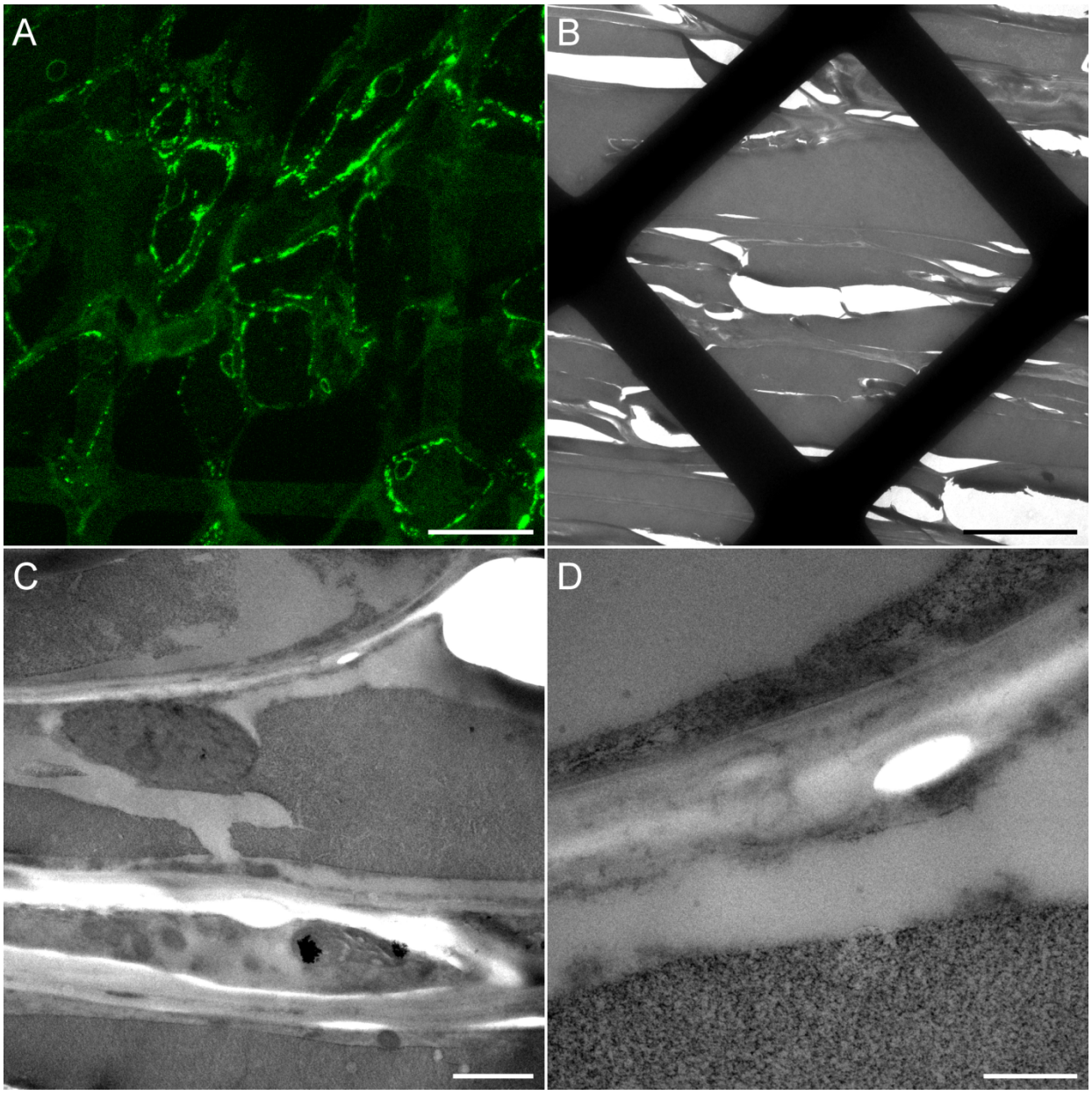

Figure 10. High Pressure Freezing and Cryosubstitution of micrograft of grapevine

(A) The fluorescence of Pinot Noir – GFP is maintained by cryomethods **(B)** Grapevine sample are not well infiltrated with HM20 resin **(C)** the ultrastructure is not preserved but the cells are not empty **(D)** Plasma membranes are not visible

Scale bars: (A) 20 µm, (B) 10 µm, (C) 2 µm, (D) 500 nm

PM. The incubation times should be specifically adapted for grapevine samples and also the thickness of vibratome sections. Thinner sections could help to improve the impregnation steps but thicker sections could help to have plenty cells. Thus, to investigate the ultrastructure at the graft interface of *in vitro* grapevine micro-grafts, efforts have to be pursued. The development of rootstock genotypes expressing 35S::HDEL_mRFP is necessary to localize the graft interface and perform CLEM.

During the first steps of graft union formation in the micro-graft of grapevine, cells divide actively and form a callus. Thus, the first contact between scion and rootstock occurs between callus cells. Callus cell grafting appeared as an alternative to study the cell-to-cell communication establishment between the scion and the rootstock. We grafted callus cultured cells of PN-GFP and 1103P on top of each other (Fig. 7D). After 24 DAG, graft interface was isolated thanks to the separation of both calluses. For the better visualization of 1103P cells, calluses were stained with propidium iodide before observation. PN-GFP fluorescent cells in close contact with 1103P cells were present (Fig. 11). They were harvested before being placed in the HPF carrier. Before fixation, the contact between fluorescent and non-fluorescent cells was systematically validated thanks to a fluorescent macroscope (Fig 11B). Afterwards, callus cells were fixed as previously described for the hypocotyl of *A. thaliana*. Fluorescence and ultrastructure were preserved (Fig. 11 C, D, E). Plasma membrane, desmotubule and cytoplasmic sleeve of PD were notably well preserved. Unfortunately, no close contact between fluorescent and non-fluorescent cells could be observed on ultrathin sections indicating that no common cell walls were formed between both kinds of callus. To avoid blind approach, new fluorescent genotypes are absolutely required. To follow symplastic communication establishment callus genotypes expressing a cytosolic mRFP grafted onto callus cells expressing 35S::HDEL_GFP are required. The screening of cell groups showing the HDEL_GFP pattern and cytosolic RFP could be selected before performing HPF.

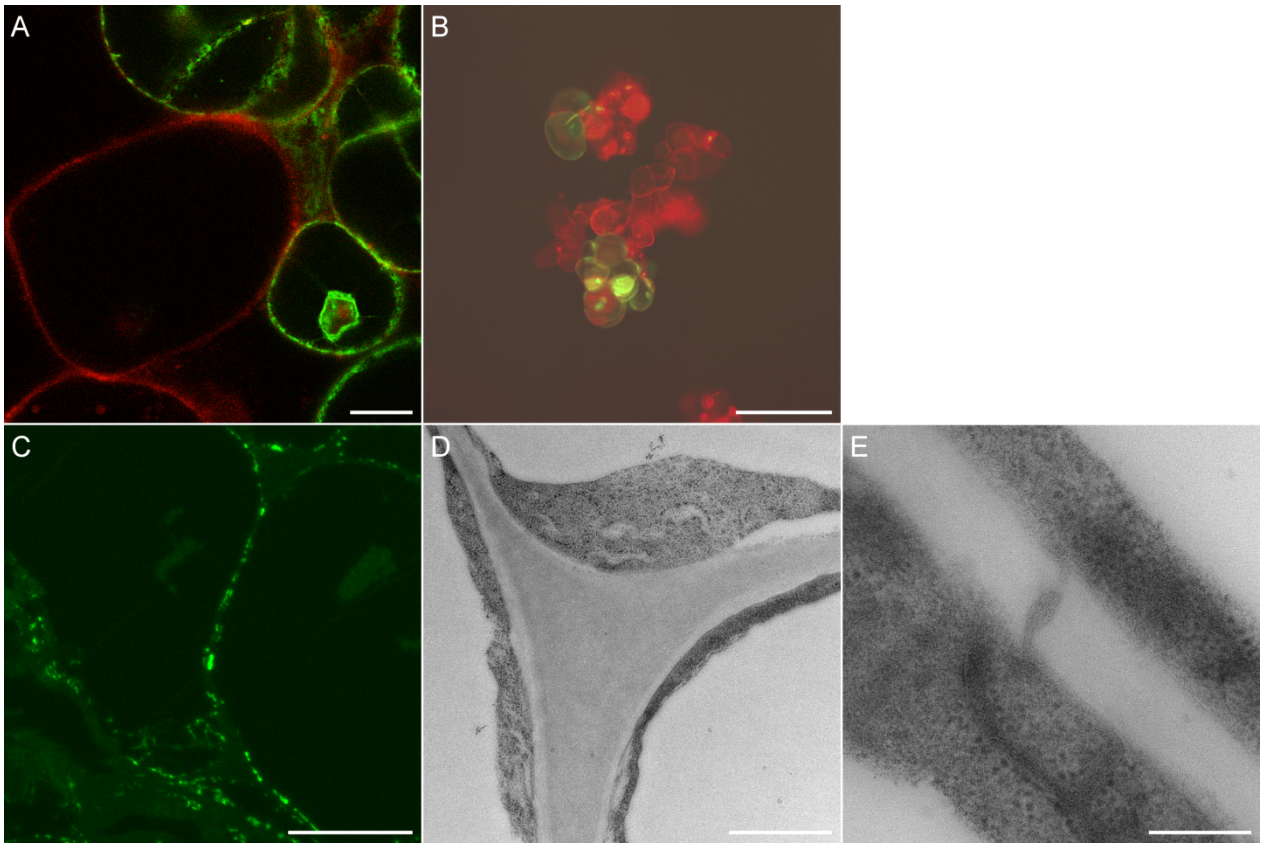

Figure 11. Callus grafting experiments

(A) Callus cells have been colored using propidium iodide. Contacts between Pinot Noir-GFP callus cells and 1103 Paulsen cells colored with propidium iodide have been observed **(B)** Small bulks of cells in contact have been selected and deposited in the carrier for high pressure freezing **(C)** resin section of 150 nm of callus cells. No contact between pinot noir GFP and 1103 Paulsen cells have been observed. The GFP fluorescence has been preserved **(D)** Transmission electron microscopy observations of the ultrastructure. Endoplasmic reticulum is visible **(E)** plasmodesmata with a good ultrastructural preservation are observed between two pinot noir GFP cells

Scale bars: (A) 20 µm, (B) 200 µm, (C) 20 µm, (D) 1 µm, (E) 200 nm

2. Article 2: Scion/rootstock communication pathways at the graft interface of Arabidopsis thaliana: extracellular vesicles, plasmodesmata and vascular connectivity

SCION/ROOTSTOCK COMMUNICATION PATHWAYS AT THE GRAFT INTERFACE OF ARABIDOPSIS THALIANA: EXTRACELLULAR VESICLES, PLASMODESMATA AND VASCULAR CONNECTIVITY

Clément Chambaud[1], Emmanuelle Bayer[2], Sarah J. Cookson[1], Lysiane Brocard[3]

[1] EGFV, Bordeaux Sciences Agro, INRA, Université de Bordeaux, ISVV, 210 Chemin de Leysotte, Villenave d'Ornon, France

[2] Laboratoire de Biogenèse Membranaire, UMR5200, CNRS, Université de Bordeaux, Villenave d'Ornon, France

[3] Université de Bordeaux, CNRS, INSERM, UMS 3420, INRA, Bordeaux Imaging Center, Plant Imaging Plateform, Villenave d'Ornon, France

[*]For correspondence: lysiane.brocard@inra.fr

1/Abstract

Combining interesting traits of shoots and roots of different genotypes through grafting has been used for over a thousand years in horticulture. Despite recent progress in understanding mechanisms of graft union formation using transcriptomic analysis and grafting of *Arabidopsis thaliana* mutants, we have little knowledge of the cellular events underlying graft union formation. This is because it is difficult to reliably target the graft interface under electron microscope to study its ultrastructure. To overcome this technological bottle neck, a correlative light electron microscopy approach (CLEM) was developed for the first time in grafted hypocotyls of *A. thaliana*. During the early stages of graft union formation, four potential pathways of communication between the scion and rootstock were identified: extracellular vesicles, plasmodesmata, phloem and xylem. In absence of cytokinesis, exclusively secondary plasmodesmata are formed across the graft interface. While plasmodesmata crossing the cell wall between the scion and rootstock are found, a third of them are hemi-plasmodesmata meaning that they do not span the cell wall entirely to connect the scion and rootstock cells. The progression of hemi-plasmodesmata seems to be physically stopped by the middle lamella of the cell wall. This can lead to the formation of "ball of wool" plasmodesmata, which are characterized by the aberrant accumulation of desmotubule structures in a central cavity. In addition, hemi-plasmodesmata are formed by the scion and the rootstock indicating that plasmodesmata biogenesis can be initiated independently by both partners. The ultrastructural characteristics of plasmodesmata obtained by electron tomography led us to propose a new model for secondary plasmodesmata biogenesis in which cell preparation events are required to facilitate the successful formation of plasmodesmata. For the first time, cytoplasmic exchanges between the

scion and rootstock cells were observed at 3 days after grafting, opening new theories of the mechanisms of vascular re-connection and graft union formation.

2/ Introduction

For thousands of years, people have used grafted plants to combine agronomical or ornamental traits that are difficult to obtain with simple cuttings or breeding. Grafting, between a scion and a rootstock is now commonly used for a variety of perennial (e.g. *Citrus spp., Prunus spp*., apples and grapevines) and even for annual crops (e.g. tomatoes and melons) to control growth, productivity and confer resistance to pathogens. Despite the widespread use of grafting, we know little of the cellular events underpinning graft union formation (Gautier *et al.,* 2019).

For the development of multicellular organisms such as higher plants, intercellular communications are crucial, and in plants many molecules are transported from cell-to-cell through plasmodesmata (PD). These nanometric channels span the cell wall to connect the symplast of two neighboring cells. Plasmodesmata are composed of a central cylindrical element deriving from the endoplasmic reticulum (ER) called the desmotubule (Ding *et al,.* 1992; Tilney and al., 1991), and are bordered by a specialized plasma membrane domain (Grison *et al.,* 2015). The space between the desmotubule and the plasma membrane forms the cytoplasmic sleeve in which cytosolic molecules can traffic from cell-to-cell; whilst the desmotubule could be a trafficking pathway from cell-to-cell for lipids and membranous proteins (Cantrill *et al.,* 1999). Plasmodesmata allow the cell-to-cell communication between almost all plant cells by establishing both cytosolic and membrane continuities between cells of the entire plant body. These channels are required for plant life because of their role in key biological processes such as photoassimilate transport (Turgeon, 1996) and development (as reviewed by Otero *et al.,* 2016) through the transport of transcription factors, RNA and metabolites (Lucas & Lee, 2004; Furuta *et al.,* 2012 Benitez-alfonso *et al.,* 2009; Stonebloom *et al.,* 2009; Xu *et al.,* 2011).

While PD are crucial for cell-to-cell communication, long-distance signaling is ensured by vascular tissues: phloem and xylem. They are formed by highly specialized cells that come from the differentiation of meristematic cells of the procambium. Phloem is formed of (1) sieve elements (SE) which are responsible of transport of photoassimilates and signaling molecules from source to sink organs, (2) companion cells (CC) which support the metabolism of SE and (3) parenchyma cells which have the role of support cells. The differentiation process of SE is characterized by cell wall thickening, a loss of several organelles, ultrastructural modifications of plastids and mitochondria, a draining process of the nucleus content and an accumulation of P-proteins (Batailler *et al.,* 2012; Froelich *et al.,* 2011; Furuta *et al.,* 2014). The SE continuum is ensured by specialized pores, derived from PD where the desmotubule is absent. Sieve elements and CC come from the division of the

same cambial cell and they are connected together through PD that are thought to be formed during the new cell plate formation (Cheadle *et al.,* 1962; Esau & Thorsch, 1985). Companion cells have a high number of mitochondria and a dense cytoplasm (Esau, 1973). Xylem is notably composed of (1) tracheary elements (TE) and (2) parenchyma cells. Tracheary elements are lignified dead cells responsible for the transport of water and minerals from root to shoot. The TE differentiation begins with the deposition of secondary cell wall (composed of lignin) before the induction of a programmed cell death involving nuclear DNA condensation and vacuole collapse processes (Aoyagi *et al.,* 1998; Avci *et al.,* 2008; Farage-Barhom *et al.,* 2008). The walls of adjacent pre-TE are perforated leading to the formation of continuous tubes specialized for mineral and water transport (Nakashima *et al.,* 2000). During grafting, as opposed to the wounding, all physical cell communications are interrupted by cutting at the grafting point. To survive, both grafted partners with sectioned opened cells, have to interact together quickly and effectively enough to establish new exchange pathways (Fuentes *et al.,* 2014; Lu *et al.,* 2017; Sidorov *et al.,* 2018; Stegemann *et al.,* 2009). Recent progress has been made in understanding of graft union formation by using the *Arabidopsis thaliana* hypocotyl grafting model. In this model, developmental framework and transcriptomic events have been well-documented (Melnyk *et al.,* 2018; Melnyk *et al.,* 2015). The disruption of vascular tissues induces the accumulation of sucrose and auxin just above the grafting point. These accumulations permit a new polarization of PIN-FORMED 1 (PIN1) above the wounding site, facilitating the cell alignment of future vascular cells (Mazur *et al,.* 2016). The establishment of a vascular continuum begins by phloem reconnection at 3 day after grafting (DAG) and then, xylem reconnection from 5 to 7 DAG. New vascular tissue formation is initiated above, and then below, the graft interface indicating that the scion could be the leader of this cellular differentiation processes. At the graft interface, new differentiated vascular cells expand and divide to bypass the wounded regions and permit the vascular reconnection between both partners (Melnyk *et al.,* 2015). Despite the recent advances in the understanding graft union formation, studying the ultrastructure of the graft interface is still challenging due to the difficulty of distinguishing reliably the scion and rootstock cells among the cell mixture at the interface. Until now, the studies of Kollmann and Glockmann (Kollmann & Glockmann, 1985, 1991; Kollmann *et al,.* 1985) were the only ones which targeted, without ambiguity, the graft interface by transmission electron microscopy (TEM). They demonstrated the existence of PD at the graft interface thanks to the study of a heterograft between *Vicia faba* and *Helianthus annuus* in which callus cells possess species-specific plastids and nuclei. This approach did not allow the identification without ambiguity of every cell studied because of the intrinsic ultrastructural cell heterogeneity between differentiated cells. Moreover, an identification method linked to organelles markers limits the study to only certain and very different species.

In order to gain insights into the ultrastructural events underpinning graft union formation, we developed a Correlative Light and Electron Microscopy approach (CLEM) on grafted hypocotyls of *A. thaliana*. Fluorescent proteins (FPs) were used to label the graft interface under light microscopy before accessing to its ultrastructure with TEM and Electron Tomography (ET). This work provides novel insights into the cell-to-cell communication processes occurring at the graft interface during graft union formation.

3/ Materials & Methods

- Plant material, growth conditions and plant grafting.

Arabidopsis thaliana were grown vertically in a growth chamber on solid medium composed of half Murashige and Skoog medium including vitamins (1/2 MS) and plant-Agar (8 g L^{-1}), pH 5.8. Growth conditions were set at 22 °C in a growth chamber with a short day 10 h photoperiod with photosynthetic photon flux density of 120 µmol m^{-2} s^{-1}). All lines (35S::HDEL_mRFP, 35S::HDEL_YFP and 35S::GFP) were previously published (Clark *et al.,* 2016; Lee *et al.,* 2013; Nelson *et al.,* 2007). 35S::TagRFP were produced in a Col-0 background.
For grafting, seven-day-old plants were selected and grafted using the transverse cut and butt alignment from the method described by Melnyk (Melnyk, 2017). A modification is that water plus plant-Agar (1.6 g L^{-1}) was used instead of humid paper to maintain the moisture level required for graft union formation.

- High Pressure Freezing and Cryosubstitution

Copper carriers (100 µm deep and 1.5 mm wide) were filled with water plus 20% bovine serum albumin (BSA) (which functions as a cryoprotectant). Rapidly, grafts were cut above and below the graft point and installed in the well of the carrier. Samples were frozen in the carriers using an EM-PACT high-pressure freezer (Leica) and then transferred at −90 °C into an AFS 2 freeze-substitution device (Leica). Grafts were incubated in a cryosubstitution mix containing only uranyl acetate 0.1 % in pure acetone for 30 h. Afterwards temperature was raised progressively until −50 °C is reached at 3 °C h^{-1}. The cryosubstitution mix was removed and thoroughly washed 3 times with pure acetone followed by 3 times in pure ethanol. Low temperature and the limited amount of chemical compounds help in preserving the fluorescence of fluorescent proteins while preserving a sufficient staining for TEM and ET. Samples were then carefully removed from the carriers before progressive embedding in HM20 Lowicryl resin (Electron Microscopy Science): HM20 25 % 2 h, 50 % 2 h, 75 % overnight (diluted in pure ethanol), HM 20 100 % 2 h twice before a last 100 % for 8 h 25 %, 50 % (2 h each), 75 % (overnight), 100 % (twice for 2 h) and a last 100 % for 8 h. The polymerization was done

under UV light for 24 h at −50 °C followed by 12h at +20 °C. Samples in resin blocks were stored at -20 °C protected from light.

- Microscope acquisitions and correlations

Prior to observation, sections were made with an EM UC7 ultramicrotome (Leica). For an optimal balance between resolution under the electron microscope and signal quantity under the confocal microscope, sections from 150 nm to 200 nm were collected on on parlodion coated 200-square mesh copper grids with thin bars (Electron Microscopy Science). Fluorescence Z-stack acquisitions were made on a Zeiss LSM 880 with excitation 488 nm for YFP and 561 nm for mRFP. The acquisitions were achieved with a 63× apochromatic N.A 1.4 oil objective. The tile acquisition tool of the Zen black software was used to get the large field of view with the best resolution. Moreover, the Z-stack tool was use to acquire the maximum of photons emitted by the samples. Afterwards maximal or summed Z-projections were used to improve the visualization. Transmission electron microscopy observations were carried out on a FEI TECNAI Spirit 120 kV electron microscope equipped with an Eagle 4Kx4K CCD camera. Correlation was based on natural landmarks such as cell shapes, plastids and nucleus. Correlated images were obtained thanks to Adobe Photoshop software.

- Tomogram acquisition and reconstruction

We used the process described by (Nicolas *et al.,* 2018). Before tomogram acquisition, sections need to be coated with gold fiducials for later alignment, a 1:1 mixture of 0.5 % BSA and 5 nm colloidal gold solution from BBI solutions (referenced as EM-GC5 on http://bbisolutions.com) was used. Tilt series were acquired with a single tilt specimen holder (Fichione instruments, model-2020), using the batch mode of FEI 3D Explore tomography software. Each tilt series was acquired between -65° to 65° when it was possible, with an acquisition every degree. For dual axis, the grid was turned to 90° manually. The raw tilt series were aligned and then reconstructed using the fiducial alignment mode with the eTomo software (http://bio3d.colorado.edu/imod/). 10 to 25 fiducials were used to accurately align all images. Aligned stacks were binned two times before reconstruction. Reconstruction was performed using the back-projection with SIRT-like filter (10 to 50 iterations).

- Image processing and analysis

Image analysis was carried out using the ImageJ software (https://imagej.nih.gov/ij/download.html) with the Bio-Format plugin (https://www.openmicroscopy.org/bio-formats/) to open and process the Zeiss .czi files and to open the .mrc tilt series files and tomograms. Measurement of cell wall thickness was done using ImageJ. Mosaic images of confocal microscope were assembled with the

BigStitcher plugin of Fiji. Mosaic images of TEM were assembled using Photomerge function of Adobe Photoshop. Correlated images were obtained by a rough alignment of confocal and TEM images using layers in Adobe Photoshop. No image analysis was carried out on mosaic and correlated images, they were only used as a visualization tools.

- Data analysis

Data analysis and presentation was done using SigmaPlot, Systat Software Inc.

4/ Results

- Correlative Light Electron Microscopy gives access to the graft interface ultrastructure unambiguously

In order to target the *A. thaliana* graft interface, scions and rootstocks expressing FPs with different colors were grafted (Fig. 1A). To avoid erroneous targeting of the graft interface, transgenic lines transformed with 35S::HDEL_YFP or 35S::HDEL_mRFP were selected. HDEL motif is known to be retained in the lumen of the ER and to be unable to pass through PD (Knox *et al.,* 2015). To validate the HDEL_FP lines for graft interface studies, confocal microscopy observations were performed. As positive controls for cell-to-cell diffusion, HDEL_YFP and HDEL_mRPF were respectively replaced by lines expressing cytosolic either GFP or mRFP, which freely diffuse from cell-to-cell. At 5 DAG, in the positive controls, cells near the graft interface contained fluorescence of both the cytosolic FP and HDEL_FP (Fig. 1 C and D). In contrast, for grafted hypocotyls between HDEL_YFP and HDEL_mRFP, no bicolored cells were observed close to the graft interface (Fig. 1B). These results show that HDEL_FPs cannot cross the graft interface. HDEL_FPs lines are convenient to tag the graft interface.

A CLEM approach was developed on the grafted hypocotyls between HDEL_YFP and HDEL_mRFP (Fig. 2). Unfortunately, the fragility of young *A. thaliana* grafts makes it impossible to fix the samples before 3 DAG. During the TEM sample preparation, the preservation of YFP and mRFP fluorescence as well as of the ultrastructure is absolutely required. To this end, fixative contrasting compounds were limited to uranyl acetate and high pressure freezing followed by a rapid freeze substitution and polymerization was used. To evaluate the fluorescence preservation, ultrathin sections were observed by confocal microscope. Despite these preventive measures during fixation, the fluorescence of the fixed samples decreased, indicating that a strong fluorescence signal is initially required. Moreover, to slow eventual photo-bleaching reactions, embedded samples are systematically stored in the dark at -20 °C. Even though mRPF and YFP signals were preserved, YFP appears weaker and sometimes difficult to detect under confocal microscopy requiring an increase of excitation power and the compression of the display of YFP signal (see supplemental data 1). After resin embedding, plastids have the same emission spectrum as mRFP, but can be easily identified by

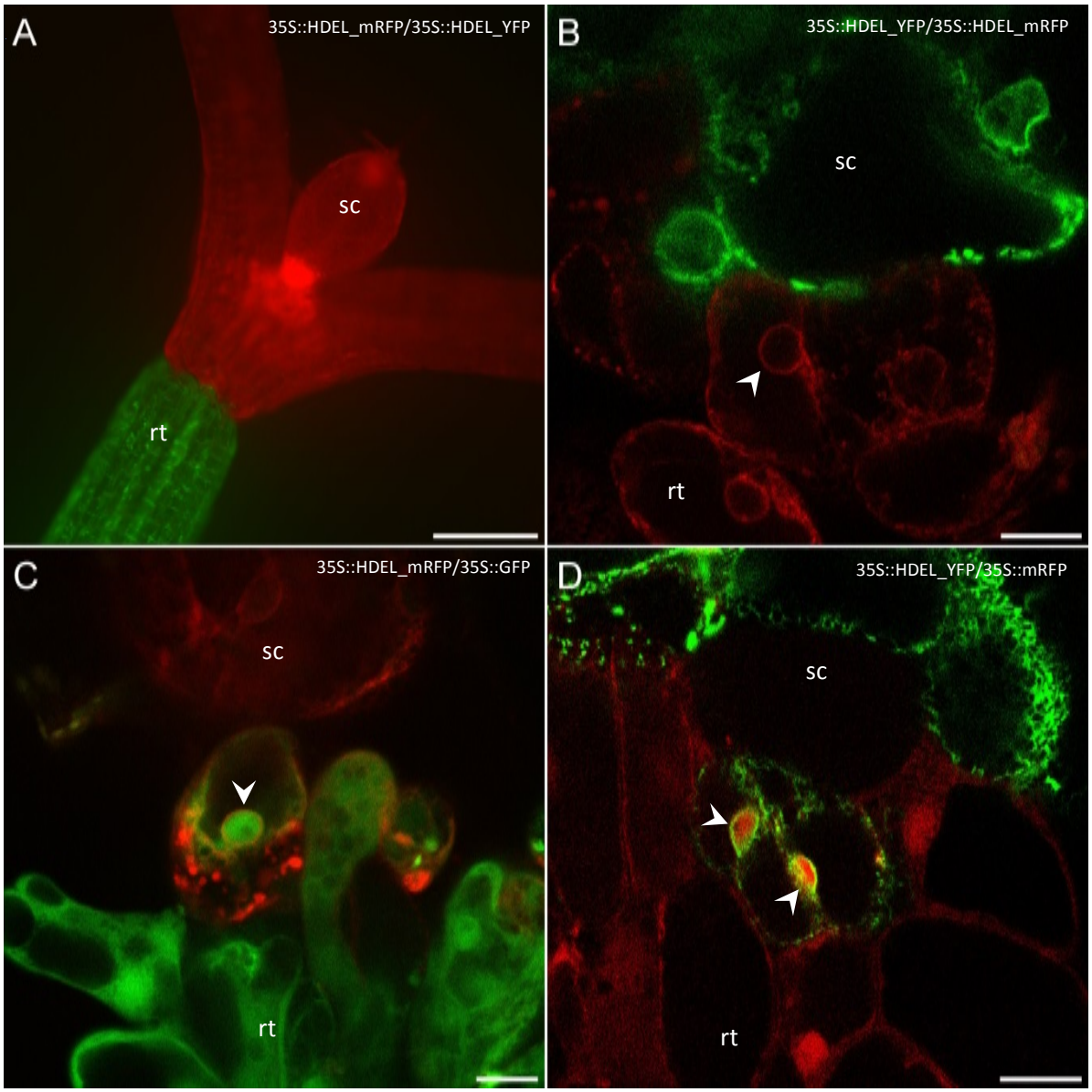

Figure 1. Graft interface targeting in *A. thaliana* by grafting hypocotyls of HDEL-YFP and HDEL-mRFP lines

The scion and the rootstock are respectively at the top and bottom positions. **(A)** Large view of a graft between a scion expressing 35S::HDEL_mRFP (red) onto a rootstock expressing 35S::HDEL_YFP (green). **(B)** Observation by confocal microscopy of a graft interface of 35S::HDEL_YFP (scion) / 35S::HDEL_RFP (rootstock). No YFP nor RFP signal is found in the opposite partner. **(C)** Observation by confocal microscopy of a graft interface of 35S::HDEL_RFP (scion) / 35S::GFP (rootstock). GFP and HDEL-mRFP can be observed in same cells. **(D)** Observation by confocal microscopy of a graft interface of 35S::HDEL_YFP (scion) / 35S::mRFP (rootstock). mRFP and HDEL-YFP can be observed in same cells. White arrowheads pinpoint nuclei. sc: scion, rt: rootstock

Scale bars (A) 200 µm, (B, C and D) 10 µm

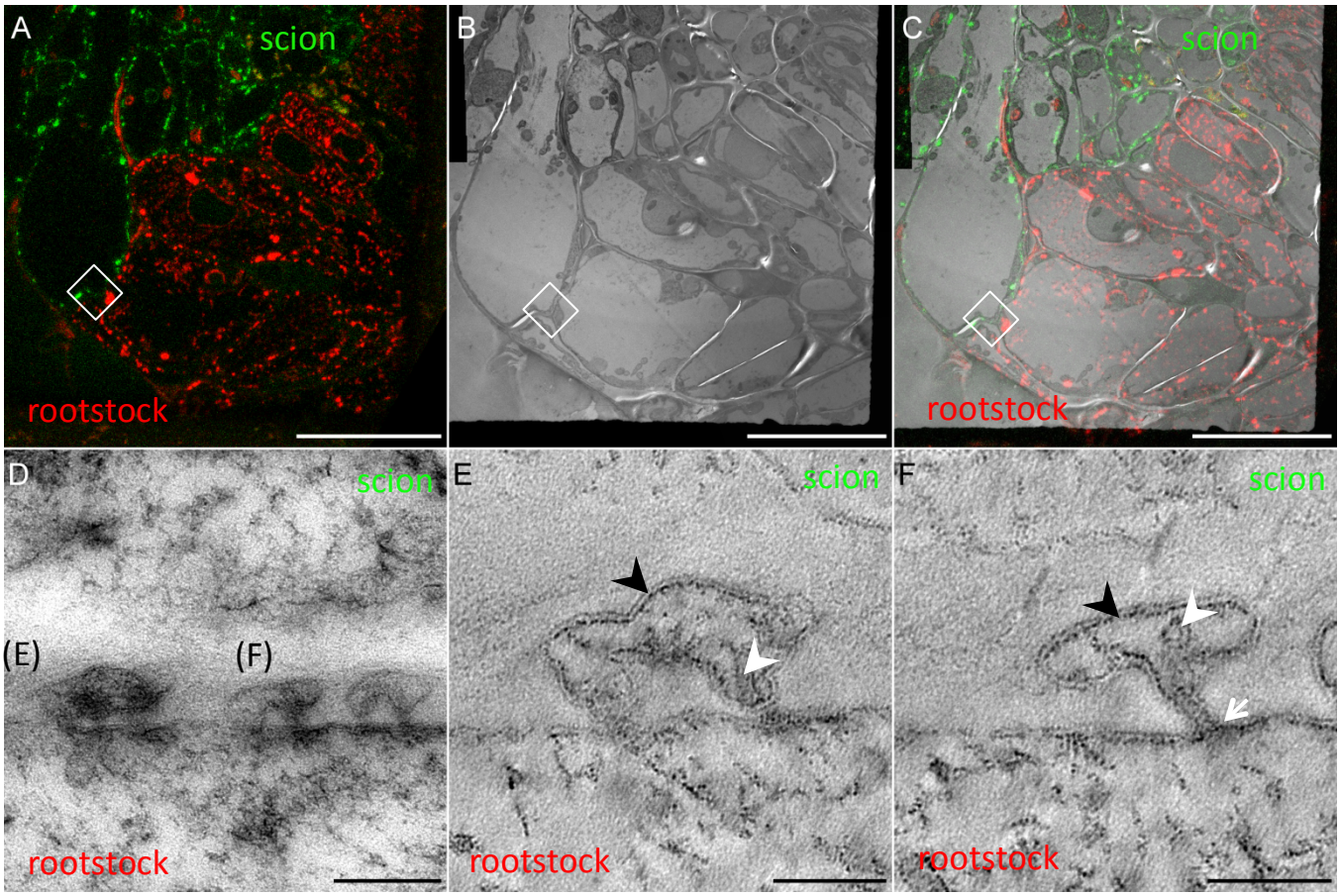

Figure 2. Correlative Light Electron Microscopy as a tool to investigate the ultrastructure of the graft interface

The scion and the rootstock are respectively at the top and bottom positions. **(A)** Confocal acquisition of the graft interface of a 35S::HDEL_YFP scion grafted onto a 35S::HDEL_mRFP rootstock **(B)** Transmission electron micrograph tiles of the regions observed in (A). **(C)** Correlated light electron microscopy view of the graft interface which allows the precise identification of the scion and rootstock cells. **(D)** Enlarged view of the white square shown in A, B and C, plasmodesmata (PD) found at the graft interface. **(E)** Electron tomogram of section of one PD labelled (E) in image (D). **(F)** Electron tomogram section of another PD labelled (F) in image (D). Black arrowheads show the plasma membrane of PD, white arrowheads indicate the desmotubule of PD longitudinally oriented in (E) and transversally in (F). On (F) the open white arrow highlights continuity between the plasma membrane of PD and the cell plasma membrane.

Scale bars: (A, B and C) 20 µm, (D) 200 nm, (E and F) 100 nm

their structure (see supplemental data 2). To get enough fluorescence signal, without compromising the ultrastructure observations with a TEM at 120kV, thickness of ultrathin sections was increased up to 200 nm. Sections were collected on TEM grids before optimizing the photon collection and fluorescence visualization by z stacks acquisitions. We successfully observed the same ultrathin sections under both confocal and TEM (Fig. 2A and B). The acquisition of fluorescence was used to target specifically the graft interface and was then correlated with TEM images thanks to endogenous cell markers such as the cell shapes, nuclei and plastids (Fig. 2C). Good ultrastructure preservation was obtained even in the absence of osmium tetroxide. In fact, the bilayer of the plasma membrane as well the desmotubule were well conserved (Fig. 2D, E, F). In order to restore the fine resolution, which is impaired by the increasing in thickness of the section, ET in one or two axis can be done. Therefore we can conclude that our CLEM approach permits the unambiguous targeting of the grafting interface the study of its ultrastructure.

- Four pathways to communicate at the graft interface

In order to have a temporal view on the process of graft union formation, especially communications between both partners, TEM observations were performed on *A. thaliana* hypocotyl grafts at 3 and 6 DAG. The physical contact between both partners was confined in the central part of the graft interface, in contrast cellular debris were systematically observed at the periphery (see supplemental data 3). In the center of the graft although cells where well-organized in a continuous tissue at 6 DAG, at 3 DAG interfaces still show a heterogeneous cell organization at certain regions of the graft (Fig. 3A and M), where some scion and rootstock cells were still physically separated by several layers of electron-dense residues and cell walls. Interestingly, theses cell wall layers presented a stratum organization with different electron densities that could indicate modifications in the cell wall composition (Fig. 3B and D). In these cell wall layers, several kinds of parietal elements surrounded by a lipid bilayer were present. Some of them could be PD-like structures with a diameter around 22 nm and a dense electron central element (Fig. 3C) whereas other extracellular vesicles (EVs) were bigger and could contain punctuated electron dense complexes (Fig. 3E). These EVs are likely to result from residual cell compartments after the wounding. However, in more conventional cell wall regions at the graft interface, EVs in contact to the plasma membrane were also found potentially indicating an active process. These EVs could ensure the first steps of cell communication between the scion and the rootstock by passing through the cell wall layers that separate both partners. This wide physical barrier tended to disappear at 6 DAG (Fig. 3G). Outside the cell wall layers, PD were observed from 3 DAG indicating that symplastic connections were already established between the scion and the rootstock. Moreover, cells coming from scion and rootstock were well aligned, presented no vacuole compartment and contained P-proteins. A

nucleus, with a visible nucleolus, interacting with mitochondria, could be observed in one scion cell. It indicates that SE are still in differentiation (Fig. 3F and I). Once, one immature incomplete pore, which is not crossed by P-proteins, was observed between a scion and stock pre-SE (Fig. 3J). At 3 DAG, differentiating SE cells are often surrounded by cells with a dense nucleus content and dilated nuclear envelope (Fig. 3K). These cells present a dense cortical cytoplasmic layer with mitochondria and vacuole invaginations. They could correspond to ultrastructural specificities that could occur during the vacuole elimination during the SE differentiation process. At 6 DAG, SE differentiation was accomplished with mitochondria surrounded by a halo (Fig. 3O), differentiated plastids and sieve plates (Fig. 3Q and R). Similarly, CC were fully differentiated showing cytosolic characteristics: dense cytoplasm and numerous black mitochondria. Moreover, at 6 DAG the fluorescent pattern of SE did not correspond to HDEL but to auto-fluorescence signal which is characteristic of mature SE (supplemental data 4). It indicates that the "cytoplasmic draining process" accompanying the SE differentiation was achieved. Even if the graft interface between SE cannot be reliably localized because of the HDEL_FP signal disappearance, scion and stock SE were connected at 6DAG because SE strands with SE associated with their own respective CC can be observed (Fig. 3Q, R, S and T).

No connected mature xylem was found between both partners at 3 DAG. However, cells with lignin deposition on the cell wall were observed remote from the interface (3 or more cell layers) as well as in scion and rootstock (Fig. 3L). These kind of differentiating cells were never observed at the cut site that could indicate that the xylem differentiation process is not initiated at the cut point. At 6 DAG, mature connected TE were well established (Fig. 3U).

Thus, observations of the graft at 3 DAG and 6 DAG indicate that EVs and PD could be the first ways of grafted partner to communicate allowing phloem reconnection which is ongoing at 3 DAG. Xylem and phloem continuum are well established at 6 DAG.

- Scion and rootstock can initiate secondary PD biogenesis at the graft interface

Primary PD are formed during the cytokinesis by the trapping of ER strands during the cell plate formation. In the context of grafting, the establishment of cell-to-cell connectivity between the scion and rootstock requires the biogenesis of PD in the pre-existing cell walls at the graft interface; PD formed after the cell wall are called secondary PD. To elucidate the mechanisms of *de novo* secondary PD biogenesis, the ultrastructural characteristics of PD exactly at the graft interface, as well as their cellular environment, were observed by TEM and ET at 3, 6 and 8 DAG. Electron tomography gives access to a three dimensional (3D) view of these tiny channels with an improved resolution (Fig. 4). Four classes of PD were observed (Fig. 5). The first class, observed with a rate of 32.4 %, is simple PD. They are formed of one continuous channel (Fig. 5A).

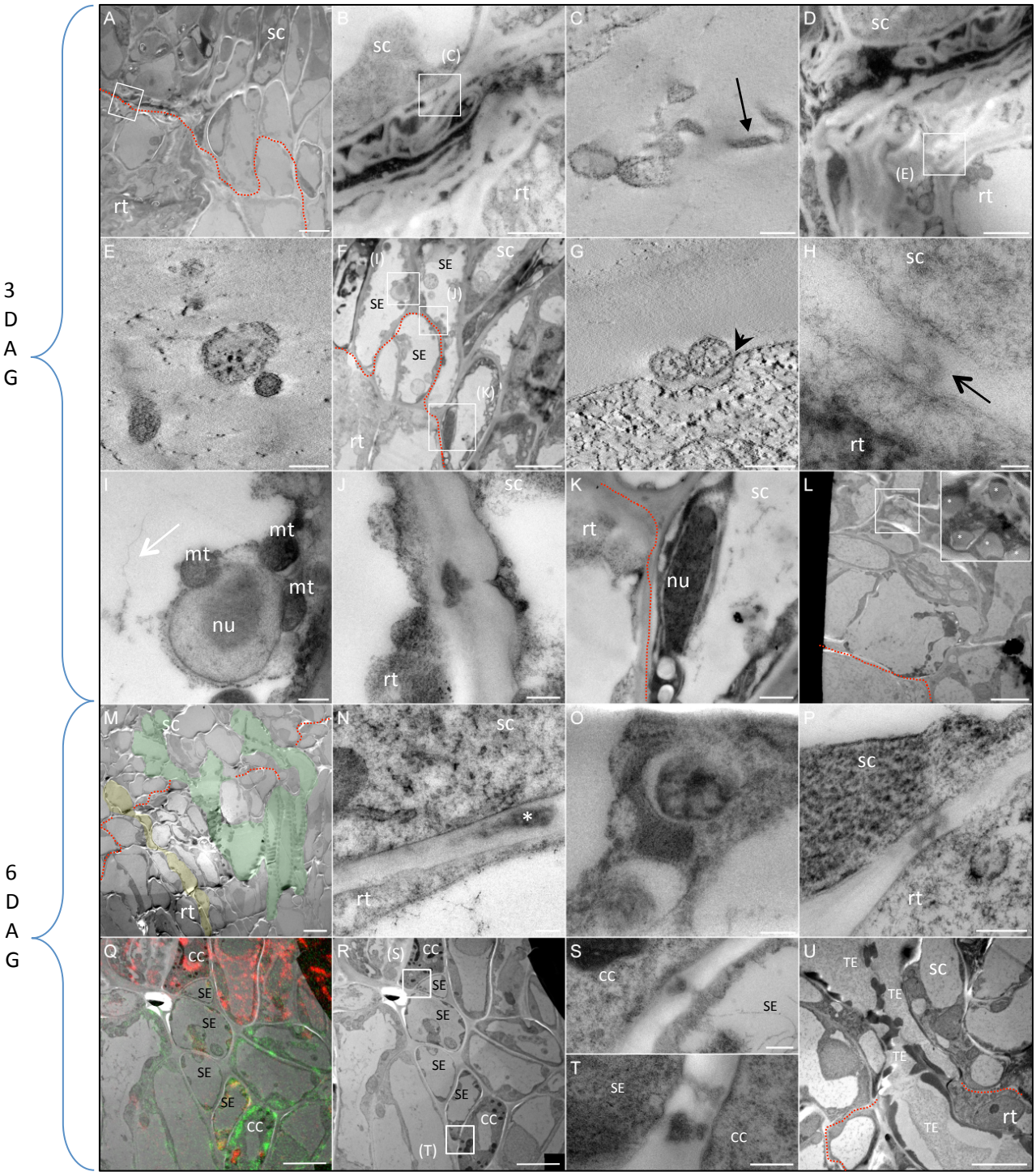
3
D
A
G
6
D
A
G
A
sc
rt
B
sc
(C)
rt
C
D
sc
(E)
rt
E
F
(I)
SE
sc
SE
(J)
SE
(K)
rt
G
H
sc
rt
I
mt
mt
mt
nu
J
sc
rt
K
sc
rt
nu
L
M
sc
rt
N
sc
*
rt
O
P
sc
rt
Q
CC
SE
SE
SE
SE
CC
R
(S)
CC
SE
SE
SE
SE
CC
(T)
S
CC
SE
T
SE
CC
U
TE
SC
TE
TE
TE
rt

Figure 3. Ultrastructural comparison of 3 vs 6 days after grafting graft interface of *A. thaliana*

The scion and the rootstock are respectively at the top and bottom positions. **(A-L)** Ultrastructure of a 3 days after grafting (DAG) graft interface **(A)** Overview of the 3 DAG graft interface shows two heterogenous cell organization with tissue discontinuity and continuity at the graft interface. The two region of interest in the discontinuous region are shown with white squares **(B)** Enlarged view of the white square (B) in (A) showing electron dense material and cell wall layers between the scion and the rootstock on the following section. **(C)** Tomogram of the white square in (B) showing a PD-like structure (Black closed arrow) and extracellular vesicles found into the cell wall. **(D)** Enlarged view of the (D) white square in (A) showing electron dense material and cell wall layers between the scion and the rootstock **(E)** tomogram of the extracellular vesicles found in (D). One vesicle contains dense granules. **(F)** Overview of a 3 DAG graft interface showing contiguous sieve elements (SE). **(G)** Two extracellular vesicles at region of the graft interface in contact with the plasma membrane (Black arrowhead). **(H)** Continuous plasmodesmata observed at the graft interface (open black arrow). **(I)** Enlarged view of (F) in which the nucleus (nu) is surrounded by mitochondria (mt) in a differentiating sieve element containing P-proteins (white open arrow) **(J)** Enlarged view of (F) showing an incomplete pore between two sieve elements at the interface **(K)** Enlarged view of (F) showing a dense nucleus (nu) with dilated nuclear envelop (L). At 3 DAG, differentiating xylem is observed remote from the graft interface. **(M-U)** Ultrastructure of a 6 DAG graft interface. **(M)** Overview of the 6 DAG graft interface showing no dense material nor additional cell wall layers. Aligned sieve elements are highlighted in light yellow, aligned tracheary elements are highlighted in light green. **(N)** Small electron dense material are occasionally found at the graft interface. **(O)** Round mitochonchria, characteristic of mature sieve elements. **(P)** Branched plasmodesmata observed at the graft interface. **(Q)** Correlated view of sieve elements aligned at the interface, connected to their respective companion cell with plasmodesmata. **(R)** Ultrastructure of the sieve element (SE) alignment. **(S-T)** Enlarged view of the plasmodesmata connecting sieve elements and companion cells (CC) observed in (R). **(U)** Xylem tracheary element (TE) properly aligned at the graft interface.

Red dotted lines indicate graft interfaces Scale bars: (A, F, L, Q, R and U) 5 µm, (B and D) 2 µm, (K) 1 µm, (G, J, N, O, P, S and T) 200 nm, (C, E and H) 100 nm

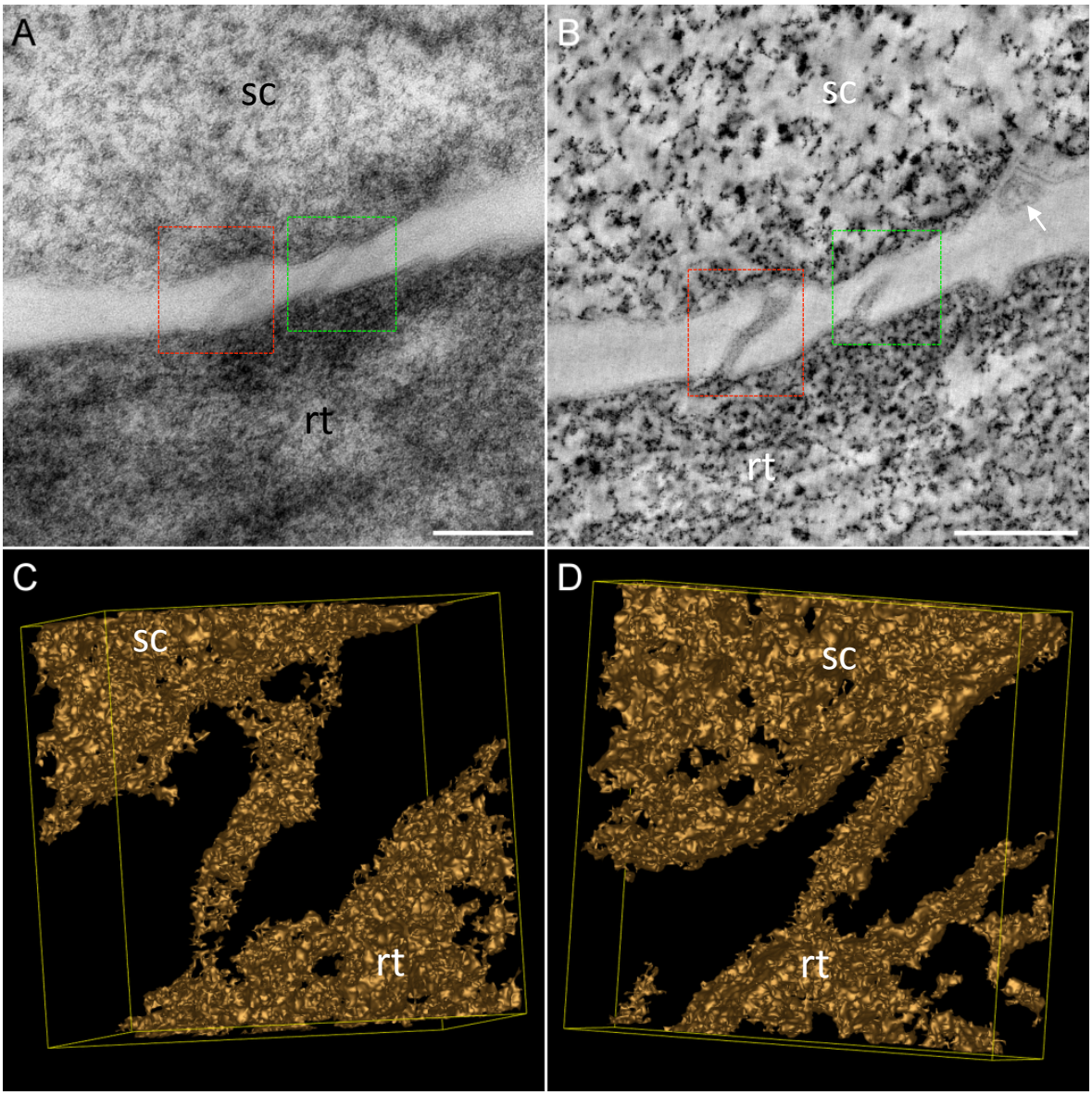

Figure 4. Electron tomography reveals the three dimensional shape of plasmodesmata

The scion and the rootstock are respectively at the top and bottom positions. **(A)** Plasmodesmata (PD) are observed at the graft interface by transmission electron microscopy (TEM). **(B)** Resolution is further improved by electron tomography (ET). The white arrow shows an extracellular vesicle. The 3D shape of PD can be characterized by ET. PD is **(C)** branched (red dotted square) or **(D)** simple (green dotted square). sc: scion, rt: rootstock

Scale bars: (A and B) 200 nm

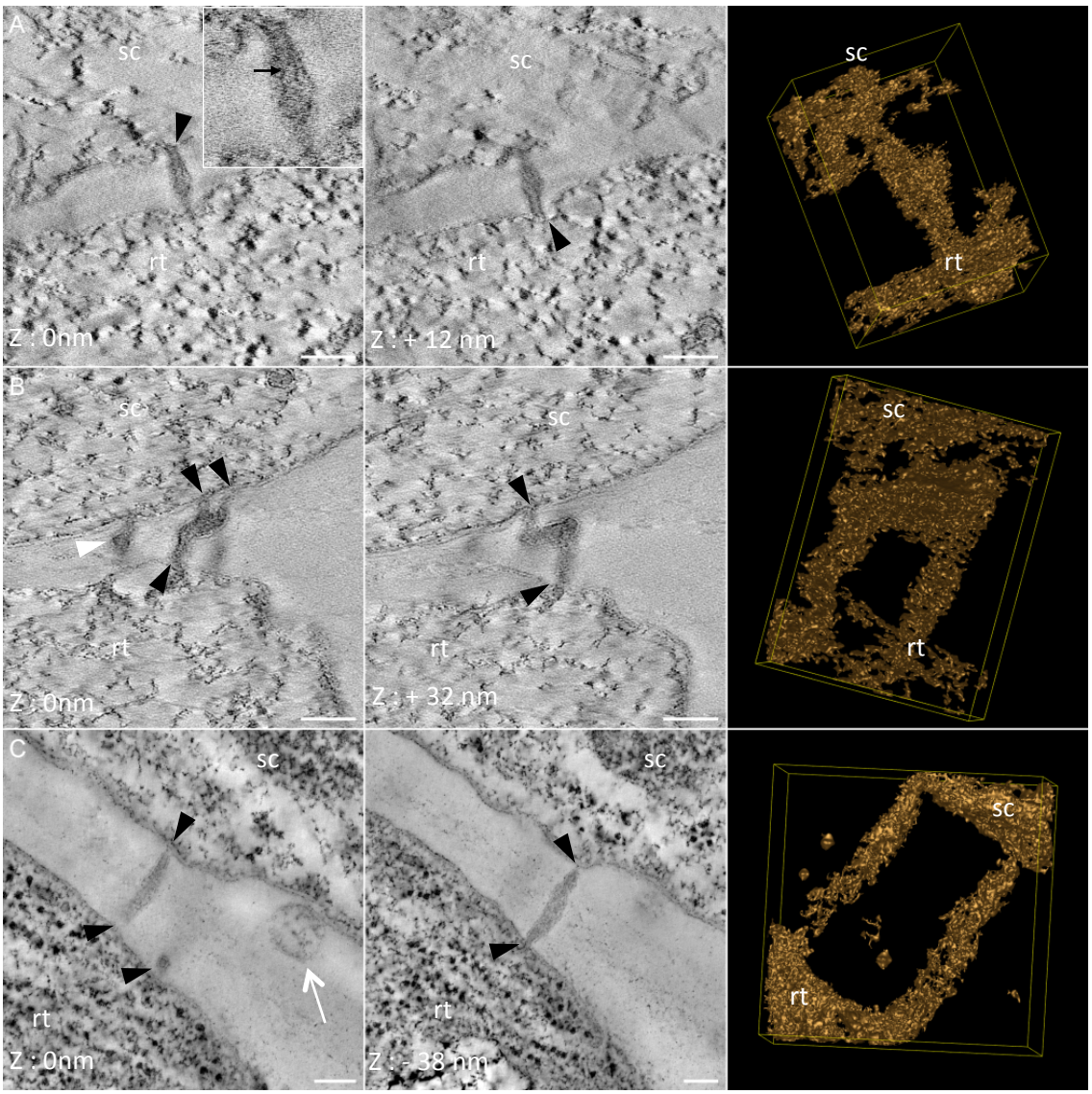

D

Shapes of PD at the graft interface	n	%
Branched	38	20.5
Hemi	73	39.5
Simple	60	32.4
Twin	14	7.6
Total	**185**	**100**

Figure 5. Electron tomograms and three dimensional (3D) visualization of simple, branched and twin plasmodesmata (PD)

The scion and the rootstock are respectively at the top and bottom positions. Black arrowheads pinpoint the extremities of simple **(A)**, branched **(B)** and twin **(C)** PD. For each shape of PD, two Z plans and one 3D segmentation are presented. **(A)** Simple PD with a visible desmotubule (black arrow). **(B)** Branched PD with three branches on the scion side and two on the rootstock side, and another PD in its vicinity (B, filled white arrowhead). **(C)** Twin PD characterized by the close proximity of two simple PD. Open white arrow shows an extracellular vesicle. **(D)** Number and proportion of the different shapes of PD at the graft interface. sc: scion, rt: rootstock

Scale bars: (A, B and C) 100 nm

The second class, named branched PD, presents several continuous ramifications of at least three and up to six branches (Fig. 5B). They are observed with the rate of 20 %. The third one, twin PD, corresponds to at least two simple PD in very close proximity, when the distance between PD is inferior to their length. They are the rarest ones observed with a rate of 7.6 % (Fig. 5C). Twin PD could come from the separation of branched PD occurring during the cell wall elongation. These first three types of PD seem to pass through the cell wall completely. Finally, a fourth class, hemi PD, is the most frequently observed class of PD at the graft interface (39.5 %). Hemi PD do not completely cross the cell wall. Hemi PD are found at the scion and rootstock sides with the same frequency indicating that PD biogenesis could be initiated as well as by scion or rootstock cells (Xhi-squared = 0.22857, df = 1, p-value = 0.632) (Fig. 6).

Moreover, when the middle lamella is visible, hemi PD progression into the cell wall seems blocked by it and hemi PD can even run along it (Fig. 6A). Almost every hemi-PD observed form loop-like structures with at least 2 cytosolic openings (called neck region) into the same cell (Fig. 6B). The desmotubule and the plasma membrane are in intimate contact at the neck regions of PD (Fig. 2F and 6B) whereas a weaker interaction leads to the formation of a central cavity in the middle of the cell wall (Fig. 2E, F and Fig. 6B, E). Some other hemi PD seemed to be straight with only one cytosolic opening, but more detailed 3D observations of corresponding tomograms show that they could correspond in fact to a partial view of hemi PD in loop (Fig. 6C). Strikingly, hemi PD in a 'ball of wool' structure were observed twice in thick cell walls of around 500 nm at the graft interface of 8 DAG (Fig. 6D). In 'ball of wool' PD, after the straight progression of the desmotubule (in close interaction with plasma membrane) into the first 70 nm of the cell wall, a huge central cavity is formed with a diameter of around 300 nm. In this cavity, the desmotubule, still compressed, is archaically accumulated and wrapped on itself. A second cytosolic opening for the 'ball of wool' PD was not found even after detailed observations of the different axis of the corresponding tomogram. The absence of at least one exit for these 'ball of wool' PD could be the cause of the accumulation of elements that usually transit through PD from one cytosolic opening to another one. Unfortunately, the entire volume of 'ball of wool' PD is only just obtained and so the presence of only one cytosolic opening cannot be completely confirmed.

Cell wall thickness was measured for each PD (n = 185) and ranges from 23 nm to 1 µm. While no significant difference was observed between the cell wall thickness of single, branched and twin PD, the cell wall around hemi PD is significantly thicker (p value < 0.001, Supplemental Data 5).

- Partner coordination is required for the biogenesis of spanning secondary PD

Secondary PD biogenesis process is still unknown. Different mechanisms of biogenesis could exist simultaneously at the graft interface depending on the cellular context when PD are formed (i.e. cell

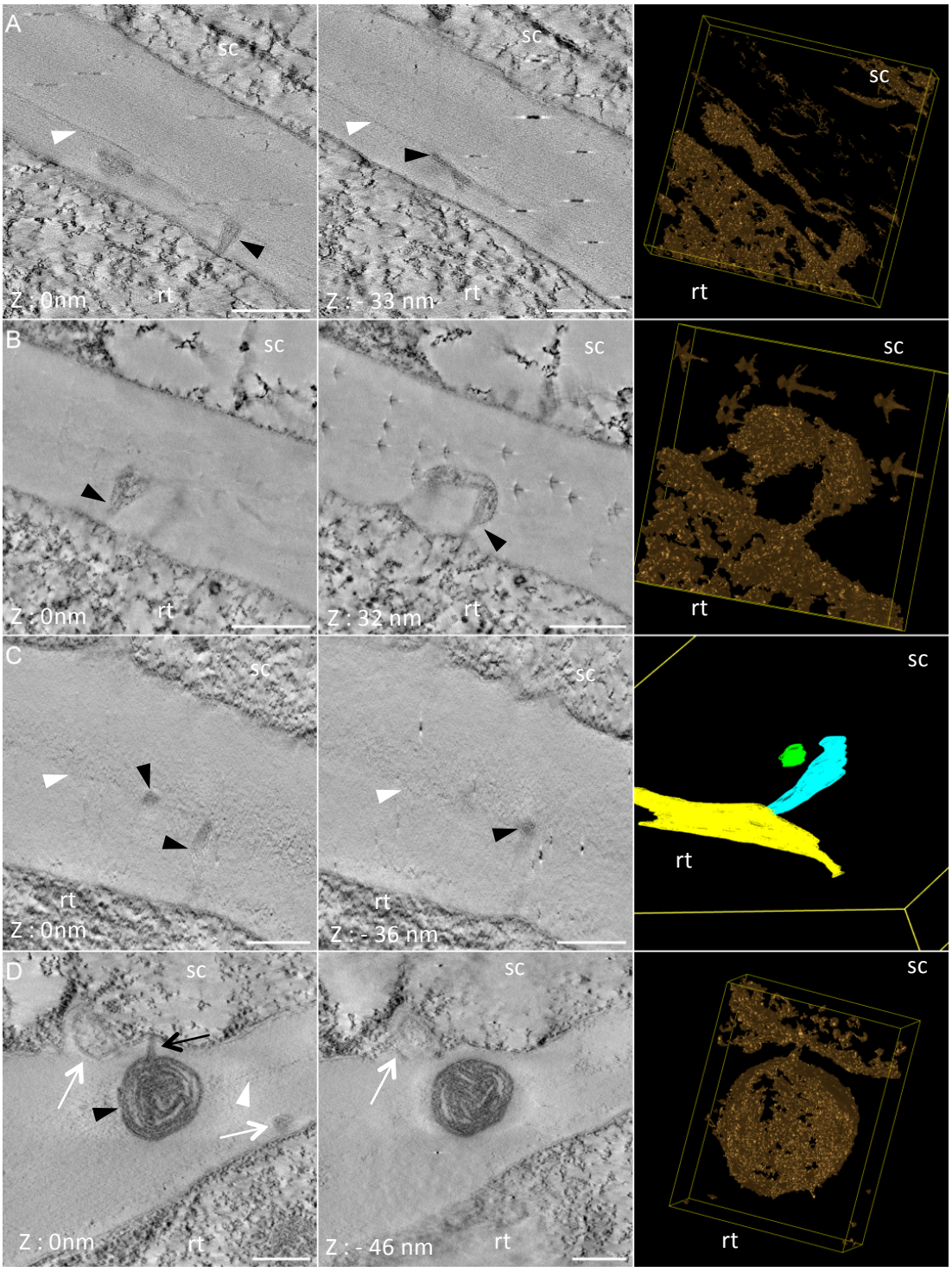

E

Orientation	Observed orientation	Observed distribution	Expected distribution
Rootstock	37	0.53	0.50
Scion	33	0.47	0.50
Total	70	1	1
Xhi-square p -value	0.6326		

Figure 6. Tomograms of of hemi plasmodesmata (hemi-PD) that do not span the cell wall found at the graft interface

The scion and the rootstock are respectively at the top and bottom positions. For each PD, two Z plans and one 3D reconstruction are presented. **(A)** A hemi-PD (black arrowheads) that does not cross the middle lamella (white arrowheads) but runs along it (the full volume of PD is not available for this section). **(B)** Dual axis tomogram of hemi-PD forming a loop-like structure with three branches as seen on the 3D reconstruction. **(C)** When not sectioned longitudinally, hemi-PD in loops can be misidentified as simple hemi-PD. **(D)** A hemi-PD in a 'ball of wool' shape with an aberrant accumulation of desmotubule in a large central cavity in the middle of the cell wall. Only one opening connects the PD to one cell. Extracellular vesicles are visible near this PD (open white arrows). **(E)** Occurrence of hemi-PD in scion and rootstock. sc: scion, rt: rootstock

Scale bars: (A, B and C) 200 nm

wall thickness). One hypothesis is that it could be initiated by an ER-plasma membrane attachment that could be coordinated with a local thinning of the cell wall. Afterwards ER could be trapped while new cell wall material is brought at this plasma membrane-ER tethering site and form a hemi-PD. To end up with PD that span the cell wall, a coordinated event could occur at the opposite side of the cell wall followed by a fusion of both hemi-PD. In order to elucidate the secondary PD biogenesis, ET observations were performed on the cell walls of the graft-interface. Hemi-PD were found facing each other into a cell wall presenting a middle lamella (Fig. 7A, B, C and D). The progression in the cell wall of one of these hemi-PD was stopped by the middle lamella before running along it. A second hemi-PD progress into the cell wall in front of the first one and began to enter in contact with the central part of this first hemi-PD. A following fusion event between both hemi-PD at the middle lamella place could lead to a complete secondary PD.

Some cell walls appeared irregular with regions of different thicknesses from around 23 nm to around 100 nm (Fig. 7I and J). On a thinner part of the cell wall, a cytoplasmic structure, surrounded by a membrane bilayer, was associated with the plasma membrane by a continuous electron dense layer of around 15 nm thick (Fig. 7E). The correlated fluorescence pattern allowed us to confirm unequivocally that this structure (Fig. 7G and H), which presents some ribosomes on its surface is actually ER. Just above this ER-plasma membrane interaction, a local thinning of the cell wall up to 23 nm was primed (Fig. 7E). A more electron dense area, indicating a strictly localized structural modification of the cell wall composition, spanned the cell wall just under this interaction site (Supplemental data 6). Interestingly, not strictly at the opposite site of the cell wall, a similar interaction between ER and plasma membrane as well as an electron densification across the cell wall were also observed (Fig. 7F). These symmetric events showed that both partners at the graft interface were temporally and spatially coordinated to induce cell wall modifications and ER-plasma membrane interactions. Further on the graft interface between the same rootstock cell and another scion cell, fluorescence patterning showed that ER strands could be organized symmetrically on both sides of the cell wall (Supplemental data 6). Electron dense tubes that span completely a very thin part of the cell wall have been observed (Fig. 7I and J). These elements share PD ultrastructural characteristics: bordered by the plasma membrane, and contain an electron dense central element with a diameter around 14 nm that could be a desmotubule. No space between the central element and the PM could be observed leading to a total width of around 25 nm, similar to very young primary PD. Unfortunately, these channels were difficult to observe in continuity with ER structures maybe due to the lack of osmium tetroxide staining. The correlated fluorescence pattern allowed us to confirm the presence of ER strands from the scion partner (Fig. 7K and L). No middle lamella could be observed at the sites where PD spanned the cell wall. Moreover, around the cell wall at the graft interface, several electron dense vesicles with a diameter around 40 nm were found at both scion

and rootstock sides (Fig. 7I and J). These vesicles could bring key materials indispensable for a cell wall remodeling leading to a symplastic connection. In summary, these symmetric events could indicate that both partners at the graft interface are temporally and spatially coordinated at the ultrastructural level. The middle lamella seems to block the PD progression in the cell wall. The thinning of portions of the cell wall, until the elimination of the middle lamella, could be a starting point to establish the conditions required for secondary PD biogenesis.

- Cytosolic fusion events occur during the grafting process

During the examination of graft interfaces of HDEL_YFP/HDEL_mRFP, truly bicolored cells, with both YFP and mRFP signals were seen exclusively on 3 DAG graft interface and with a low frequency (1 out of the 4 samples studied for bicolored cells) (Fig. 8A, B, C and D). However, the HDEL sequence is known to target proteins to the ER and prevent cell-to-cell movement through the conventional symplastic pathway. Twelve sections of this cell were carefully observed by confocal microscopy and showed the same result, the cell was bicolored. To ensure that the YFP fluorescence signal is specific, and not due to auto-fluorescence in this bicolored cell, immuno-gold labelling with antibodies against YFP was used (see negative control in supplemental data 7). As expected, a specific ER labelling was obtained (Fig. 8H, I and J). The distribution of the two colors was different, with mRFP mainly at the periphery of the cell and at the periphery of the YPF region, whereas YFP is exclusively in the central part of the cell (Fig. 8F, G). The two labels were not found on the same part of the cell and remained separated. The cytoplasm appeared fragmented around the vacuole traversed by cytoplasmic strands. In this bicolored cell, the proportion of cytosol remains high as in young cells. To better understand these bicolored events, several sections were done on this sample in order to screen for other bicolored cells. Several bicolored cells were observed near the central part of the graft interface (Fig. 9). They were aligned with one another and localized in proximity of vascular cells. Further examinations of the scion cells close to the bicolored cells permitted to catch the transit of organelles from cell-to-cell through a wide cell wall opening. As during the cell division the cell plate formation is a centrifuge process, the gap observed in the middle of the cell wall could not be associated to a cell division event (Fig. 9F). Moreover, a perforated bicolored cell presenting two nuclei was also found at graft interface (Fig. 9K). One nucleus was more surrounded with YFP labelling in contrast to the other one which was more associated with mRFP labelling. On the same section, further away from the graft, in the rootstock, a cytoplasmic compartment that could be a nucleus was found transiting from a cell to another one (Fig. 9L).

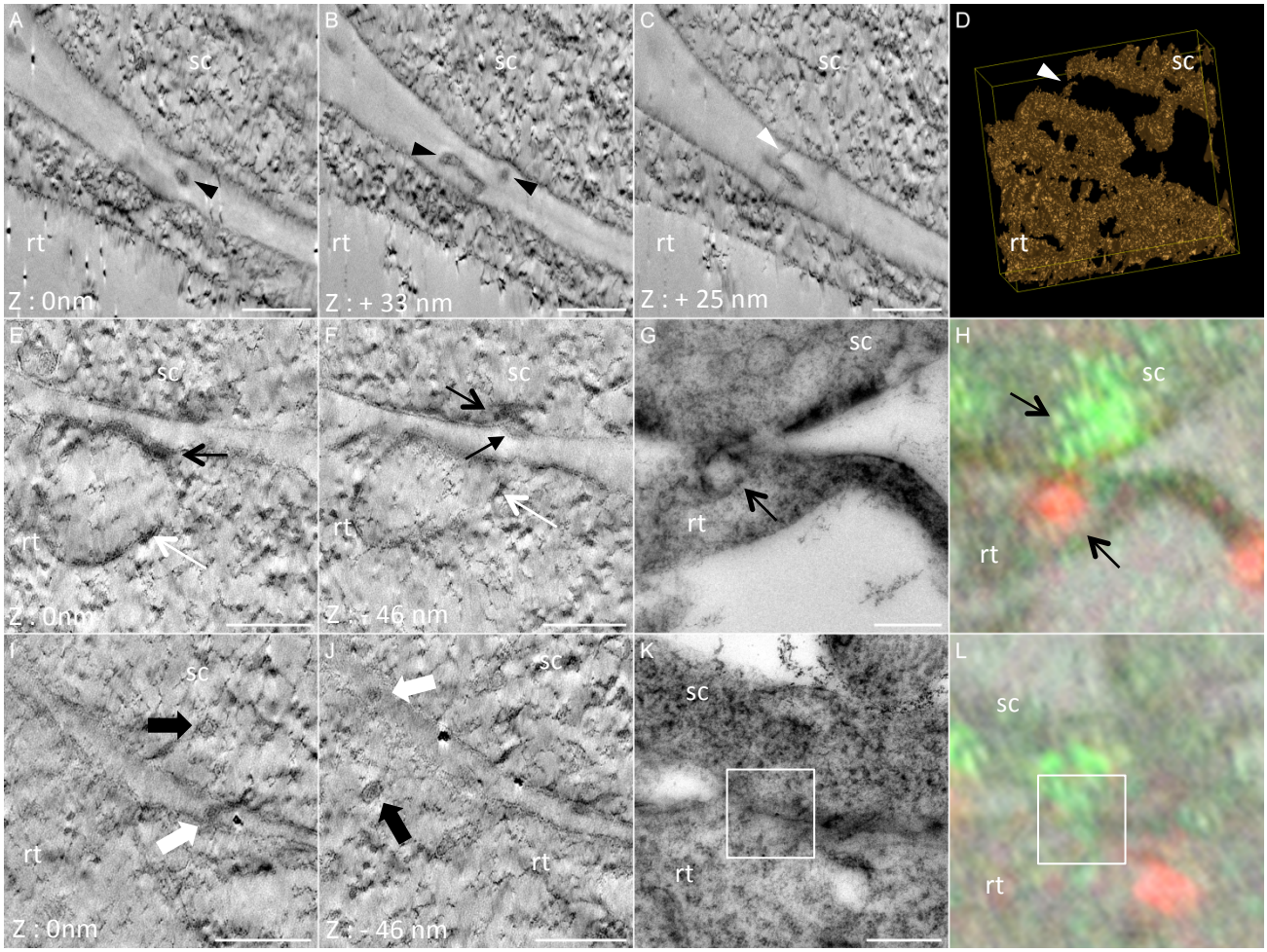

Figure 7. Plasmodesmata (PD) biogenesis events by electron tomography and correlative light electron microscopy

The scion and the rootstock are respectively at the top and bottom positions. **(A-C)** Three Z plans and **(D)** one 3D segmentation of two hemi-PD facing each other at the graft interface (black arrowheads); on the rootstock (rt) hemi-PD running along the middle lamella begin to enter in close contact to the hemi-PD coming from the scion (sc) (white arrowheads). **(E-F)** Two events of ER apposition to the plasma membrane are facing each other at the graft interface (black open arrows). Electron densification in the cell wall (black closed arrows), ribosomes associated with the ER (white open arrows). **(I-J)** Two plasmodesmata are present in a very thin wall; there is no space between the central element and the plasma membrane as typical of very young primary PD (white solid arrows). 40 nm wide vesicles (black solid arrow) around the cell wall at the PD biogenesis hotspot **(G and K)** At this region where PD span the cell wall, the ER is not clearly visible, but correlative microscopy reveals the presence of ER labeled with YFP in the scion.

Scale bars: (A, B, C, E and F) 200 nm, (I and J) 200 nm (G and K) 500 nm

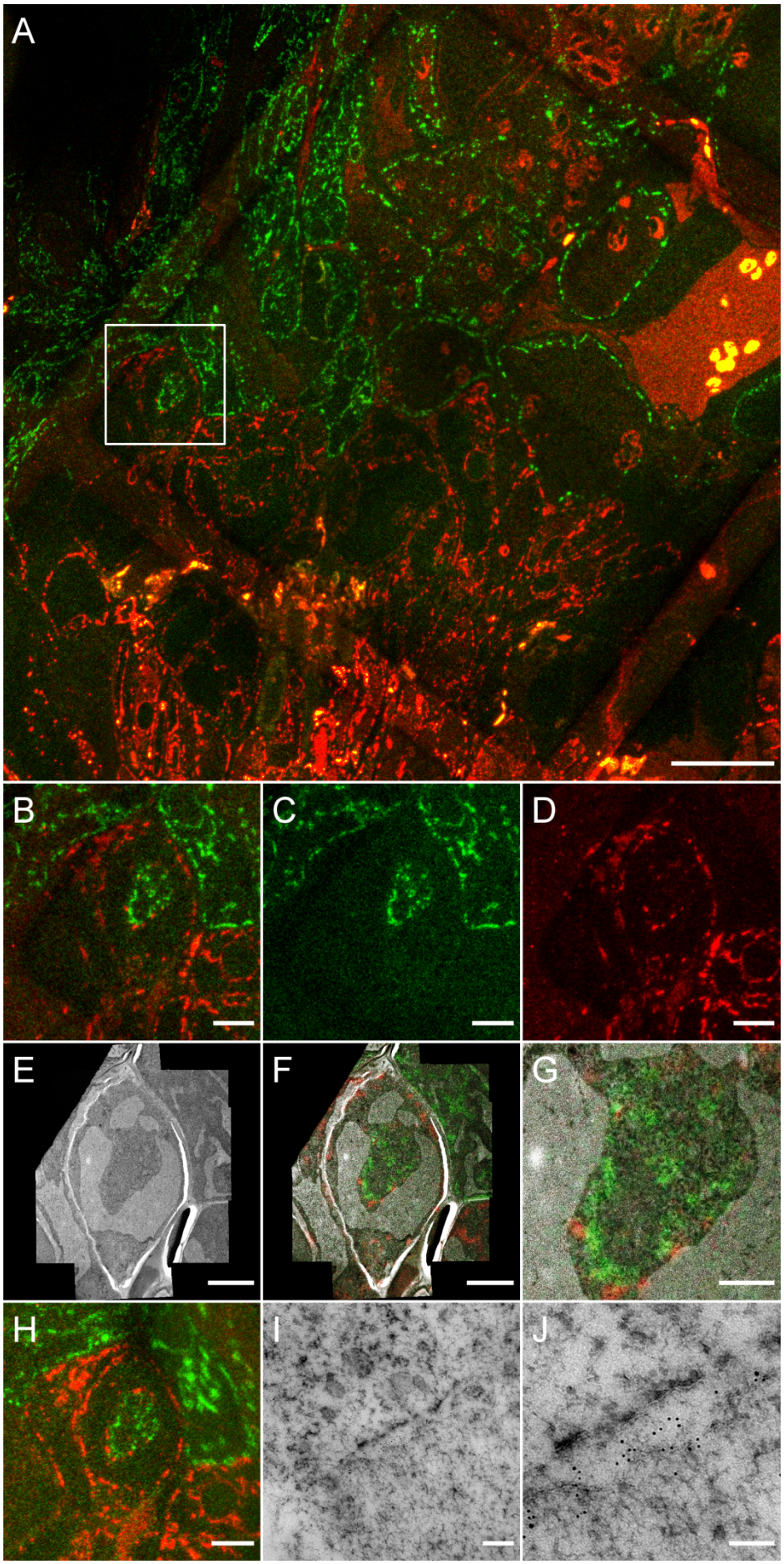

Figure 8. Bicolored cells are visible at the graft interface of *Arabidopsis thaliana* when scions expressing 35S::HDEL_YFP are grafted onto rootstocks expressing 35S::HDEL_mRFP three days after grafting

The scion and the rootstock are respectively at the top and bottom positions. **(A)** overview of a 150 nm-thick section of a graft interface, **(B)** crop of the bicolored cell highlighted with a white square in image (A), **(C)** the splitted YFP channel of (B), **(D)** the splitted RFP channel of (B), **(E)** stitched tiles of transmission electron micrographs of the same cell, **(F)** correlated light electron on the same cell, **(G)** crop of the correlated bicolored region, **(H)** the same cell is observed on another section, **(I-J)** immunogold labelling with antibodies angainst GFP reveals beads on the ER inside the HDEL_RFP cell (white square)

Scale bars: (A) 20 µm, (B, C, D, E, F, H) 5µm, (G) 2 µm, (I) 200 nm, (J) 100 nm

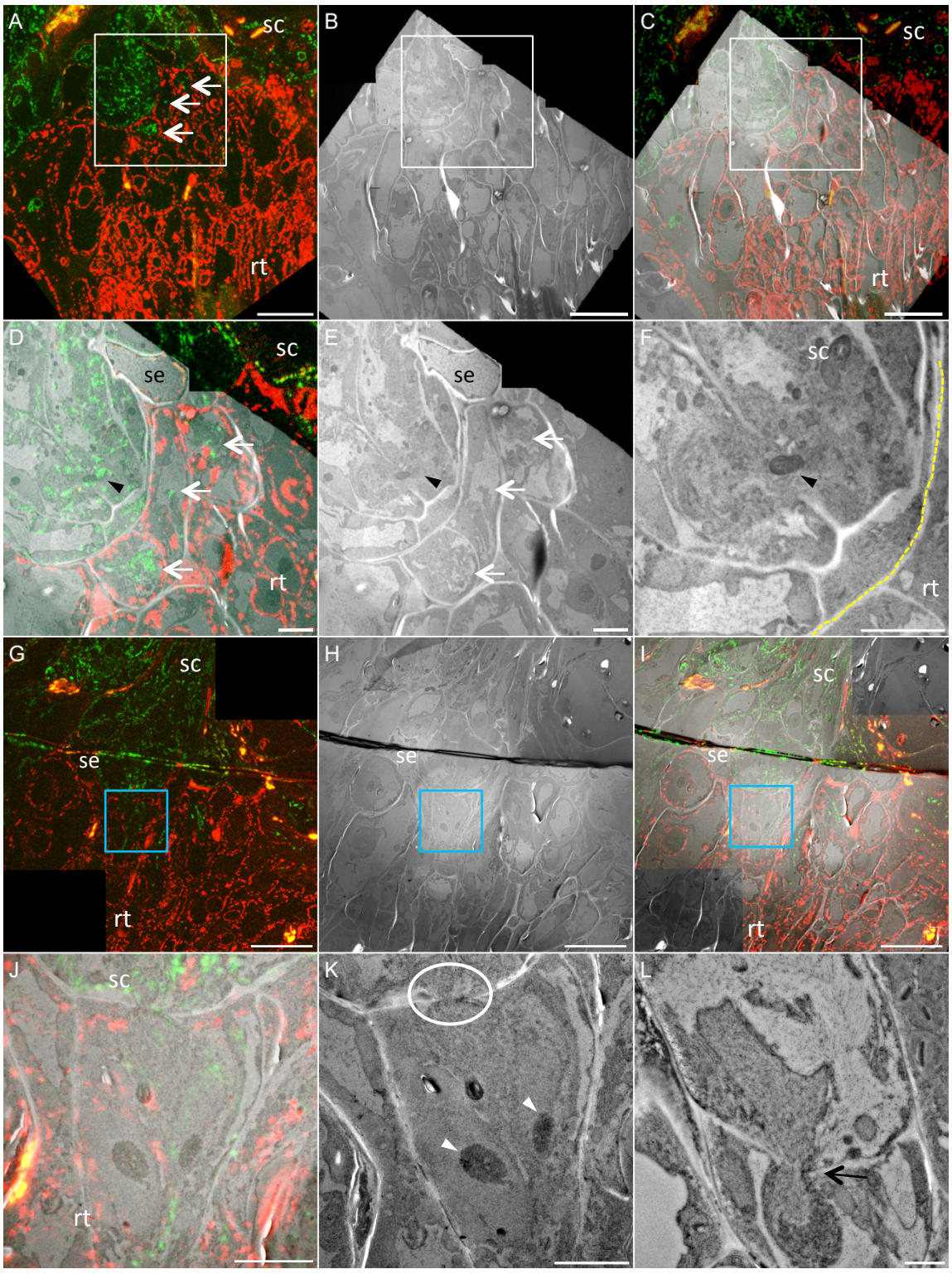
A
sc
rt
B
C
sc
rt
D
sc
se
rt
E
se
F
sc
rt
G
sc
se
rt
H
se
I
sc
se
rt
J
sc
rt
K
L

Figure 9. Bicolored cells and organelle transfer from cell-to-cell at the graft interface

The scion and the rootstock are respectively at the top and bottom positions. **(A-E)** Correlative light and electron microscopy reveals the presence of aligned bicolored cells (white arrows) at the graft interface. The superposition of fluorescent and electron microscopy acquisitions was based on cytological landmarks. On large field of view (C), the section deformations under the electron beam avoid a perfect correlation. **(D-F)** At higher magnification, sieve element (se) can be identified near to the bicolored cells, and just above the interface, a plastid is seen crossing a cell wall opening (black arrowheads). The graft interface is labeled with yellow dotted line on (F). **(G-I)** Correlative light and electron microscopy reveals the presence of bicolored cells (white arrows) that are in proximity of a with sieve element (se) at the graft interface. **(J-K)** A magnification of the white square region reveals a cell wall perforation at the interface (blue circle) and two nuclei with their nucleolus (white arrowheads). On the correlated view (D), one nucleus is surrounded by HDEL_YFP labeled ER while the other is surrounded by HDEL_mRFP labeled ER. **(L)** Near the interface, a structure that could be a nucleus was found passing through a cell wall perforation between two rootstock cells (black arrow).

Scale bars: (A, B, C, G, H and I) 20 µm, (D, E, J and K) 5 µm, (F and L) 2 µm

5/ Discussion

Ultrastructure of the graft interface has long remained difficult to target. The emergent high end microscopy technique, CLEM, allowed us to access for the first time the kinetics of the ultrastructural events occurring at the graft interface. The study of Melnyk (2015) shows a first attachment at 2 DAG. Unfortunately, for us, the fragility of the graft interface did not permit the cryofixation of the samples before 3 DAG because of scion and rootstock detachment. This fragility could be because of, before 3 DAG, the scion and the rootstock cells do not share enough common cell walls at the graft interface and that vascular tissues are not yet well connected.

At 3 DAG, a large part of the graft interface contains cellular and cell wall debris. The degradation of this necrotic layer to give way to the formation of common cell walls that may be the first step required for a robust graft union. Several kinds of EVs, divergent by their sizes and contents, were notably found in this necrotic layer. Extracellular vesicles could result from residues formed from sectioned cells, but they could be also the result of an active cell process. Graft union formation involves a lot of stress responses, notably associated with wounding (Melnyk *et al.,* 2018). In plants, EVs are of multiple types and are known to play a role in stress responses, immunity and mediate plant-microbe interactions (Rutter & Innes, 2017, 2018; Rybak & Robatzek, 2019). Extracellular vesicles can transport small RNAs from host plant cells to targeted cells in order to modulate its gene expression (Cai *et al.,* 2018). They are also able to bring enzymes, ribosomes into the cell wall in order to induce cell wall remodeling (Regente *et al.,* 2017). Moreover, EVs have been associated with PD, by acting to block PD permeability and stop the hypersensitive response spreading (An *et al.,* 2006). EV formation can be increased, as the number of branched PD, by salicylic acid treatments (Fitzgibbon *et al.,* 2013; Rutter & Innes, 2017). Thus, every previously cited EV functions could be required during the first steps of graft union formation. They could bring material needed to digest the necrotic layer and remodel the cell wall to make a common unique cell wall at the graft interface. This could provide tissue cohesion at the graft point. Moreover, by transporting elements permitting the gene regulation from one partner to the other, EVs might ensure the temporal and spatial synchronization between the scion and rootstock cells. Thus, before all symplastic connections, EVs could be the first communication pathway between the grafted partners. They could act as a first cell "sensor" of the wounding response during grafting as they are presumably easier to set up than secondary PD that requires preliminary partner synchronization. These sensors may permit the evaluation of compatibility level from the partner of the other wounded side. If there is the correct response, synchronized cell events may be triggered, leading to the formation of a common cell wall, secondary PD biogenesis and coordinated cell differentiation. Thus, the induction of EV formation during grafting could be the starting point to ensure the scion and rootstock communications. Salicylic acid treatments by inducing EVs formation as well as secondary PD formation could help the

cell wall fusion and the cell-to-cell connection between the scion and the rootstock. Measurements of the robustness of the graft interface throughout its development, in presence of salicylic acid could permit to answer this question.

In the cell wall at the graft interface, there is initially no PD. The only way to establish a symplastic connection requires *de novo* PD biogenesis. As in the heterograft between *H. annuus* and *V. faba* (Kollmann & Glockmann, 1985), in *A. thaliana* homografts spanning PD and hemi-PD, coming from scion and rootstock, are formed. Thus, even between cells of the same species, secondary PD biogenesis at the graft interface appears not to be a simple mechanism. In *A. thaliana* hypocotyl grafts, more than a third of PD fail to span entirely the cell wall. Surprisingly, the PD progression into the cell wall is stopped at the middle lamella position, which is known to be composed of pectin, a rather malleable compound (Knox & Benitez-Alfonso, 2014). Thus, secondary PD formation seems to require a drastic cell wall remodeling concerning maybe the middle lamella or the cell wall which is at the other side of this middle lamella. In fact, on the side where the PD biogenesis is initiated, ER-plasma membrane tethering and a thinning/weakening of the cell wall have to be synchronized to allow correct PD progression into the cell wall. If this cell wall remodeling is induced asymmetrically in relation to the middle lamella, meaning only on the side of the cell wall where ER is tethered, PD progression into the cell wall is deviated and PD evolves in a loop after running along the middle lamella to form, finally, one hemi-PD. However, if the cell wall remodeling and thinning is well coordinated at both sides, *de novo* desmotubule, in close contact with the plasma membrane will succeed to cross the cell wall. Afterwards, both plasma membranes fuse and a continuous PD is finally formed. The close interaction between the desmotubule and the plasma membrane is systematically observed at the cytosolic entries of every PD observed. This interaction could be essential to lead the desmotubule to the other side of the cell wall. In the PD in “ball of wool”, after this close interaction with the plasma membrane, the desmotubule grows into the cell wall and accumulates aberrantly into the central cavity where the close interactions between the desmotubule and the plasma membrane are lost. This PD class demonstrates that PD inclusion in the cell wall is a directed process not only governed by the deposition of new cell wall material. Moreover, the important number of secondary simple PD reinforced the hypothesis of a directed PD biogenesis process. This process, in contrast to the hemi-PD fusion proposed by Kollmann et al. (1991) where hemi-PD have to be in front to each other and where each opposite PM and each opposite desmotubule membranes have to fuse, requires less precision and steps. In fact, these straight simple PD derive probably from an unidirectional new PD penetration in the cell wall followed by both plasma membrane fusion. However, in heterograft system, PD observed are mainly branched (Kollmann & Glockmann, 1985), which could indicate that in less compatible grafts, directed secondary PD biogenesis use another mechanism. In *A. thaliana* homograft, the presence of

simple PD, branched PD and the hemi-PD in front of each other let us think that secondary PD biogenesis is an emergency that uses several pathways. Thus, *de novo* PD biogenesis is a complex event involving cell wall remodeling and PM/ER tethering, which are followed by at least one plasma membrane hemi-fusion, lead to connect *de novo* two cells.

The presence of branched PD at the graft interface could indicate two different things. The first one is that branched PD could be the result of the fusion of two hemi-PD well aligned. The second possibility is that, due the difficulty to form new PD crossing the middle lamella, increasing the cell-to-cell connectivity could be easier by adding new ramifications of a pre-existing PD rather than forming them *de novo*. This idea is supported by the facts that only newly divided cells have a majority of simple PD and that mature cells have a majority of branched PD (Nicolas *et al.,* 2017; Oparka *et al.,* 1999). Moreover, the evolution of branched PD into twin PD during the cell wall expansion could permit a relatively easily increase of the number of PD (Faulkner *et al.,* 2008). After a common cell wall formation, new PD formation could occur through the formation of hot spots of PD biogenesis by synchronized cells. On these spots, remodeling of the cell wall and plasma membrane-ER tethering takes place. These ERs can evolve into compressed strands closely interacting with the plasma membrane and capable of spanning entirely the cell wall and finally form a simple PD. During the cell expansion, the cell-to-cell connectivity is ensured by adding new PD ramifications on the pre-existing PD rather than making *de novo* PD, which is a symmetric landmark to allow a perfect spatial synchronization between both cells.

During PD biogenesis, if the thinning of the cell wall is excessive, partial plasma membrane fusion between both cells can occur from PD, as described during protoplast fusion (Withers & Cocking, 1972), and lead to the bicolored cell formation. Organelle transfers between partially fused cells can occur. These “cellmixis” events may explain the hybrid plants obtained from grafted callus cells (Fuentes *et al.,* 2014; Lu *et al.,* 2017; Stegemann & Bock, 2009). These cells fusion events could be favorited by an imperfect coordination between the cell wall thinning and the ER-plasma membrane tethering. In fact, the close interaction between the desmotubule and the plasma membrane plus the rigid frame of the cell wall can limit the plasma membrane pore opening. Thus, in absence of these two parameters, the expansion of the plasma membrane pore is not regulated. Another possibility is that the cell wall openings could correspond to the cell wall perforation processes occurring during the TE differentiation. However, perforations are known to occur after the characteristic lignin deposition in TE. Therefore, no lignin was observed on these bicolored cells. In order to recover quickly, grafted plants have to be able to exchange water and photoassimilates rapidly. In this context, plants would have an interest in maintaining cell viability and using all possible rescue mechanisms to ensure cell survival. The “cellmixis” events between wounded cells (originating from the same partner or not) could be emergency process for the cell rescue where cell

synchronization events are secondary. These cellmixis event could allow avoiding the formation of the thick necrotic layer that would delay the grafting union formation. Moreover, cellmixis events could ensure the formation of a more continuous tissue at the grafting unions. In fact, these hybrid cells are in endogenous continuity with both partners in the same time and their presence could constitute a key advantage in the graft sustainability. Unfortunately, these fusions events are difficult to observe maybe due to their precocity during the grafting process, their rarity or their future. New fluorescent lines allowing following different organelles have to be grafted to better understand these cellmixis events during grafting process. Secondary PD biogenesis and cellmixis seem to be processes ensuring the tissue cohesion at the graft interface because they allow establishing a membrane and cytoplasmic continuities between the scion and the rootstock. Our CLEM approach applied on different mutant lines of *A. thaliana* will permit to take up the challenge to identify protein actors which are required to end up the symplastic connections between both grafted partners.

6/ Acknowledgments

This work was supported by the French Nationnal Institute for Agronomical Research (INRA), the Region Nouvelle Aquitaine and the Institute of Vine and Wine Science (ISVV) (travel grant to Melnyk's lab to learn grafting procedure). Thanks to Charles Melnyk and Remi Lemoine that invited me to learn the grafting procedure of *A. thaliana*. Thanks to Claire Bréhélin for providing HDEL_YFP lines. All sample preparation and imaging was done on the Pôle Imagerie du Végétale, from Bordeaux Imaging Centre (http://www.bic.u-bordeaux.fr/). The authors declare having no conflicts of interests.

7/ References

An, Q., Ehlers, K., Kogel, K. H., Van Bel, A. J. E., & Hückelhoven, R. (2006). Multivesicular compartments proliferate in susceptible and resistant MLA12-barley leaves in response to infection by the biotrophic powdery mildew fungus. *New Phytologist*, *172*(3), 563–576. https://doi.org/10.1111/j.1469-8137.2006.01844.x

Aoyagi, S., Sugiyama, M., & Fukuda, H. (1998). BEN1 and ZEN1 cDNAs encoding S1-type DNases that are associated with programmed cell death in plants. *FEBS Letters*, *429*(2), 134–138. https://doi.org/10.1016/S0014-5793(98)00563-8

Avci, U., Earl Petzold, H., Ismail, I. O., Beers, E. P., & Haigler, C. H. (2008). Cysteine proteases XCP1 and XCP2 aid micro-autolysis within the intact central vacuole during xylogenesis in Arabidopsis roots. *Plant Journal*, *56*(2), 303–315. https://doi.org/10.1111/j.1365-313X.2008.03592.x

Batailler, B., Lemaître, T., Vilaine, F., Sanchez, C., Renard, D., Cayla, T., … Dinant, S. (2012). Soluble and filamentous proteins in Arabidopsis, 1258–1273. https://doi.org/10.1111/j.1365-3040.2012.02487.x

Cai, Q., Qiao, L., Wang, M., He, B., Lin, F., Palmquist, J., & Jin, H. (2018). Plants send small RNAs in extracellular vesicles to fungal pathogen to silence virulence genes. *Science*, *360*(June), 1126–1129. https://doi.org/10.1126/science.aar4142

Cantrill, L. C., Overall, R. L., & Goodwin, P. B. (1999). CELL-TO-CELL COMMUNICATION VIA PLANT ENDOMEMBRANES. *Cell Biology International*, *23*(10), 653–661.

Cheadle, V. I., Risley, E. B., & Esau, K. (1962). DEVELOPMENT OF SIEVE-PLATE PORES. *Botanical Gazette*, *123*(4), 233–243.

Clark, N. M., Hinde, E., Winter, C. M., Fisher, A. P., Crosti, G., Blilou, I., … Benfey, P. N. (2016). Tracking transcription factor mobility and interaction in Arabidopsis roots with fluorescence correlation spectroscopy, 1–25. https://doi.org/10.7554/eLife.14770

Ding, B., Turgeon, R., & Parthasarathy, M. V. (1992). Substructure of freeze-substituted plasmodesmata. *Protoplasma*, *169*(1–2), 28–41. https://doi.org/10.1007/BF01343367

Esau, K. (1973). Comparative Structure of Companion Cells and Phloem Parenchyma Cells in Mimosa pudica L .

Esau, K., & Thorsch, J. (1985). SIEVE PLATE PORES AND PLASMODESMATA , THE COMMUNICATION CHANNELS OF THE SYMPLAST : ULTRASTRUCTURAL ASPECTS AND DEVELOPMENTAL RELATIONSl. *American Journal of Botany*, *72*(10), 1641–1653. https://doi.org/10.1002/j.1537-2197.1985.tb08429.x

Farage-Barhom, S., Burd, S., Sonego, L., Perl-Treves, R., & Lers, A. (2008). Expression analysis of the BFN1 nuclease gene promoter during senescence, abscission, and programmed cell death-related processes. *Journal of Experimental Botany*, *59*(12), 3247–3258. https://doi.org/10.1093/jxb/ern176

Faulkner, C., Akman, O. E., Bell, K., Jeffree, C., & Oparka, K. J. (2008). Peeking into Pit Fields: A Multiple Twinning Model of Secondary Plasmodesmata Formation in Tobacco. *The Plant Cell Online*, *20*(6), 1504–1518. https://doi.org/10.1105/tpc.107.056903

Fitzgibbon, J., Beck, M., Zhou, J., Faulkner, C., Robatzek, S., & Oparka, K. (2013). A Developmental Framework for Complex Plasmodesmata Formation Revealed by Large-Scale Imaging of the Arabidopsis Leaf Epidermis, *25*(January), 57–70. https://doi.org/10.1105/tpc.112.105890

Froelich, D. R., Mullendore, D. L., Jensen, K. H., Ross-Elliott, T. J., Anstead, J. A., Thompson, G. A., … Knoblauch, M. (2011). Phloem Ultrastructure and Pressure Flow: Sieve-Element-Occlusion-Related Agglomerations Do Not Affect Translocation. *The Plant Cell*, *23*(12), 4428–4445. https://doi.org/10.1105/tpc.111.093179

Fuentes, I., Stegemann, S., Golczyk, H., Karcher, D., & Bock, R. (2014). Horizontal genome transfer as an asexual path to the formation of new species. *Nature*. https://doi.org/10.1038/nature13291

Furuta, K., Lichtenberger, R., & Helariutta, Y. (2012). The role of mobile small RNA species during root growth and development. *Current Opinion in Cell Biology*, *24*(2), 211–216. https://doi.org/10.1016/j.ceb.2011.12.005

Furuta, K. M., Yadav, S. R., Lehesranta, S., Belevich, I., Miyashima, S., Heo, J. ok, … Helariutta, Y. (2014). Plant development. Arabidopsis NAC45/86 direct sieve element morphogenesis culminating in enucleation. *Science (New York, N.Y.)*, *345*(6199), 933–937. https://doi.org/10.1126/science.1253736

Gautier, A. T., Chambaud, C., Brocard, L., Ollat, N., Gambetta, G. A., Delrot, S., & Cookson, S. J. (2019). Merging genotypes: Graft union formation and scion-rootstock interactions. *Journal of Experimental Botany*, *70*(3), 805–815. https://doi.org/10.1093/jxb/ery422

Grison, M. S., Brocard, L., Fouillen, L., Nicolas, W., Wewer, V., Dörmann, P., … Bayer, E. M. (2015). Specific membrane lipid composition is important for plasmodesmata function in Arabidopsis.

The Plant Cell, *27*(4), 1228–1250. https://doi.org/10.1105/tpc.114.135731

Knox, J. P., & Benitez-Alfonso, Y. (2014). Roles and regulation of plant cell walls surrounding plasmodesmata. *Current Opinion in Plant Biology*, *22*(Figure 1), 93–100. https://doi.org/10.1016/j.pbi.2014.09.009

Knox, K., Wang, P., Kriechbaumer, V., Tilsner, J., Frigerio, L., Sparkes, I., … Oparka, K. (2015). Putting the Squeeze on Plasmodesmata: A Role for Reticulons in Primary Plasmodesmata Formation. *Plant Physiology*, *168*(4), 1563–1572. https://doi.org/10.1104/pp.15.00668

Kollmann, R., & Glockmann, C. (1985). Studies on graft unions. I. Plasmodesmata between cells of plants belonging to different unrelated taxa. *Protoplasma*, *124*(3), 224–235. https://doi.org/10.1007/BF01290774

Kollmann, R., & Glockmann, C. (1991). Studies on graft unions - III. On the mechanism of secondary formation of plasmodesmata at the graft interface. *Protoplasma*, *165*(1–3), 71–85. https://doi.org/10.1007/BF01322278

Kollmann, R., Yang, S., & Glockmann, C. (1985). Studies on graft unions - II. Continuous and half plasmodesmata in different regions of the graft interface. *Protoplasma*, *126*(1–2), 19–29. https://doi.org/10.1007/BF01287669

Lee, H., Sparkes, I., Gattolin, S., Dzimitrowicz, N., Roberts, L. M., Hawes, C., & Frigerio, L. (2013). An Arabidopsis reticulon and the atlastin homologue RHD3-like2 act together in shaping the tubular endoplasmic reticulum, 481–489.

Lu, Y., Stegemann, S., Agrawal, S., Karcher, D., Ruf, S., Bock, R., … Bock, R. (2017). Horizontal Transfer of a Synthetic Metabolic Pathway between Plant Species Report Horizontal Transfer of a Synthetic Metabolic Pathway between Plant Species. *Current Biology*, 1–8. https://doi.org/10.1016/j.cub.2017.08.044

Lucas, W. J., & Lee, J.-Y. (2004). Plasmodesmata as a supracellular control network in plants. *Nature Reviews. Molecular Cell Biology*, *5*(9), 712–726. https://doi.org/10.1038/nrm1470

Mazur, E., Benková, E., & Friml, J. (2016). Vascular cambium regeneration and vessel formation in wounded inflorescence stems of Arabidopsis. *Scientific Reports*, *6*, 1–15. https://doi.org/10.1038/srep33754

Melnyk, C. W. (2017). *Grafting with Arabidopsis* (Vol. 137).

Melnyk, C. W., Gabel, A., Hardcastle, T. J., Robinson, S., & Miyashima, S. (2018). Transcriptome dynamics at Arabidopsis graft junctions reveal an intertissue recognition mechanism that activates vascular regeneration, *115*(10). https://doi.org/10.1073/pnas.1718263115

Melnyk, C. W., Schuster, C., Leyser, O., & Meyerowitz, E. M. (2015). A developmental framework for graft formation and vascular reconnection in arabidopsis thaliana. *Current Biology*, *25*(10), 1306–1318. https://doi.org/10.1016/j.cub.2015.03.032

Nakashima, J., Takabe, K., Fujita, M., & Fukuda, H. (2000). Autolysis during in vitro tracheary element differentiation: Formation and location of the perforation. *Plant and Cell Physiology*, *41*(11), 1267–1271. https://doi.org/10.1093/pcp/pcd055

Nelson, B. K., Cai, X., & Nebenfu, A. (2007). A multicolored set of in vivo organelle markers for co-localization studies in Arabidopsis and other plants, 1126–1136. https://doi.org/10.1111/j.1365-313X.2007.03212.x

Nicolas, W. J., Bayer, E., & Brocard, L. (2018). Electron Tomography to Study the Three-dimensional Structure of Plasmodesmata in Plant Tissues–from High Pressure Freezing Preparation to Ultrathin Section Collection, *8*, 1–25. https://doi.org/10.21769/BioProtoc.2681

Nicolas, W. J., Grison, M. S., Trépout, S., Gaston, A., Fouché, M., Cordelières, F. P., … Bayer, E. M. (2017). Architecture and permeability of post-cytokinesis plasmodesmata lacking cytoplasmic

sleeves. *Nature Plants*, *17082*(June). https://doi.org/10.1038/nplants.2017.82

Oparka, K. J., Roberts, A. G., Boevink, P., Cruz, S. S., Roberts, I., Pradel, K. S., … Epel, B. (1999). Simple, but not branched, plasmodesmata allow the nonspecific trafficking of proteins in developing tobacco leaves. *Cell*, *97*(6), 743–754. https://doi.org/10.1016/S0092-8674(00)80786-2

Otero, S., Helariutta, Y., & Benitez-Alfonso, Y. (2016). Symplastic communication in organ formation and tissue patterning. *Current Opinion in Plant Biology*, *29*, 21–28. https://doi.org/10.1016/j.pbi.2015.10.007

Regente, M., Pinedo, M., Clemente, H. S., Balliau, T., Jamet, E., & De La Canal, L. (2017). Plant extracellular vesicles are incorporated by a fungal pathogen and inhibit its growth. *Journal of Experimental Botany*, *68*(20), 5485–5495. https://doi.org/10.1093/jxb/erx355

Rutter, B. D., & Innes, R. W. (2017). Extracellular vesicles isolated from the leaf apoplast carry stress-response proteins. *Plant Physiology*, *173*(1), 728–741. https://doi.org/10.1104/pp.16.01253

Rutter, B. D., & Innes, R. W. (2018). Extracellular vesicles as key mediators of plant–microbe interactions. *Current Opinion in Plant Biology*, *44*, 16–22. https://doi.org/10.1016/j.pbi.2018.01.008

Rybak, K., & Robatzek, S. (2019). Functions of extracellular vesicles in immunity and virulence. *Plant Physiology*, *179*(4), 1236–1247. https://doi.org/10.1104/pp.18.01557

Sidorov, V., Armstrong, C., Ream, T., Ye, X., & Saltarikos, A. (2018). " Cell grafting ": a new approach for transferring cytoplasmic or nuclear genome between plants. *Plant Cell Reports*, *37*(8), 1077–1089. https://doi.org/10.1007/s00299-018-2292-7

Stegemann, S., & Bock, R. (2009). Exchange of genetic material between cells in plant tissue grafts. *Science (New York, N.Y.)*, *324*(5927), 649–651. https://doi.org/10.1126/science.1170397

Tilney, L. G., Cooke, T. J., Connelly, P. S., & Tilney, M. S. (1991). The structure of plasmodesmata as revealed by plasmolysis, detergent extraction, and protease digestion. *Journal of Cell Biology*, *112*(4), 739–747. https://doi.org/10.1083/jcb.112.4.739

Turgeon, R. (1996). Phloem loading and plasmodesmata. *Trends in Plant Science*, *1*(12), 418–423. https://doi.org/10.1016/S1360-1385(96)10045-5

Withers, L. A., & Cocking, E. C. (1972). Fine-structural studies on spontaneous and induced fusion of higher plant protoplasts. *Journal of Cell Science*, *11*(1), 59–75.

8/ Supplemental data

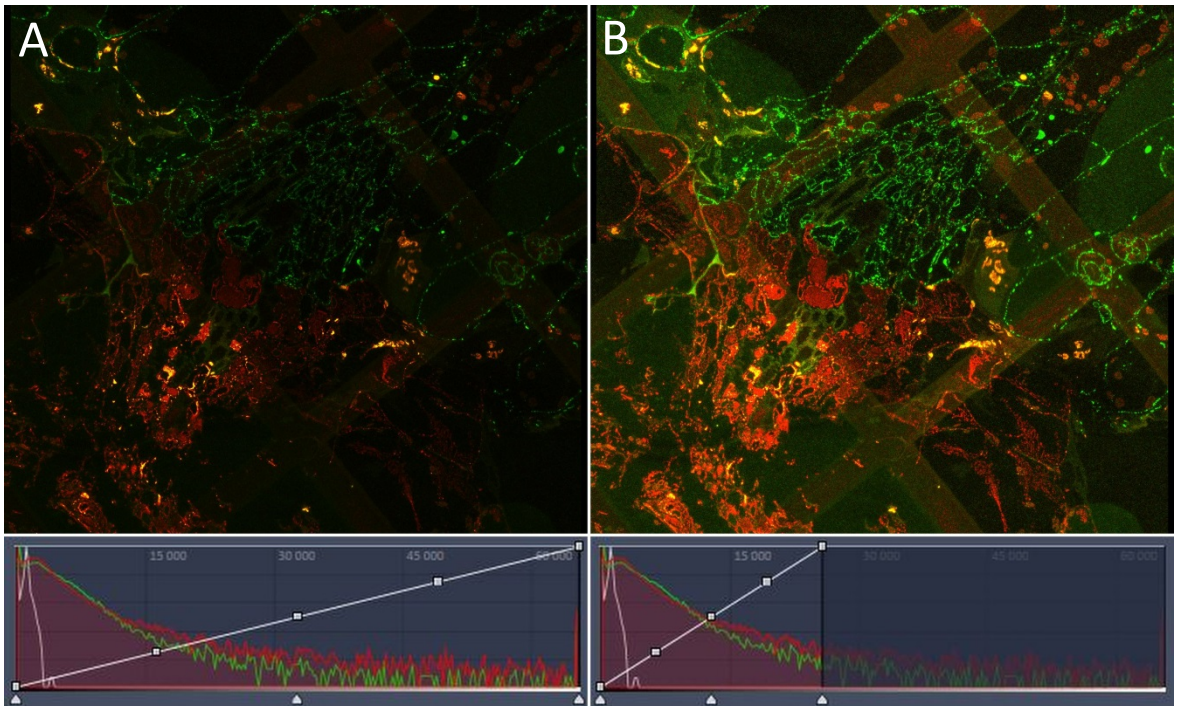

Supplemental Figure 1. Histogram display and laser power

Yellow fluorescent protein: 488 nm laser at the power of 24 %

Red fluorescent protein: 561nm laser at the power of 1.5 %

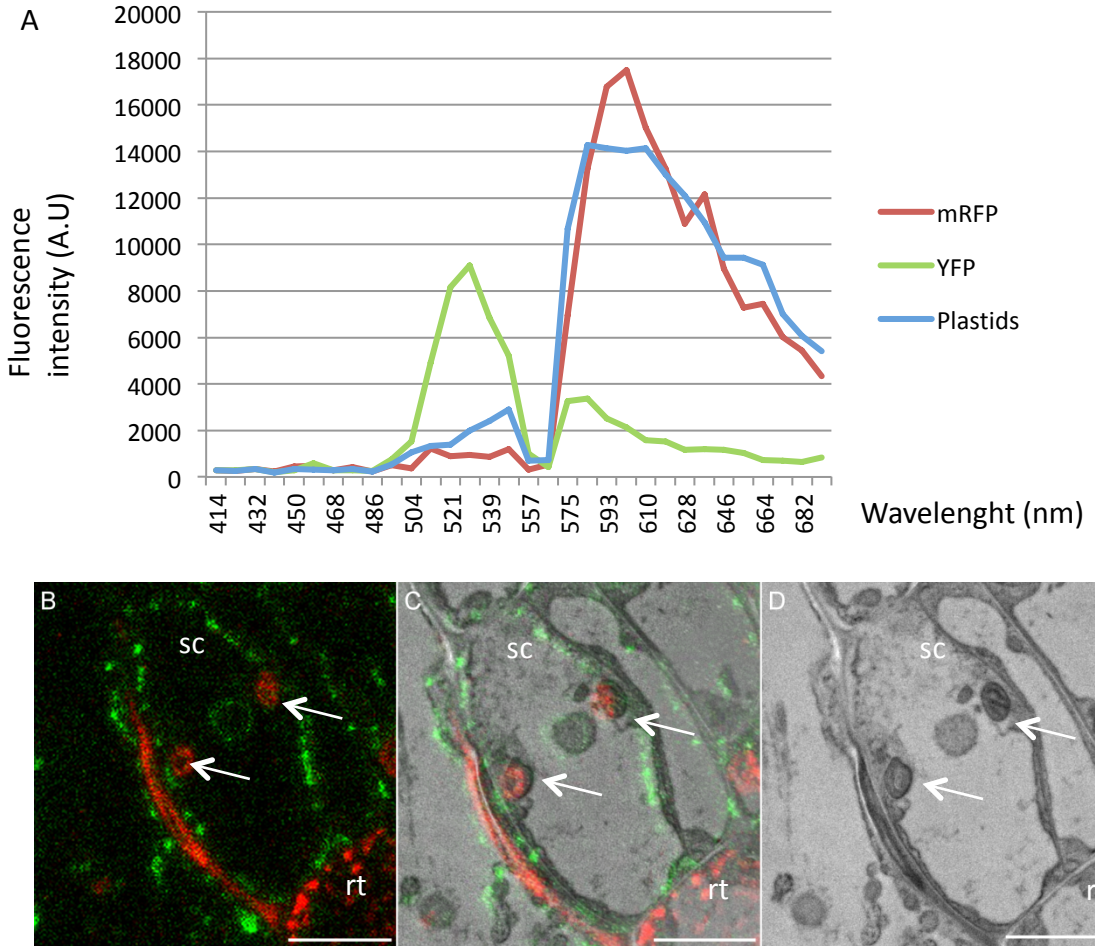

Supplemental Figure 2. Emission spectra of chloroplast, mRFP and YFP after embedding in HM20

When illuminated with 488 nm line, chloroplast crosstalk in the mRPF channel **(A)** Fluorescence emission spectra of mRFP (red), YFP (green) and plastids (blue) illuminated with 488 and 561 lines **(B)** Confocal, **(C)** Correlated, and **(D)** TEM imaging permit to identify chloroplast

sc: scion, rt: rootstock

Scale bars: 5 µm

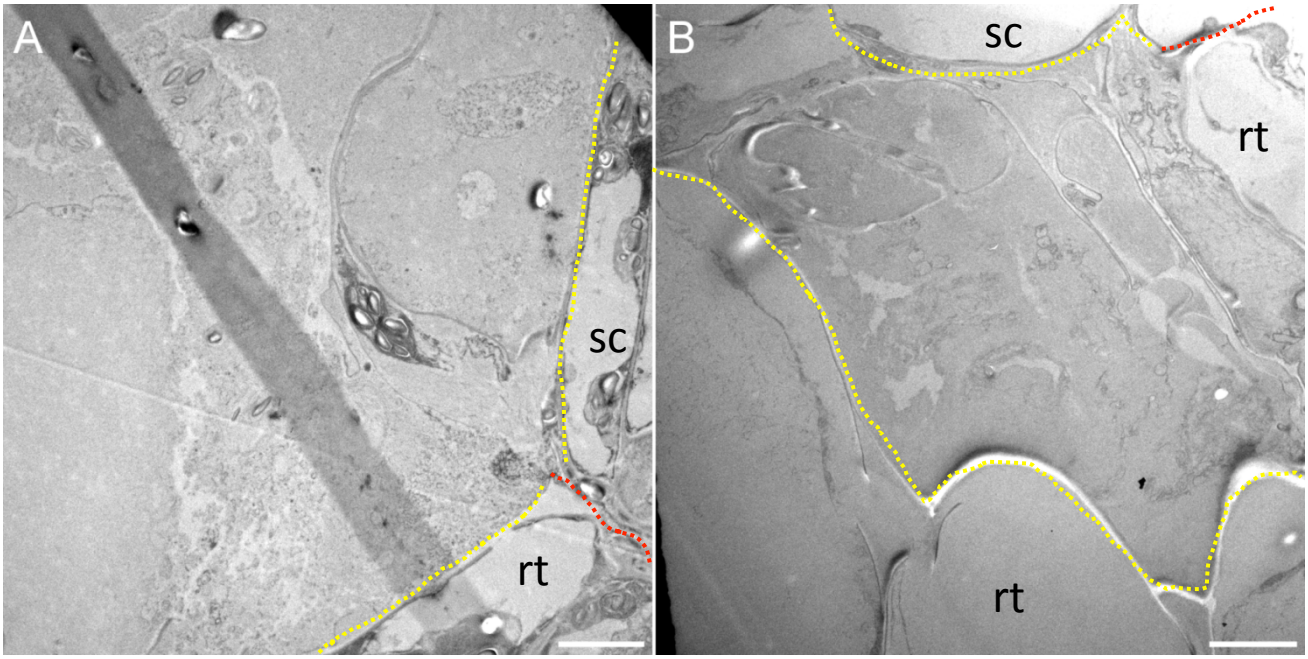

Supplemental Figure 3. Cellular debris are commonly found both at 3 DAG (A) and 6 DAG (B) at the periphery of the graft interface

Yellow dashed lines show the border of the grafts, red dashed arrows show the graft interface. sc: scion, rt: rootstock

Scale bars: 5 µm

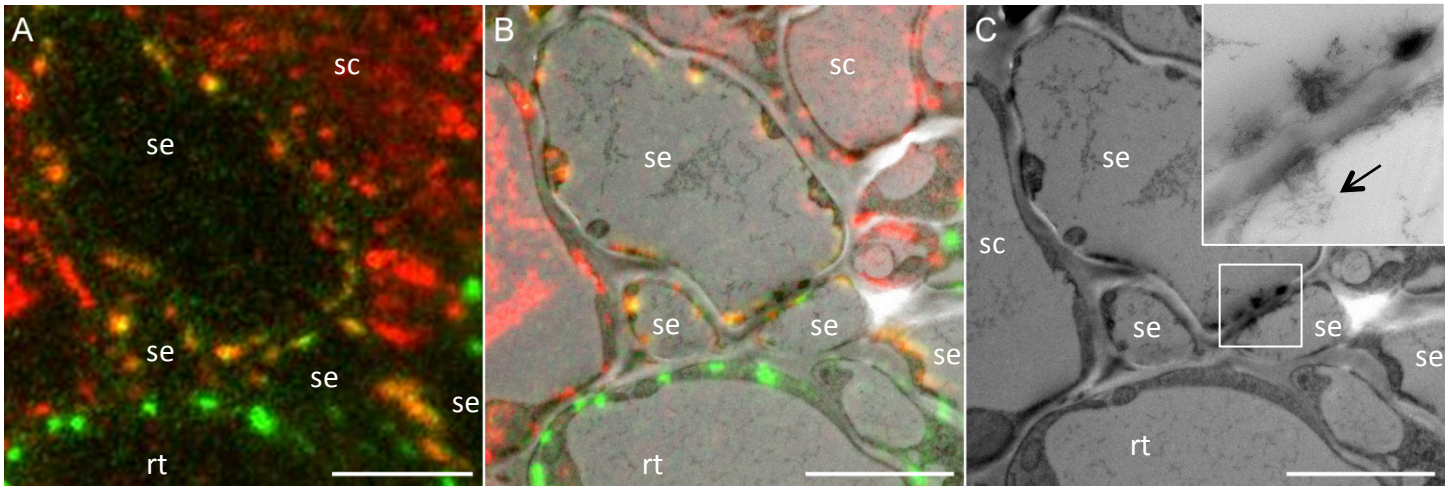

Supplemental Figure 4. Autofluorescence pattern of sieve element

(A) Confocal, **(B)** Correlated, and **(C)** TEM imaging of sieve elements, black arrow shows P-proteins

sc: scion, rt: rootstock, se: sieve element,

Scale bars: 5 µm

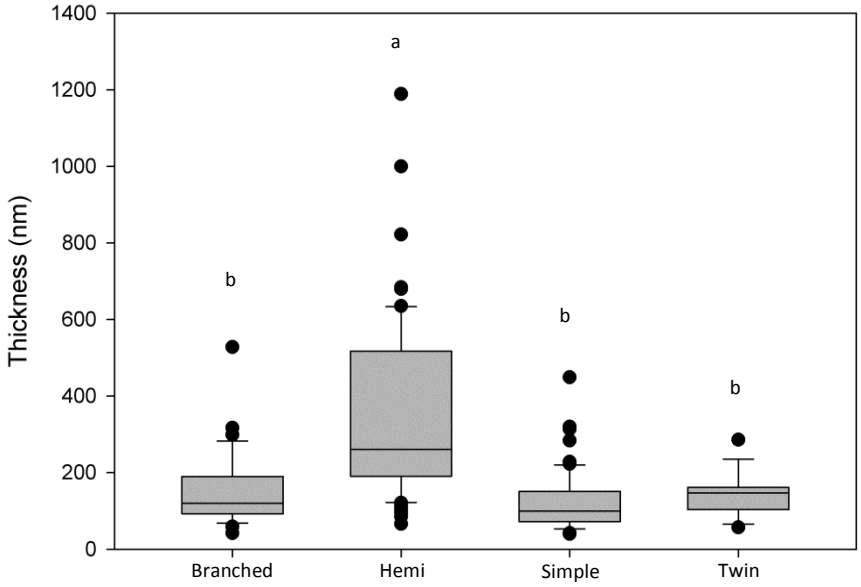

Supplemental Figure 5. Box plot of thickness of the cell wall near to the plasmodesmata found at the graft interface of *Arabidopsis thaliana* by classes of plasmodesmata

Box plots depict, interquartiles and outliers. Letters indicate the results of ANOVA on ranks and Dunn's tests (p-value < 0.001).

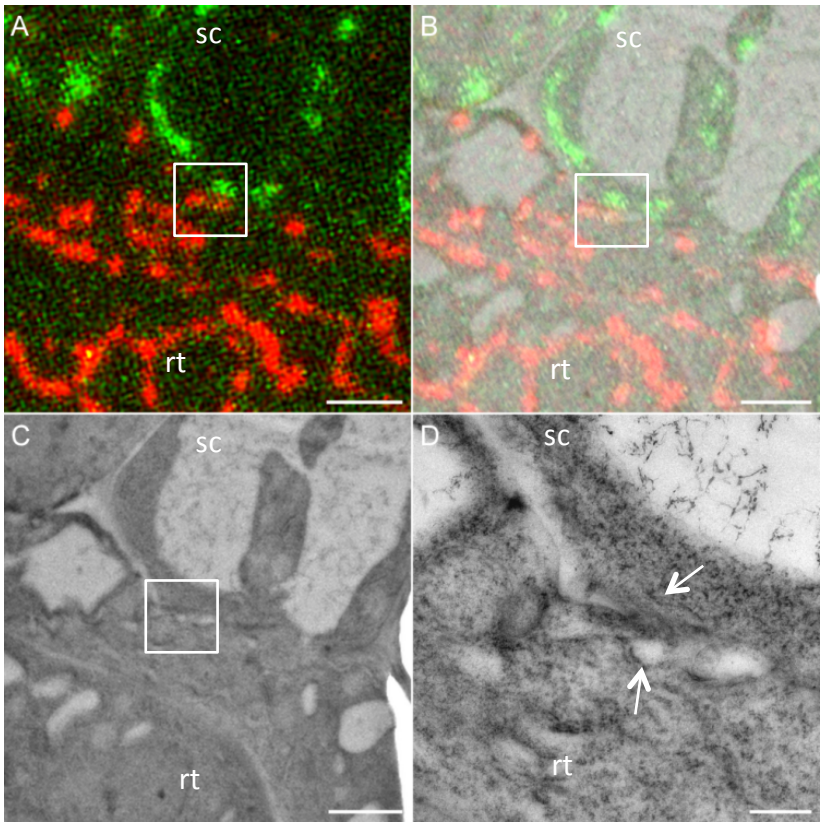

Supplemental Figure 6. Alignment of cortical ER is observed at the graft interface in a region of thin cell wall

(A) Confocal, **(B)** correlative light and electron microscopy, and **(C)** electron microscopy of the same graft interface showing endoplasmic reticulum facing each other at the graft interface of *Arabidopsis thaliana.* (D) Enlarged electron micrographs of the white square shown in (A), (B) and (C)

Scale bars: (A-C) 2 µm, (D) 500 nm

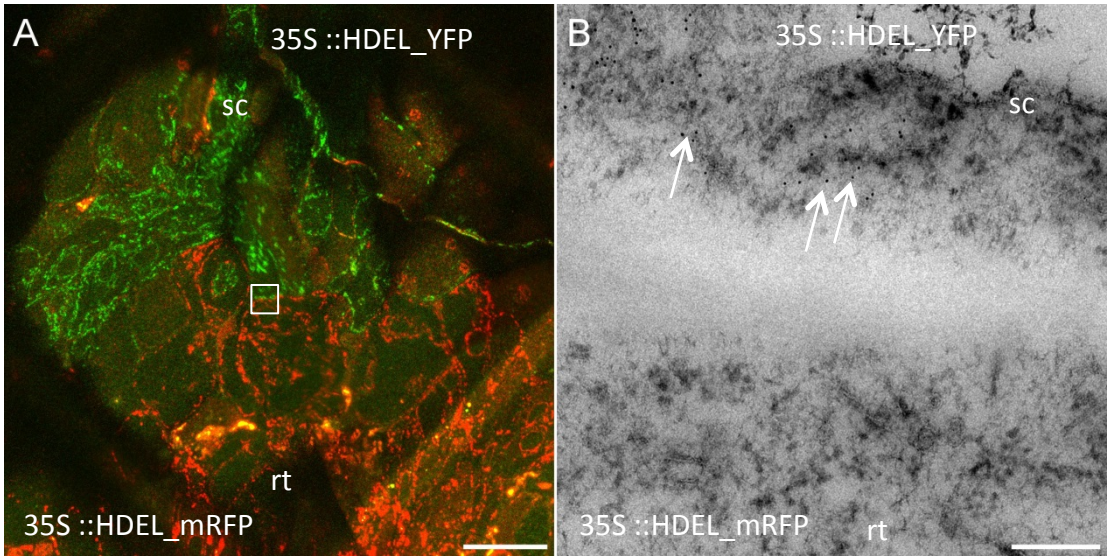

Supplemental Figure 7. Negative control of yellow fluorescent protein immunogold labelling

The scion and the rootstock are respectively at the top and bottom positions. Endoplasmic reticulum (ER) from 35S::HDEL_mRFP partner is not labeled with gold beads while ER from 35S::HDEL_YFP partner is labeled (white arrows highlight some beads)

Scale bars: (A) 20 µm, (B) 200 nm

3. Additional results

3.1. Assessing the permeability of PD at the graft interface

3.1.1. Grafting 35S::GFP onto 35S::HDEL_mRFP

Thanks to our CLEM approach, the presence of PD at the graft interface from 3 DAG was demonstrated. They are formed as well by scion and rootstock. Even if the link between ultrastructural characteristics and permeability begin to be studied, simply having the ultrastructure does not permit to access to the permeability. Indeed, counterintuitive results were obtained in Nicolas *et al.,* (2017). Plasmodesmata of type I, which do not have an apparent cytoplasmic sleeve, are permeable. Additionally, it is known that PD could change of permeability throughout development of the plant, especially during the sink-source transition (Oparka *et al.,* 1999). This permeability modification is also associated to an ultrastructural modification of PD. They demonstrated that simple PD are found in young leaf tissues (sink) were more permeable than branched PD found in older leaf tissues (source). A cytoplasmic sleeve is observed for branched PD. However, no information about PD permeability could be obtained directly from their ultrastructure. To access to the functional cell-to-cell connectivity between the scion and the rootstock, dynamic studies need to be performed. Determining and following the permeability of PD specifically at the graft interface would highlight their roles during the graft establishment. Moreover, in the context of graft, PD could have an asymmetric permeability at the graft interface, with a preferential transport from one partner to the other or an asymmetric SEL. Finally, studying the permeability of PD at the graft interface is an opportunity to focus on the permeability of secondary PD, established or not between two different genomic backgrounds that could not be addressed in a non-grafted plant because of the presence of numerous primaries PD.

To study symplastic connection establishment at the graft interface, we started by grafting plants expressing 35S::GFP with HDEL_mRFP lines. Both combinations 35S::GFP grafted onto HDEL_mRFP and HDEL_mRFP grafted onto 35S::GFP were used. 35S::GFP is a cytosolic protein that could freely diffuse through PD whereas HDEL_mRFP is retained in the lumen of ER and it is not able to pass through the desmotubule of PD (Knox *et al.,* 2015). We tracked the GFP diffusion at the graft junction at different time 3, 4, 5 and 8 DAG (Fig. 12).

Whatever the direction of the combination, free GFP was observed in the cytoplasm and nuclei of cells of HDEL_mRFP lines. These results could indicate that PD at the graft interface are functional and permeable. However, as observed in ultrastructural studies, SE were already connected at 3 DAG. Thus, the presence of GFP in HDEL_mRFP could be due to either cell-to-cell movement or phloem unloading process. Phloem flux is orientated from source to sink (Complainville *et al.,* 2003). In *A. thaliana* hypocotyl grafts, the source tissues are composed by the residual cotyledon and

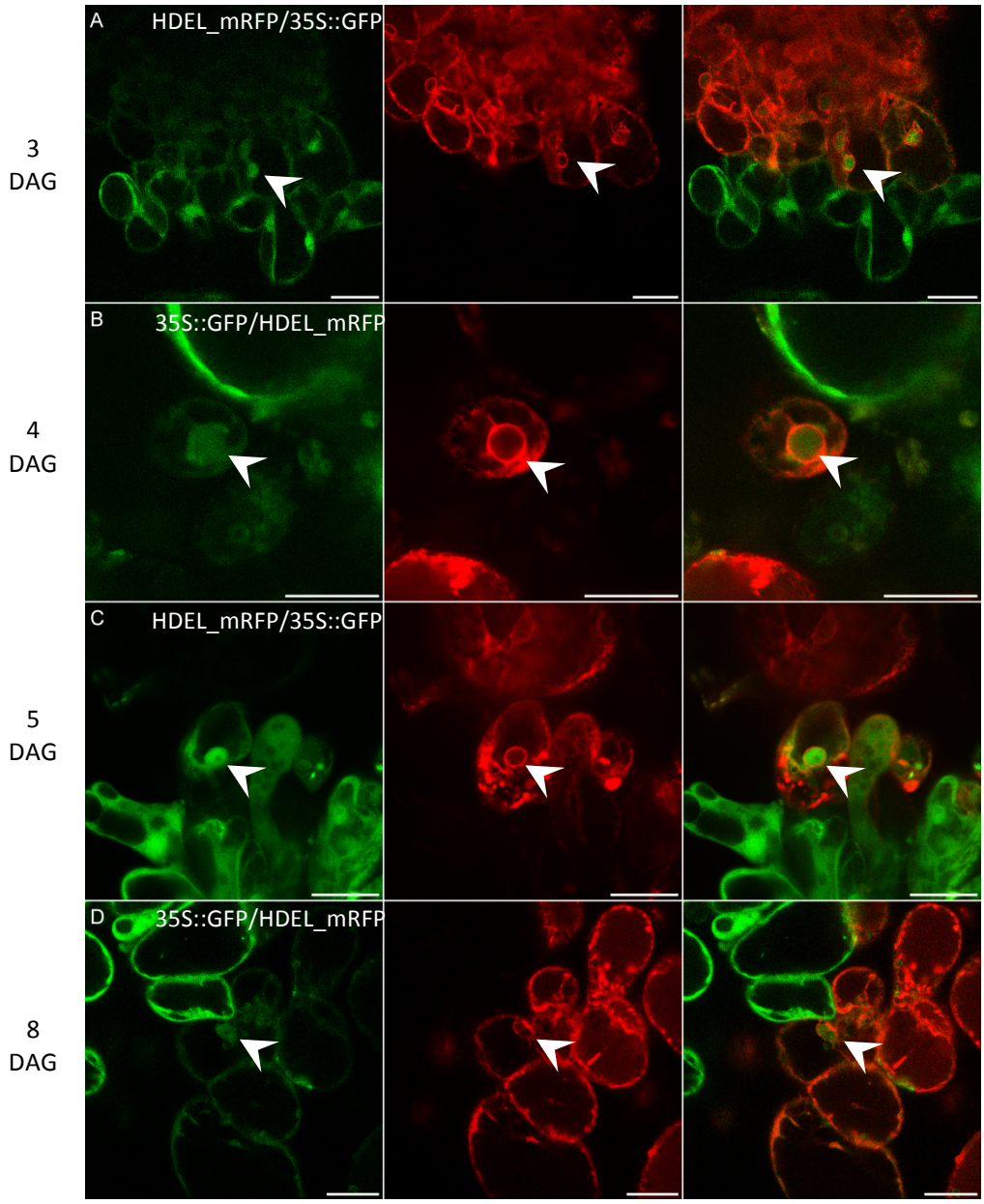

Figure 12. Cytosolic Green Fluorescent Protein (GFP) is able to move at the graft interface at 3, 4, 5 and 8 days after grafting (DAG)

For each time point, GFP channel, mRFP channel and the composite are shown.

(A) 3 DAG, HDEL_mRFP grafted onto 35S::GFP, **(B)** 4 DAG, 35S::GFP grafted onto HDEL_mRFP, **(C)** 5 DAG, HDEL_mRFP grafted onto 35S::GFP, **(D)** 8 DAG, 35S::GFP grafted onto HDEL_mRFP

The movement of GFP has been observed at each time either toward scion or rootstock

White arrowheads indicate the GFP found in the grafted partner

Scale bars: (A-D) 20 µm

potentially the first leaves. Thus, the GFP diffusion, when observed from rootstock to scion could almost be linked to symplastic connection rather than the phloem unloading process. Nevertheless, it is not possible to exclude that this GFP movement was actually unloaded from the phloem.

3.1.2. Development of new tools to assess plasmodesmata permeability only

To overcome this problem, we designed a new strategy based on the grafting of one transgenic line expressing 35S::HDEL_YFP and a photoactivable variant of the GFP (PA-GFP (Patterson *et al*., 2002)) and a transgenic line expressing 35S::tagRFP, (Fig. 13). The UV illumination with 405nm photodiode permits to switch on the PA-GFP which becomes excitable such as the conventional GFP. Thanks to HDEL-YFP, the graft interface can be reliably localized. The cytosolic tagRFP can freely pass through PD from cell-to-cell. Then, cells presenting at the same time HDEL_YFP and tagRFP are targeted. The presence of tagRFP could be due to direct symplastic connections or phloem unloading. To discriminate both pathways, PA-GFP will be activated in the HDEL_YFP plus tagRFP cells. If the passage of PA-GFP from the photo activated cell into the adjacent 35S::tagRFP cells occurs in a lapse time of few minutes, it will mean that functional PD connect both cells in which the molecule traveled and not that it is due to phloem loading/unloading. On the contrary, if the transport of the PA-GFP occurs a long time after, it means that it has been unloaded by phloem and then recaptured by the grafted partners.

Our results demonstrated that 35S::tagRFP was able to move through the graft interface at 5 DAG. However, we only succeed to activate the PA-GFP on the graft surface. Unfortunately, cells showing the two labels are usually localized deeper in the tissue of the graft interface. Thus due to the scattering of the light, the activation was either too weak (Fig. 14) or not enough precise leading to the activation of several cells including 35S::tagRFP.

To overcome this difficulty, a photoswitchable FP, DRONPA (Gerlitz *et al.,* 2018), became to be grafted with HDEL_mRFP. DRONPA can be switched off with a high power of excitation line and switched on by a low power of UV line multiple times. DRONPA is very bright and can be excited in deeper tissue layer due to the low amount of energy needed. Unfortunately, even if it was easy to bleach the cells at the graft interface; as with PA-GFP we were not able to perform a precise photo-activation at the center of the graft interface and the surrounded cells were also activated (Fig. 15). These live approaches still require technical improvements.

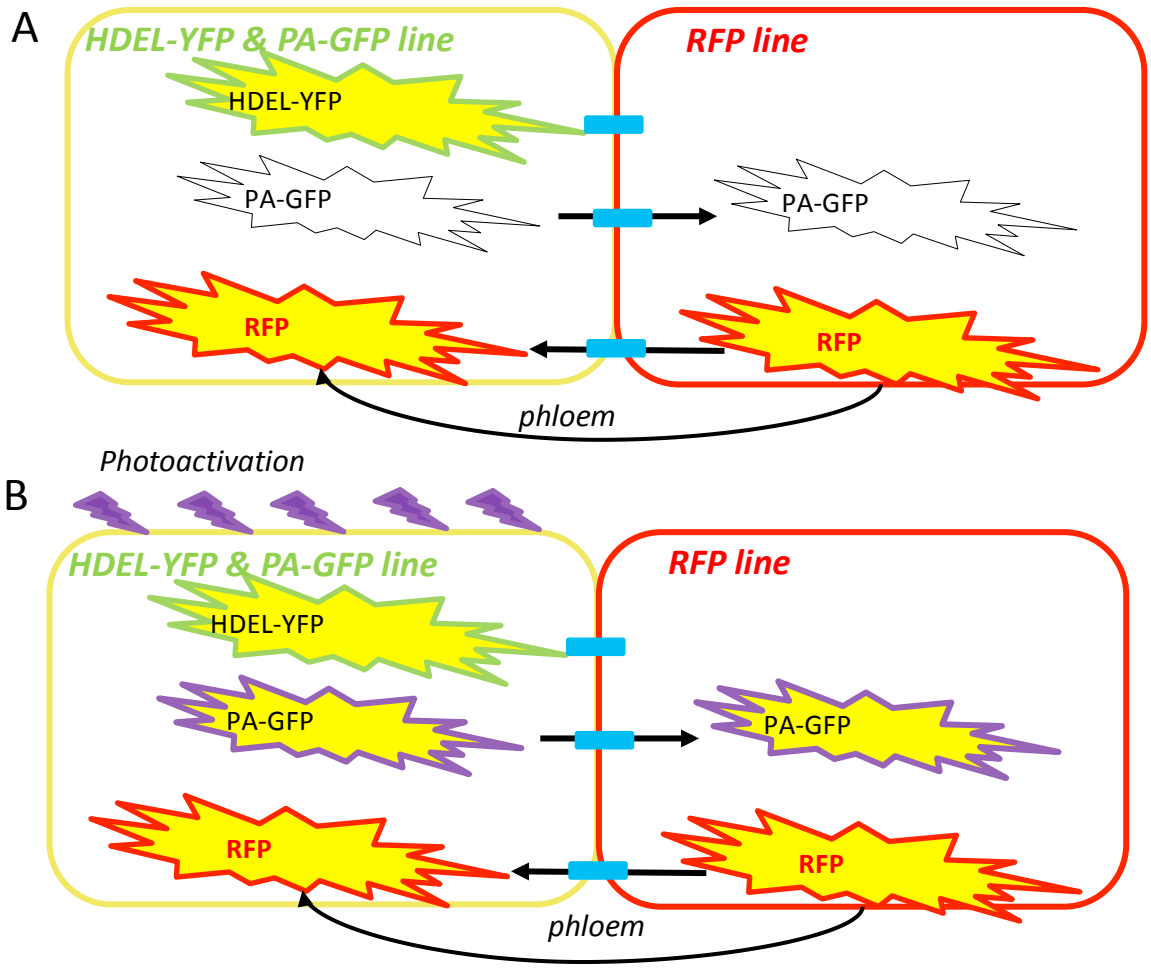

Figure 13. Assessing symplastic traffic across the graft interface of *Arabidopsis thaliana* by photo-activation approach.

HDEL_YFPxPA-GFP is grafted onto 35S::tagRFP.

(A) At the graft interface, cytosolic tagRFP and photoactivable (PA)-GFP are able to traffic in the phloem and/or plasmodesmata pathways (blue rectangle), before photoactivation PA-GFP is not visible **(B)** After photo-activation of a HDEL-YFPxPA-GFP cell containing cytosolic tagRFP, if PA-GFP traffic is observed quickly, it will mean that traffic occurs in a PD-dependant manner.

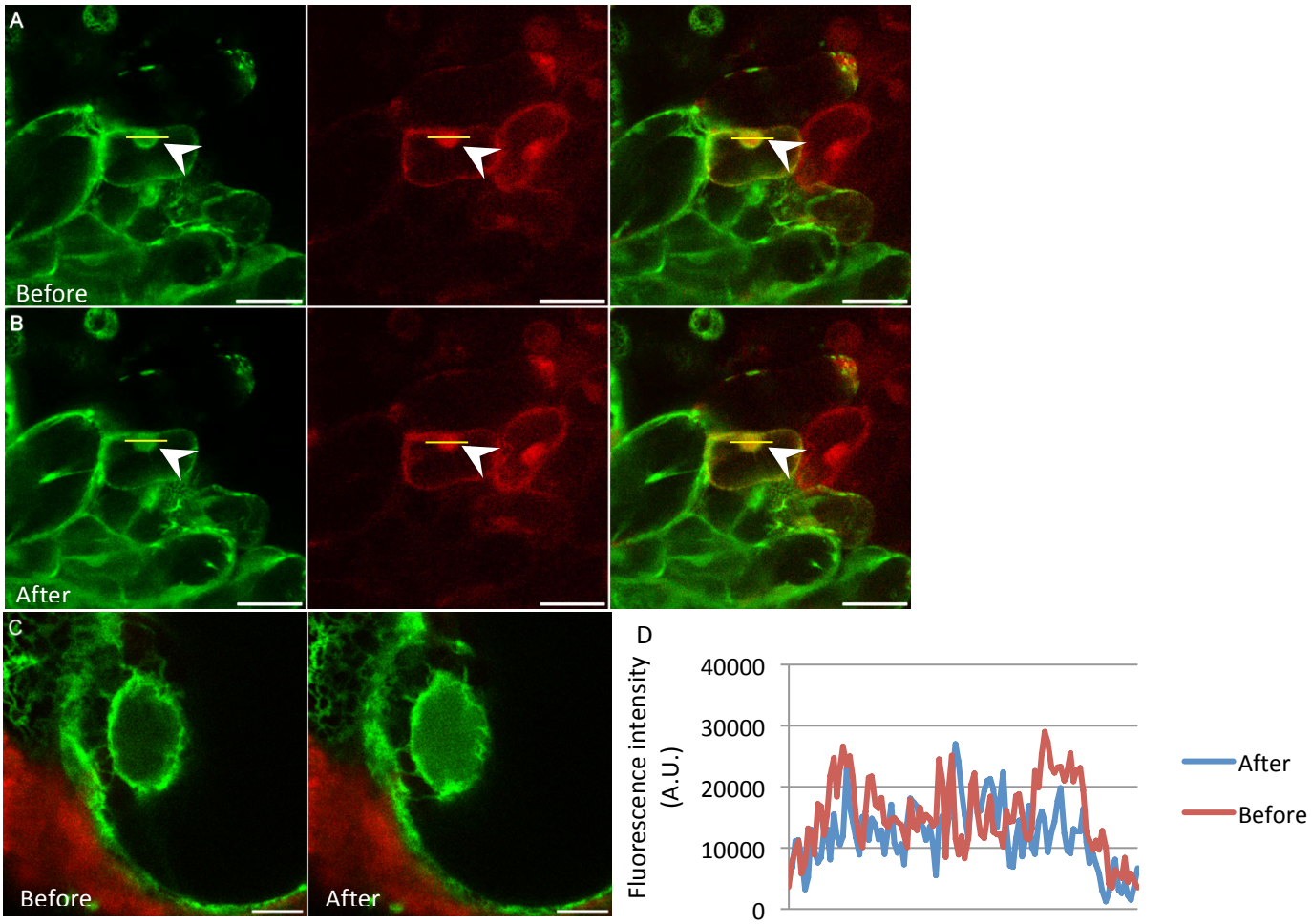

Figure 14. Photoactivation of the photoactivable Green Fluroscent Protein (PA-GFP) is not effective with confocal microscope in too deep tissue

For (A) and (B) the GFP, RFP channels and composite are presented. 5 DAG HDEL_YFPxPA-GFP grafted onto 35S::tagRFP.

(A) Before photoactivation of a HDEL_YFPxPA-GFP cell containing cytosolic tagRFP and **(B)** after its photoactivation **(C)** When exposed at the surface, PA-GFP is easily photoactivable **(D)** The fluorescence intensity plot of PA-GFP is traced along the yellow line on (A) and (B) and shows not significant differences before and after photoactivation.

Scale bars: (A, B) 20 µm, (C) 5 µm

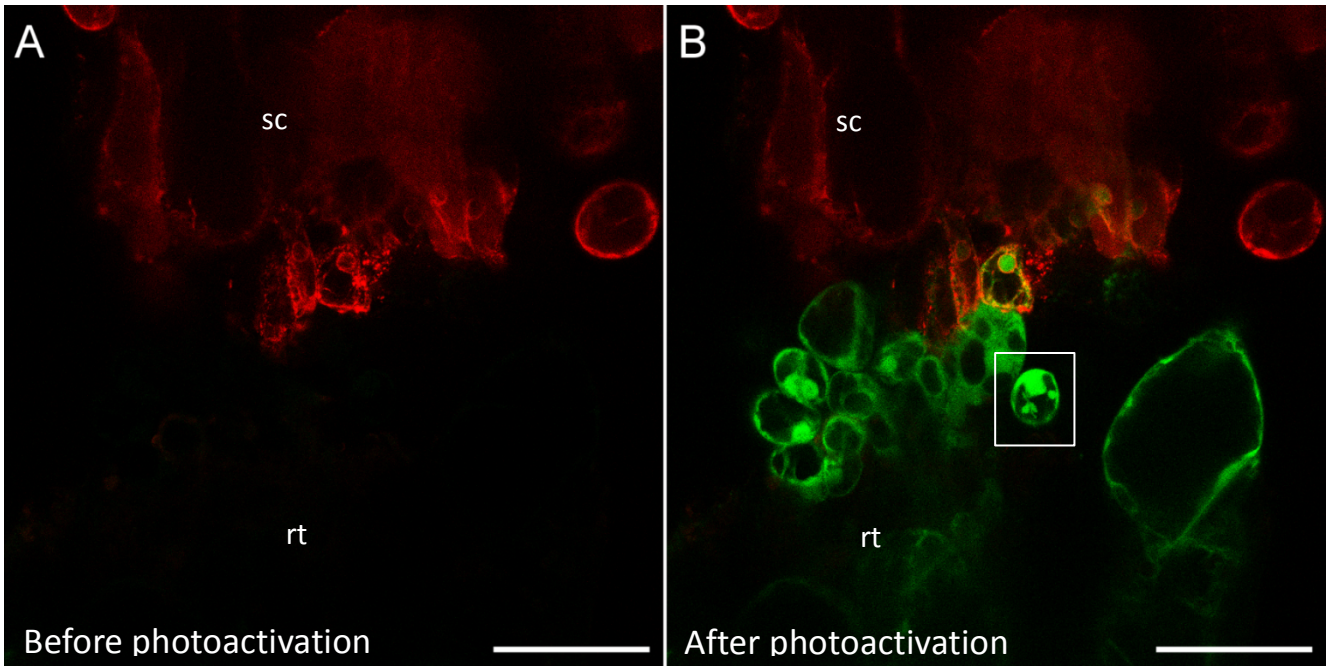

Figure 15. Photoactivation of the DRONPA at the graft interface of 5 DAG HDEL_mRFP grated onto 35S::DRONPA

(A) Before photoactivation of a DRONPA cell and **(B)** after its photoactivation . The photoactivated cell is showed in the white square but photoactivation of DRONPA occurs in the entire graft interface due to scattering of the UV light

sc: scion, rt: rootstock

Scale bars: (A, B) 20 µm

3.2. Three dimensional comprehension of cellular organization and mapping of PD at the graft interface

3.2.1. Context

To integrate these results at a more global scale, it is necessary to access to the cellular organization of the graft interface in 3D in both grapevine and *Arabidopsis.* It is crucial to understand and to assign a role for the different types of tissues involved in the process of graft union formation. For example, following the establishment of new symplastic connections, at different time points could allow understanding their importance during the establishment and the development of the graft union. To now, several questions remained to be answered especially when exactly PD are formed and where at the graft interface of *A. thaliana*? We have demonstrated in the present work that they were already formed at 3 DAG, while SE connecting the two partners are found. Because pores that connect SE are deriving from PD, they should at least be formed when mature SE connect toghether. A mapping in 3D of the PD at the graft interface would permit to determine if certain tissues are preferentially connected first and thus, if there is a chronology in the establishment of new PD. They could for example connect in priority in the regions where the future vascular elements will be established to allow a fast reestablishment of a vascular continuity and then only later in other tissues. On the contrary, they could be established at the same time at the whole graft interface.

Finally, deepest investigations are necessary to determine the frequency, the origin and the potential role of the cellular exchanges we observed at the graft interface. During my Ph.D., I was able to participate to an EMBO workshop on 3D imaging. This workshop was the opportunity to test several approaches to obtain the three dimension of the graft interface. Working with living samples has the advantage to allow studying dynamic events however, due to the light scattering of biological samples, special microscopy techniques that allow in-depth imaging such as light sheet microscopy or two-photon microscopy have to be used. Instead of working with living samples, it is also possible to work with fixed and “cleared” tissue. The clearing allows reducing the turbidity and opaqueness of tissues mostly causes by changes of refractive index. Indeed, when imaging, the light usually have to pass through multiple material with different refractive index (*e.g.* glass, air, water, oil, biological membranes, proteins, etc.). Clearing aims to homogenize the refractive index throughout the tissue to allow an optimized excitation and emission light propagation.

3.2.2. Results

With living *A. thaliana* grafted hypocotyls, we were not able to visualize the entire sample in the three dimensions using both light sheet and two photon microscopes. The best results were obtained with the light sheet, which allowed us to acquire up to 4 cell layers in depth (Fig. 16 A). In our hands,

two-photon microscopy did not permit to obtain significantly better results than confocal and only allowed us to image the two first cell layers (Fig. 16B). However, these tests are only preliminary. They were obtained in a workshop context, thus very rapidly, not with optimal conditions and with plant not grown under the proper conditions (notably long day leading to thicker hypocotyls with more chlorophyll) and not grafted under good conditions leading to a rather large amount of callus cells at the interface.

The challenge when working with cleared samples is to preserve the intrinsic fluorescent properties of the FPs to still be able to target the graft interface reliably. Working with cleared samples permitted to have significantly improved results on *A. thaliana*. Samples were cleared using a very effective, safe and rapid protocol with ethyl cinnamate that has a refractive index close to that of class (Masselink *et al.,* 2019). The protocol required a light fixation with paraformaldehyde 4% and a progressive dehydration with increasing concentration of ethanol buffered at pH 9 (from 25% to 95%). The not complete dehydration allowed to keep the pH buffered (as it is not possible to buffer pure ethanol) and to maintain a little amount of water. These two criteria help in preserving the fluorescence properties of FPs by ensuring the preservation of their conformation. It allowed us to preserve mRFP and YFP in a 6 DAG graft HDEL_YFP / HDEL_mRFP of *A. thaliana* hypocotyls (Fig. 17A) and to visualize the entire volume of the grafts. Unfortunately, on grapevine grafts, even after 24 h clearing in ethyl cinnamate, the sample stays opaque and brownish, certainly due to the presence of lignin. Moreover, the long clearing step did not preserve GFP (Fig. 17B).

To decipher the 3D organization of grafted grapevine, other clearing methods have been tested (Fig. 18). Before clearing with these two techniques, grapevine samples were chemically fixed with 4 % paraformaldehyde in 0.1 M phosphate buffer. Samples were cleared for one week. While clearing with 100 % 2,2 thiodiethanol (Staudt *et al.,* 2007) was better, it did not permit to preserve the fluorescence of GFP. On the other hand, ClearSee methods (Kurihara *et al.,* 2015) permitted to preserve more the GFP, but in this case, the tissue clearing was not significant. It would have been interesting to work with 95 % 2,2 thiodiethanol to maintain a little amount of water and to buffer at pH 9 as for the ethyl cinnamate clearing to improve the preservation of fluorescence.

Accessing to the 3D of the graft interface of *A. thaliana* is now possible with the clearing method using ethyl cinnamate, thus access to the 3D tissue organization seems to be possible. This method combined with fluorescent lines expressing PD markers could allow mapping the PD specifically at the graft interface. More improvements are required to access at the 3D organization of ligneous tissues. This challenge has to be faced in order to access different cell organization specific of different compatibility levels.

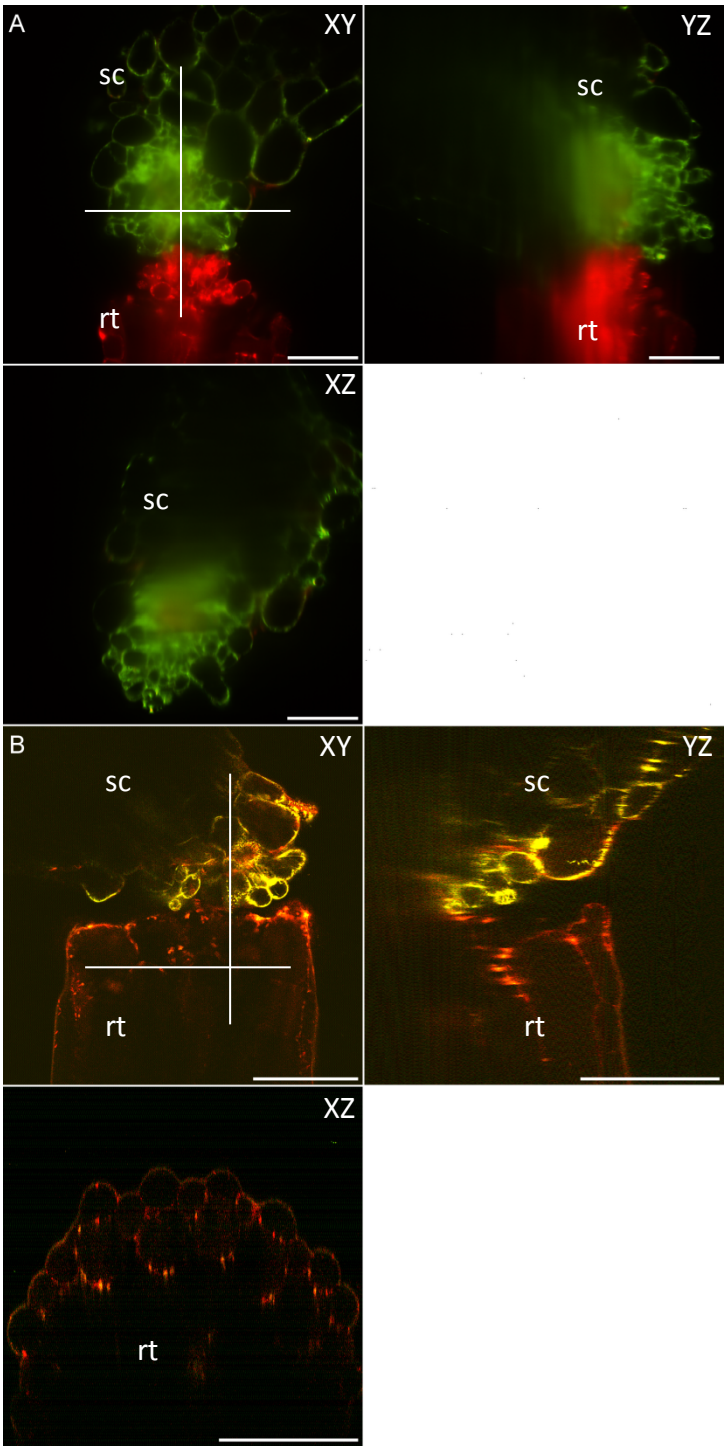

Figure 16. Live imaging of 6 DAG grafts of HDEL_YFP grafted onto HDEL_mRFP

(A) Orthogonal view of the graft using lightsheet microscopy. It allows us to visualize 3 to 4 cell layers deep in the tissue **(B)** Orthogonal view of the graft using two-photons microscopy. It allows imaging around 2 cell layer deep in the tissue.

Scale bars: (A) 100 µm, (B) 50 µm

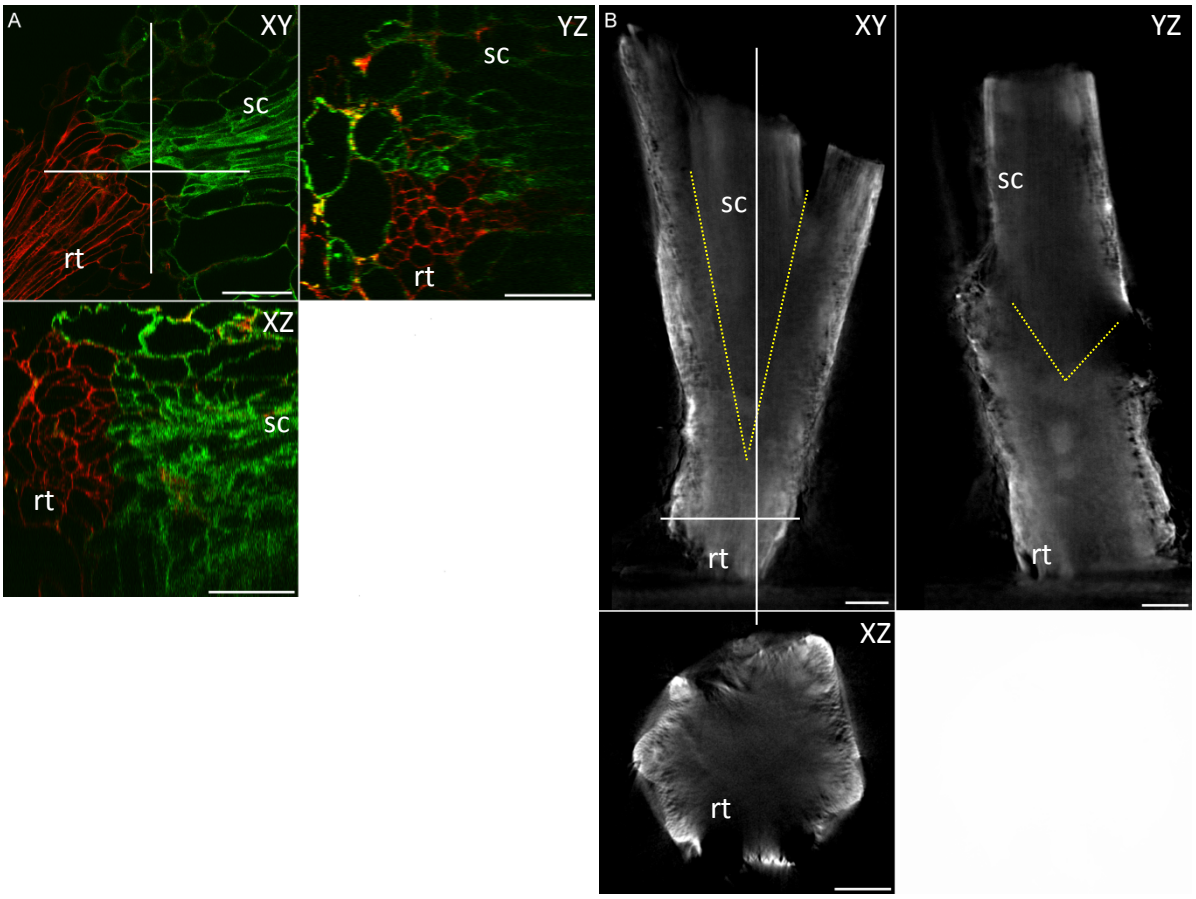

Figure 17. Three dimensionnal imaging of tissues cleared with Ethyl Cinnamate *Arabidopsis thaliana* and grapevine grafts

(A) Orthogonal view of confocal microscopy of HDEL_YFP grafted onto HDEL_mRFP, 6 DAG. The grafted sample could be imaged entirely. **(B)** Orthogonal view of optical tomography of Pinot Noir GFP grafted onto Riparia Gloire de Montpellier cleared with ethyl cinnamate did not permit to image the entire graft. Graft interface is represented by the yellow lines. GFP channel. After one day clearing in ethyl cinnamate, there is no more GFP flurorescence but only autofluorescence

White lines indicates the orthogonal slices, sc: scion, rt: rootstock

Scale bars: (A) 50 µm (B) 200 µm

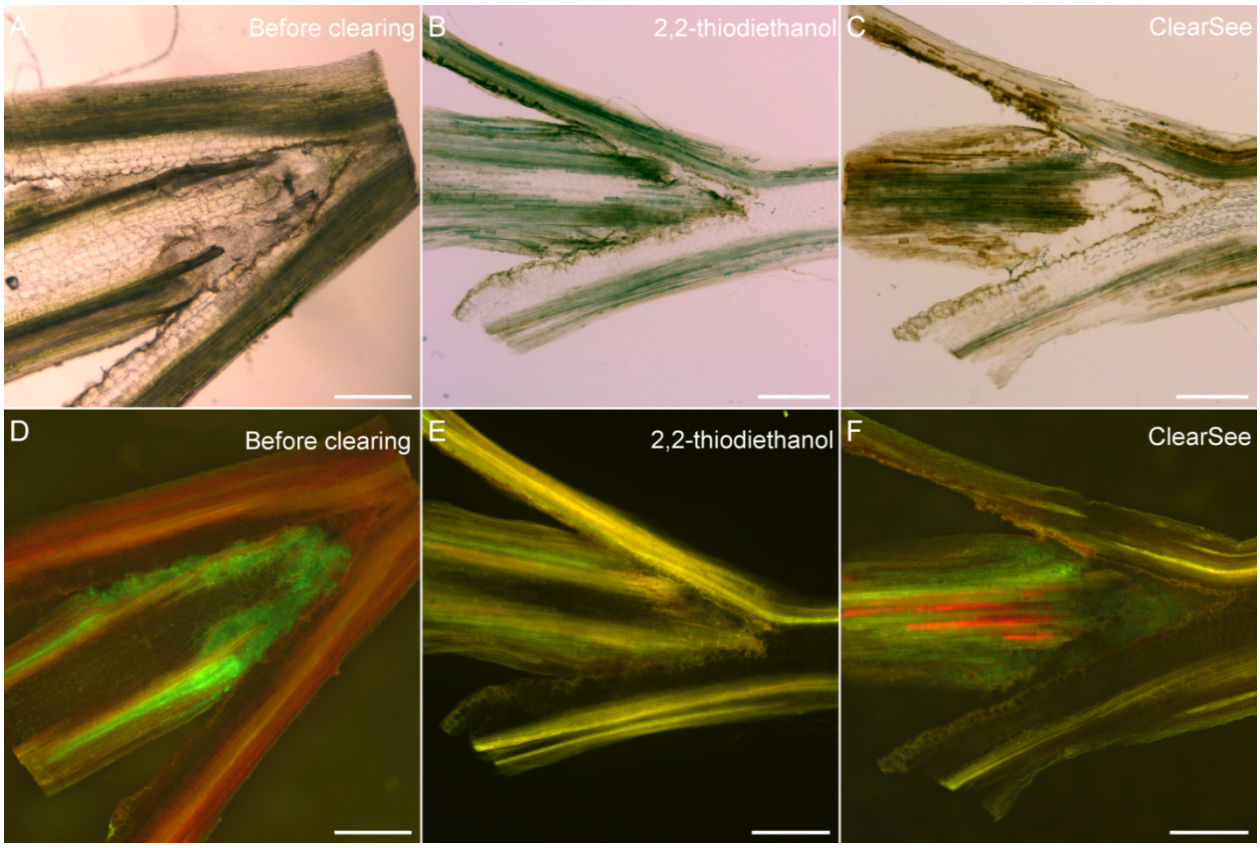

Figure 18. Clearing of 150µm-thick section of grapevine Pinot Noir-GFP grafted onto Riparia Gloire de Montpellier

(A and D) When not cleared, samples are not transparent enough to acquire the volume. Before clearing, the fluorescence of GFP is clearly visible. **(B and E)** Clearing using 2,2 thiodiethanol increases slightly the tissue transparency but was still not optimal. Moreover, the GFP fluorescence was not preserved **(C and F)** Clearing with the ClearSee method did not significantly increase the tissue transparency but preserves more GFP than with 2,2 thiodiethanol.

Scale bars: (A-F) 500 µm

DISCUSSION AND PERSPECTIVES

1. Development of the CLEM method

During my Ph.D. project, I focused on the characterization of the ultrastructure of the graft interface. For this purpose, a CLEM approach has been developed. It is a very powerful tool, allowing a precise targeting of the graft interface. Moreover, this CLEM method allows the use of a variety of complementary approaches such as ET and immunogold labelling.

However, it is still a complex task, where every small mistake during the process, such as the break of the parlodion film on the TEM grid, will automatically result in the loss of the sample. Indeed, many criteria should be fulfilled such as fluorescence signal in living samples and quality of HPF. There are also numerous steps that are critical: good balance for the duration of the different freeze-substitution steps, storage of samples, thickness of sections, montage of grids between the glass slide and the cover slip, removing the cover slip, manipulation of the grids, presence of nanometric dust, and coating with gold particles.

Setting up a CLEM approach already begins from the choice of the genotypes to study. The plants should have a strong expression of the FP as the preparation steps will affect the fluorescence properties of the FPs. In our hands, mRFP is more suitable than eGFP or YFP. It could be due to the short polymerization wavelength that could impair more the FPs that are excited with short wavelength. However, for mEos2, 4a and 4b, for which the emission spectrum can be converted from green to red under 405 nm, the green emission is better preserved than the red one (Paez-Segala *et al.,* 2015). Additionally, working with grafted hypocotyls of *A. thaliana* added an extra level of difficulty. It was particularly challenging due to the inherent fragility of the graft point. Correlative Light Electron Microscopy required several handling steps during the preparation of samples, notably cutting before the HPF and handling during the FS. The grafted samples will often break at the graft point, especially when they are very young, such as 3 DAG. For this reason, we were not able to obtain samples before 3 DAG. However, being able to study younger grafts would be highly informative to capture developmental events before 3DAG such as PD biogenesis, EVs production and vascular tissue development. Even though many samples will be lost, it worth the effort to try to obtain younger graft interfaces for CLEM studies in the future.

When samples are fixed and embedded in resin, the first step is to determine the optimal thickness for CLEM of the resin section. The CLEM approaches are always a matter of balance and compromise. Generally, what is optimal for TEM, such as the use of chemical agents for contrasting (such as osmium tetroxide) or working with ultrathin section (less than 100 nm thick) is not appropriate for LM as it drastically reduces or impaires fluorescence and *vice versa*. Working with thick sections and

no contrasting agent reduces the resolution under TEM but permits the observation of fluorescence. In our hands, 150nm-thick sections permit us to obtain a convenient resolution under a 120 kV TEM while maintaining sufficient fluorescence in the section. To work with proteins that have an insufficient level of expression could be challenging with CLEM approaches, however it is still possible to increase the thickness, especially if a TEM with higher tension, such as a Scanning TEM (STEM) 200 kV, is available. Moreover, to restore the fluorescence signal of one partner, immunofluorescence with a first antibody against YFP following by a secondary antibody conjugated with fluorophore can permit us to amplify the residual endogenous fluorescent signal. Additionally, as our CLEM method is compatible with ET, ET could be used to significantly increase the resolution in X, Y and Z when necessary. One of the most critical steps of the CLEM approach is the visualization of the fluorescent signal on ultrathin sections. To image sections under LM with an optimal resolution, working with immersion objectives is required and the grids have to be mounted in water between a slide and a coverslip. When mounting, and even more when unmounting the grid, great precautions should be taken to not break the parlodion film, otherwise subsequent observation under TEM will not be possible. Indeed, we have noticed that after long laser expositions the TEM grids often stick to the glass and thus, have great chance to break if not handled very carefully. Additionally, when considering doing ET, another handling step of the grids is necessary to coat with fiducial, however, at this time, the grids is already weakened due to the previous LM and TEM observations. This additional step often breaks them. For all the reasons mentioned above, it was not possible to obtain a high number of samples. However, the powerfulness of the CLEM tool makes the effort worth it.

2. Ultrastructural changes occurring at the graft interface of *A. thaliana*

The use of this approach on *A. thaliana* grafted hypocotyls allows us to better understand the fine ultrastructural processes occurring during the graft union formation. In particular, we were able to compare the ultrastructure of two time points; 3 DAG and 6 DAG. Three DAG appeared to be a transient state where the connections between grafted partners are not complete, notably characterized by regions separated by electron dense material, while others appeared continuous with PD and connected SE. Also at 3 DAG, cells are still not fully differentiated while the differentiation process is advanced at 6 DAG, showing already mature SE, and TE connected at the graft interface.

Plasmodesmata of different shapes have been observed from 3 DAG. It is intriguing how they could form between two cells not originating from the same plant. These secondary PD biogenesis events necessarily involve a plasma membrane pore biogenesis *via* the plasma membrane fusion of the two newly connected cells as proposed in the theoretical pore formation model (Fig. 19 A). This step of

plasma membrane fusion could be a key step to finalize the cell connection. It is involved in the species barrier in fecundation and so could be involved in grafting compatibility. In the context of homograft, we only capture two tomograms where plasma membrane apposition has been observed (Fig.19 B and C). Then, the desmotubule passed through this pore. Interestingly, numerous hemi-PD have been observed at the graft interface. We postulated that they could result from a failed attempt in making cell-to-cell connection and thus, they inform us on how PD form at the graft interface. Our results in *A. thaliana* show that even in homograft context, hemi-PD are formed. These "half" PD are not the consequence of an incompatibility between both partners. Secondary PD biogenesis is a highly regulated process where cells positioned at each part of the cell wall have to be well coordinated. As hemi-PD are stopped by the middle lamella, both cells have to modify the composition of their respective side of the common cell wall for continuous PD formation. The cell wall could become more "fluid" allowing the PD to pass through it. The cell-to-cell connectivity is a regulated process. Between scion and rootstock, the hierarchy of cell development events could be different between two cells in contact but coming from two different plants. Thus, the need for one cell to increase its connections could be the not priority for the cell in the front it. If the conditions are not reunited, if only one cell initiate cell wall thinning or modification of the cell wall at its side, it will results in the formation of hemi-PD on this side. Scion and rootstock take the same part in the process of making new PD because hemi-PD are found in the same proportion in scion and rootstock side. The "secondary PD biogenesis permission" has to be given by both cells at the same time and the same place to permit the connection of both cells. In the context of homografts, the presence of simple PD and PD in "ball of wool" indicates that making new PD could be an active process. Thus, cells that require an increasing of intracellular connections "send" a PD into the cell wall. In fact, a coordination between (1) the cell wall thinning, (2) ER-plasma membrane tethering, (3) ER compression into desmotubule during new PD progression into the cell wall, (4) following by the plasma membrane pore formation lead to new continuous PD. If the recipient cells do not give permission, PD progression is blocked at the middle of the cell wall. Once stopped, almost all hemi-PD come back to form a loop before to exit by a new cytosolic opening in the same cell. In rare cases, PD is blocked in the cell wall and the desmotubule continue to be sent in the cell wall where it aberrantly accumulates. The presence of hemi-PD has been also observed in the outer cell wall of developing protoplast of *Solanum nigrum* (Ehlers & Kollmann, 1996). In their study, they proposed that these PD on the outer cell wall could meet each other to form a new continuous PD. However, this study is questionable due to the nature of initial material. PD observed on the outer cell wall could be residual PD that resulted from an incomplete cell wall digestion during the protoplast preparation. Moreover, no element allows us to know if the cell wall interface is the product of a cell

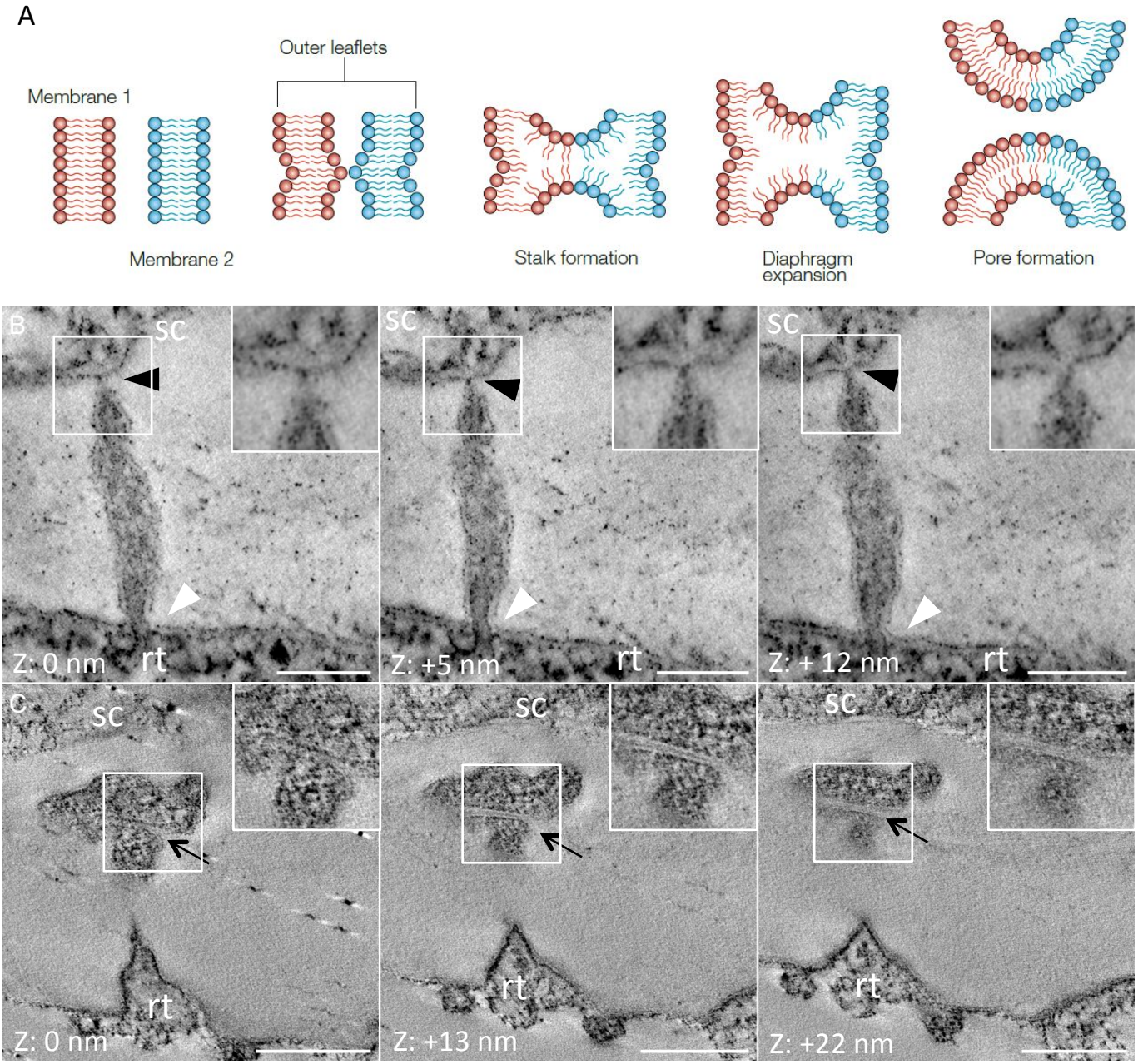

Figure 19. Close apposition of plasma membranes at site of plasmodesmata biogenesis

(A) At one side of the plasmodesmata (PD), membrane continuity is clear (white arrowheads) while at the other side of the PD, the opening is never found in the entire thickness of the electron tomogram. Plasmodesmata plasma membrane and cell plasma membrane seem to have a very close proximity **(B)** Incomplete pore between two differentiating sieve elements. Two membranes in close contact separate the two half of the pore are visible (Black open arrow). **(C)** A theoretical model of the mechanism pore formation (extracted from *Ogle et al.,* 2005). The same type of hemi fusion of membranes could occur to form continuous PD. sc: scion, rt: rootstock

Scale bars: (A) 100 nm, (B) 200 nm

division or comes from the fusion of both cell walls. Thanks to our CLEM approach, the identification of a cell wall that comes from the stitching together of two cell walls is reliable.

In graft, in addition to these simple PD, branched PD were also observed at the graft interface in homograft and heterograft contexts. These branched PD can derive from the fusion of two hemi-PD facing each other. In this case, in addition to the plasma membrane fusion, an alignment between both hemi-PD and a desmotubule membrane fusion are required to give a continuous PD. Several secondary PD biogenesis mechanisms could coexist within the same graft.

More investigation is needed to decipher the process of secondary PD biogenesis. By grafting lines that express membrane contact site protein (between ER and PM) coupled to FPs, we could search for events of ER and PM tethering. This close proximity of ER and PM could show potential hotspots for PD biogenesis. Using CLEM, and validating the approach through immunogold labelling against the FPs, it would be possible to link these events of ER/PM tethering and PD biogenesis. In this way, we may be able to select the very first event of PD biogenesis. Among membrane contact sites, the MULTIPLE C2 DOMAINS AND TRANSMEMBRANE REGION PROTEINS (MCTP) family appears as a good candidate. Proteins of this family showed an association with ER and some members; MCTP3 and 4 have been demonstrated to localize at PD and act as ER/PM in *A. thaliana* (Brault et al., 2018). By grafting mutant lines of these proteins, we could search for event of PD biogenesis and eventually address a role for these proteins family and ER/PM contact site in secondary PD biogenesis. It would be particularly interesting to see if *mctp* loss of function mutants grafted onto themselves are affected in their efficiency of grafting and if there is a difference when only one of the two grafted partner is a *mctp* mutant. For example, it could lead to the formation of hemi-PD mostly at the side of wild plant. Moreover other mutant lines have been demonstrated to be affected in secondary PD biogenesis, such as ISE1, ISE2 and Choline Transporter Like 1 (CHER). Graft efficiency could be impaired with these mutants. Moreover, thanks to CLEM, ultrastructure of resulting PD could be investigated.

Another approach to better understand the PD biogenesis is to use desmotubule fluorescent lines of *A. thaliana.* During the formation of primary PD, ER strands are being trapped during the development of the cell plate, resulting in the formation of the central part of the PD, the desmotubule. In this way, PD allow a continuity of both ER and plasma membranes between the two daughter cells. In grafts, secondary PD at the interface present a visible desmotubule. At the graft interface, PD are not originating from a cell division, their biogenesis is still no fully understood. Ultrastructural data obtained during my Ph.D. indicate that PD biogenesis can be primed by the scion and the rootstock. Moreover, complex PD could be the result from the fusion of two facing hemi-PD and simple PD could result from the unidirectional desmotubule cell wall spanning. To go further, stably labelling the desmotubule at the graft interface would allow us to answer to the following

questions: (1). does the desmotubule come from the fusion of ER of both partners? (2) Can it come only from one of the two partners? Also, it is better to not put aside the probability that all of these possibilities could coexist within the same graft, depending on how PD are formed. Being able to determine the origin of desmotubule in PD at the graft interface and correlate this to ultrastructural observations could help to shed light on the role of each partner in the symplastic communication establishment.

RETICULON-LIKE 6 (RTNLB6) belongs to a multigenic family for which proteins are associated to the ER. RTNBL6 was localized by 3D-Structured illumination microscopy (SIM) in the desmotubule on the Bright Yellow 2 (BY2) tobacco cultured cells (Knox et al., 2015). Grafting two RTNBL6 lines expressing mRFP and YFP respectively could permit us to observe the origin of desmotubules at the graft interface. However, this approach could be time consuming due to the difficulty to catch PD biogenesis events. Moreover, the technique of super resolution microscopy could help to reach the resolution needed to visualize the desmotubule labelling. Stimulation Emission Depletion (STED) observations after immunofluorescence labelling could be done. The observation of a bicolored desmotubule could be due to the fusion of two desmotubule that are facing each other or due to RTNLB6 diffusion along a spanning desmotubule after PD have been formed with the ER originating from only one grafted partner. In fact, spanning ER can fuse with the ER of the other grafting partner and membrane ER proteins, such as RTNLB6, could maybe move on the desmotubule leading to the formation of the bicolored desmotubule.

Additionally, the importance of cell wall remodeling for PD biogenesis specifically at the graft interface should be addressed. Several studies focused on the cell wall composition around PD and its influence on PD permeability, ultrastructure and biogenesis (reviewed by Knox & Benitez-Alfonso, 2014). Notably, the importance of callose that accumulate at neck regions of PD to regulate PD permeability is important for developmental processes (Benitez-Alfonso et al., 2013). Pectins and cellulose are also regulated (Faulkner et al., 2008). In our experiments, for the graft union formation, the middle lamella seems to be a bottleneck to permit the formation of continuous secondary PD. Thus, it would be interesting to access specifically to the composition of the cell wall at the graft interface. Like that, the cell wall around continuous PD and hemi-PD could be compared. For this purpose, immunolabelling against the different types of pectin such as homogalacturonan or rhamnogalacturonan II that are involved in cell wall strengthening (Caffall & Mohnen, 2009) or rhamnogalacturonan I that is rather associated with softening (Ulvskov et al., 2005) could be performed (Domozych et al., 2017; Giannoutsou et al., 2013; Roy et al. 1997). In addition, following the localization of proteins implicated in cell wall remodeling such as pectin methyl esterase (PME), the enzyme involved in pectic homogalacturonan de-esterification that may contribute to localized

softening of the cell wall could help to understand the role of cell wall composition in the formation of secondary PD at the graft interface. A recent study study showed that pectin unmethyl-esterified homogalacturonan (Sala *et al.,* 2019).

For the first time, we highlight the presence of EVs at the graft interface. Until now, functions of EVs in plant only begin to be addressed. They have been reported to play role in pathogens defense and symbiosis as they contain various defense-related proteins, sRNA, (Rutter & Innes, 2017; Rybak & Robatzek, 2019). A possible role in the graft union formation remains to be elucidated. Interestingly, some EVs have been characterized to contain cell wall remodeling enzymes (as reviewed by de la Canal & Pinedo, 2018). They have been found in the proteome of EVs in sunflower (Prado et al., 2014; Rutter & Innes, 2017). Thus, it is possible that they contribute to the localized changes in cell wall composition needed for establishment of a common cell wall and new PD. Extracellular vesicles could also be one of the first steps to clean-up the cellular debris in order to make possible the close contact between the two partners. Moreover, by transporting proteins and RNAs, they could be a way for the partners to exchange signals rapidly and in very localized areas for the first steps of graft union formation. Using EVs pathway permits plants to ensure that their content will be only delivered into another cell thanks to membrane fusion event and not in intercellular spaces. Such EVs have been regularly observed surrounding PD, in this context, we propose that they could participate in the establishment of new PD, notably by modifying the cell wall composition or by helping to the opening of PD into the "targeted cell" thanks to membrane fusion process.
Several pathways have been proposed, notably the EXPO pathway that mediates exocytosis and the Multi Vesicular Bodies pathways (MVBs). To do so, finding specific markers of EVs is necessary. As EVs are supposedly from several origins, they are heterogeneous in composition and there are no markers that allow us to identify specifically EVs. However, some genes potentially related to their biogenesis have been proposed as markers such as TETRASPANIN 8 (TET8), PENETRATION 1 (PEN1) syntaxin and the exocyst subunit Exo70E2.

Finally, to demonstrate the importance of cell-to-cell communication at the graft interface, impairing secondary PD biogenesis and modification of PD permeability have to be tested. In this way, measurements of grafting efficiency in different context will have to be evaluated according to the Melnyk's protocol (Melnyk et al., 2015). The use of CFDA allows quantifying the vascular reattachment over time. It would be particularly interesting to measure the effect of certain compounds such as salicylic acid, a plant hormone that can increase EVs formation and the number of branched PD (Fitzgibbon et al., 2013; Rutter & Innes, 2017). The same way, we could graft *A. thaliana* genotypes affected in PD biogenesis and measure the success rate overtime and if there is

delay in vascular reattachment. It would be particularly interesting to focus on the phloem continuity, as sieve pore derived from PD. Thus it is possible to expect a delayed reconnection or even no connection at all between SE from the grafted partners. However, these mutants have several developmental defects; thus, the change in grafting success may not be only due to the absence of secondary PD formed at the graft interface.

Until now, it is not possible to determine which from EVs, PD or SE are established first as they both have been observed at 3 DAG. Being able to study younger graft interfaces, appears crucial to establish the kinetics of graft union formation and decipher the interconnection between these events.

Besides PD, more investigation is needed to characterize precisely the development of vascular tissues at the graft interface. Indeed, it is still not known how vessels reconnect. Are they differentiating from the pre-existing vascular tissues toward the graft interface, or from the graft interface toward the existing vascular tissues? In his, work Melnyk (2015) described that new xylem vessels form a bridge to reconnect the two partners and with the two-segment graft, he demonstrated that the process of reconnecting xylem begin apically in the scion. Appropriate markers such as pMtSEOR::GFP5-ER that label differentiating SE (Ross-elliott *et al.,* 2017) or Atxyn3::YFP that transiently label the nucleus of differentiating TE just before the collapse of vacuole (Sawa *et al.,* 2005) could be used to follow the differentiation process of vascular tissues.

Not less importantly, the use of CLEM approaches allows us to visualize for the first time exchanges of nucleus and ER between scion and rootstock through cell wall openings. Near the graft interface, cell openings between cells from the same partner have been found with a transient plastid. Exchanges of genetic material was already observed in few studies of Bock's team (Fuentes et al., 2014; Lu et al., 2017; Stegemann & Bock, 2009) by grafting transgenic tobacco lines that have different markers and reporter genes respectively in nucleus and plastids. By regenerating plants from callus cell of the graft interface on selective medium, they were able to obtain plants that have the two resistances. Their technique is now even used for transplastomic (Sidorov et al., 2018). However, the use of antibiotics to select these exchanges could have permitted to select very rare events or could even have induced these exchanges as a mechanism for the cells to survive. The work of Sidorov *et al*. (2018) shows that wounding may be necessary for the plant to exchange genetic material. Other studies have used the graft system to study the cell-to-cell movement of organelles (Gurdon et al., 2016; Thyssen et al., 2012), they both proposed that these exchanges could occur through newly formed PD, in regions where cell wall is thinned. Our experimental did not permit us to answer if the cell wall openings observed resulted from spontaneous fusion of damaged

membranes during the wounding or if a drastic cell wall thinning in certain regions could lead to the fusion of PM of the adjacent cells. Interestingly, spontaneous cell fusion has been observed when plant tissues underwent an enzymatic treatment to digest cell wall components (Withers & Cocking, 1972). They observed the appearance of large cytoplasmic connections alongside a reduction in the proportion of PD. Thus, they suggest that the formation of these large opening resulted from the expansion of PD, that are not constrained anymore by the cell wall. This would mean that the establishment of PD between cell of the scion and the rootstock is necessary to form these large channels. In their work, these connections were observed containing ribosomes, ER and mitochondria. Until now, their biological relevance and frequency *in planta* are not known yet. They could result from a passive mechanism where two adjacent wounded cells are opened. Organelles could diffuse from a cell to another before cell reparation. On second thought, these exchanges could be very important for the grafted partners to communicate. They would permit faster exchanges of signaling material rather than establishing new PD or to release EVs, in order to start communication at the graft interface. The fusion would permit to form a hybrid zone, where the graft interface is not well defined. For the plant, it could be a faster and more efficient strategy to ensure the continuity of grafted tissues. We observed these cell wall openings only on young grafts, suggesting that it is a very transient state. After a first exchange of material, the exogenous nucleus could degenerate and the expression of the second fluorescent marker disappears. Given that they have been observed relatively close to existing vascular tissues and that they have been found aligned, they could be implicated in the formation of continuous vessels at the graft interface but to now it remains to be elucidated.

3. Visualization of the three dimension of graft interfaces

Being able to access to the spatial organization of the graft interface is important to understand the graft union formation. Until now the graft interface has mostly been studied using 2D techniques, with the exception of magnetic resonance imaging (Bahar et al., 2010) and X-ray tomography (Milien et al., 2012) on *V. vinifera.* The resolution obtained with these techniques has left a gap in our understanding of fundamental cellular events such as processes involved in the establishment of a vascular tissue continuum, cell organization and symplastic connections. Nowadays, new 3D imaging techniques could help to reach an unprecedented level of resolution to study the graft union formation. Reaching the 3D ultrastructure of biological samples is possible through EM methods such as Serial Block Face (SBF), which consists of a combination of an ultra-microtome and a scanning electron microscope (SEM). The surface of the block of resin is scanned before being removing thanks an ultra-microtome section. After that, the block of resin is scanned again and so forth. This

SBF-SEM approach could give access to a volume of around 200 µm x 200 µm x 200 µm. In this way, the ultrastructural data, linked to the phloem differentiation and the phloem unloading in the root tip, could be observed in 3D (Furuta *et al.,* 2014; Ross-elliott *et al.,* 2017). However, SBF-SEM requires samples highly contrasted by using osmium tetroxide, uranyl acetate and lead citrate during preparation. These chemical agents impair the fluorescent preservation of almost every FP and prevents the targeting of the graft interface. An interesting volume CLEM approach has been developed in *Caenorhabditis elegans* (Burel et al., 2018). By performing serial sectioning of HM20 blocks outside the SEM, they were able to collect up to 500 sections of thickness from 50 to 150 nm on glass slide. They performed firstly confocal imaging followed by SEM imaging before correlating confocal and SEM images. Applying this technique to grafted hypocotyl of *A. thaliana* would be beneficial to follow particularly the establishment of vascular continuum. Using lines expressing PIN1 fused to GFP, it will be possible to correlate the ultrastructural events associated to the auxin repolarization for canalization and determination of SE. Moreover, the 3D PD mapping at the graft interface thanks to HDEL grafted lines could be realized. Confocal imaging will ensure the interface targeting and SEM imaging will permit to visualize PD distribution. Serial sectioning is labor intensive, time consuming and the loss of a region of the sample constitutes a permanent risk. The thickness of grafted hypocotyls of *A. thaliana* are around 100 µm. Performing sections of 150 nm will represent more than 600 sections and consequently lots of time for LM and SEM acquisitions.

Another possible solution is to perform a CLEM approach directly “en bloc” imaging, *i.e* fluorescent imaging directly in the resin bloc followed by SBF. In their work, Prior *et al.,* (1999) used the autofluorescence of their sample to localize precisely their region of interest, particularly being able to find its depth in the resin bloc to facilitate the sectioning step before TEM. In this way, it could be possible to obtain the 3D volume of samples embedded in resin with the fluorescence of FPs and with SBF to obtain the corresponding ultrastructure in 3D. Recent studies suggest that lots of improvement can be done on the choice of the appropriate markers. For example, the fluorescence of specific variants of the mEos, such as mEos4b (Sun *et al.,* 2015) and mEosEM (Fu *et al.,* 2019) can withstand osmium staining. Henceforth, the use of such FPs, in combination to osmium tetroxide could allow us to improve resolution obtained with serial sectioning or SBF-CLEM.

Plasmodesmata mapping at the graft interface could be realized without EM imaging by taking advantages of LM and fluorescent labelling of PD thanks to fluorescent-tagged PD-proteins. Particular attention has to be paid on the choice of the PD-marker that has to not impair the grafting efficiency. For example, lines overexpressing PDLP increase callose deposition to PD that affects the plant development. Thus, using the native promotor of these PD markers is a mandatory. A first possibility to access to the 3-D volume of the graft interface is to work with samples lightly fixed with paraformaldehyde before being embedded in agarose blocs. Serial sections of around 100 µm are

harvested on glass slide after vibratome cutting before confocal imaging (Lartaud et al., 2015). To avoid the loss of sections, a vibratome, this time, combined to a confocal microscope, could be used to perform SBF. Another possibility is to clear the samples in order to avoid scattering of the light in order to improve the imaging in thick samples. The methods developed on *A. thaliana* allowed us to access to its full volume using regular confocal microscopy. This method using ethyl cinnamate (Masselink *et al.,* 2019) is easy to set up and is user safe in comparison to other clearing procedures that use toxic compounds such as chloral hydrate (Sing *et al.,* 1996; Villani *et al.,* 2013). Few adjustments are still necessary to further enhance the preservation of fluorescence and to reduce the auto fluorescence background. Combined with light sheet or two-photon microscopies that are suitable for thick samples, it will permit us to access to the 3D view of the graft interface with a resolution around 200 nm. The possibility to study graft interface of etiolated hypocotyl of *A. thaliana* should be explored. Etiolated hypocotyls have a thinner and longer hypocotyl with less chlorophyll. These characteristics should be highly beneficial for light imaging. However, in his grafting protocol, Melnyk (2017) mentioned that grafting with etiolated hypocotyl is usually more difficult as plant are very fragile for handling. He also developed modified petri dishes with a cover slip that allow imaging the plant directly in the petri dish without having to handle them. In this way, it will allow access to very early steps of the graft union formation and to follow a same sample over time to focus on very particular aspect of the graft development. It will permit the targeting of these aspects and fix the sample with HPF to study the associated ultrastructure. Special effort should be done to decipher if PD are established before SE differentiation or if sieve plate are established after the SE differentiation. One of our observations makes one think that sieve plate pore could be establish independently of ER. A complete view and more observations are required to answer this question.

4. Assessing PD permeability

Our CLEM approach permitted to confirm the presence of PD at the graft interface of *A. thaliana*. However, their presence and ultrastructure alone cannot reveal their functionality and permeability. During my Ph.D. project, we developed biological tools to evaluate the permeability of PD. The first results obtained with the traffic of a cytosolic GFP between grafted partners did not confirm reliably the functionality of PD because the phloem unloading of GFP can also occur at 3 DAG. We show that GFP was also able to pass from the rootstock to the scion and thus *a priori* in the opposite direction of phloem flux. In the graft, where the sink/source gradient is perturbed, it could not be excluded that molecules can traffic in the opposite direction. Thus, we developed experiments based on selective photoactivation and photobleaching of cells at the interface, to measure the speed of

fluorescence recovery and determine if it is due to PD (rapid recovery) or phloem transport (slower recovery). However, time constraints of my Ph.D. did not allow me to perform successfully these experiments. Indeed, the cells which are in contact at the graft interface were often deep in the graft interface and are difficult to reach for photobleaching and photoactivation due to light scattering.

By using other techniques, such as light sheet or two-photon microscopy and by working on etiolated hypocotyls, it could be possible to study cells deeper in the tissues, where we mostly found connected cells. In this way, targeting cells with a selective FRAP (Fluorescence Recovery After Photobleaching) or photoactivation experiments should be easier. Fluorescence Recovery After Photobleaching has been reported to be able to integrate into a light sheet or two-photon microscope (Rieckher et al., 2015; Sullivan et al., 2016). In this context, grafting experiments with DRONPA seem particularly appropriate because it has been reported to be convenient for accurate activation of individual cells with a two-photon microscope.

Cell-to-cell connectivity depends in fact, on two parameters: the number of PD and the permeability of PD. A way to evaluate the permeability of PD could be to study the Size exclusion limit (SEL) of PD. Whereas the PD mapping allows to identify the number of PD, using lines expressing either 35S::PA-1xGFP, 2xPA-GFP, 3xPA-GFP (two, three PA-GFP fused together) will permit to evaluate the SEL of the secondary PD at the graft interface over time (GFP could be replaced by DRONPA if it appears more suitable).

Finally, all these graft experiments have to be tested using both lines (crossed lines and 35S-RFP) as a scion or rootstock to decipher if the traffic through PD occurs the same way or not for both partner. Is there a difference in permeability and directionality in the transport for PD at the graft interface at a particular developmental stage?

Moreover, to investigate the involvement of symplastic connection establishment during the graft union formation, efficiency of grafting establishment between different *A. thaliana* lines affected in PD permeability should be assessed. To do so, grafting *A. thaliana* affected in the homeostasis of callose which is known to control SEL, for example overexpressor of β-1,3-glucanases, that have a reduced amount of callose in the cell wall or on the contrary, β-1,3 synthetase that increase callose deposition, should be tested. However, affecting the callose deposition have pleiotropic effect on the development of the plant and thus, could have an indirect effect on grafting efficiency. Inducing callose deposition only at specific time of graft development, with inducible lines such as *icals3* (Vatén et al., 2011), or affecting the callose deposition more specifically at PD with *A. thaliana* line such as overexpressor of PDLP1 that was showed to decrease GFP trafficking (Thomas *et al,.* 2008) or pdlp5 mutant that has the opposite phenotype (Lee et al., 2011), could be tested.

Moreover, along with the traffic of molecules through PD, grafting hypocotyl of *A. thaliana* could be an excellent model to evaluate the traffic of membrane proteins along the desmotubule through the

cell wall interface. The PD in “ball of wool” shows that the desmotubule can accumulate in the cell wall indicating a probable desmotubule transit in PD. Until now, it is not yet known if the desmotubule takes part in the traffic of membrane proteins. By grafting lines expressing proteins found in the desmotubule, such as RTNLB fused with mRFP and YFP in the rootstock and scion respectively, FRAP experiments could be conducted to observe the transfer or not of membrane proteins along the desmotubule through the cell wall interface.

5. Transfer to *in vitro* grapevine micrografts

The techniques developed on grapevine samples, using PLT for *in vitro* grafting and HPF for callus grafting allowed us to obtain encouraging results. The main interest in developing such techniques is to study the ultrastructural events and the permeability of PD throughout the development of graft interface in different context of compatibility. Understanding compatibility is from a great interest for breeders as it is an economic challenge. With the methods developed, we were able to preserve the fluorescence of both *in vitro* grapevine and callus cells, a first step to implement a CLEM approach. Using PLT on *in vitro* grapevine permitted to obtain a good preservation of vascular tissues. But other cells appeared empty. Maybe the sectioning step on living sample impairs the cells and the probability to cut only between the cells that can reach up to 90 µm in diameter is very weak. Grapevine cells are relatively large compared to *A. thaliana* ones. It is probable that when doing sections of 150 µm thick, a large number of cells were actually open and their content released during sectioning. To improve the quality of ultrastructure, several adjustments have to be considered. First it is possible to work with thicker sections such up to 250 µm. Sections have to not be too thick to avoid infiltration issues. Moreover, a light chemical fixation prior to sectioning and/or sectioning directly into PFA should be considered to avoid the complete emptying of cells. In this way, we have good hopes to maintain a convenient ultrastructure to study the graft interface. On the contrary, with callus cell and HPF, the ultrastructure was satisfying, allowing to preserve ultrastructural details and to visualize ER and PD. Using this system we were not able to find graft interfaces due to the difficulty to see the cells with a very weak GFP signal and the cell contours in transmission light on ultrathin sections. It was a mandatory to use propidium iodide to visualize the non-fluorescent cell and find the region of interest on a large sample. However, the cells in contact not necessarily have established PD between them. For both grapevine systems, the introduction of new fluorescent genotype is necessary to study the graft interface. Other genotypes of *in vitro* grapevine have to been transformed with 35S::HDEL_mRFP to facilitate the targeting of graft interface as with *A. thaliana*. Special concern should be taken in the choice of genotypes. Indeed, transforming both compatible and incompatible rootstocks would permit to reach a new level of understanding in graft compatibility, by notably focusing on the early events for graft union

formation such as the establishment of PD. For callus grafting, compatible and incompatible "rootstock" should be transformed with a cytosolic mRFP. Being able to visualize cell with the two FPs will automatically means that they have established cell-to-cell communication as callus systems are deprived of vascular tissues. In this way, it would permit us to study both the permeability of PD in different levels of compatibility and select these cells for subsequent HPF to investigate for potential changes in the PD ultrastructure.

CONCLUSION

In summary, CLEM has been a valuable and innovative approach to study the ultrastructure of graft union formation by allowing the reliable targeting of the graft interface. I demonstrate unequivocally that PD are established at the graft interface. This *de novo* PD biogenesis is a highly controlled process, which necessitates very well temporally and spatially coordinated events in the cells of both the scion and rootstock. Understanding precisely how these cell-to-cell connections are established and are maintained over time (particularly in perennial crops), in addition to their functional characterization stays a major issue to decipher the mechanisms of compatibility/incompatibility during graft union formation in species of agricultural interest.

TRANSFERABLE SKILLS AND EXPERIENCE

During my thesis, I had several opportunities to present my work by oral presentation and posters to national congresses. First, I presented a poster and a flash-talk at the "15eme colloque de la société française des microscopies" in Bordeaux, July 2017 the 4th to 7th, a congress specialized in the microscopy domain where I introduced the development of the CLEM methods on plants samples and presented its application to the research field of grafting. This allows me to be selected by the "Radio des Chrétiens de France" (RCF) to comply with the exercise of scientific popularization by presenting my thesis work at "Que cherchent-ils?", a radio program to promote the work of young researchers (PhD and post-docs) and to confront the general public. (October 2017, the 28th)(https://rcf.fr/culture/lunion-porte-greffegreffon-chez-la-vigne-0)

Moreover, I had the opportunity to present my work to the Bordeaux Cell Biology Gathering (BCBG), a congress specialized in cell biology in which I did an oral presentation, April 2018, the 4th.

I presented my thesis in 3 minutes for "Conférence du millesime" at La Cité du Vin, Bordeaux (December 2017, the 13th), an event organized by Vintage Report. Each year, "Conférences du millésime" are the opportunity for vine and wine professionals to discuss and exchange about the past year and present the new advances and durable practices. This time, the experience permit to confront again to a nonscientific audience but professionals of the field of vine and wine industry, permitting to conciliate the fundamental research with professional world. On the same principle, I participated to the French edition of the contest three minute thesis, 'Ma these en trois minutes', for which I followed training for public oral presentations and writing. It allows me to work on explaining my project in three minutes, assisted with only one slide, to a non-specialist audience, thus training to be precise and concise

I invited and organized the venue of Charles Melnyk, from the Swedish University of Agricultural Sciences (Uppsala, Sweden) to give a seminar on his research on Arabidopsis grafting for the "Sructure Fédérative de Recherche" de "Biologie Integrative et Ecologie" that in feed-backgive me the opportunity to come in his lab, in Sweden, to learn *A. thaliana* grafting techniques and measurement of grafting success with several methods. He also gave me the opportunity to present my work on plasmodesmata in his lab. For the one week Arabidopsis grafting training, I applied for and obtained a travel grant from ISVV to fund this project.

I also have the opportunity to take part in the organization of the JJC (Journées Jeunes Chercheurs) of INRA BAP (20-21 April 2017, ISVV) with the DNAS (Doctors iN Agronomical Sciences) association of Bordeaux and present a scientific poster. This workshop is intended for the PhD students and post-docs to present their work and meet with other young researchers from BAP department of INRA (Plants Biology and Breeding).

The PhD has been a great opportunity for me to follow multiple disciplinary trainings to strengthen my competences notably a workshop on high resolution with Zeiss AiryScan, a workshop on the ImageJ software but more importantly, I was selected to participated to the 9 days EMBO workshop training on 3D developmental imaging in Portugal where I had the unique opportunity to follow both theoretical and practical courses on 3D imaging of organisms. I had the opportunity to follow courses on confocal, light sheet, two-photon microscopy and optical tomography as well as to practice these types of microscopy with state of the art equipments. During this workshop, I was also introduced to different techniques of clearing to be able to image in 3D and to analyzing the data with different software such as Amira, Huygens or ImageJ. Above all, this workshop was a unique opportunity to exchange with many experts from different biological domains to contribute to open mindedness.
Finally, I followed an introductive course to the python programming language, a very common language in the development of imaging software. I also followed training in ethics and integrity of the research, on entrepreneurship and self-assertion.

REFERENCES

Abandowitz, H. M., & Geissinger, H. D. (1975). Preparation of cells from suspensions for correlative scanning electron and interference microscopy. *Histochemistry*, *45*(2), 89–94. https://doi.org/10.1007/BF00495152

Albacete, A., Martínez-Andújar, C., Martínez-Pérez, A., Thompson, A. J., Dodd, I. C., & Pérez-Alfocea, F. (2015). Unravelling rootstock×scion interactions to improve food security. *Journal of Experimental Botany*, *66*(8), 2211–2226. https://doi.org/10.1093/jxb/erv027

Asahina, M., Iwai, H., Kikuchi, A., Yamaguchi, S., Kamiya, Y., Kamada, H., & Satoh, S. (2002). Gibberellin produced in the cotyledon is required for cell division during tissue reunion in the cortex of cut cucumber and tomato hypocotyls. *Plant Physiology*, *129*(1), 201–210. https://doi.org/10.1104/pp.010886

Assunção, M., Santos, C., Brazão, J., Eiras-Dias, J. E., & Fevereiro, P. (2019). Understanding the molecular mechanisms underlying graft success in grapevine. *BMC Plant Biology*, *19*(1), 1–17. https://doi.org/10.1186/s12870-019-1967-8

Bahar, E., Korkutal, I., Carbonneau, A., & Akcay, G. (2010). Using magnetic resonance imaging technique (MRI) to investigate graft connection and its relation to reddening discoloration in grape leaves. *Journal of Food, Agriculture and Environment*, *8*(3-4 PART 1), 293–297.

Bailey, J. (1923). *A microscopic study of apple graft unions*. Iowa State University of Science and Technology.

Batailler, B., Lemaître, T., Vilaine, F., Sanchez, C., Renard, D., Cayla, T., … Dinant, S. (2012). Soluble and filamentous proteins in Arabidopsis, 1258–1273. https://doi.org/10.1111/j.1365-3040.2012.02487.x

Bell, K., Mitchell, S., Paultre, D., Posch, M., & Oparka, K. (2013). Correlative Imaging of Fluorescent Proteins in. *Plant Physiology*, *161*(April), 1595–1603. https://doi.org/10.1104/pp.112.212365

Benitez-Alfonso, Y., Faulkner, C., Pendle, A., Miyashima, S., Helariutta, Y., & Maule, A. (2013). Symplastic Intercellular Connectivity Regulates Lateral Root Patterning. *Developmental Cell*, *26*(2), 136–147. https://doi.org/10.1016/j.devcel.2013.06.010

Biberfeld, P., Biberfeld, G., Molnar, Z., & Fagraeus, A. (1974). Fixation of cell-bound antibody in the membrane immunofluorescence test. *Journal of Immunological Methods*, *4*(2), 135–148. https://doi.org/10.1016/0022-1759(74)90056-8

Brault, M. L., Petit, J. D., Immel, F., Nicolas, W. J., Brocard, L., Gaston, A., … Bayer, E. M. (2018). Multiple C2 domains and Transmembrane region Proteins (MCTPs) tether membranes at plasmodesmata. *BioRxiv*, *44*, 1–26. https://doi.org/10.1101/423905

Brocard, L., Immel, F., Coulon, D., Esnay, N., Tuphile, K., Pascal, S., … Bréhélin, C. (2017). Proteomic Analysis of Lipid Droplets from Arabidopsis Aging Leaves Brings New Insight into Their Biogenesis and Functions. *Frontiers in Plant Science*, *8*(May). https://doi.org/10.3389/fpls.2017.00894

Burel, A., Lavault, M. T., Chevalier, C., Gnaegi, H., Prigent, S., Mucciolo, A., … Kolotuev, I. (2018). A targeted 3d em and correlative microscopy method using sem array tomography. *Development (Cambridge)*, *145*(12). https://doi.org/10.1242/dev.160879

Caffall, K. H., & Mohnen, D. (2009). The structure, function, and biosynthesis of plant cell wall pectic polysaccharides. *Carbohydrate Research*, *344*(14), 1879–1900. https://doi.org/10.1016/j.carres.2009.05.021

Cantrill, L. C., Overall, R. L., & Goodwin, P. B. (1999). CELL-TO-CELL COMMUNICATION VIA PLANT ENDOMEMBRANES. *Cell Biology International*, *23*(10), 653–661.

Carron, C., Balor, S., Delavoie, F., Plisson-Chastang, C., Faubladier, M., Gleizes, P. E., & ODonohue, M. F. (2012). Post-mitotic dynamics of pre-nucleolar bodies is driven by pre-rRNA processing. *Journal of Cell Science*, *125*(19), 4532–4542. https://doi.org/10.1242/jcs.106419

Cheadle, V. I., Risley, E. B., & Esau, K. (1962). DEVELOPMENT OF SIEVE-PLATE PORES. *Botanical Gazette*, *123*(4), 233–243.

Chen, Z., Zhao, J., Hu, F., Qin, Y., Wang, X., & Hu, G. (2017). Transcriptome changes between compatible and incompatible graft combination of Litchi chinensis by digital gene expression profile, (January), 1–12. https://doi.org/10.1038/s41598-017-04328-x

Complainville, A., Brocard, L., Roberts, I., Dax, E., Sever, N., Sauer, N., … Crespi, M. (2003). Nodule Initiation Involves the Creation of a New Symplasmic Field in Specific Root Cells of Medicago Species. *Plant Cell*, *15*(December), 2778–2791. https://doi.org/10.1105/tpc.017020.of

Cookson, S. J., Clemente Moreno, M. J., Hevin, C., Nyamba Mendome, L. Z., Delrot, S., Magnin, N., … Ollat, N. (2014). Heterografting with nonself rootstocks induces genes involved in stress responses at the graft interface when compared with autografted controls. *Journal of Experimental Botany*, *65*(9), 2473–2481. https://doi.org/10.1093/jxb/eru145

Cookson, S. J., Clemente Moreno, M. J., Hevin, C., Nyamba Mendome, L. Z., Delrot, S., Trossat-Magnin, C., & Ollat, N. (2013). Graft union formation in grapevine induces transcriptional changes related to cell wall modification, wounding, hormone signalling, and secondary metabolism. *Journal of Experimental Botany*, *64*(10), 2997–3008. https://doi.org/10.1093/jxb/ert144

Cordeau, J. (1998). Création d'un vignoble : Greffage de la vigne et porte-greffes, élimination des maladies à virus. Retrieved from http://sbiproxy.uqac.ca/login?url=http://international.scholarvox.com/book/88834499

Cui, W., & Lee, J. Y. (2016). Arabidopsis callose synthases CalS1/8 regulate plasmodesmal permeability during stress. *Nature Plants*, *2*(5). https://doi.org/10.1038/NPLANTS.2016.34

de la Canal, L., & Pinedo, M. (2018). Extracellular vesicles: A missing component in plant cell wall remodeling. *Journal of Experimental Botany*, *69*(20), 4655–4658. https://doi.org/10.1093/jxb/ery255

Ding, B., Turgeon, R., & Parthasarathy, M. V. (1992). Substructure of freeze-substituted plasmodesmata. *Protoplasma*, *169*(1–2), 28–41. https://doi.org/10.1007/BF01343367

Domozych, D., Lietz, A., Patten, M., Singer, E., Tinaz, B., & Raimundo, S. C. (2017). Imaging the Dynamics of Cell Wall Polymer Deposition in the Unicellular Model Plant, Penium margaritaceum David. In *Methods in Molecular Biology* (Vol. 1563, pp. 107–125). https://doi.org/10.1007/978-1-4939-6810-7

Ehlers, K., & Kollmann, R. (1996). Formation of branched plasmodesmata in regenerating Solanum nigrum-protoplasts. *Planta*, *199*(1), 126–138. https://doi.org/10.1007/BF00196889

Ehlers, K., & van Bel, A. J. E. (2010). Dynamics of plasmodesmal connectivity in successive interfaces

of the cambial zone. *Planta*, *231*(2), 371–385. https://doi.org/10.1007/s00425-009-1046-8

Esau, K. (1973). Comparative Structure of Companion Cells and Phloem Parenchyma Cells in Mimosa pudica L.

Esau, K., & Thorsch, J. (1985). Sieve plate pores and plasmodesmata, the communication channels of the symplast: ultrastructural aspects and developmental relations. *American Journal of Botany*, *72*(10), 1641–1653. https://doi.org/10.1002/j.1537-2197.1985.tb08429.x

Estrada-Luna, A., Lopez-Peralta, C., & Cardenas-Soriano, E. (2002). In vitro micrografting and the histology of graft union formation of selected species of prickly pear cactus (Opuntia spp.). *Scientia Horticulturae*, *92*, 317–327. https://doi.org/10.1016/S0304-4238(01)00296-5

Faulkner, C., Akman, O. E., Bell, K., Jeffree, C., & Oparka, K. J. (2008). Peeking into Pit Fields: A Multiple Twinning Model of Secondary Plasmodesmata Formation in Tobacco. *The Plant Cell Online*, *20*(6), 1504–1518. https://doi.org/10.1105/tpc.107.056903

Fernández-García, N., Carvajal, M., & Olmos, E. (2004). Graft union formation in tomato plants: Peroxidase and catalase involvement. *Annals of Botany*, *93*(1), 53–60. https://doi.org/10.1093/aob/mch014

Fitzgibbon, J., Beck, M., Zhou, J., Faulkner, C., Robatzek, S., & Oparka, K. (2013). A Developmental Framework for Complex Plasmodesmata Formation Revealed by Large-Scale Imaging of the Arabidopsis Leaf Epidermis, *25*(January), 57–70. https://doi.org/10.1105/tpc.112.105890

Flaishman, M. A., Loginovsky, K., Golobowich, S., & Lev-Yadun, S. (2008). Arabidopsis thaliana as a model system for graft union development in homografts and heterografts. *Journal of Plant Growth Regulation*, *27*(3), 231–239. https://doi.org/10.1007/s00344-008-9050-y

Froelich, D. R., Mullendore, D. L., Jensen, K. H., Ross-Elliott, T. J., Anstead, J. A., Thompson, G. A., … Knoblauch, M. (2011). Phloem Ultrastructure and Pressure Flow: Sieve-Element-Occlusion-Related Agglomerations Do Not Affect Translocation. *The Plant Cell*, *23*(12), 4428–4445. https://doi.org/10.1105/tpc.111.093179

Fu, Z., Peng, D., Zhang, M., Xue, F., Zhang, R., He, W., … Xu, P. (2019). mEosEM withstands osmium staining and Epon embedding for super-resolution CLEM. *Nature Methods*. https://doi.org/10.1038/s41592-019-0613-6

Fuentes, I., Stegemann, S., Golczyk, H., Karcher, D., & Bock, R. (2014). Horizontal genome transfer as an asexual path to the formation of new species. *Nature*. https://doi.org/10.1038/nature13291

Funk, V., Kositsup, B., Zhao, C., & Beers, E. P. (2002). The Arabidopsis xylem peptidase XCP1 is a tracheary element vacuolar protein that may be a papain ortholog. *Plant Physiology*, *128*(1), 84–94. https://doi.org/10.1104/pp.010514

Furuta, K., Lichtenberger, R., & Helariutta, Y. (2012). The role of mobile small RNA species during root growth and development. *Current Opinion in Cell Biology*, *24*(2), 211–216. https://doi.org/10.1016/j.ceb.2011.12.005

Furuta, K. M., Yadav, S. R., Lehesranta, S., Belevich, I., Miyashima, S., Heo, J. -o., … Helariutta, Y. (2014). Arabidopsis NAC45/86 direct sieve element morphogenesis culminating in enucleation. *Science*, *345*(6199), 933–937. https://doi.org/10.1126/science.1253736

Furuta, Kaori Miyashima, Yadav, S. R., Lehesranta, S., Belevich, I., Miyashima, S., Heo, J. ok, … Helariutta, Y. (2014). Plant development. Arabidopsis NAC45/86 direct sieve element morphogenesis culminating in enucleation. *Science (New York, N.Y.)*, *345*(6199), 933–937.

https://doi.org/10.1126/science.1253736

Gautier, A. T., Chambaud, C., Brocard, L., Ollat, N., Gambetta, G. A., Delrot, S., & Cookson, S. J. (2019). Merging genotypes: Graft union formation and scion-rootstock interactions. *Journal of Experimental Botany*, *70*(3), 805–815. https://doi.org/10.1093/jxb/ery422

Gerlitz, N., Gerum, R., Sauer, N., & Stadler, R. (2018). Photoinducible DRONPA-s: a new tool for investigating cell–cell connectivity. *Plant Journal*, *94*(5), 751–766. https://doi.org/10.1111/tpj.13918

Giannoutsou, E., Sotiriou, P., Apostolakos, P., & Galatis, B. (2013). Early local differentiation of the cell wall matrix defines the contact sites in lobed mesophyll cells of Zea mays. *Annals of Botany*, *112*(6), 1067–1081. https://doi.org/10.1093/aob/mct175

Glauert, A. M., & Lewis, P. R. (2014). *Biological Specimen Preparation for Transmission Electron Microscopy*.

Goldschmidt, E. E. (2014). Plant grafting: new mechanisms, evolutionary implications. *Frontiers in Plant Science*, *5*(December), 1–9. https://doi.org/10.3389/fpls.2014.00727

Gregory, P. J., Atkinson, C. J., Bengough, A. G., Else, M. A., Fernández-Fernández, F., Harrison, R. J., & Schmidt, S. (2013). Contributions of roots and rootstocks to sustainable, intensified crop production. *Journal of Experimental Botany*, *64*(5), 1209–1222. https://doi.org/10.1093/jxb/ers385

Grison, M. S., Brocard, L., Fouillen, L., Nicolas, W., Wewer, V., Dörmann, P., … Bayer, E. M. (2015). Specific membrane lipid composition is important for plasmodesmata function in Arabidopsis. *The Plant Cell*, *27*(4), 1228–1250. https://doi.org/10.1105/tpc.114.135731

Groover, A., DeWitt, N., Heidel, A., & Jones, A. (1997). Programmed cell death of plant tracheary elements differentiating in vitro. *Protoplasma*, *196*(3–4), 197–211. https://doi.org/10.1007/BF01279568

Gurdon, C., Svab, Z., Feng, Y., Kumar, D., & Maliga, P. (2016). Cell-to-cell movement of mitochondria in plants, *113*(12), 3395–3400. https://doi.org/10.1073/pnas.1518644113

Guseman, J. M., Lee, J. S., Bogenschutz, N. L., Peterson, K. M., Virata, R. E., Xie, B., … Torii, K. U. (2010). Dysregulation of cell-to-cell connectivity and stomatal patterning by loss-of-function mutation in Arabidopsis chorus (glucan synthase-like 8). *Development (Cambridge, England)*, *137*(10), 1731–1741. https://doi.org/10.1242/dev.049197

Harrison, N., Harrison, R. J., Barber-Perez, N., Cascant-Lopez, E., Cobo-Medina, M., Lipska, M., … Fernández-Fernández, F. (2016). A new three-locus model for rootstock-induced dwarfing in apple revealed by genetic mapping of root bark percentage. *Journal of Experimental Botany*, *67*(6), 1871–1881. https://doi.org/10.1093/jxb/erw001

Hepler, P. K. (1982). Endoplasmic reticulum in the formation of the cell plate and plasmodesmata. *Protoplasma*, *111*(2), 121–133. https://doi.org/10.1007/BF01282070

Irisarri, P., Binczycki, P., Errea, P., Martens, H. J., & Pina, A. (2015). Oxidative stress associated with rootstock-scion interactions in pear/quince combinations during early stages of graft development. *Journal of Plant Physiology*, *176*, 25–35. https://doi.org/10.1016/j.jplph.2014.10.015

Ito, J., & Fukuda, H. (2002). ZEN1 is a key enzyme in the degradation of nuclear DNA during programmed cell death of tracheary elements. *Plant Cell*, *14*(12), 3201–3211.

https://doi.org/10.1105/tpc.006411

Ito, Y., & Fukuda, H. (2006). Dodeca-CLE Peptides as Suppressors. *Science*, (August), 842–845. https://doi.org/10.1126/science.1128436

Jeffree, C. E., & Yeoman, M. M. (1982). Development of intercellular connections between opposing cells in a graft union. *New Phytologist*, *93*, 491–509.

Jens Tilsner, William Nicolas, Abel Rosado, and E. M. B. (2016). Staying Tight: Plasmodesmal Membrane Contact Sites and the Control of Cell-to-Cell Connectivity in Plants. *Annual Review of Plant Biology*, *67*(February), 1–28. https://doi.org/10.1146/annurev-arplant-043015-111840

Kieber, J. J., & Schaller, G. E. (2014). Cytokinins. *The Arabidopsis Book / American Society of Plant Biologists*, *12*, e0168. https://doi.org/10.1199/tab.0168

Knox, J. P., & Benitez-Alfonso, Y. (2014). Roles and regulation of plant cell walls surrounding plasmodesmata. *Current Opinion in Plant Biology*, *22*(Figure 1), 93–100. https://doi.org/10.1016/j.pbi.2014.09.009

Knox, K., Wang, P., Kriechbaumer, V., Tilsner, J., Frigerio, L., Sparkes, I., … Oparka, K. (2015). Putting the Squeeze on Plasmodesmata: A Role for Reticulons in Primary Plasmodesmata Formation. *Plant Physiology*, *168*(4), 1563–1572. https://doi.org/10.1104/pp.15.00668

Kollmann, R., & Glockmann, C. (1985). Studies on graft unions. I. Plasmodesmata between cells of plants belonging to different unrelated taxa. *Protoplasma*, *124*(3), 224–235. https://doi.org/10.1007/BF01290774

Kollmann, R., & Glockmann, C. (1991). Studies on graft unions - III. On the mechanism of secondary formation of plasmodesmata at the graft interface. *Protoplasma*, *165*(1–3), 71–85. https://doi.org/10.1007/BF01322278

Kollmann, R., Yang, S., & Glockmann, C. (1985). Studies on graft unions - II. Continuous and half plasmodesmata in different regions of the graft interface. *Protoplasma*, *126*(1–2), 19–29. https://doi.org/10.1007/BF01287669

Kousik, C. S., Mandal, M., & Hassell, R. (2018). Powdery mildew resistant rootstocks that impart tolerance to grafted susceptible watermelon scion seedlings. *Plant Disease*, *102*(7), 1290–1298. https://doi.org/10.1094/PDIS-09-17-1384-RE

Kubo, M., Udagawa, M., Nishikubo, N., Horiguchi, G., Yamaguchi, M., Ito, J., … Demura, T. (2005). Transcription switches for protoxylem and metaxylem vessel formation. *Genes & Development*, 1855–1860. https://doi.org/10.1101/gad.1331305.GENES

Kukulski, W., Schorb, M., Kaksonen, M., & Briggs, J. A. G. (2012). Plasma membrane reshaping during endocytosis is revealed by time-resolved electron tomography. *Cell*, *150*(3), 508–520. https://doi.org/10.1016/j.cell.2012.05.046

Kukulski, W., Schorb, M., Welsch, S., Picco, A., Kaksonen, M., & Briggs, J. A. G. (2011). Correlated fluorescence and 3D electron microscopy with high sensitivity and spatial precision, *192*(1), 111–120. https://doi.org/10.1083/jcb.201009037

Kumar, D., Kumar, R., Hyun, T. K., & Kim, J. Y. (2014). Cell-to-cell movement of viruses via plasmodesmata. *Journal of Plant Research*, *128*(1), 37–47. https://doi.org/10.1007/s10265-014-0683-6

Kurihara, D., Mizuta, Y., Sato, Y., & Higashiyama, T. (2015). ClearSee: a rapid optical clearing reagent for whole-plant fluorescence imaging. *Development*, 4168–4179.

https://doi.org/10.1242/dev.127613

Lartaud, M., Perin, C., Courtois, B., Thomas, E., Henry, S., Bettembourg, M., … Dievart, A. (2015). Phiv-Rootcell: A supervised image analysis tool for rice root anatomical parameter quantification. *Frontiers in Plant Science*, *5*(JAN), 1–7. https://doi.org/10.3389/fpls.2014.00790

Lee, J., Wang, X., Cui, W., Sager, R., Modla, S., Czymmek, K., … Lakshmanan, V. (2011). A Plasmodesmata-Localized Protein Mediates Crosstalk between Cell-to-Cell Communication and Innate Immunity in Arabidopsis, *23*(September), 3353–3373. https://doi.org/10.1105/tpc.111.087742

Lehmann, K., Hause, B., Altmann, D., & Köck, M. (2001). Tomato ribonuclease LX with the functional endoplasmic reticulum retention motif HDEF is expressed during programmed cell death processes, including xylem differentiation, germination, and senescence. *Plant Physiology*, *127*(2), 436–449. https://doi.org/10.1104/pp.010362

Levy, A., Erlanger, M., Rosenthal, M., & Epel, B. L. (2007). A plasmodesmata-associated ??-1,3-glucanase in Arabidopsis. *Plant Journal*, *49*(4), 669–682. https://doi.org/10.1111/j.1365-313X.2006.02986.x

LINDSAY, D. W., YEOMAN, M. M., & BROWN, R. (1974). An Analysis of the Development of the Graft Union in Lycopersicon esculentum. *Annals of Botany*, *38*(3), 639–646. https://doi.org/10.1093/oxfordjournals.aob.a084849

López-Sáez, J. F., Giménez-Martin, G., & Risueño, M. C. (1966). Fine structure of the plasmodesm. *Protoplasma*, *61*(1–2), 81–84. https://doi.org/10.1007/BF01247912

Lu, Y., Stegemann, S., Agrawal, S., Karcher, D., Ruf, S., Bock, R., … Bock, R. (2017). Horizontal Transfer of a Synthetic Metabolic Pathway between Plant Species Report Horizontal Transfer of a Synthetic Metabolic Pathway between Plant Species. *Current Biology*, 1–8. https://doi.org/10.1016/j.cub.2017.08.044

Lucas, W. J., & Lee, J.-Y. (2004). Plasmodesmata as a supracellular control network in plants. *Nature Reviews. Molecular Cell Biology*, *5*(9), 712–726. https://doi.org/10.1038/nrm1470

Marion, J., Le Bars, R., Satiat-Jeunemaitre, B., & Boulogne, C. (2017). Optimizing CLEM protocols for plants cells: GMA embedding and cryosections as alternatives for preservation of GFP fluorescence in Arabidopsis roots. *Journal of Structural Biology*, *198*(3), 196–202. https://doi.org/10.1016/j.jsb.2017.03.008

Masselink, W., Reumann, D., Murawala, P., Pasierbek, P., Taniguchi, Y., Bonnay, F., … Tanaka, E. M. (2019). Broad applicability of a streamlined ethyl cinnamate-based clearing procedure. *Development (Cambridge)*, *146*(3). https://doi.org/10.1242/dev.166884

Matsuoka, K., Sugawara, E., Aoki, R., Takuma, K., Terao-Morita, M., Satoh, S., & Asahina, M. (2016). Differential cellular control by cotyledon-derived phytohormones involved in graft reunion of arabidopsis hypocotyls. *Plant and Cell Physiology*, *57*(12), 2620–2631. https://doi.org/10.1093/pcp/pcw177

Maule, A. J., Gaudioso-pedraza, R., Benitez-alfonso, Y., Maule, A. J., Gaudioso-pedraza, R., & Benitez-alfonso, Y. (2013). Callose deposition and symplastic connectivity are regulated prior to lateral root emergence Callose deposition and symplastic connectivity are regulated prior to lateral root emergence, *0889*. https://doi.org/10.4161/cib.26531

May, P., Grape, Research, W., & (Australia), D. C. (1994). *Using Grapevine Rootstocks: The Australian Perspective*. Winetitles Pty Limited. Retrieved from

https://books.google.fr/books?id=MNtJAAAAYAAJ

Melnyk, C. W. (2017). *Grafting with Arabidopsis* (Vol. 137).

Melnyk, C. W., Gabel, A., Hardcastle, T. J., Robinson, S., & Miyashima, S. (2018). Transcriptome dynamics at Arabidopsis graft junctions reveal an intertissue recognition mechanism that activates vascular regeneration, *115*(10). https://doi.org/10.1073/pnas.1718263115

Melnyk, C. W., Schuster, C., Leyser, O., & Meyerowitz, E. M. (2015). A developmental framework for graft formation and vascular reconnection in arabidopsis thaliana. *Current Biology*, *25*(10), 1306–1318. https://doi.org/10.1016/j.cub.2015.03.032

Milien, M., Renault-Spilmont, A. S., Cookson, S. J., Sarrazin, A., & Verdeil, J. L. (2012). Visualization of the 3D structure of the graft union of grapevine using X-ray tomography. *Scientia Horticulturae*, *144*, 130–140. https://doi.org/10.1016/j.scienta.2012.06.045

Moore, C. L., Cheng, D., Shami, G. J., & Murphy, C. R. (2016). Correlated light and electron microscopy observations of the uterine epithelial cell actin cytoskeleton using fluorescently labeled resin-embedded sections. *Micron*, *84*, 61–66. https://doi.org/10.1016/j.micron.2016.02.010

Moore, R., & Walker, D. B. (1981). Studies of Vegetative Compatibility-Incompatibility in Higher Plants. I. A STRUCTURAL STUDY OF A COMPATIBLE AUTOGRAFT IN SEDUM TELEPHOIDES (CRASSULACEAE). *American Journal of Botany*, *68*(6), 820–830. https://doi.org/10.2307/2443189

Mudge, K. (2009). A History of Grafting, *35*, 437–494.

Müller-Reichert, T., & Verkade, P. (2012). Introduction to correlative light and electron microscopy. *Methods in Cell Biology*, *111*. https://doi.org/10.1016/B978-0-12-416026-2.03001-6

Nicolas, W. J., Grison, M. S., Trépout, S., Gaston, A., Fouché, M., Cordelières, F. P., … Bayer, E. M. (2017). Architecture and permeability of post-cytokinesis plasmodesmata lacking cytoplasmic sleeves. *Nature Plants*, *17082*(June). https://doi.org/10.1038/nplants.2017.82

Nixon, S. J., Webb, R. I., Floetenmeyer, M., Schieber, N., Lo, H. P., & Parton, R. G. (2009). A single method for cryofixation and correlative light, electron microscopy and tomography of zebrafish embryos. *Traffic*, *10*(2), 131–136. https://doi.org/10.1111/j.1600-0854.2008.00859.x

Nocito, F. F., Espen, L., Fedeli, C., Lancilli, C., Musacchi, S., Serra, S., … Sacchi, G. A. (2010). Oxidative stress and senescence-like status of pear calli co-cultured on suspensions of incompatible quince microcalli, (March), 450–458. https://doi.org/10.1093/treephys/tpq006

Notaguchi, M., Abe, M., Kimura, T., Daimon, Y., Kobayashi, T., Yamaguchi, A., … Araki, T. (2008). Long-distance, graft-transmissible action of Arabi... [Plant Cell Physiol. 2008] - PubMed result. *Plant Cell Physiology*, *49*(11), 1645–1658. https://doi.org/10.1093/pcp/pcn154

Ohashi-Ito, K., Oda, Y., & Fukuda, H. (2010). Arabidopsis VASCULAR-RELATED NAC-DOMAIN6 directly regulates the genes that govern programmed cell death and secondary wall formation during xylem differentiation. *Plant Cell*, *22*(10), 3461–3473. https://doi.org/10.1105/tpc.110.075036

Oparka, K. J., Roberts, A. G., Boevink, P., Cruz, S. S., Roberts, I., Pradel, K. S., … Epel, B. (1999). Simple, but not branched, plasmodesmata allow the nonspecific trafficking of proteins in developing tobacco leaves. *Cell*, *97*(6), 743–754. https://doi.org/10.1016/S0092-8674(00)80786-2

Ormenese, S., Havelange, A., Deltour, R., & Bernier, G. (2000). The frequency of plasmodesmata increases early in the whole shoot apical meristem of Sinapis alba L. during floral transition. *Planta*, *211*(3), 370–375. https://doi.org/10.1007/s004250000294

Osugi, A., & Sakakibara, H. (2015). Q and A: How do plants respond to cytokinins and what is their importance? *BMC Biology*, *13*(1), 1–10. https://doi.org/10.1186/s12915-015-0214-5

Otero, S., Helariutta, Y., & Benitez-Alfonso, Y. (2016). Symplastic communication in organ formation and tissue patterning. *Current Opinion in Plant Biology*, *29*, 21–28. https://doi.org/10.1016/j.pbi.2015.10.007

Overall, R. L., & Blackman, L. M. (1996). A model of the macromolecular structure of plasmodesmata. *Trends in Plant Science*, *1*(9), 307–311. https://doi.org/10.1016/1360-1385(96)88177-5

Paez-Segala, M. G., Sun, M. G., Shtengel, G., Viswanathan, S., Baird, M. A., Macklin, J. J., … Looger, L. L. (2015). Fixation-resistant photoactivatable fluorescent proteins for CLEM. *Nature Methods*, *12*(3), 215–218. https://doi.org/10.1038/nmeth.3225

Pandey, K. K. (1976). Genetic transformation and "graft-hybridization" in flowering plants. *Theoretical and Applied Genetics*, *47*(6), 299–302. https://doi.org/10.1007/BF00281935

Patterson, G. H., & Lippincott-Schwartz, J. (2002). A Photoactivatable GFP for Selective Photolabelling of Proteins and Cells. *Science*, *297*(September), 1873–1878. https://doi.org/10.1126/science.1074952

Paultre, D. S. G., Gustin, M.-P., Molnar, A., & Oparka, K. J. (2016). Lost in transit: long-distance trafficking and phloem unloading of protein signals in Arabidopsis homografts. *The Plant Cell*, *28*(September), tpc.00249.2016. https://doi.org/10.1105/tpc.16.00249

Pina, A., & Errea, P. (2005). A review of new advances in mechanism of graft compatibility-incompatibility. *Scientia Horticulturae*, *106*(1), 1–11. https://doi.org/10.1016/j.scienta.2005.04.003

Pina, A., & Errea, P. (2008). Differential induction of phenylalanine ammonia-lyase gene expression in response to in vitro callus unions of Prunus spp. *Journal of Plant Physiology*, *165*(7), 705–714. https://doi.org/https://doi.org/10.1016/j.jplph.2007.05.015

Pina, A., Errea, P., Schulz, A., & Martens, H. J. (2009). Cell-to-cell transport through plasmodesmata in tree callus cultures. *Tree Physiology*, *29*(6), 809–818. https://doi.org/10.1093/treephys/tpp025

Prado, N., De Dios Alché, J., Casado-Vela, J., Mas, S., Villalba, M., Rodríguez, R., & Batanero, E. (2014). Nanovesicles are secreted during pollen germination and pollen tube growth: A possible role in fertilization. *Molecular Plant*, *7*(3), 573–577. https://doi.org/10.1093/mp/sst153

Prior, D. A. M., Oparka, K. J., & Roberts, I. M. (1999). En bloc optical sectioning of resin-embedded specimens using a confocal laser scanning microscope. *Journal of Microscopy*, *193*(1), 20–27. https://doi.org/10.1046/j.1365-2818.1999.00433.x

Radford, J. E., & White, R. G. (2011). Inhibitors of myosin, but not actin, alter transport through Tradescantia plasmodesmata. *Protoplasma*, *248*(1), 205–216. https://doi.org/10.1007/s00709-010-0244-3

Ribeiro, L. M., Nery, L. A., Vieira, L. M., & Mercadante-Simões, M. O. (2015). Histological study of micrografting in passionfruit. *Plant Cell, Tissue and Organ Culture*, *123*(1), 173–181. https://doi.org/10.1007/s11240-015-0824-1

Rieckher, M., Kyparissidis-kokkinidis, I., & Zacharopoulos, A. (2015). A Customized Light Sheet Microscope to Measure Spatio-Temporal Protein Dynamics in Small Model Organisms, 1–15. https://doi.org/10.1371/journal.pone.0127869

Ripper, D., Schwarz, H., & Stierhof, Y.-D. (2008). Cryo-section immunolabelling of difficult to preserve

specimens: advantages of cryofixation, freeze-substitution and rehydration. *Biology of the Cell*, *100*(2), 109–123. https://doi.org/10.1042/bc20070106

Robards, A. W. (1971). The ultrastructure of plasmodesmata. *Protoplasma*, *72*(2–3), 315–323. https://doi.org/10.1007/BF01279056

Ross-elliott, T. J., Jensen, K. H., Haaning, K. S., Wager, B. M., Knoblauch, J., Howell, A. H., … Oparka, K. J. (2017). Phloem unloading in Arabidopsis roots is convective and regulated by the phloem-pole pericycle, 1–31. https://doi.org/10.7554/eLife.24125

Roy, S., Watada, A. E., & Wergin, W. P. (1997). Characterization of the cell wall microdomain surrounding plasmodesmata in apple fruit. *Plant Physiology*, *114*(2), 539–547. https://doi.org/10.1104/pp.114.2.539

Rutter, B. D., & Innes, R. W. (2017). Extracellular vesicles isolated from the leaf apoplast carry stress-response proteins. *Plant Physiology*, *173*(1), 728–741. https://doi.org/10.1104/pp.16.01253

Rybak, K., & Robatzek, S. (2019). Functions of extracellular vesicles in immunity and virulence. *Plant Physiology*, *179*(4), 1236–1247. https://doi.org/10.1104/pp.18.01557

Rybel, B. De, Mähönen, A. P., Helariutta, Y., & Weijers, D. (2015). Plant vascular development : from early specification to differentiation. *Nature Publishing Group*, *17*(1), 30–40. https://doi.org/10.1038/nrm.2015.6

Sager, R., & Lee, J. Y. (2014). Plasmodesmata in integrated cell signalling: Insights from development and environmental signals and stresses. *Journal of Experimental Botany*, *65*(22), 6337–6358. https://doi.org/10.1093/jxb/eru365

Satoh, S., Asahina, M., Azuma, K., Pitaksaringkarn, W., Yamazaki, T., & Mitsuda, N. (2011). Spatially selective hormonal control of RAP2. 6L and ANAC071 transcription factors involved in tissue reunion in Arabidopsis, *108*(38), 16128–16132. https://doi.org/10.1073/pnas.1110443108

Sawa, S., Demura, T., Horiguchi, G., Kubo, M., & Fukuda, H. (2005). The ATE genes are responsible for repression of transdifferentiation into xylem cells in arabidopsis. *Plant Physiology*, *137*(1), 141–148. https://doi.org/10.1104/pp.104.055145

Schaller, G. E., Bishopp, A., & Kieber, J. J. (2015). The yin-yang of hormones: Cytokinin and auxin interactions in plant development. *Plant Cell*, *27*(1), 44–63. https://doi.org/10.1105/tpc.114.133595

Shaner, N. C., Steinbach, P. A., & Tsien, R. Y. (2005). A guide to choosing fluorescent proteins. *Nature Methods*, *2*(12), 905–909. https://doi.org/10.1038/nmeth819

Sidorov, V., Armstrong, C., Ream, T., Ye, X., & Saltarikos, A. (2018). " Cell grafting ": a new approach for transferring cytoplasmic or nuclear genome between plants. *Plant Cell Reports*, *37*(8), 1077–1089. https://doi.org/10.1007/s00299-018-2292-7

Sieburth, L. E. (1999). Auxin is required for leaf vein pattern in Arabidopsis. *Plant Physiology*, *121*(4), 1179–1190. https://doi.org/10.1104/pp.121.4.1179

Sing, K., Erickson, T., Amitai, Y., & Hryhorczuk, D. (1996). Chloral hydrate toxicity from oral and intravenous administration. *Journal of Toxicology - Clinical Toxicology*, *34*(1), 101–106. https://doi.org/10.3109/15563659609020242

Sleighter, R. L., Hatcher, P. G., Johnston, M. V, Seinfeld, J. H., Marston, G., Akimoto, H., … Division, M. S. (2012). Sucrose Efflux Mediated by SWEET Proteins as a Key Step for Phloem Transport, *745*(January), 207–211.

Smith, R. A., Schuetz, M., Roach, M., Mansfield, S. D., Ellis, B., & Samuels, L. (2013). Neighboring parenchyma cells contribute to Arabidopsis xylem lignification, while lignification of interfascicular fibers is cell autonomous. *Plant Cell*, *25*(10), 3988–3999. https://doi.org/10.1105/tpc.113.117176

STAUDT, T., LANG, M. C., MEDDA, R., ENGELHARDT, J., & HELL, S. (2007). 2,20-Thiodiethanol: A NewWater Soluble Mounting Medium for High Resolution Optical Microscopy. *MICROSCOPY RESEARCHAND TECHNIQUE*, *70*. https://doi.org/10.1002/jemt

Stegemann, S., & Bock, R. (2009). Exchange of genetic material between cells in plant tissue grafts. *Science (New York, N.Y.)*, *324*(5927), 649–651. https://doi.org/10.1126/science.1170397

Storme, N. De, & Geelen, D. (2014). Callose homeostasis at plasmodesmata : molecular regulators and developmental relevance, *5*(April), 1–23. https://doi.org/10.3389/fpls.2014.00138

Sullivan, K. D., Majewska, A. K., & Brown, E. B. (2016). Single and Multiphoton Fluorescence Recovery after Photobleaching. *Cold Spring Harb Protoc*, *2015*(1), 1–16. https://doi.org/10.1101/pdb.top083519.Single

Sun, M., Shtengel, G., Viswanathan, S., Baird, M., Macklin, J., Patel, R., … Looger, L. (2015). Fixation-resistant photoactivatable fluorescent proteins for correlative light and electron microscopy. *Nature Methods*, *12*(3), 215–218. https://doi.org/10.1038/nmeth.3225

Thieme, C. J., Rojas-Triana, M., Stecyk, E., Schudoma, C., Zhang, W., Yang, L., … Kragler, F. (2015). Endogenous Arabidopsis messenger RNAs transported to distant tissues. *Nature Plants*, *1*(April). https://doi.org/10.1038/nplants.2015.25

Thomas, C. L., Bayer, E. M., Ritzenthaler, C., Fernandez-Calvino, L., & Maule, A. J. (2008). Specific targeting of a plasmodesmal protein affecting cell-to-cell communication. *PLoS Biology*, *6*(1), 0180–0190. https://doi.org/10.1371/journal.pbio.0060007

Thyssen, G., Svab, Z., & Maliga, P. (2012). Cell-to-cell movement of plastids in plants, *109*(7), 2439–2443. https://doi.org/10.1073/pnas.1114297109

Tilney, L. G., Cooke, T. J., Connelly, P. S., & Tilney, M. S. (1991). The structure of plasmodesmata as revealed by plasmolysis, detergent extraction, and protease digestion. *Journal of Cell Biology*, *112*(4), 739–747. https://doi.org/10.1083/jcb.112.4.739

Turgeon, R. (1996). Phloem loading and plasmodesmata. *Trends in Plant Science*, *1*(12), 418–423. https://doi.org/10.1016/S1360-1385(96)10045-5

Turnbull, C. G. N. (2010). Grafting as a Research tool. *Plant Developmental Biology*, *655*, 11–26. https://doi.org/10.1007/978-1-60761-765-5_2

Turnbull, C. G. N., Booker, J. P., & Leyser, H. M. O. (2002). Micrografting techniques for testing long-distance signalling in Arabidopsis. *Plant Journal*, *32*(2), 255–262. https://doi.org/10.1046/j.1365-313X.2002.01419.x

Ulvskov, P., Wium, H., Bruce, D., Jørgensen, B., Qvist, K. B., Skjøt, M., … Sørensen, S. O. (2005). Biophysical consequences of remodeling the neutral side chains of rhamnogalacturonan I in tubers of transgenic potatoes. *Planta*, *220*(4), 609–620. https://doi.org/10.1007/s00425-004-1373-8

Vatén, A., Dettmer, J., Wu, S., Stierhof, Y.-D., Miyashima, S., Yadav, S. R., … Helariutta, Y. (2011). Callose Biosynthesis Regulates Symplastic Trafficking during Root Development. *Developmental Cell*, *1*, 1144–1155. https://doi.org/10.1016/j.devcel.2011.10.006

Villani, T. S., Koroch, A. R., & Simon, J. E. (2013). An Improved Clearing and Mounting Solution to Replace Chloral Hydrate in Microscopic Applications. *Applications in Plant Sciences*, *1*(5), 1300016. https://doi.org/10.3732/apps.1300016

Watanabe, S., Punge, A., Hollopeter, G., Willig, K. I., Hobson, R. J., Davis, M. W., … Jorgensen, E. M. (2011). Protein localization in electron micrographs using fluorescence nanoscopy. *Nature Methods*, *8*(1), 80–84. https://doi.org/10.1038/nmeth.1537

Webster, R. E., Osborn, M., & Weber, K. (1978). Visualization of the same PtK2 cytoskeletons by both immunofluorescence and low power electron microscopy. *Experimental Cell Research*, *117*(1), 47–61. https://doi.org/10.1016/0014-4827(78)90426-3

Withers, L. A., & Cocking, E. C. (1972). Fine-structural studies on spontaneous and induced fusion of higher plant protoplasts. *Journal of Cell Science*, *11*(1), 59–75.

Wu, S. W., Kumar, R., Iswanto, A. B. B., & Kim, J. Y. (2018). Callose balancing at plasmodesmata. *Journal of Experimental Botany*, *69*(22), 5325–5339. https://doi.org/10.1093/jxb/ery317

Yin, H., Yan, B., Sun, J., Pengfei, J., Zhang, Z., Yan, X., … Liu, H. (2012). Graft-union development: a delicate process that involves cell–cell communication between scion and stock for local methylation and chromatin patterning auxin accumulation. *Journal of Experimental Botany*, *63*(11), 4219–4232. https://doi.org/10.1093/jxb/ers109

Zarrouk, O. (2010). Changes in Cell / Tissue Organization and Peroxidase Activity as Markers for Early Detection of Graft Incompatibility in Peach / Plum Combinations, *135*(1), 9–17.